Fibre reinforced sands:
experiments and constitutive modelling

by

Andrea Diambra

University of BRISTOL

A dissertation submitted to the University of Bristol in accordance
with the requirements of the degree of Doctor of Philosophy
in the Faculty of Engineering, Department of Civil Engineering

March 2010

ABSTRACT

The technique of reinforcing soils with discrete flexible fibres is slowly gaining acceptance and support between practising engineers. However, little is known about the main factors governing the behaviour of this material and the main characteristics of its behaviour. This means that the applicability and potential of this soil improvement method have not been resolved. The present research aims to provide a considerable contribution in understanding the mechanisms governing the behaviour of this reinforced material and to develop a modelling tool which allows the prediction of its mechanical behaviour.

A procedure for the determination of the distribution of the orientation of fibre in reinforced specimens has been developed herein. It was found that the most common procedure for preparing reinforced specimens, moist tamping, leads to preferred sub-horizontal orientation of fibres. In view of these preliminary results an extensive campaign of compression and extension conventional triaxial tests for both drained and undrained condition has been performed. Fibres were found to be effective in increasing the strength of the material but their effectiveness was found to be dependent on the orientation with respect to tensile strains. Fibres were also found to be effective in preventing the liquefaction of loose sand specimens: addition of fibres results in a densification of the sand matrix not only for the volume that they occupy but also for preventing the sand matrix from using some of the voids during the deformation process.

A new constitutive modelling framework has been developed on the basis of the rule of mixtures of composite materials. This approach allows the adoption of separate constitutive laws for each constituent and to combine their effects in characterising the behaviour of the composite material. In this manner it is possible to select the complexity of the constitutive model of each constituent and to simulate peculiar aspect of its behaviour. Application of the model demonstrated how accurately the mechanical behaviour of fibre reinforced sand can be simulated with particular regard to the anisotropy of strength and the prevention of liquefaction.

ACKNOWLEDGEMENTS

I wish to express my sincere thanks to Dr. E. Ibraim for his supervision, knowledge, patience and continual encouragement during the development of this research. He has guided me towards this achievement with great enthusiasm and commitment.

I would like to thank Prof. D. Muir Wood for his invaluable advices and guidance in developing this research. He has had a considerable and beneficial influence on the progress of this project. I have acquired a lot from his extensive professional experience.

I would like to thank Dr. A Russell for proposing me to undertake this research and for his supervision throughout this project. Beyond his support and continuous advices, he gave me the possibility to collaborate with him in Australia and to visit such a beautiful country.

I wish to thank Mr. M. Pope for his invaluable technical support, without his skills this project would never have been accomplished.

Also, acknowledgement is expressed to the University of Bristol and the Department of Civil Engineering for sponsoring the research project on which this thesis is based.

I would like to thank my parents and my sister who have ever supported me in my studies and without their support I would have never reached this achievement.

Finally the greatest thank to my wife Francesca that pulled me through this adventure with great enthusiasm. We have faced the challenge of the doctorate together and she has supported me at any stage of this project. She has also recently given me the greatest joy of my life: the little Rachele. Thanks, Francesca.

AUTHOR'S DECLARATION

I declare that the work in this dissertation was carried out in accordance with the requirements of the University's Regulations and Code of Practice for Research Degree Programmes and that it has not been submitted for any other academic award. Except where indicated by specific reference in the text, the work is the candidate's own work. Any views expressed in the dissertation are those of the author.

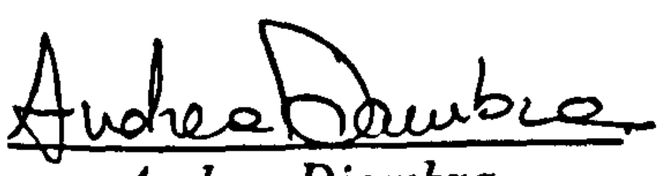

Andrea Diambra

March 2010

TABLE OF CONTENTS

LIST OF FIGURES

CHAPTER 4

LIST OF TABLES

LIST OF SYMBOLS AND ABBREVIATIONS

A	Constant to define the orientation distribution of the fibres
A	Multiplier in the flow rule of the Severn-Trent sand model
A_{ij}	Terms of the matrix stiffness for the fibres when expressed in volumetric and distortional terms
a_0	Material parameter for defining the maximum angle of dilatancy
a	Constant to define the orientation distribution of the fibres (Eq. 7.48)
b	Constant to define the orientation distribution of the fibres (Eq. 7.48)
b	Distance between the centre of the reference sphere and a vertical plane
B	Skempton's saturation coefficient
B	Parameter controlling hyperbolic stiffness relationship in Severn Trent model
C	Constant to define the orientation distribution of the fibres
c_1	Constant to define the approximated limit introduced to solve the integral for the determination of the fibre orientation distribution (Eq.4.11)
c_2	Constant to define the approximated limit introduced to solve the integral for the determination of the fibre orientation distribution (Eq.4.11)
cs	Constant to define the sliding function f_b
A_L	Lateral surface of the specimen
C_g	Coefficient of gradation
C_u	Coefficient of uniformity
D	Diameter of the specimen
D_{50}	Mean grain size
$\mathbf{D}^e$	Elastic matrix of the sand
d	Dilatancy
d_t	Diameter of the membrane
d_f	Diameter of a fibre
e	Void ratio
e_0	Void ratio after fabrication prior the consolidation stage

e_c	Void ratio after consolidation
e_{min}	Minimum void ratio
e_{max}	Maximum void ratio
E	Young modulus
E_f	Elastic modulus of a fibre
E_m	Elastic modulus of the membrane
E_{tg}	Tangential modulus of the stress-strain response
F_{ij}	Terms of the matrix stiffness for the fibres when expressed in axial and radial terms
f_b	Sliding function between fibres and sand grains
G	Shear modulus
G_s, G_f	Specific gravity of the sand /fibres
I_D	Relative density
I_{D0} , I_{Dc}	Relative density after fabrication/consolidation
K_e	Constant to define the sliding function f_b
k_d	State parameter contribution in flow rule for Severn Trent model
k_r	Link between changes in state parameter and current strength in Severn Trent model
k_v	Constant for the evolution of the specific volume of fibres
LVDT	Linear Variable Differential Transformer
l_f	Length of fibre
l_1 l_2	Dimension of the parallelepiped used to determine the number of fibres intersecting a plane
l_1 l_2	Integration for the integral to derive terms of stiffness matrix for the fibres
M_c , M_e	Stress ratio at critical state in compression/extension
M_c^{ss} , M_e^{ss}	Stress ratio at steady state in compression/extension
MT	Moist tamping
MV	Moist vibration
$[M_m]$	Stiffness matrix for the sand matrix

$[M_f]$	Stiffness matrix for the fibres agglomerate
m	Unit normal vector of the plastic flow
$\mathbf{m}^*$	Unit normal vector of the plastic flow in the normalised stress space
N^H_{tot}	Number of fibres intersecting the finite area on a horizontal plane cut through a sample
N^V_{tot}	Number of fibres intersecting the finite area on a vertical plane cut through a sample
n	Unit normal vector to the yield surface
n	Constant to define the orientation distribution of the fibres
P	Ratio of the volume of the fibres having orientations within an angle $\pm\beta$ from the horizontal to the total volume of fibres
p	Total mean stress of the composite
p^*, p', p_f	Effective mean stress of the composite /sand matrix/fibres
p'_f	Effective mean stress at the end of the test
p_{crit}	Mean stress at critical state
p'_{cs}	Corresponding effective mean stress at critical state
p_c	Mean stress at the end of consolidation
p_{ref}	Reference pressure =0.1 MPa
Q	Material parameter for defining the maximum angle of dilatancy
q	Deviatoric stress of the composite
q^*, q', q_f	Effective deviatoric stress of the composite /sand matrix/fibres
$q_{10\%}, q_{20\%}$	Deviatoric stress at 10% / 20% axial strain
$q_{peak}, q_{failure}$	Deviatoric stress at peak/failure
R	Radius of the reference sphere
R	Ratio of size of yield and strength surfaces for Severn Trent model
R^2	Correlation coefficient
t_m	Thickness of the membrane
u	Pore water pressure
V	Volume of the specimen

V_0	Initial volume of the specimen
V_f	Volume of the fibres
V_{sphere}	Volume of the reference sphere
V^H_{tot}	Volume of fibres intersecting the finite area on a horizontal plane cut through a sample
V^V_{tot}	Volume of fibres intersecting the finite area on a vertical plane cut through a sample
V_{1f}	Volume of a fibre
V_v V_{vs}, V_{vf}	Volume of voids of the composite/sand/fibres
$\upsilon, \upsilon_m, \upsilon_f$	Specific volume of the composite/sand matrix/fibres
$\upsilon_{\Delta f}$	Constant for the evolution of the specific volume of fibres
w	Water content
w_f	Average weight concentration of fibres
W_f	Weight of fibres
W_s	Weight of dry sand
$\boldsymbol{\alpha}$	Direction of the yield or loading surface in Severn Trent model
α	Angle on the horizontal plane
α^*	Approximated limit introduced to solve the integral for the determination of the fibre orientation distribution (Eq.4.11)
β	Angle from the horizontal plane
Γ	Intercept for critical-state line on υ_m- $ln\, p'$ plane at p'=1 kPa
γ	Material parameter for defining the maximum angle of dilatancy
Δe_{corr}	Correction to the initial void ratio
$\Delta\sigma_{a,corr}$	Correction to the measured axial **stress** due to membrane stiffness
$\Delta\sigma_{r,corr}$	Correction to the measured axial stress due to membrane stiffness
$\Delta\tau$	Extra strength provided by the reinforcement
$(\Delta u)'$	Effective stress part of the excess pore pressure
ΔV_m	Parasitic volume due to membrane penetration
ε	Strain

ε_a , ε_r	Axial/Radial strain
ε_q , ε_v	Distortional/volumetric strain of the composite
ε_θ	Strain in a direction θ
ε_f	Strain of the fibres agglomerate
ε_m	Strain of the sand matrix
$\tilde{\varepsilon}_f$	Deformation of the fibre skeleton
θ	Angle from horizontal direction
θ_0	Direction of zero incremental strains
κ	Slope of the elastic loading –unloading line on the υ_m- ln p' plane
η_f	Aspect ratio of a fibre
λ	Slope of the critical-state line on υ_m- ln p' plane
μ_m , μ_f	Volumetric fraction of the sand matrix/fibres
ν	Poisson's ratio
ξ	State parameter
$\bar{\rho}$	Average volumetric concentration of fibres
$\hat{\rho}$	Volumetric concentration of the fibres intersecting a plane cutting the reinforced specimen
$\rho(\theta)$	Volume concentration of fibres as function of the angle θ
σ	Stress of the composite
σ'_{30}, σ'_3	Value of initial/final confining pressure used for the determination of the parasitic volume
σ_a , σ_r	Axial/Radial stress of the composite
$\sigma_{a,mes}$, $\sigma_{r,mes}$	Axial/Radial stress measured from triaxial experiments
σ_{af} σ_{rf}	Axial/Radial stress on a single fibre
$\sigma_{\theta f}$	Stress on a single fibres oriented in a direction θ

σ_{fa} σ_{fr}	Axial/Radial effective stress of the fibre agglomerate
σ'_a , σ'_r	Axial/Radial effective stress of the sand matrix
σ^*_a , σ^*_r	Axial/Radial effective stress of the sand matrix
σ_f^L	Sliding stress limit
τ_{UNR} , τ_R	Strength of an unreinforced/reinforced specimen
ϕ	Friction angle
$\phi_{10\%}$, $\phi_{20\%}$	Friction angle at 10%/20% axial strain
ϕ_{peak} , $\phi_{failure}$	Friction angle at peak/failure
ϕ_m *	Effective mobilised friction angle
ϕ_y'	Friction angle of yield surface of the sand in Severn Trent model
ψ	Dilatancy angle
ψ_{max}	Maximum angle of dilatancy
Overscript " $\cdot$ "	Indicates increments
Superscript " ^{e} "	Indicates elastic parameters
Superscript " ^{p} "	Indicates plastic parameters
Superscript " * "	Indicates effective parameters in the composite
Superscript " ' "	Indicates effective parameters in the sand
Subscript "$_f$"	Indicates parameters of the fibres
Subscript "$_m$"	Indicates parameters of the sand matrix
Bold symbols (e.g. "$\boldsymbol{\sigma}$")	Indicates vector or matrix quantities

CHAPTER 1
INTRODUCTION

1.1 Background

Reinforcing soils using tension resisting elements is an attractive means of improving the performance of soil in a cost effective manner. The use of random discrete flexible fibres mimics the behaviour of plant roots and gives the possibility of enhancing the strength and the stability of near surface soil layers. Practising engineers are employing this technique for the stabilisation of thin layers of soil, repairing failed slopes, soil strengthening around footings and earth retaining structures. However, more research is needed to further understand the potential benefits and limitations of this technique and to allow its application to more complex geotechnical structures.

The Geomechanics group of the Department of Civil Engineering at Bristol University has had an active interest in the experimental investigation of the behaviour of fibre reinforced sands and the present research is part of a more extensive project which aims to fully explore and understand the behaviour of this composite material. In particular, this study will try to complement the already performed experimental investigations and it will pursue the development of a theoretical model with the capability of predicting the mechanical response of this composite material.

1.2 Research Objectives

The two main goals of this project were to experimentally investigate the mechanical properties of fibre reinforced sands and to develop a constitutive model able to predict their mechanical response. Experimental tests have been performed using the conventional triaxial apparatus which allowed the specimens to be tested in both drained and undrained conditions and for both compressive and extensive loading. The objectives set for each of the goals are summarised below:

1) Experimental investigation:
   - Study the orientation of fibres in the prepared specimens and propose a procedure that enables the determination of the fibre orientation distribution;
   - Explore and eventually quantify the possibility of improving the strength and deformation characteristics of a sand with the addition of discrete flexible fibres;
   - Explore the possibility of improving the undrained response of a clean loose sand which normally appears susceptible to the phenomenon of static liquefaction;
   - Explore the main factors that influence the mechanical response of fibre reinforced sands and seek the relevant information for the development of a constitutive model.

2) Theoretical development:
   - Develop a new constitutive model able to predict mechanical response of fibre reinforced sands under triaxial loading conditions;
   - Challenge the proposed model to simulate the experimental results achieved in the above mentioned experimental investigation.

1.3 Outline of the Thesis

The thesis comprises eight chapters. Following this chapter, Chapter 2 presents a short review on the published findings from experimental and theoretical researches on fibre reinforced soils and from field scale applications of this technique.

Chapter 3 describes the equipment, the materials and the specimen preparation technique employed in the laboratory investigation. The conventional triaxial apparatus has been used for testing specimens of Hostun sand reinforced with three different types of polypropylene fibres. Specimens have been prepared with either the moist tamping or moist vibration technique.

Chapter 4 introduces a new procedure for the determination of the orientation distribution of fibres in reinforced specimens. The procedure is applied to specimens prepared with both moist

tamping and moist vibration techniques. Performance of the specimens prepared with the two different techniques are also compared with a series of conventional triaxial tests.

Chapter 5 reports and analyses the results of drained triaxial tests on both unreinforced and reinforced specimens. Tests have been performed in both compression and extension for a range of cell confining pressures, specimen densities and fibre contents.

Chapter 6 studies the undrained behaviour and the susceptibility to liquefaction of unreinforced and fibre reinforced specimens. Very loose specimens have been tested in both compression and extension for a range of cell confining pressures and fibre contents.

Chapter 7 proposes a new constitutive model for predicting the behaviour of fibre reinforced specimens. The proposed modelling framework is first applied by assuming a simple linear elastic-perfectly plastic model for the sand matrix, then it is refined by adopting a more complex bounding surface and kinematic hardening model (Severn-Trent sand model) for the sand.

Chapter 8 draws conclusions from the performed experimental investigation and the proposed theoretical development, summarising the main findings and limitations of this study, and making suggestions for further research.

1.4 Notation

The notation adopted in this research mainly uses the conventional stress and strain variables for axisymmetric triaxial conditions which are schematically shown in Figure 1.1. Any stress state acting on the fibre reinforced specimen is expressed in terms of total mean (or isotropic) (p) and deviatoric (q) stresses while the strain variables of this composite material are the volumetric strain (ε_v) and distortional strain (ε_q). These stress and strain quantities are related to the axial and radial stresses and strains according to:

$$p = \frac{\sigma_a + 2\sigma_r}{3} \qquad q = \sigma_a - \sigma_r \tag{1.1}$$

$$\varepsilon_v = \varepsilon_a + 2\varepsilon_r \qquad \varepsilon_q = \frac{2}{3}(\varepsilon_a - \varepsilon_r) \tag{1.2}$$

where subscripts $_a$ and $_r$ denote the axial and radial components respectively. The pairs of stresses and strains are abbreviated in vector form $\boldsymbol{\sigma} = [p, q]^T$ and $\boldsymbol{\varepsilon} = [\varepsilon_v, \varepsilon_q]^T$.

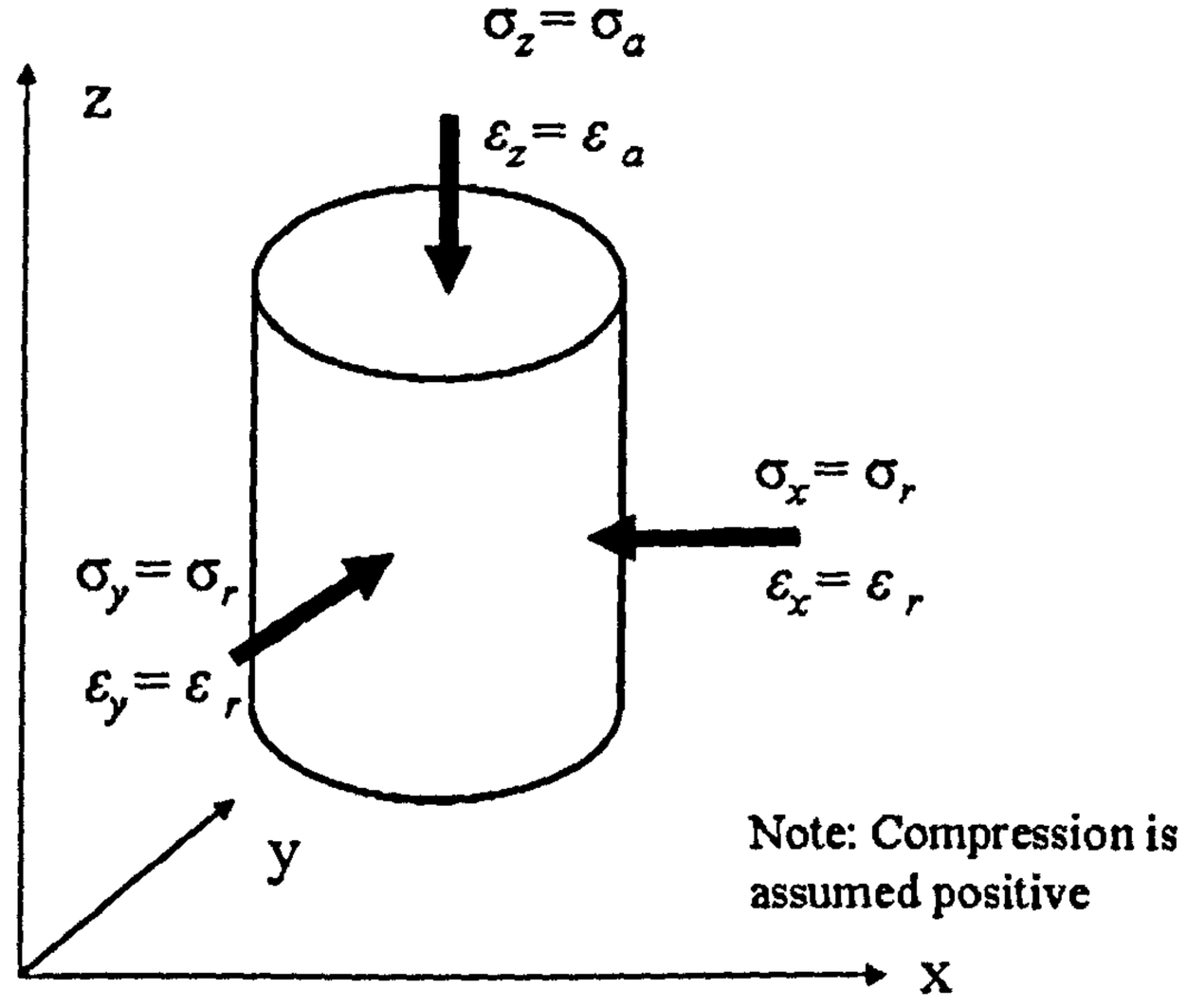

Fig. 1.1 Axysimmetric triaxial conditions

Compression is assumed positive and rate affects are ignored. Volumetric strain is linked to specific volume (v) according to:

$$\dot{\varepsilon}_v = -\frac{\dot{v}}{v} \tag{1.3}$$

where $v = 1 + e$ and e is the voids ratio defined as the ratio between the volume of voids (V_v) and the volume of solids (V_s) in the material:

$$e = \frac{V_v}{V_s} \tag{1.4}.$$

In an elastic-plastic framework, the elastic and plastic strain increments sum to give total strain increments in the normal way:

$$\begin{bmatrix} \dot{\varepsilon}_v \\ \dot{\varepsilon}_q \end{bmatrix} = \begin{bmatrix} \dot{\varepsilon}_v^e \\ \dot{\varepsilon}_q^e \end{bmatrix} + \begin{bmatrix} \dot{\varepsilon}_v^p \\ \dot{\varepsilon}_q^p \end{bmatrix} \tag{1.5}$$

where the superscripts ^{e} and ^{p} denote the elastic and plastic components respectively.

The effective mean and deviatoric stresses of the composite are respectively denoted by the variables $p*$ and $q*$ and abbreviated in vector form as $\boldsymbol{\sigma}^* = [p^*, q^*]^T$. Total and effective stresses are linked by the usual relationship:

$$p = p^* + u \qquad q = q^* \tag{1.6}$$

where u is the pressure of the water filling the pores between soil particles.

The investigation and the analysis performed in the following of this research require the definition of stress and strain components of both the constituents of the composite material. The effective stress state of the soil matrix will be denoted with dash $\left(\boldsymbol{\sigma}' = [p', q']^T\right)$ while its strain state with the subscript '$_m$' $\left(\boldsymbol{\varepsilon}_m = [\varepsilon_{mv}, \varepsilon_{mq}]^T\right)$ to be easily differentiated from the strain state of the composite. The effective stress and strain states of the fibres will be denoted with the subscript '$_f$' $\left(\boldsymbol{\sigma}_f = [p_f, q_f]^T, \boldsymbol{\varepsilon}_f = [\varepsilon_{fv}, \varepsilon_{fq}]^T\right)$. The relationship defined in Eqs (1.1), (1.2) and (1.3) are considered valid for both the constituents. Therefore, stress and strain quantities of the soil matrix are related to the axial and radial stresses and strains according to:

$$p' = \frac{\sigma'_a + 2\sigma'_r}{3} \qquad q' = \sigma'_a - \sigma'_r \tag{1.7}$$

$$\varepsilon_{mv} = \varepsilon_{ma} + 2\varepsilon_{mr} \qquad \varepsilon_{mq} = \frac{2}{3}(\varepsilon_{ma} - \varepsilon_{mr}) \tag{1.8}$$

and the relationships for the fibre agglomerate can be defined as:

$$p_f = \frac{\sigma_{fa} + 2\sigma_{fr}}{3} \qquad q_f = \sigma_{fa} - \sigma_{fr} \tag{1.9}$$

$$\varepsilon_{fv} = \varepsilon_{fa} + 2\varepsilon_{fr} \qquad \varepsilon_{fq} = \frac{2}{3}(\varepsilon_{fa} - \varepsilon_{fr}) \tag{1.10}.$$

CHAPTER 2

LITERATURE REVIEW

2.1 Introduction

The basics and principles of improving the mechanical characteristics of soil with the addition of some inclusions are largely demonstrated in nature by the activity of animals and by the action of plant roots. Nonetheless, humans understood the possibility of strengthening soil by mixing with other materials in ancient times: the Ziggurat at Aqar Quf which was built 3000 years ago and the Great Wall of China which was partially completed around 200 BC are reinforced soil structures that still stands today. Through the years, the practice of reinforcing soil has obviously been enhanced, has employed many different types of inclusions and has been applied to a wider and wider range of applications. However, only recently, experimental techniques and analytical studies have been employed to fully understand the mechanics and the real benefits of strengthening the soil by adding inclusions.

Of the many kinds of reinforcement, the use of short fibres is now becoming a promising and attractive means of improving the performance of soil in a cost effective manner. The use of random discrete flexible fibres mimics the behaviour of plant roots and provides the possibility of improving the strength and the stability of near surface soil layers. Practising engineers are employing this technique for the stabilisation of thin layers of soil, repairing failed slopes, soil strengthening around footings, earth retaining structures, sports pitches, horse racing tracks, lightly trafficked pavements and car parking areas. However, more research is needed to further understand the potential benefits and limitations of this technique and to allow its application to more complex geotechnical structures including stronger and liquefaction resistant earthfills, foundations for buildings, dams, heavily trafficked pavements and large scale slope stabilisation where a construction process involving mixing of random fibres with soil appears more attractive than current procedures.

2.2 Laboratory investigations

Recent experimental research has focussed on evaluating the improvements on the soil behaviour caused by the addition of fibres. The majority of the work has concentrated on fibre reinforced granular materials but some investigation on reinforced clays can also be found in the literature (Maher and Ho, 1994; Kumar and Tabor, 2003; Tang et al., 2006 among others). Results are encouraging and the benefits of fibre addition are remarkable for any type of soil. It is clear that the effectiveness of fibres as reinforcement for granular materials depends on several parameters linked to fibre properties including type, content, length, aspect ratio, modulus of elasticity, orientation and also soil characteristics including particle size, shape and gradation, as well as loading mode, stress level and density.

2.2.1 Sample preparation

Fundamental laboratory studies of soil behaviour require testing of homogeneous and reproducible specimens. For fibre reinforced sands the so called moist tamping technique (Ladd, 1978) reproduces a soil fabric that resembles that of compacted soil by dynamic plates (Michałowski, 2008) and it has been generally adopted for preparing laboratory specimens. Michałowski and Zhao (1996) proposed a different technique for controlling the orientation of fibres in the specimen: a specially designed tool grid is employed for reorienting the fibres in the specimen before densification through vibration. However, the procedure may not be applicable to fibres with a tendency to segregate or agglomerate.

Modified Proctor compaction tests on unreinforced and reinforced sand specimens showed (Fig. 2.1) that for a given compaction effort the maximum dry density decreases with increasing fibre content whereas the optimum moisture content was found to be independent of fibre concentration (Ibraim and Fourmont, 2006). This means that for a given amount of sand and relative density there is a maximum amount of fibres beyond which sand reinforced specimens cannot be prepared (Fig.2.2).

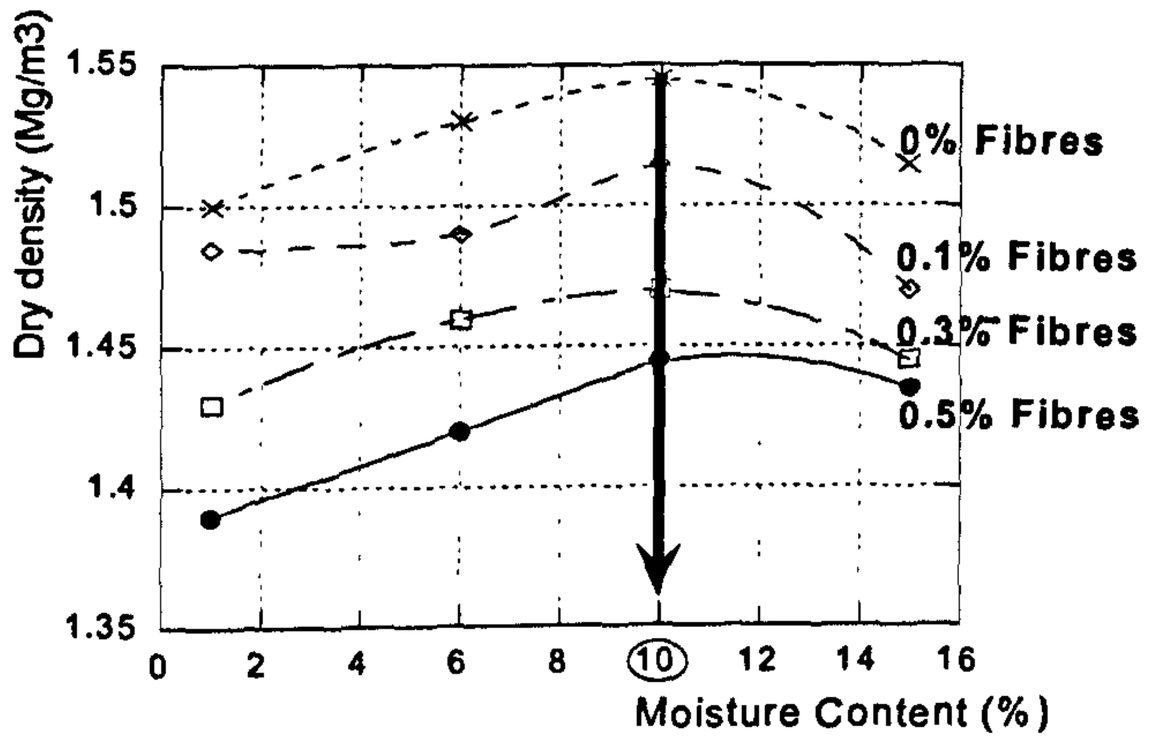

Fig. 2.1 Modified Proctor compaction tests on specimens reinforced with Loksand™ fibres (after Ibraim and Fourmont, 2006)

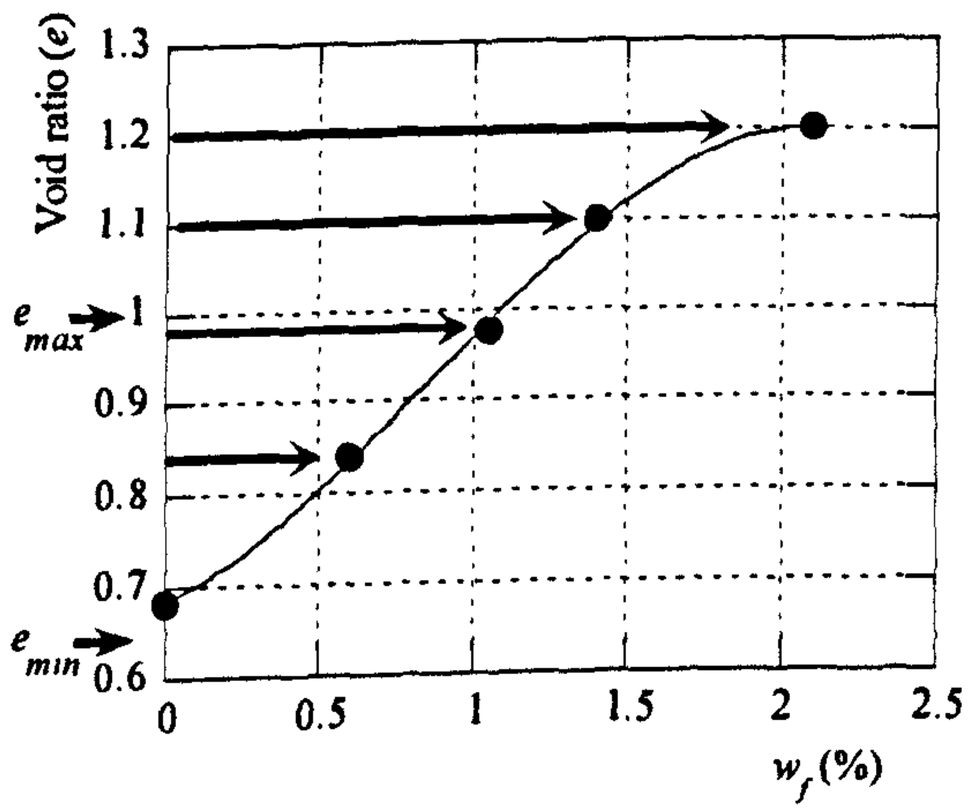

Fig. 2.2 Maximum amount of fibres that can be mixed with a fixed amount of sand without leading to a change in specimen volume using moist tamping (after Ibraim and Fourmont, 2006)

2.2.2 Test types

Direct shear tests

The direct shear has been one of the first apparatus employed for investigating the effectiveness of inclusions in improving the mechanical behaviour of sands (e.g. McGown et al. 1978, Gray and Ohashi, 1983) but it has also been used in recent research (Yetimoglu and Salbas 2003). Results mainly highlight the effectiveness of fibres in increasing the peak strength of soils, in reducing the post peak strength-loss and in increasing the strain at failure.

Ring shear tests

The performance of fibre reinforced sands at very large strains has been studied with the ring shear apparatus (Heineck et al., 2005; Consoli et al., 2007a). Addition of fibres results in an increase in the strength which is not reduced even at very large displacements.

Bender elements

Following an investigation with the bender element technique, Heineck et al. (2005) suggests that the initial stiffness of the composite soil is not influenced by the presence of fibres.

Conventional triaxial tests

The conventional triaxial apparatus has, to date, been so far the most employed for studying the behaviour of reinforced sands (e.g. Gray and Al Refeai, 1986; Al Refeai 1991; Maher and Ho, 1993; Ranjan et al., 1996; Michalowski and Zhao, 1996; Li and Ding, 2002; Michalowski and Čermák, 2003; Heineck et al., 2005; Consoli et al., 2007a; Consoli et al., 2007b). Major attention has been addressed towards the behaviour of reinforced sands during monotonic compressive loading in drained conditions and only a few investigations have studied the performance under cyclic and/or undrained loading.

- *Drained tests*

Results from compression tests confirm the findings of the investigation carried out with the direct shear apparatus: addition of fibres results in an increase in the peak strength and a reduction in the post-peak strength loss. Limited to triaxial compression loading, the failure strength envelope for reinforced sands was found to be independent from the stress path direction (Consoli et al., 2007b). However, the effectiveness of fibres was found to be linked to many factors which will be discussed in the following of this chapter.

The conventional triaxial apparatus permits the accurate determination of the deformation behaviour during loading and some authors concluded that the presence of fibres inhibits the dilative behaviour of soil (Michałowski and Zhao, 1996; Michałowski and Čermák, 2003); the dilation is referred here as the increase in volume during shearing which is typical of dense or overconsolidated soils. Contrarily, recent results published from this research (Diambra et al., 2009) showed that a more dilative behaviour was induced by the addition of fibres. This discrepancy probably depends on the different approaches that researchers have used when comparing unreinforced and reinforced specimen. The former has chosen to compare specimens with the same amount of solid considered as sand plus fibres while the latter have compared specimens where the fibres have been added to a constant amount of sand. It follows that a definitive conclusion of the influence of fibres on the volumetric behaviour of reinforced specimens can not be drawn.

When subjected to isotropic compression loading, the addition of fibres decreased the compressibility of the specimen and two distinct but parallel normal compression lines were observed for the reinforced and unreinforced specimens (Consoli et al., 2005). After testing, analysis of exhumed fibres revealed that some fibres have acted in tension even if the specimens were subjected only to compressive strains.

One of the major limitations of the conventional triaxial apparatus is the impossibility of investigating the effect of a continuous principal stress rotation, however the apparatus permits to apply a jump rotation of 90 degree on the principal stress rotation and to study the behaviour

of soils for extensive loading (see Section 3.2). Anyway, investigation of the behaviour of reinforced soils in extensive loading conditions has not yet been presented in the literature.

- *Undrained tests*

To the author's knowledge, no study is reported either on the undrained monotonic behaviour of fibre reinforced sands or on the effect of fibres on the static liquefaction response of sands. However, recent research (Ozkul and Baykal, 2007) has demonstrated the positive influence of rubber fibre addition for preventing the static liquefaction of a clayey soil and these findings encourage the investigation of the monotonic undrained behaviour of reinforced sands.

More attention has been addressed towards the cyclic undrained behaviour of reinforced sands. When subjected to undrained cyclic compression loading, reinforced specimens show an increased resistance if compared with unreinforced specimens (Maher and Ho, 1993). The number of cycles and the magnitude of strains required to reach failure is increased significantly as a result of fibre inclusion. In the case of undrained cyclic loading at small strains, fibre reinforced sands show a higher linear elastic modulus than unreinforced sands but the modulus deteriorates with loading repetition (Li and Ding, 2002).

2.2.3 Influence of test conditions

Confining stress

Typically, over a wide range of stresses, sand reinforced with randomly distributed discrete fibres exhibits either curved-linear (for uniform, rounded sand) or bilinear (for well-graded or angular sands) failure envelopes (Gray and Ohashi, 1983; Maher and Gray, 1990; Ranjan et al., 1994; Michalowski and Zhao, 1996; Michalowski and Čermák, 2003) (Fig 2.3). A marked change in the slope for the failure envelope is recorded in correspondence to a threshold confining stress, referred to as a critical confining stress σ_{crit}. Above σ_{crit} the failure envelopes for the reinforced sand become parallel to the unreinforced sand envelope and the failure mechanism is due to plastic stretching or breakage of fibres. Below σ_{crit} it is considered that the reinforcing mechanism is not fully mobilised during shearing and the fibres tend to slip or pull out.

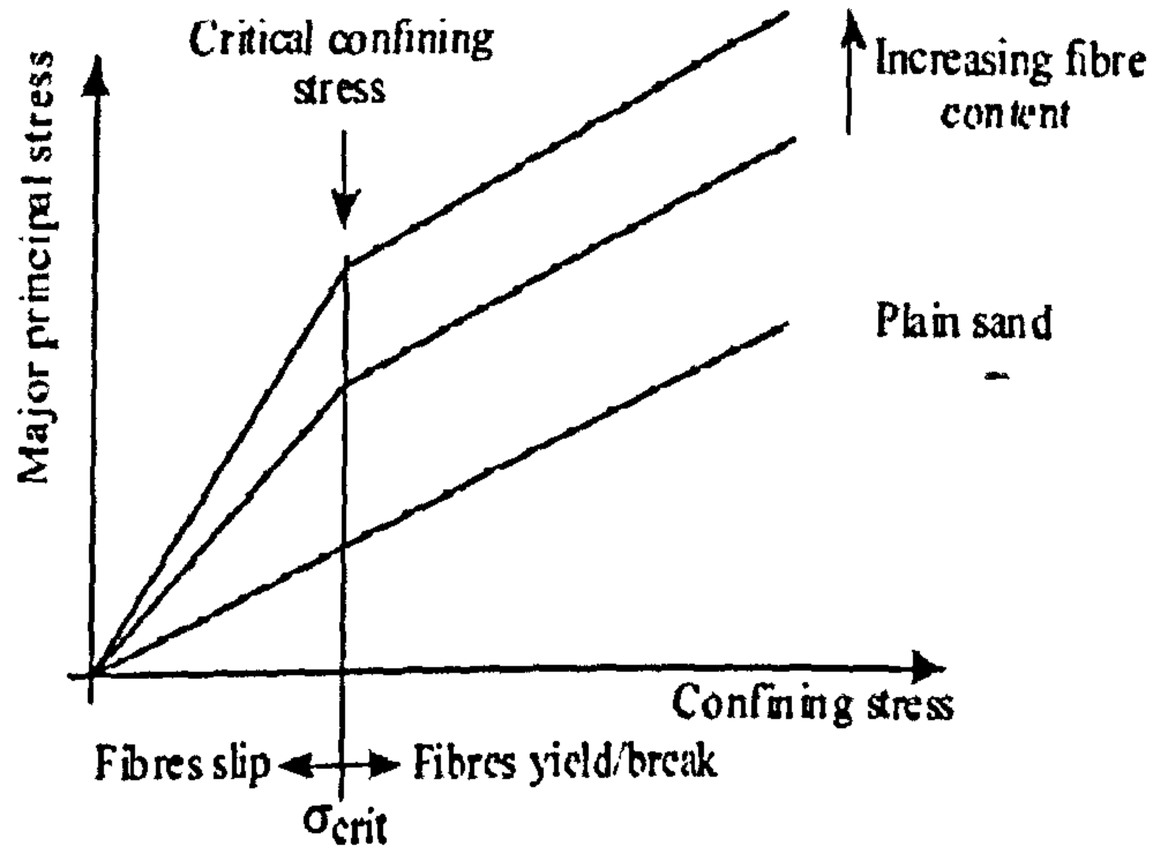

Fig. 2.3 Typical failure envelope for fibre reinforced sands

Specimen density

As for unreinforced sand specimens, reinforced ones show that the peak failure envelope is dependent on the density of the specimen. However, the average strength increase at failure due to fibres is not affected by the density of the sample (Gray and Ohashi, 1983).

2.2.4 Influence of fibres characteristics

Fibre type

Investigation of the benefits of fibre inclusion on the mechanical behaviour of sands has been performed employing both synthetic and natural types of fibres. Glass, steel, rubber, polyamide and polypropylene fibres can be mentioned among the synthetic fibres while sisal, reed, coconut and palm fibres are commonly used natural types. The effectiveness of each fibre depends on many factors that will be described in the following section.

Fibre length

The strength improvement at failure is linked with the fibre length: the longer the fibres the larger the strength increase (Al Refeai, 1991; Consoli et al., 2007a). When fibres are stretched, the mobilized tensile stress in the fibres is zero at their ends and increases towards the fibre centre. Longer fibres may accumulate enough strains to allow the tensile strength of the fibres to be reached while shorter fibres would simply slide through the sand particles before the fibre strength is reached. Indeed the portion of the fibres where the tensile strength is fully mobilised increases with the length of the fibres itself. However, there seems to be a limit to the length of fibres beyond which any further increase in length has no effect on the shear strength (Al Refeai, 1991). The length of the fibres should be at least one order of magnitude greater than the size of the grains for achieving an effective fibre-sand interaction (Michalowski and Čermák, 2003).

Fibre content

The peak and failure strengths for reinforced specimens increase with the fibre content which seems to be the main factor governing the contribution of the fibres. Nonetheless, above some limiting fibre content, the strength increase seems to reach an asymptotic upper limit (Gray and Al Refeai, 1986; Maher and Gray, 1990; Ranjan et al., 1996).

Elastic modulus

Gray and Ohashi (1983) found that the strength of reinforced sands was enhanced by the employment of stiffer fibres.

Aspect ratio

For a given fibre content, the effectiveness of the fibres increases with the fibre aspect ratio ($\sqcup_f$) (Gray and Al Refeai, 1986; Ranjan et al.1996; Michalowski and Čermák, 2003) which is defined as the ratio between fibre length (l_f) and diameter (d_f):

$$\eta_f = \frac{l_f}{d_f} \tag{2.1}$$

Gray and Al Refeai (1986) found that the increase in strength varies linearly with the aspect ratio. The slope of this envelope increases with the fibre content. Maher and Gray (1990) and Ranjan et al. (1996) found that the critical confining stress σ_{crit} decreases if the aspect ratio increases.

Fibre orientation

It is not surprising that fibre orientation was found to be particularly important for the strength of reinforced soils (Jewell and Wroth, 1987; Palmeira and Milligan, 1989; Michalowski and Čermák, 2002) and fibres were most influential when orientated in the same direction as tensile strains. However, in all the investigations the orientation of the fibres has been imposed during sample fabrication and no study has been undertaken to define the fibre orientation imposed by the specimen fabrication procedure. An investigation performed in this research (Diambra et al., 2007; Diambra et al., 2008) demonstrated that the most common procedure for preparing reinforced specimens, moist tamping, leads to a preferred sub-horizontal orientation of fibres.

2.2.5 Influence of soil characteristics

Uniformity

Maher and Gray (1990) found that the gradation of the soil may affect the shape of the strength envelope. Reinforced specimens prepared with a uniform sand exhibit a curved linear strength envelope while those prepared with well graded sand showed a bilinear strength envelope. Also, a better gradation intended as an increase in the coefficient of uniformity (C_u) resulted in a higher contribution to strength and in a lower critical confining stress (σ_{crit}).

Angularity

The shape of the strength envelope seems governed by the angularity of the sand particles with rounded sands exhibiting curved linear strength envelopes and angular sands exhibiting quite

sharp bilinear envelopes. The increase of particle sphericity seems to result in a lower critical confining stress σ_{crit} (Maher and Gray, 1990).

Particle size

At the same confining stress, the strength increase induced by the addition of fibres seems enhanced by reducing the average grain size D_{50} (Gray and Al-Refeai, 1986; Maher and Gray, 1990; Ranjan et al., 1996). Smaller grains provide greater contact area and probably more frictional resistance between sand and fibres.

2.2.6 Discussion

The interaction mechanism between fibres and sand grains is affected by several factors which have been extensively studied by using the direct shear or conventional triaxial apparatus. Among all the factors, the orientation of fibres was found to be particularly important but no investigation on the real orientation of fibres imposed by the specimen fabrication method has yet been published. An accurate method to determine the orientation of fibres in fibre reinforced specimens will be developed in the following research.

The limited loading conditions that can be imposed in the direct shear and conventional triaxial apparatus are well known and more complex apparatus such as the true triaxial apparatus or the hollow cylinder apparatus may be used to investigate the effect of principal stress directions and their rotation on the performance of reinforced sands. However, the capabilities of the conventional triaxial apparatus have not been fully exploited: the benefits of fibre addition in extensive loading or their effect on the static liquefaction response of sands have not yet been investigated. The experimental section of this research will attempt to fill this gap.

2.3 Modelling the behaviour of fibre reinforced soils

2.3.1 Models for predicting the shear strength

Several models have been proposed to explain the behaviour of discrete randomly distributed fibres throughout a soil mass but most of them are limited to the prediction of the shear strength increase and failure conditions.

Waldron (1977), Gray and Ohashi (1983) and Gray and Al-Refeai (1986) described a simple force equilibrium model for predicting the strength of soils reinforced with oriented fibres. Fibres crossing a discrete shear zone of the specimen develop tensile forces that provide additional normal stresses on the shear zone and additional shear resistance according to their orientation (Fig. 2.4). The model was further developed by Maher and Gray (1990) to account for randomly oriented fibres. However, the characterisation of the shear band thickness remains difficult to quantify (Shewbridge and Sitar, 1990).

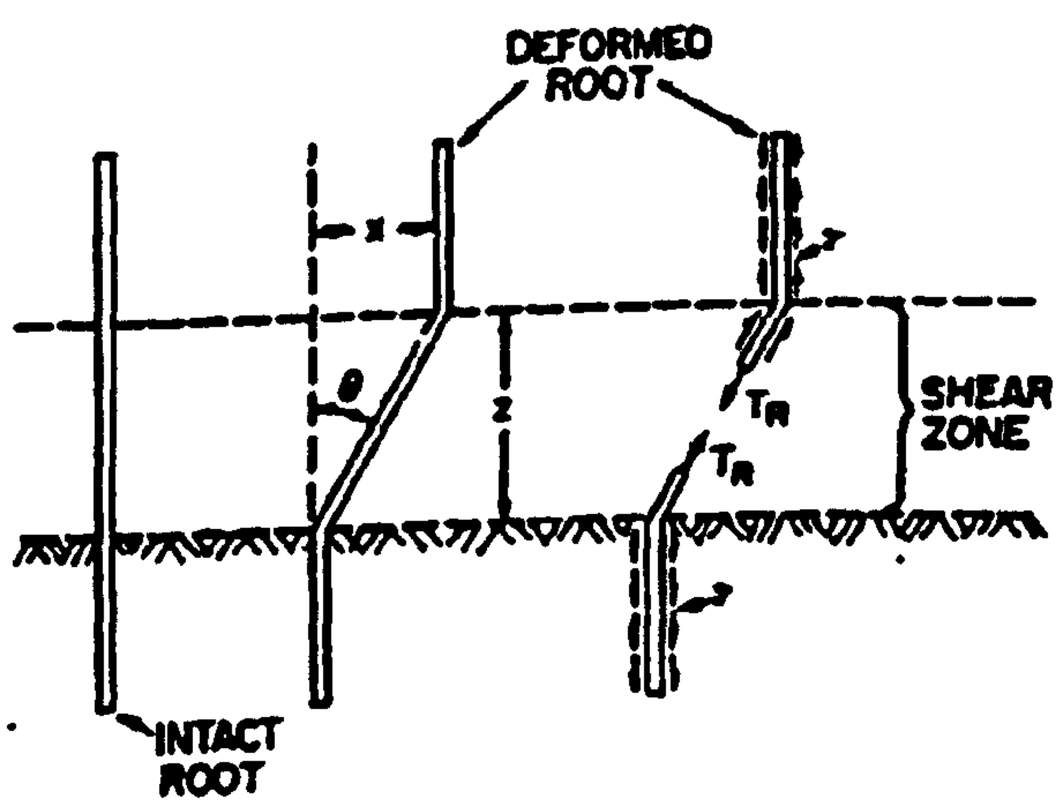

Fig. 2.4 Basic model for predicting the stresses mobilized in the fibres (after Gray and Ohashi, 1983)

Based on an energy-based homogenization technique Michałowski and Zhao (1996) proposed an analytical description of the macroscopic stress state at failure (peak strength) for sand reinforced with randomly oriented flexible discrete fibres. During plastic deformation, the rate

of the energy dissipation by external load must be equated by the rate of the energy dissipated in the composite. The model has been applied by Michalowski (1997) for predicting the strength of granular materials reinforced with continuous filaments. Michalowski and Čermák (2002) introduced an anisotropic orientation distribution of fibres which was also supposed to evolve according to the deformation process of the specimen. The evolution of fibre orientation induces a kinematic hardening effect at large strain and the composite becomes stronger in the direction of the stress path (Fig.2.5). The model has been recently applied to the limit analysis of retaining wall and bearing capacity of footing: the addition of fibres reduces the load on the retaining wall and increases the bearing capacity of the footing (Michalowski, 2008). In both cases the contribution of fibres was enhanced by the anisotropic distribution of their orientation.

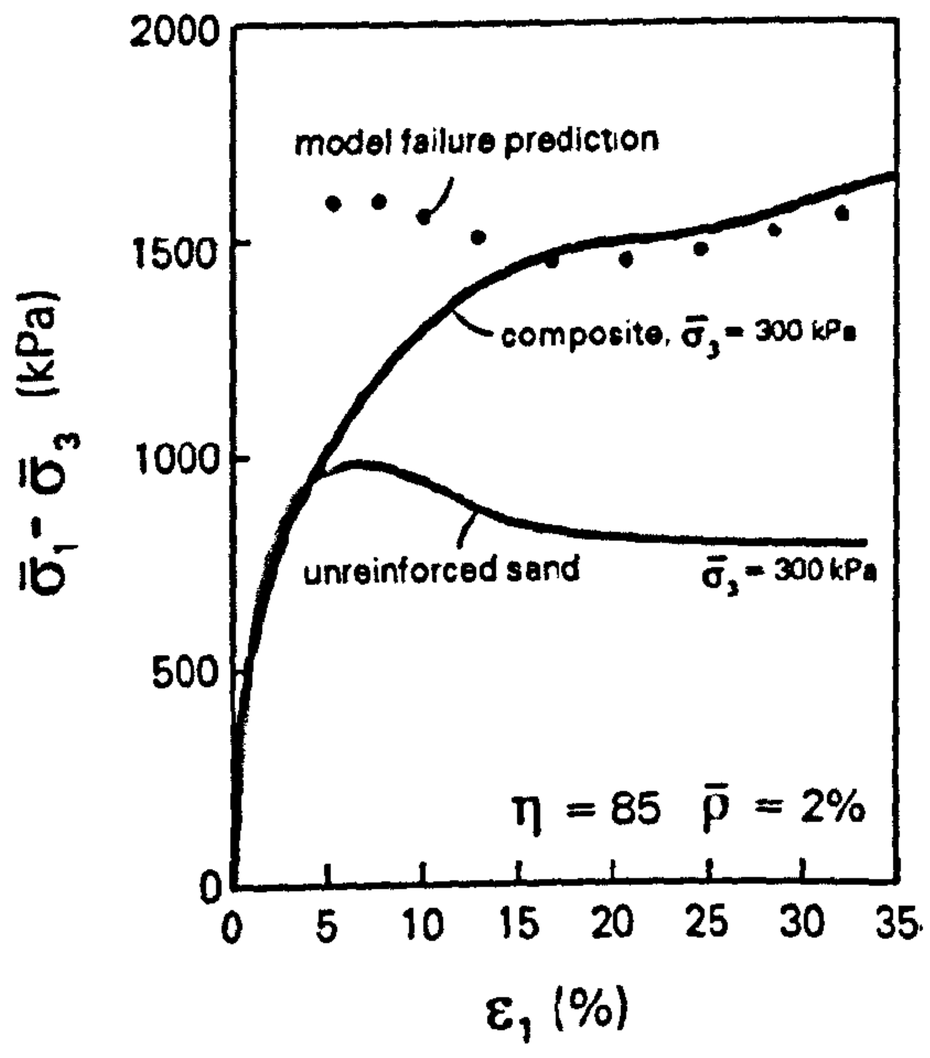

Fig. 2.5 Experimental results and model prediction of the model proposed by Michalowski and Čermák, (2002)

Recently Zornberg (2002) proposed a framework to predict the failure of different reinforced soil types based on the superposition of the sand and fibre effects. A limit equilibrium analysis is performed to characterise the equivalent shear strength of the composite material according

to the respective properties of its components (sand and fibres). Therefore this approach requires independent testing of soil specimens and fibres, rather than shear strength tests on fibre-reinforced specimens. The typical bilinear failure envelope for fibre reinforced soils is obtained (Fig.2.6).

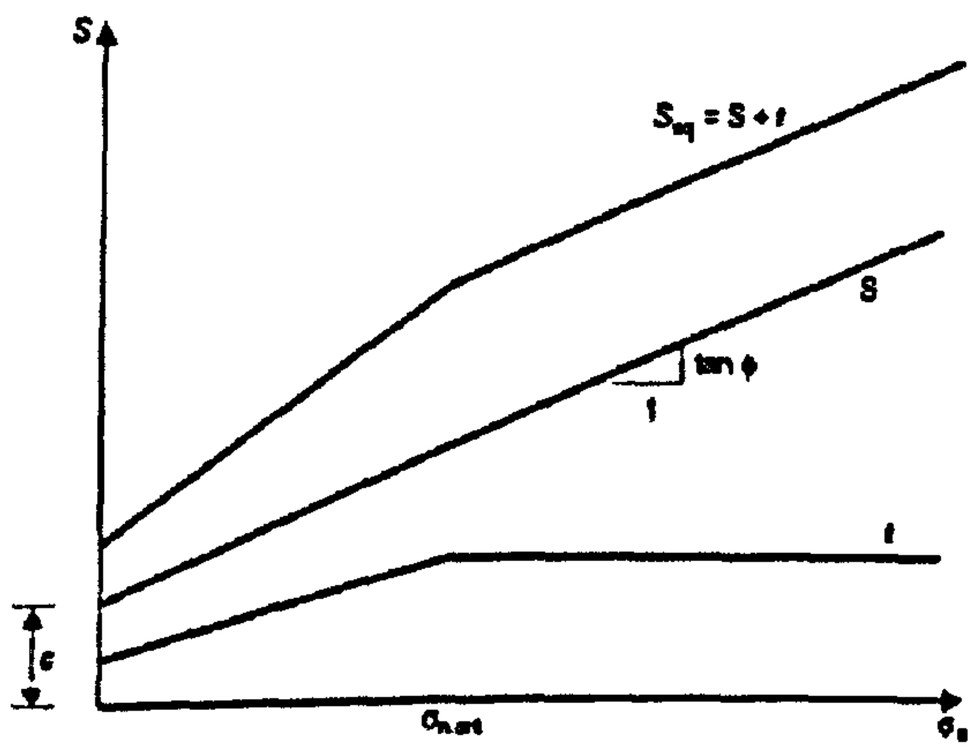

Fig. 2.6 Representation of the equivalent shear strength (S_{eq}) as the superposition of the soil contribution (S) and the fibres contribution (t) (after Zornberg, 2002)

2.3.2 Constitutive models for fibre-reinforced soils

A general constitutive law for reinforced soils has been proposed by few authors. A model based on a volumetric homogenization technique was proposed by Ding & Hargrove (2006). The model aims to describe the nonlinear elastic behaviour under monotonic loading before soil/fibres slip or fibre yielding occurs. Fibres are assumed to be randomly oriented throughout the soil matrix. The nonlinear elastic behaviour under cyclic loading has been captured by a hyperbolic shear stress-strain function proposed by Li and Ding (2002). The magnitude of the elastic modulus degrades from an initial value towards an ultimate value as function of the shear strains. The influence of fibre content, confining stresses and number of loading cycles is accounted for in the model. However, the model is limited to the prediction of the mechanical behaviour at small strains.

A full constitutive law for soils reinforced with continuous thread was proposed by Villard et al. (1990) and di Prisco and Nova (1993) employing the superposition of sand and thread effects. The reinforced soil is seen as a composite material whose stress state is derived by the superposition of the stress states of its constituents according to their volumetric fractions. The compounds are supposed to act in parallel and eventual sliding between components only occurs at failure. Di Prisco and Nova (1993) modelled both the sand matrix and the thread with a linear elastic - perfectly plastic model. The deviatoric stress-strain response for conventional compression triaxial tests is reasonably reproduced but the model does not correctly capture the post peak and volumetric behaviour. The model by Villard et al. (1990) adopts more complex models for the constituents of the composite and it also recognises the importance of the orientation of the thread as a parameter governing its effectiveness. Even if the thread is supposed to be uniformly oriented in an angular domain, it is demonstrated that the account of its orientation distribution is fundamental for the correct estimation of the strength of the reinforced material.

Numerical analyses with finite difference code have been performed by Sivakumar Babu et al. (2008) for simulating the behaviour of coir fibre reinforced sand under triaxial compression loading. An elastic - perfectly plastic model was used for describing the behaviour of the sand matrix while the fibres have been modelled as straight cable elements elastically behaving. The presence of randomly distributed fibres prevents the formation of localised shear bands and contributes to higher strength, stiffness and reduced deformation of the specimens.

2.3.3 Micromechanical approaches

Recently, the behaviour of fibre reinforced sands have been studied with a micromechanical approach in order to identify how the presence of fibres affects the kinematic and the stresses of the granular matrix. A two dimensional DEM (Distinct Element Method) has been developed for the micromechanical analysis of mixtures of granular materials and flexible fibres (Ibraim et al., 2006; Ibraim and Maeda, 2007). The contact forces between grains and fibres are calculated at small steps according to the restraints given to the contact elements. The results of the simulations show that the highest tensile stresses in the fibres are mobilized on fibre oriented

towards the tensile strains direction but local micro fabric or structural rearrangements with the deformation process may influence the tension state of the fibres.

2.3.4 Discussion

The prediction of the contribution of fibre to the shear strength increase has been extensively investigated in literature and many sophisticated models have been proposed by different authors. However the correct estimation of the behaviour of fibre reinforced structures with numerical programs is based on rigorous constitutive models which have not been largely developed in the literature. Few authors have proposed constitutive models for fibre reinforced sand and their application is still limited to the elastic behaviour or to triaxial compressive loading conditions. Therefore, a new modeling approach will be proposed here with the aim to expand the range of application and capability of existing models for fibre reinforced sands. The proposed model will be challenged in extensive triaxial loading and particular attention will be addressed to considering the influence of fibre orientation in respect of the loading conditions. Since rotations of principal axes almost always occur within a soil mass, the account of the fibre orientation distribution is considered to be fundamental for a correct prediction of the reinforced soil behaviour.

2.4 Field tests and applications of fibre reinforced soils

The results of the extensive laboratory tests proved the effectiveness of fibres in enhancing the mechanical characteristics of soils but scale and field tests are necessary and essential to verify the applicability of the proposed technique to real geotechnical structures. Some recent studies have investigated the behaviour of reinforced sands in different applications obtaining optimistic and promising conclusions:

- Plate load tests on a thick homogeneous layer of compacted sandy soil reinforced with polypropylene fibres showed improved results compared with an unreinforced soil (Consoli et al., 2003). When the top soil layer was reinforced with cement and fibres, increased bearing capacity was observed followed by very ductile post-failure behaviour with a completely different failure mechanism by formation of thick shear bands around

the border of the plate (Consoli et al., 1998). The enhanced bearing capacity of a fibre-reinforced sand fill overlying a soft clay stratum has been investigated by Yetimoglu et al. (2005) with a CBR test. Not only the peak load but also the initial stiffness was found to be increased by the reinforcement. Gray and Al-Refeai (1986) suggested that the use of internal reinforcement (with randomly distributed fibres) for granular piles to stabilise a weak clay soil should substantially increase the bearing capacity of strip footings on the soil.

- The mixing of soil with randomly oriented discrete fibres as a viable alternative for the stabilisation of the subgrade materials for temporary low-volume roads (Tingle et al., 2002), as well as for aircraft pavements and more general road design (Santoni and Webster, 2001), have been assessed with jointed results of a laboratory campaign and full-scale field tests. The densification of the material under repeated loading may limit its applicability and surfacing of the material was found to be necessary to prevent the fibre pull out mechanism. The importance of the field tests was also recognised on defining guidance criterion for the construction and maintenance of the structure.

- The use of random discrete flexible fibres mimics the behaviour of plant roots and in the stabilisation of near surface soil layers provides clear advantages over the use of traditional planar inclusions (Zornberg, 2002). The use of fibre reinforced soil for building evapotranspirative soil layer for steep landfill slopes (Zornberg et al., 2003) results in an increased surface stability, an enhanced resistance against erosion and desiccation cracking and also a greater ability to sustain vegetation. For repairing localised failed slopes, the use of discrete fibres provides advantages over continuous planar inclusions for its easy adaptability to variable site geometry and difficult site access conditions (Gregory and Chill, 1998).

2.5 Conclusions

Reinforcing soils using tension resisting elements is an attractive means of improving the performance of soil in a cost effective manner. The use of random discrete flexible fibres

mimics the behaviour of plant roots and gives the possibility of improving the strength and the stability of near surface soil layers. Practising engineers are employing this technique in a restrained range of geotechnical applications and more research is needed to further understand the potential benefits and limitations of this technique.

The advantages of using discrete flexible fibres have been proven by laboratory and field tests. Fibres are found to be effective in increasing the shear strength, the post peak reduction and the ductility of the material. The effectiveness of fibres is dependent on many factors and it is not surprising that fibre orientation is one of the governing factors. It follows that the exploration of the orientation distribution of fibres in the tested specimens is fundamental in understanding the behaviour of reinforced sands. Published laboratory investigations have concentrated on direct shear or triaxial compression tests and they have not yet investigated the effect of rotation of principal axis or at least the effect of fibres in extension triaxial tests. Also, the behaviour of fibre reinforced sands in undrained condition has not yet been fully investigated.

Most modelling approaches that have been proposed so far have concentrated on the prediction of the contribution of fibres to shear strength increase while fewer authors have tried to propose a general constitutive law for reinforced soils. The proposed constitutive models are limited to conventional compression triaxial loading and they have been developed for soil reinforced with continuous thread only. The development of a full constitutive model for sand reinforced with discrete flexible fibres is fundamental to the accurate prediction of the behaviour of a fibre reinforced sand geotechnical structure with the use of a numerical programme. Since rotations of principal axes almost always occur within a soil mass, the account of the fibre orientation distribution is fundamental for the correct estimation of soil design strength for certain loadings.

This research attempts to complement the findings of published research with new experimental tests on fibre reinforced sands and it aims to increase the range of applicability and the capabilities of the existing constitutive models.

CHAPTER 3

EXPERIMENTAL APPARATUS, MATERIALS AND SAMPLE PREPARATION

3.1 Introduction

The investigation of the parameters governing the behaviour of soils requires the acquisition of reliable information from good quality experimental tests. The knowledge of the capabilities and limitations of the apparatus used is fundamental to assess the accuracy and reliability of the experimental results. The conventional triaxial apparatus used in this study will be described in the following chapter together with information on the materials and methods for preparing the tested specimens.

3.2 The conventional triaxial apparatus

3.2.1 General

The conventional triaxial test is at present the most widespread among the test methods which can be used for soil testing. It allows the investigation of soil's properties under different boundary conditions with the limitation that the imposed horizontal stresses are equal. The main advantages of this apparatus among the others have been presented by Baldi et al. (1988) and listed below:

- relative simplicity of drainage control and measurement of pore pressure;
- ability to apply stresses in known directions;
- easy measurement of axial and volumetric strains;
- use of solid cylindrical specimens which can be conveniently obtained from standard tube samples;

- versatility of the equipment which may be used for a variety of determination besides triaxial strength and stiffness (e.g. consolidation and permeability parameters).

The loading conditions applicable in the triaxial apparatus are schematically shown in figure 3.1 and they are limited to triaxial compression (when the imposed vertical stress is greater than the horizontal stresses) or extension (when the vertical stress is lower than the horizontal stresses). It is clear that, in such apparatus, the major principal stress direction can be either vertical or horizontal and during the test only a jump rotation of 90° in the principal stress direction can be imposed. The impossibility to provide a continuous rotation of the major principal stress axis between the vertical and the horizontal direction is certainly one of the major limitations of the conventional triaxial apparatus.

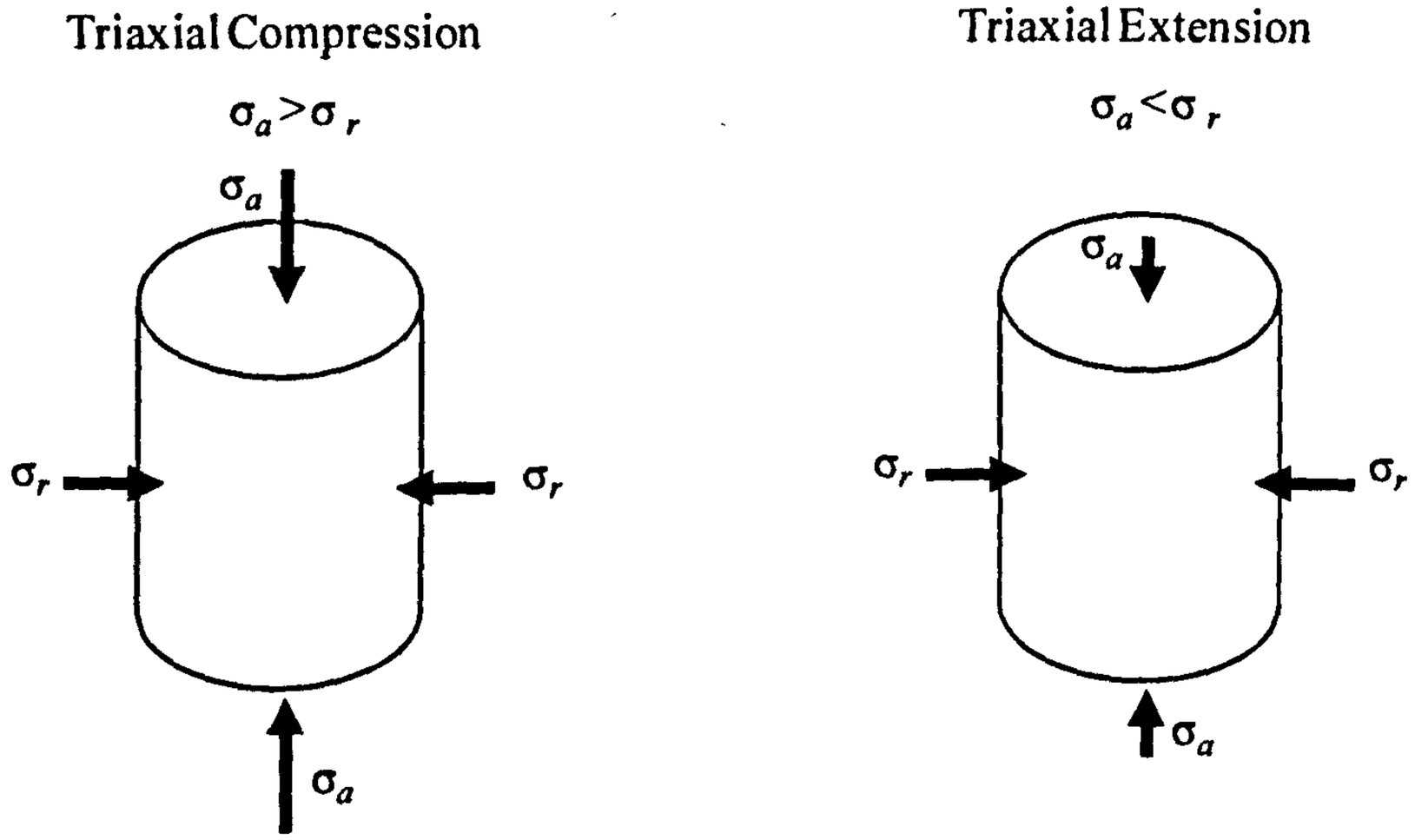

Fig. 3.1 Schematic view of loading conditions imposed in the triaxial apparatus

3.2.2 Apparatus

The apparatus used in this investigation is composed of a triaxial cell, a digital tritest 50 loading frame and systems of measurement, saturation, consolidation and data acquisition (Fig. 3.2.).

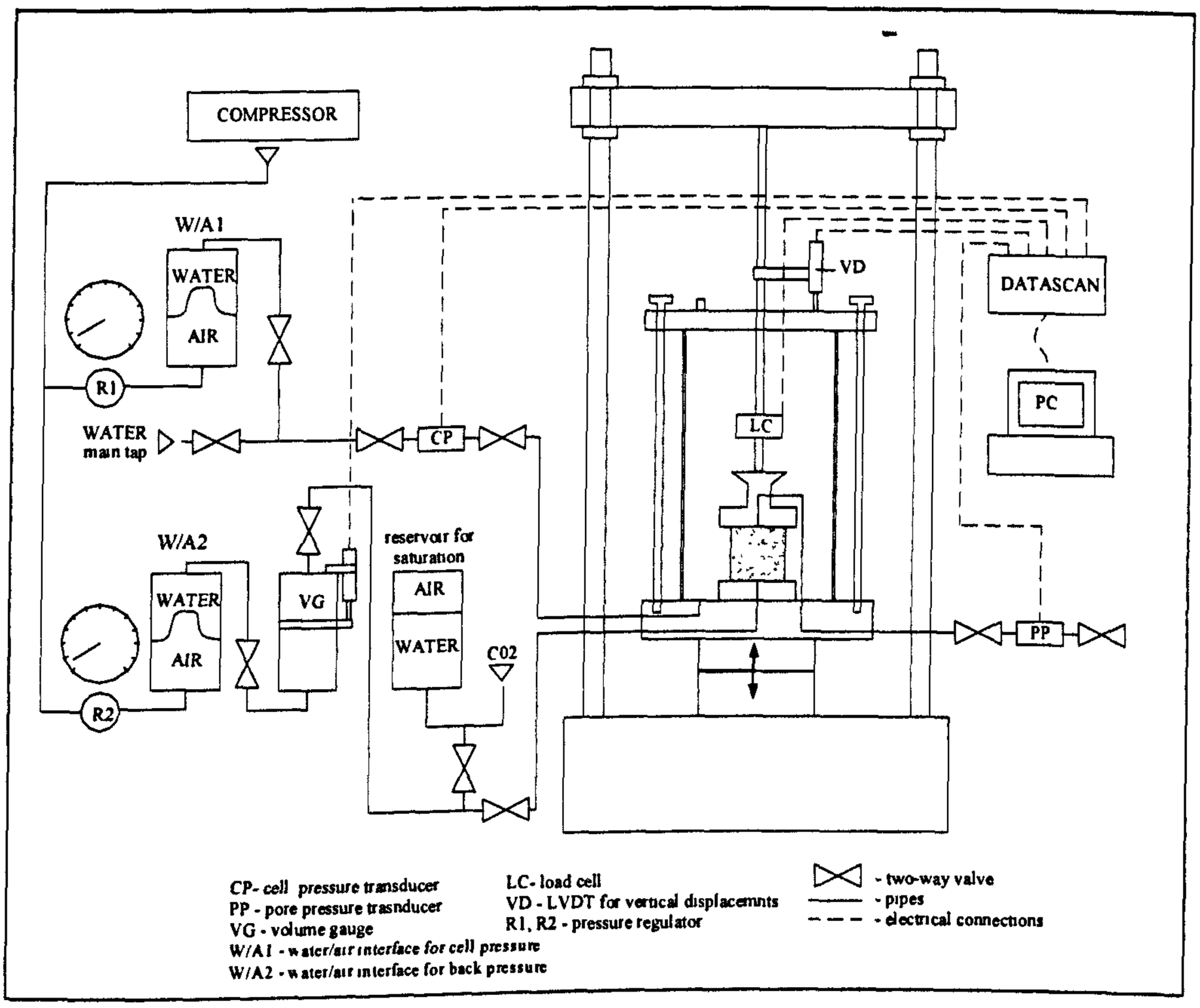

Fig. 3.2 Scheme of the experimental apparatus

Triaxial cell

The triaxial cell WF10201 provided by WIKEHAM FARRANCE (Fig. 3.3) consists of a perspex chamber reinforced to withstand a maximum pressure of 2000 kPa and it is designed for bearing water pressure only. The triaxial cell accommodates cylindrical specimens of 70 mm diameter and with a height to diameter ratio of 1. Circular enlarged top and bottom end

platens with 100 mm diameter have been used. The drainage of the specimen was ensured through a cavity in the platens of 16 mm diameter that was filled with a filter material, sand and filter paper (Fig.3.4).

Fig. 3.3 Picture of the triaxial cell and loading frame

The cell has also been further equipped with an attachment system between the loading ram and the top cap of the specimen for permitting the realisation of extension tests (Ibraim, 1988). The attachment of the top of the specimen is schematically shown in Fig. 3.5 and follows in succession stages (1) and (2) that are repeated until full top cap/ram fixity is achieved.

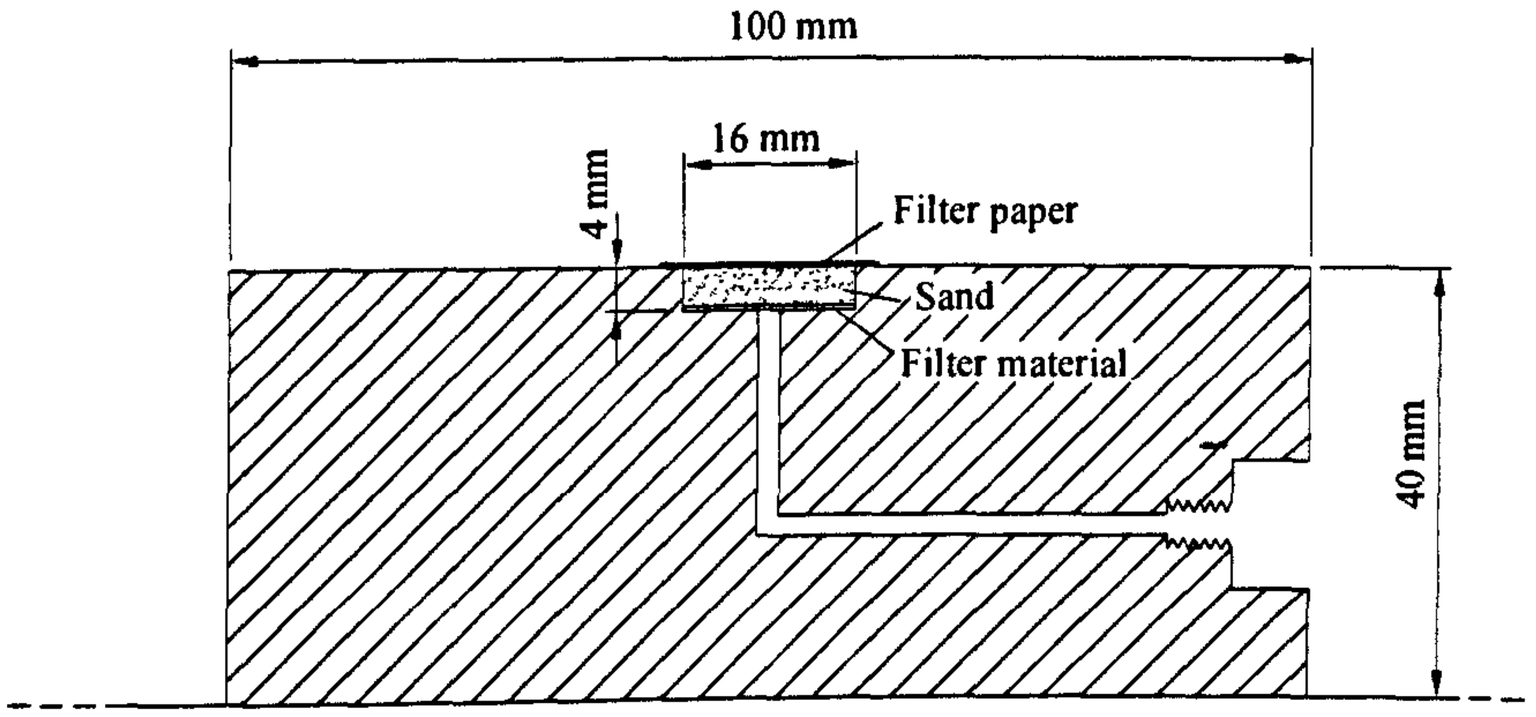

Fig. 3.4 Drainage at the bottom platen of the specimen

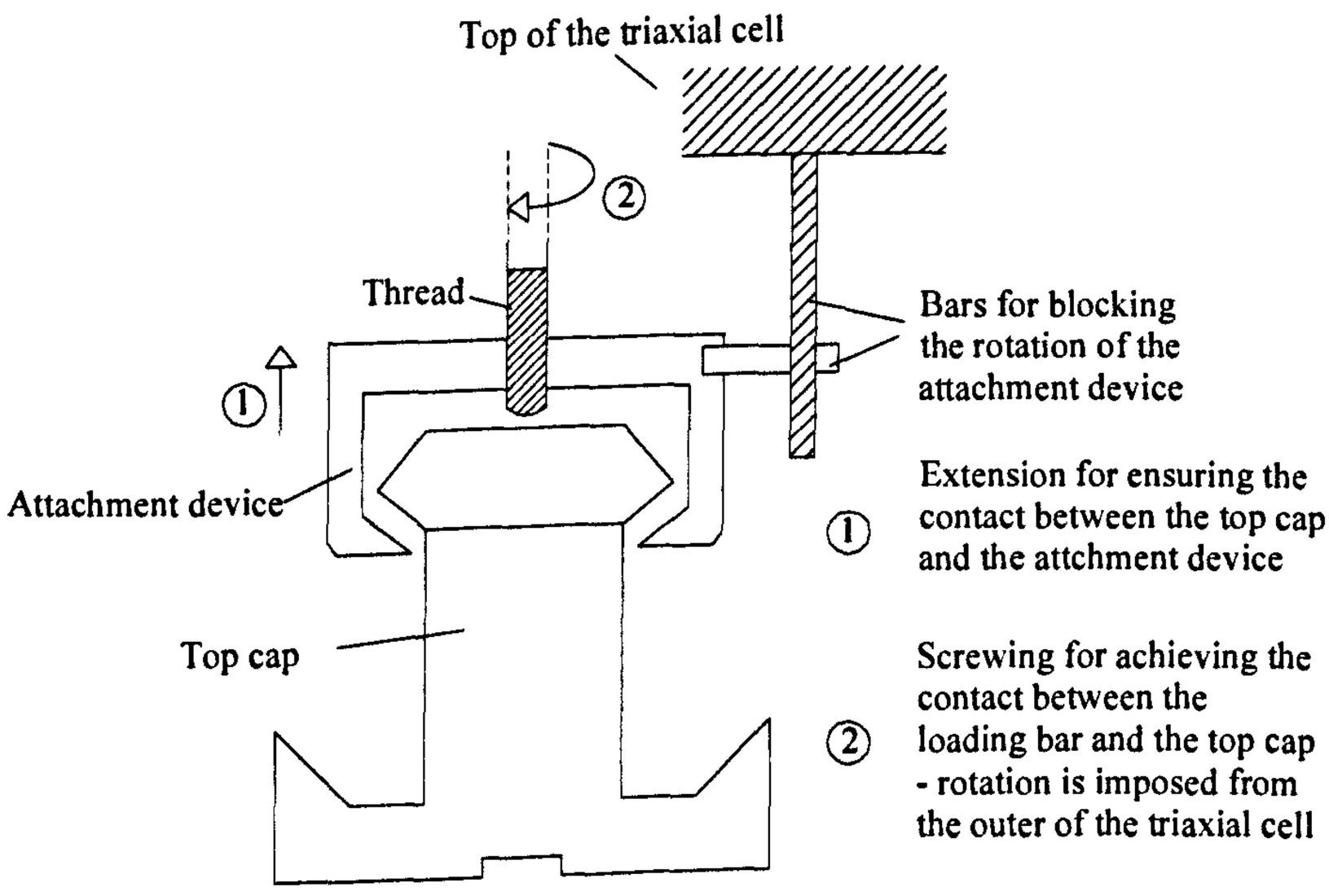

Fig. 3.5 Attachment system for the extension tests

Loading frame

The digital tritest machine (Fig. 3.3) is designed for testing soil up to maximum load of 50 kN. The forces applied are generated by a ballscrew jack driven by an electric motor and the rate of the test can be controlled by a touch panel keypad. The loading movement is applied from the bottom. The machine lifts or lowers the triaxial cell depending on the load condition and in turn the specimen is pushed against or pulled apart from the loading ram fixed to the crosshead of the tritest machine.

Measure system

The apparatus is equipped with the following devices:

- submergible load cell (LC in Fig.3.1) for measuring the axial stresses in the specimen;
- LVDT (VD in Fig.3.2) placed outside the cell for following the movement of the triaxial cell and for monitoring the axial strains of the specimen.;
- double chamber volume change gauge (VG in Fig.3.2) which uses a LVDT for measuring the volumetric strains of the specimen;
- pressure transducer (PP in Fig.3.2) connected to the top of the specimen for measuring the pore pressures inside the specimen;
- pressure transducer (CP in Fig.3.2) for monitoring the pressure inside the cell.

Pictures of the measure devices are shown in Fig. 3.6, while the details of technical specifications, calibration factors, resolution and precision are given in the following Table 3.1. According to German and Ladd (1988), the resolution reflects the smallest detectable measurement unit (from measurement display) while the precision expresses the basic scatter in the measurement and can be estimated from the observed spread of results. An example of derivation for the values of resolution and precision is reported in Fig. 3.7.

The load cell and pore pressure transducers were calibrated against a Budenberg dead weight system. The pressure is generated from the reference dead-weight placed on a known floating piston area. The displacement sensors were calibrated by a 25 mm micrometer. The sensors were fixed in a gauge block and the position of their spindles was varied by winding the

micrometer while the output voltage was recorded. The volume change gauge was calibrated with a scale of 0.01g resolution. The amount of water flowing out was converted in its volume while the corresponding output voltage was monitored.

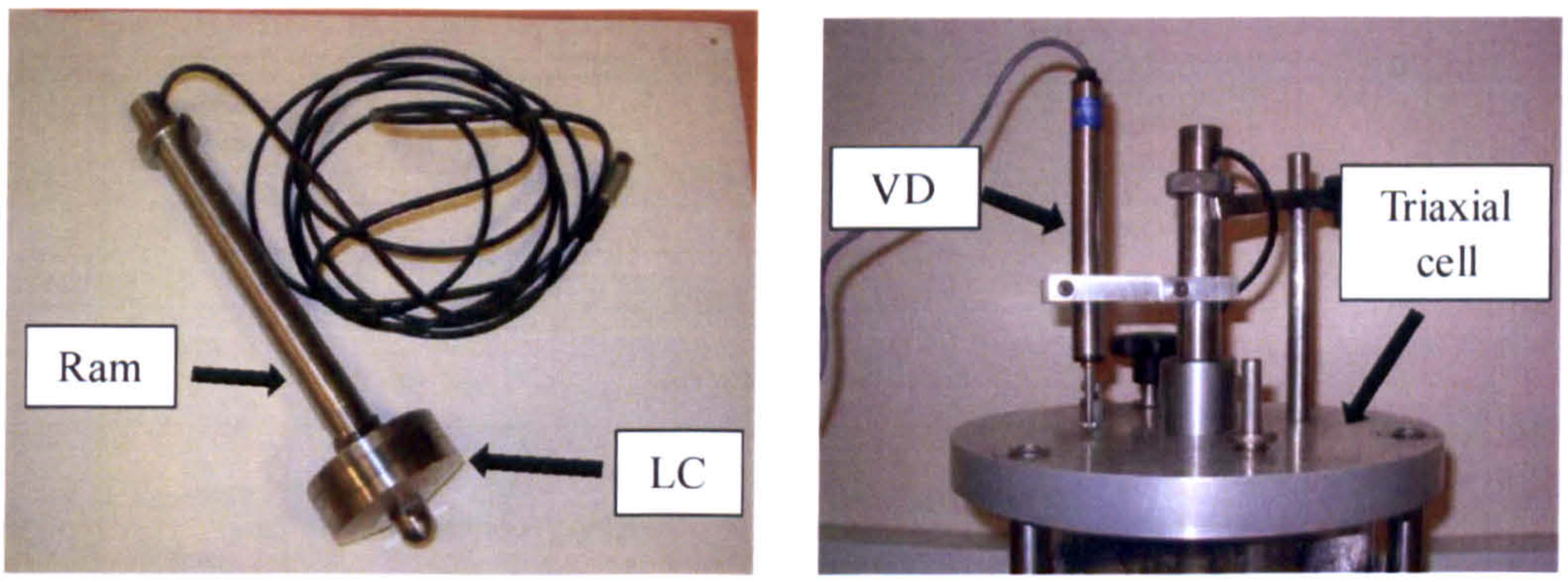

Fig. 3.6 System devices used in this investigation: (a) internal load cell, (b) LVDT, (c) pressure transducer and (d) volume change

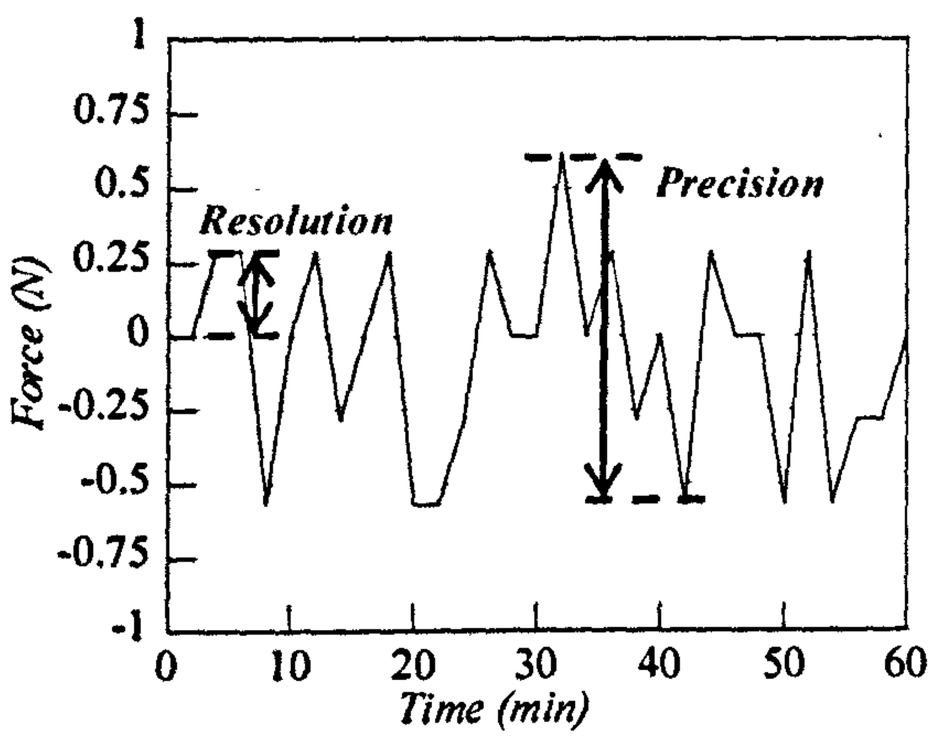

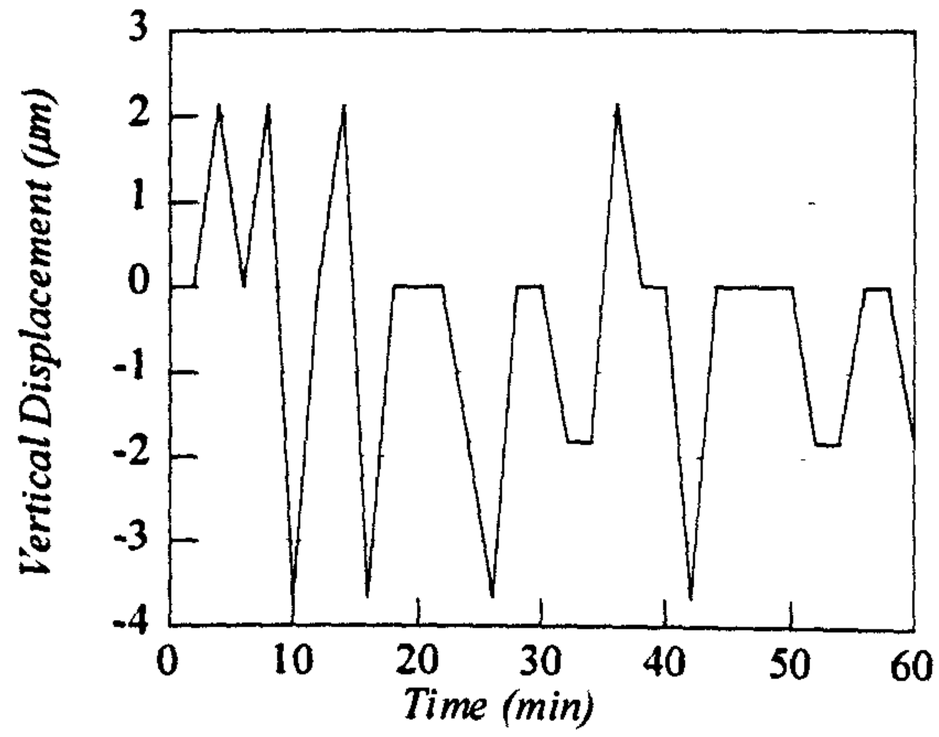

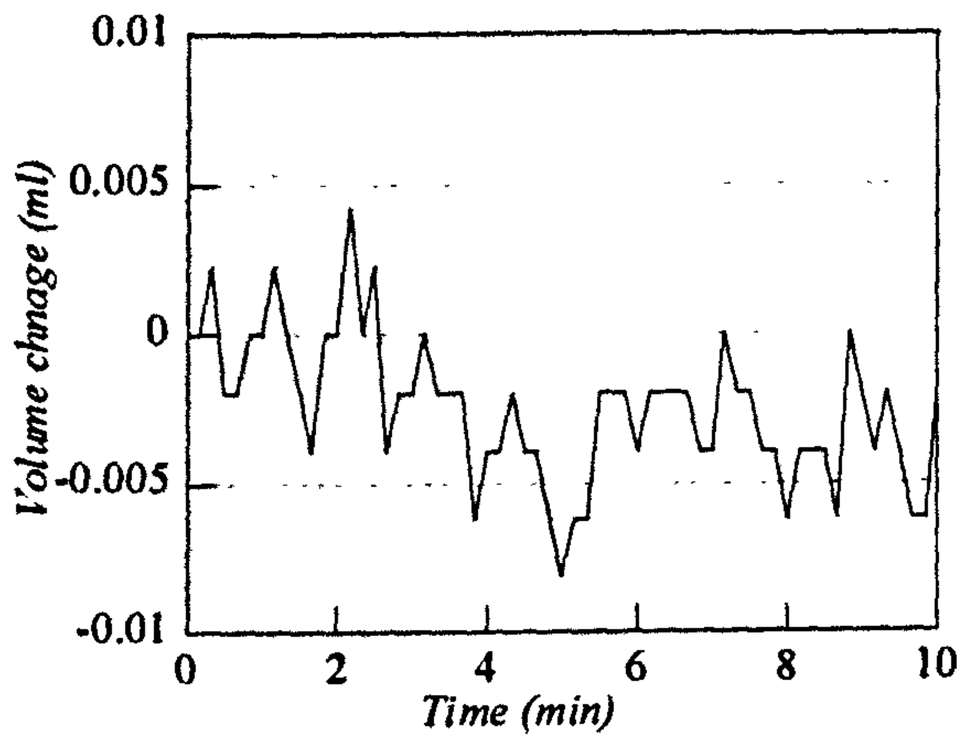

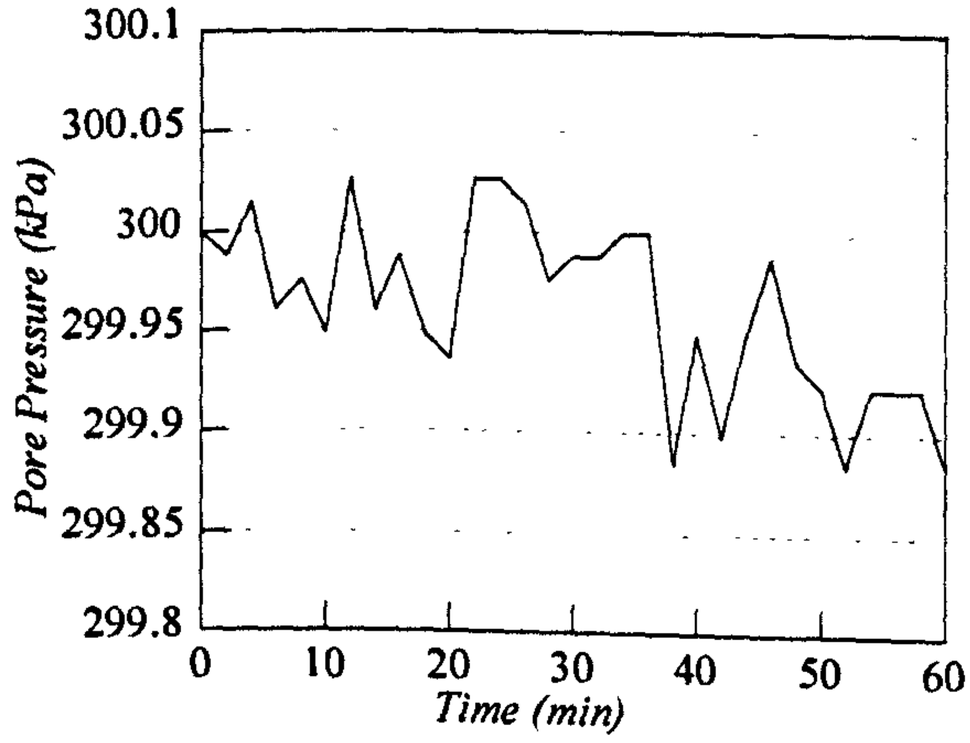

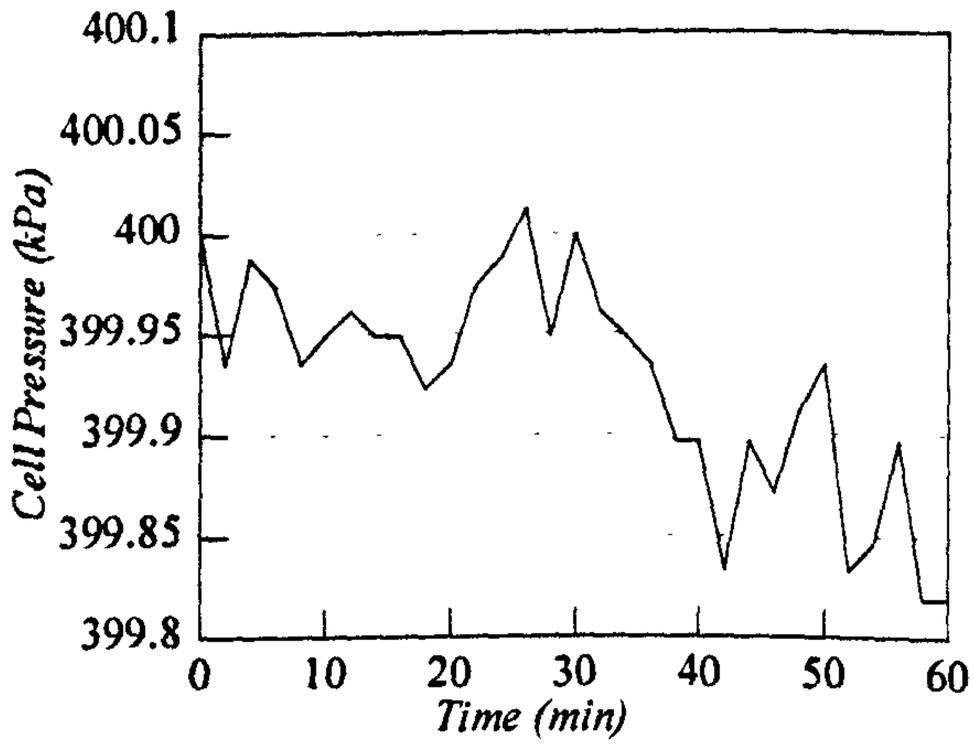

Fig. 3.7 Resolution of the measure devices

Tab. 3.1 Technical specifications, calibration factors, resolution and precision for the measure devices

Device	Device type	Manufacturer	Model	Max capacity	Calibration factor	Resolution	Precision
LC	Load cell	Wykehanm Farrance	WF17100	5 kN	471.735 kN/V	0.28 N	±0.6 N
VD	LVDT	Measurement group Inc.	HS-50	50 mm	3050.15 mm/V	2 µm	±4 µm
VG	Volume gauge	Wykehanm Farrance	WF17044	100 ml	3247.90 ml/V	0.0023 ml	±0.01 ml
	LVDT	Measurement group Inc.	HS-25	25 mm			
PP	Pressure Trans.	Druck Limited	PDCR810	800 kPa	20330.5 kPa/V	0,012 kPa	±0.5kPa
CP	Pressure Trans.	Druck Limited	PDCR810	800 kPa	20337.0 kPa/V	0,012 kPa	±0.5kPa

Systems of saturation and consolidation

The cell pressure and back pressure of the specimen are supplied through water pressure, converted from air pressure. The compressed air is generated from a main compressor air system and can be manually regulated with manometers (R1 and R2 in Fig. 3.2). The regulated air pressure is then transferred to the water through an air-water interface unit which consists of two compartments separated by an elastomeric diaphragm (W/A1 and W/A2 in Fig.3.2). The air pressure is applied to the bottom chamber while the top chamber is filled with water. The apparatus is not provided with an automatic control system, pressures are manually regulated.

The system was equipped with a saturation system for permitting the testing of completely saturated specimen. The back pressure line can be closed and the specimen can be connected

either to a CO_2 source or a water reservoir (see Fig. 3.2). CO_2 and de-aired water are flushed through the specimen from the bottom to the top.

In the cell pressure line, the triaxial cell can be filled prior to pressurisation through a connection with the water main tap as schematically shown in Fig. 3.2.

System of data acquisition

The data measured by the transducers are acquired using a RS Datascan 7200 unit connected to the computer (Fig.3.2). The module communicates with the computer through a RS232 port and it can monitor a maximum of 16 different input channels. The Datascan module is programmed to provide a 16 bit resolution and it can take up to 40 readings per second. The computer records the data received from the Datascan with a BBC basic programme called TRIAX. The version used in this research has been developed at University of Bristol from the previous DOS version (Toll, 1993; Nash, 2002)

3.3 Materials

3.3.1 Hostun RF sand

Hostun RF (S28) sand, a European standard sand for laboratory testing employed in several experimental research, has been used in this study. Its chemical components consists of an high siliceous amount (SiO_2>98%) and the grain shape varies from angular to sub-angular. Its grain size distribution is shown by Fig. 3.8 and its physical properties are as follows: mean grain size D_{50}=0.32 mm, coefficient of uniformity C_u=1.70, coefficient of gradation C_g=1.1, specific gravity G_s=2.65 and minimum and maximum void ratios e_{min}=0.62 and e_{max}=1.00 respectively (Ibraim 1998).

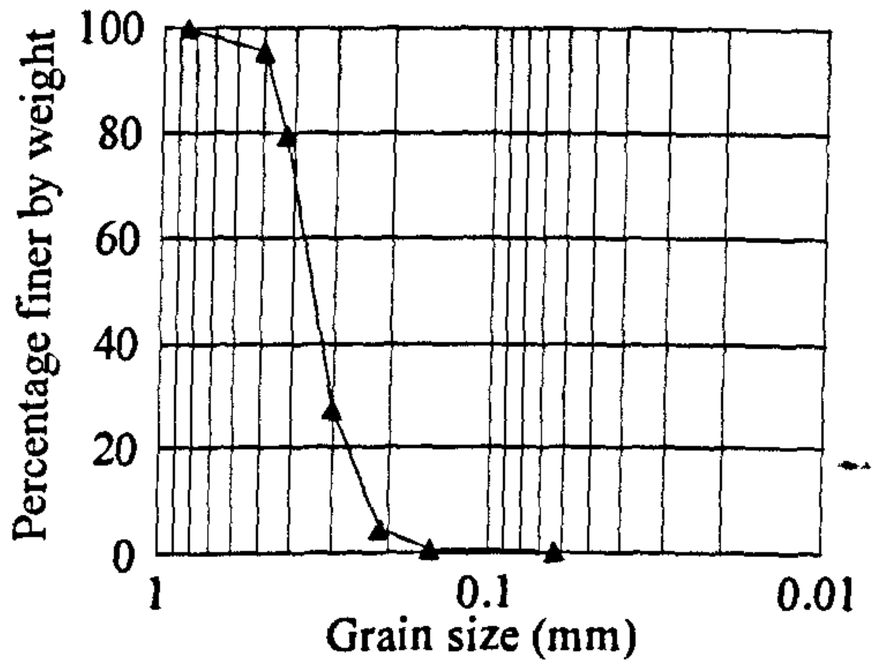

Fig. 3.8 Grain size distribution for Hostun RF (S28) sand

3.3.2 Fibres

Three different types of discrete, flexible polypropylene fibres have been used as reinforced material (Fig. 3.9):

• Type (1): crimped fibres (Loksand^{TM}) of 35mm length and circular cross section of 0.1mm diameter. These are the fibres mainly used in this investigation. They react predominately in tension and the average tensile stress-strain response (obtained through a series of 15 tension tests performed according to ASTM D2343) is shown in Fig. 3.10a;

• Type (2): fibrillated fibres with an average length of 20mm and circular cross section of 0.03mm diameter. The average tensile stress-strain response is reported in Fig. 3.10b;

• Type (3): platy fibres are flattened, ribbon shaped fibres with the following dimensions: 40mm average length, 0.1mm thickness and 1.3mm width. These fibres are different from the previous for their "linear" cross section but also because they possess a quite relevant bending stiffness. The apparatus used did not allow testing the fibres until their plastic threshold because pull-out of fibres took place before yielding. However the initial stiffness of the tensile stress-strain behaviour was deducible and reported in Fig. 3.10c.

Other characteristics of the tested fibres are given in Table 3.2.

Tab. 3.2 Characteristics of the fibres used in this study

Fibre type	Weight Denier	Cross Sect.	Aspect ratio	Tensile strength (MPa)	Elongation at Break
(1) Loksand™	50	Circular	350.0	22.5	160%
(2) Fibrillated	6	Circular	667	58.0	-
(3) Platy	900	Rectangular	98	-	-

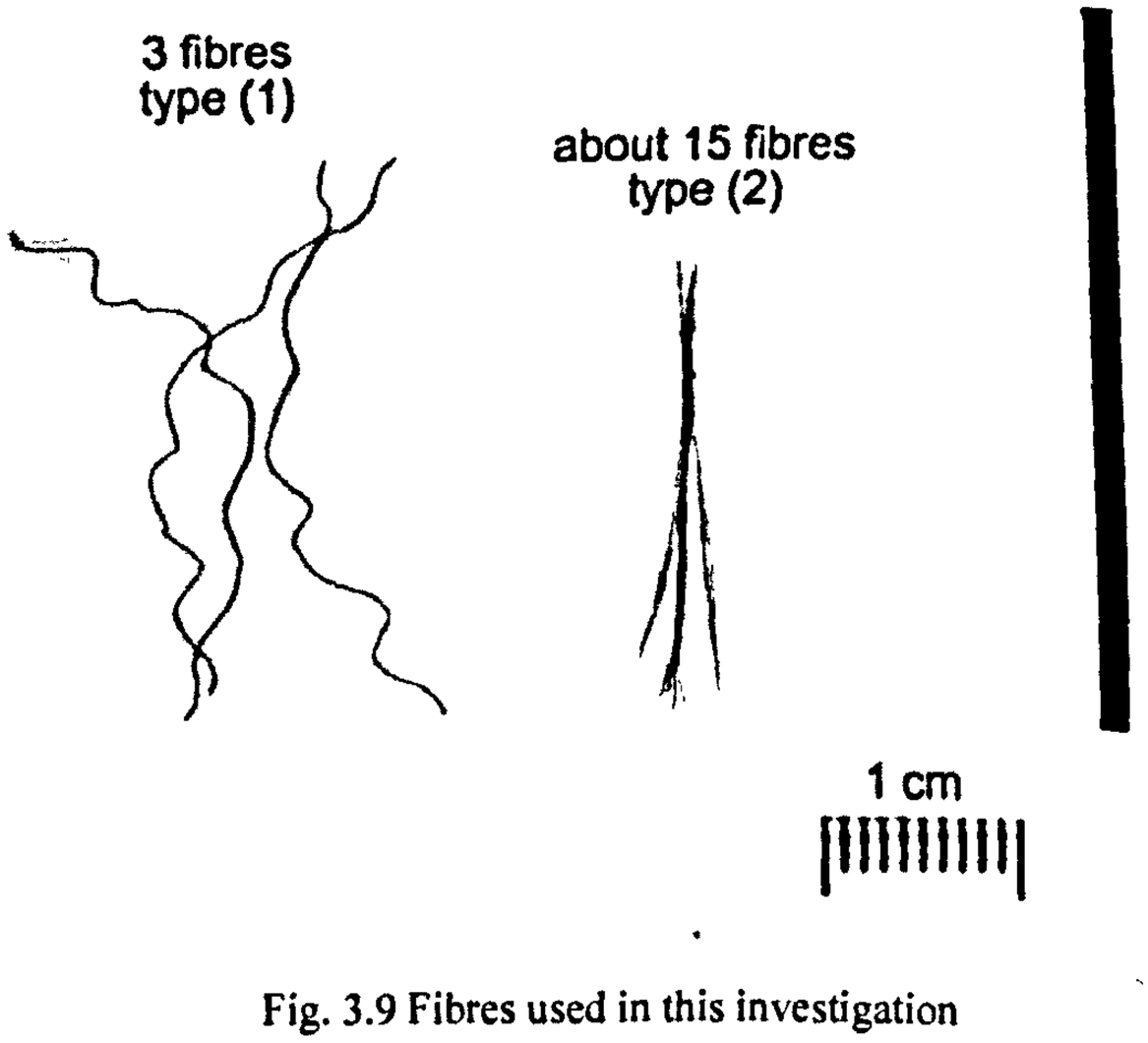

Fig. 3.9 Fibres used in this investigation

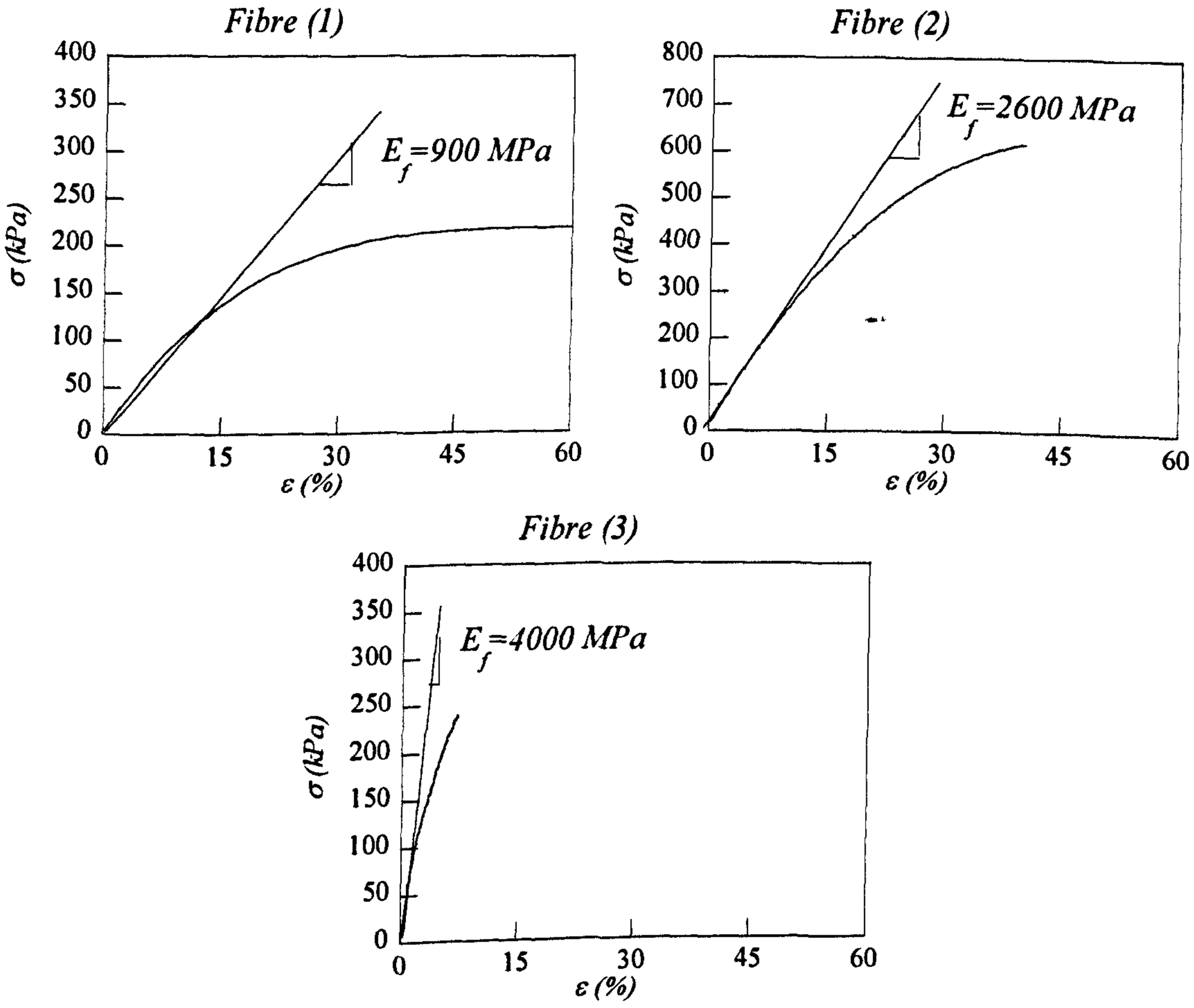

Fig. 3.10 Average tensile stress-strain curve of 15 individual (a) Loksand™ fibres, (b) fibrillated fibres and (c) platy fibres

3.4 Specimen preparation

3.4.1 Fabrication - Moist tamping technique

The moist tamping technique (Ladd, 1978) is the most widely adopted procedure for preparing fibre reinforced specimens. The technique has the advantage of easily controlling the soil density while preventing the segregation of fibres and it produces soil fabric that eventually resembles that of compacted soil by dynamic plates (Michalowski, 2008).

The fabrication procedure involved two stages: mixing and compaction. Mixing consisted of firstly adding water to dry sand (10 % by weight, which is the optimum moisture content for compaction as determined by Ibraim and Fourmont, 2006) then mixing the water through the sand manually using a small spoon until the grains became moist. Fibres were then added progressively and mixed through the moist sand also using the small spoon. The moisture in the sand was necessary to prevent the fibres from floating and becoming segregated. Mixing was stopped when, by visual examination, it was considered that the fibres were evenly distributed throughout (Fig.3.11a).

Cylindrical specimens with 70 mm height and diameter were prepared in three layers of equal thickness. The amount of mixture required to form one-third of a sample was delicately deposited into a mould (Fig.3.11b, c and d) to ensure a zero drop height and minimal disturbance to the fibre distribution. The mixture was then compacted/tamped by hand using a light-weight circular disc (Fig. 3.11e) until the layer thickness became equal to one-third of the sample height. In developing the fabrication procedure, prototype reinforced and unreinforced specimens made in a transparent Perspex tube did not show any significant over-compaction effects during the formation of the higher layers, therefore no undercompaction ratios have been considered (Ladd, 1978).

The average concentration of fibres included in a composite was defined as a percentage of dry weight of sand:

$$w_f = \frac{W_f}{W_s} \text{ x } 100\ (\%) \qquad (3.1)$$

where W_f is the weight of fibres and W_s is the weight of the dry sand. As a general procedure, different concentrations of fibres have been added to constant W_s. There is a limit to the amount of fibres that can be added to the sand so that the moist tamped composite can be effectively prepared (Ibraim and Fourmont, 2006).

The void ratio must be carefully defined for a reinforced specimen, since the volume occupied by fibres can be "attached" either to the sand or to the voids. This distinction has not always been clear in literature: in this investigation the fibres have been considered as part of solids. Specimens have been fabricated with three different densities generally named *(L)*, *(M)* and *(D)* which respectively corresponds to a nominal relative density index I_D of 0%, 25% and 50% for the unreinforced specimens. The relative density index is defined as:

$$I_D = \frac{(e_{max} - e)}{(e_{max} - e_{min})} \tag{3.2}$$

where e, e_{max} and e_{min} are respectively the actual, maximum and minimum void ratio for the tested material. Maximum and minimum void ratios for Hostun sand have been reported in section 3.3.1.

As a general procedure, different concentrations of fibres have been added to constant W_s. The amount of sand and fibres for every combination of relative density and fibre content is reported in Table 3.3.

Tab. 3.3 Amount of sand (W_s) and fibres (W_f) used for fabricate unreinforced and reinforced specimens

w_f / Density	*0%*	*0.3%*	*0.6%*	*0.9%*
(L)	W_s=356.41 g	W_s=356.41 g	W_s=356.41 g	W_s=356.41 g
	W_f= 0.00 g	W_f= 1.07 g	W_f= 2.14 g	W_f= 3.21 g
(M)	W_s=375.16 g	W_s=375.16 g	W_s=375.16 g	-
	W_f= 0.00 g	W_f= 1.13 g	W_f= 2.25 g	-
(D)	W_s=396.01 g	W_s=396.01 g	-	-
	W_f= 0.00 g	W_f= 1.18 g	-	-

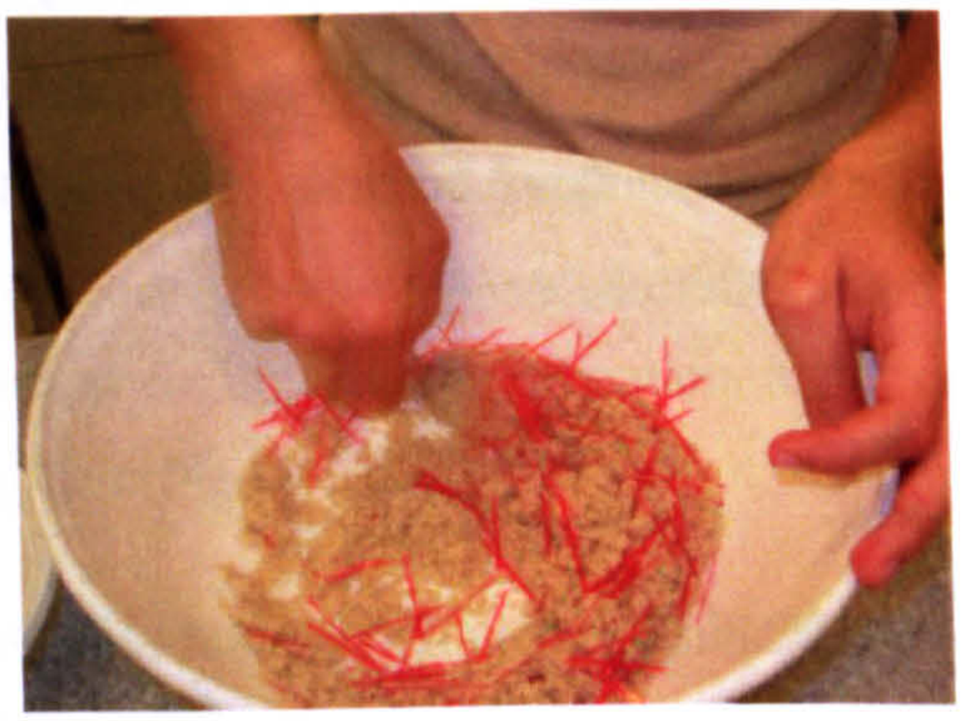

(a)

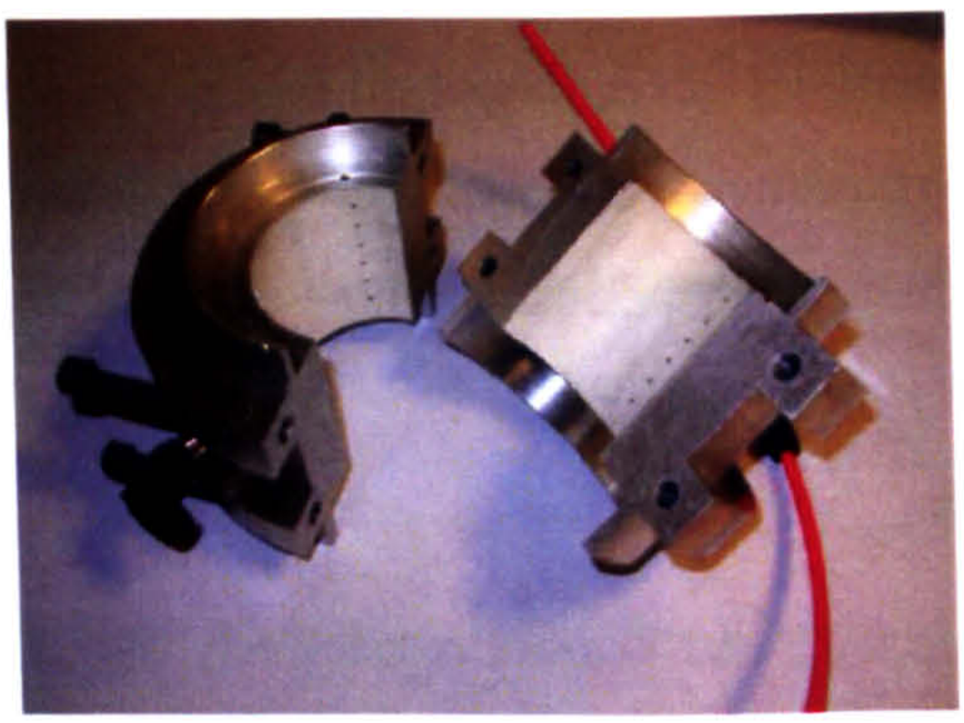

(b)

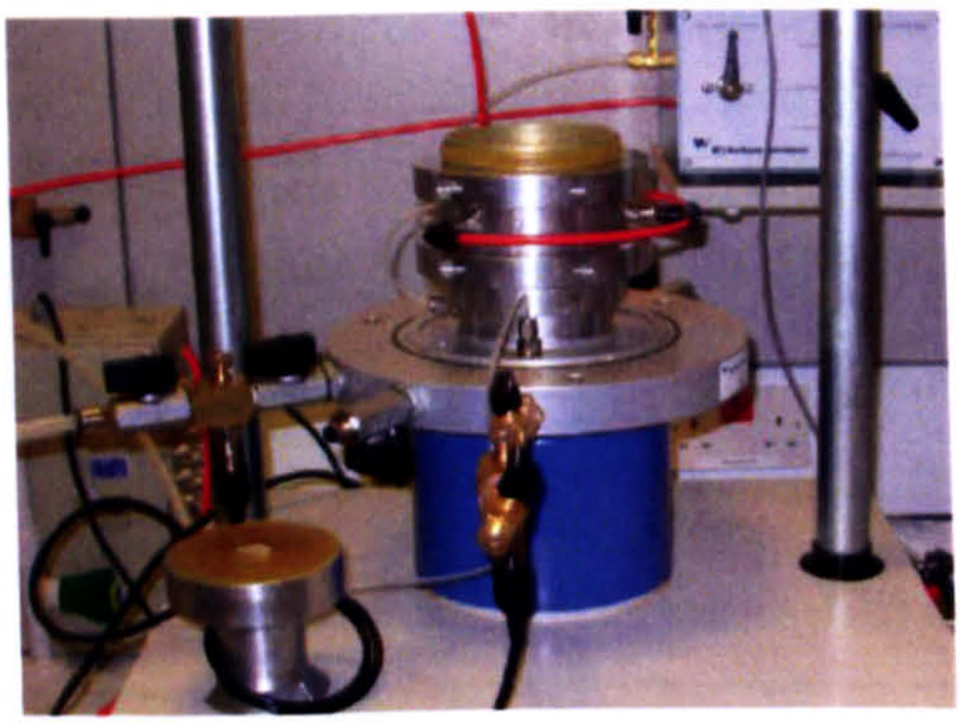

(c)

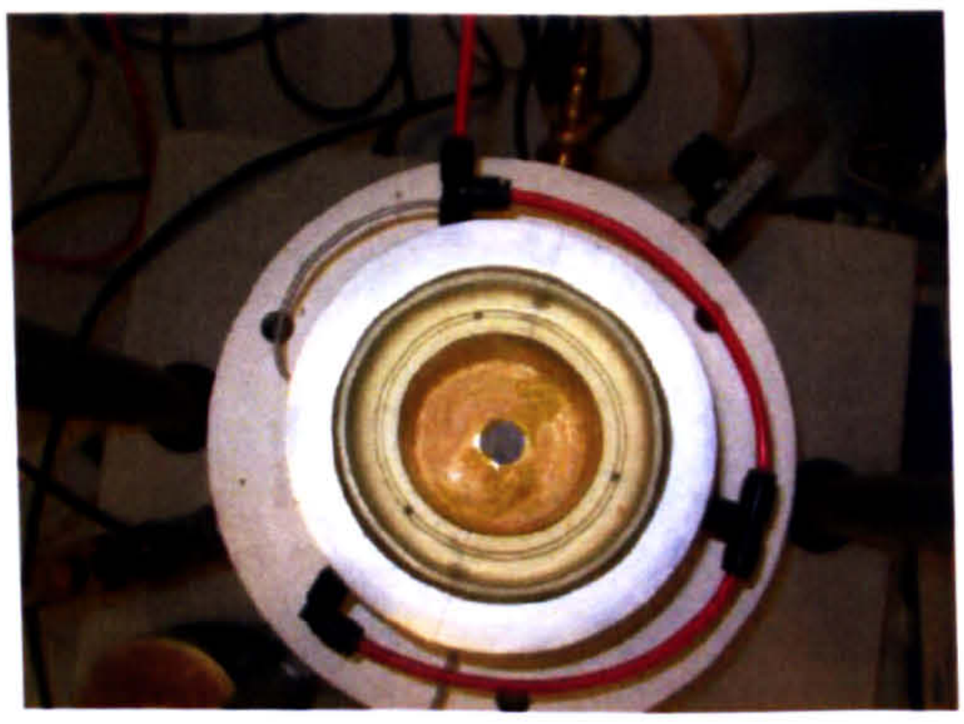

(d)

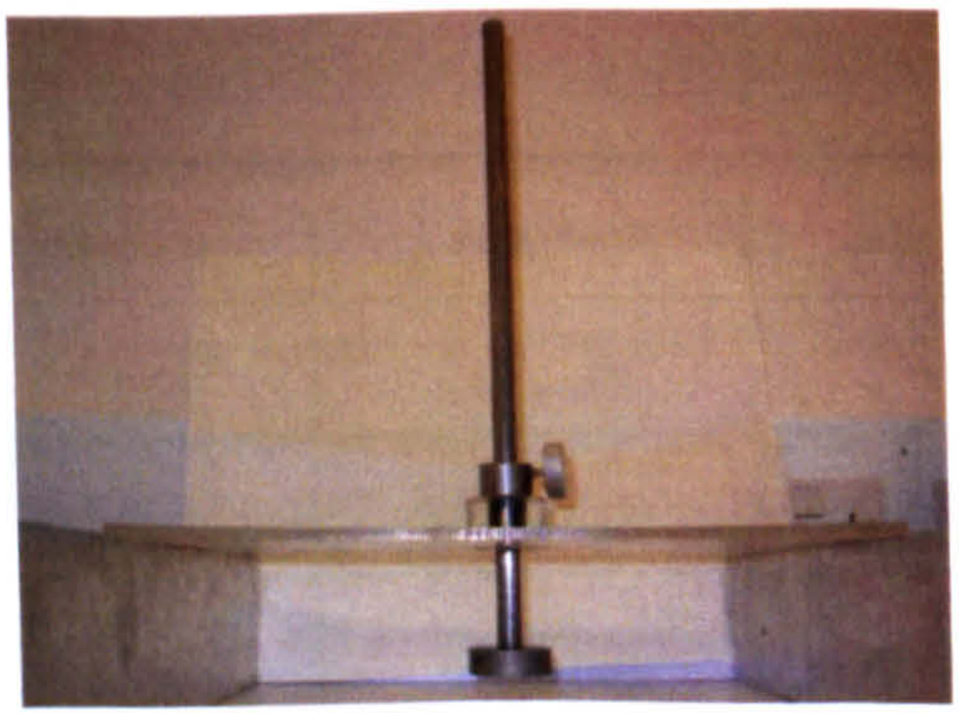

(e)

(f)

Fig. 3.11 Specimen fabrication: (a) mixing, (b),(c) and (d) particular of the mould, (e) light hammer for tamping and (f) specimen after tamping

Removal of the mould was performed by confining the specimen under -20 kPa vacuum to avoid the collapse of the specimen (Fig.3.12). After removal, three measurement of height and diameter of the specimen were taken. The triaxial cell was then delicately posed and slowly filled with water ensuring minimal disturbance to the specimen. Once the cell was fully filled with water, the vacuum was slowly released and at the same time the cell pressure was increased up to 20 kPa.

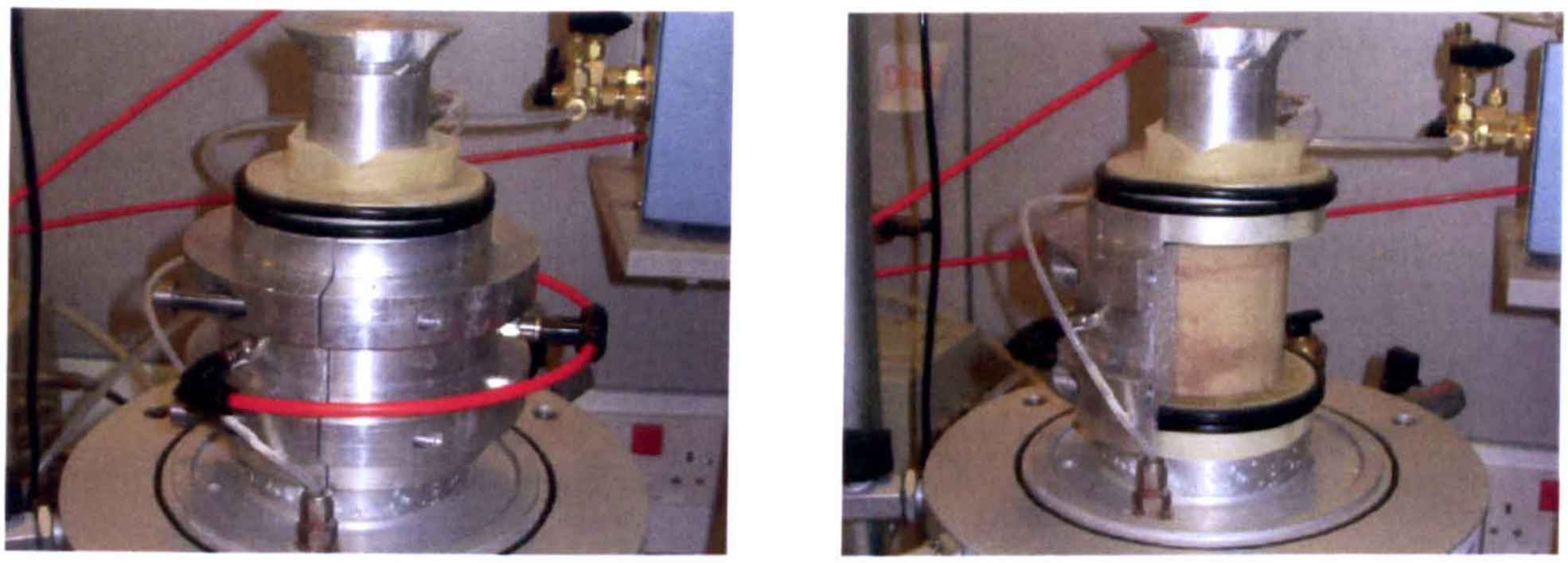

Fig. 3.12 Removal of the mould

Enlarged and lubricated ends were used at the top and bottom of the specimen to eliminate the problem of the friction at the ends of the specimen. The lubrication consisted of silicone grease and two/three latex rubber disks respectively at the bottom/top of the specimen. The latex disks had a 12 mm diameter hole in their centre to permit the drainage of the specimen and they have been randomly perforated to increase their deformability. By visual inspection, the homogeneous shape of the specimen was well preserved at least up to 20% of axial strain (ε_a) and up to 10% in extension conditions (Fig.3.13).

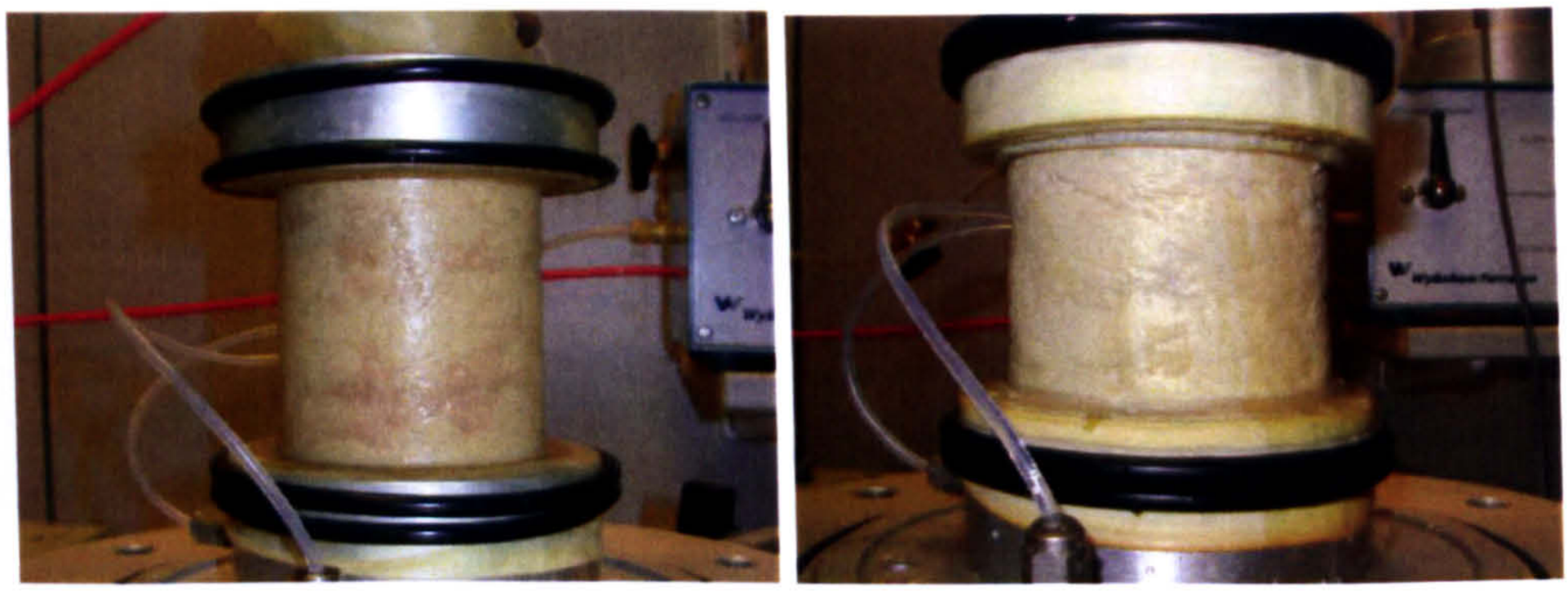

(a) (b)

Fig. 3.13 Effect of enlarged lubricated ends. Specimen (a) before the test and (b) after the test

3.4.2 Saturation and consolidation

Saturation has been achieved by firstly flushing CO_2 and subsequently water through the specimen. CO_2 was flushed from the bottom to the top of the specimen for at least 25 minutes under a gradient of pressure of 2 kPa. De-aired water was then flushed in the specimen under a very low gradient of pressure to fill the voids in the specimen and replace the CO_2. Saturation with water lasted for a couple of hours and it was stopped when a quantity of water equal to two times the volume of the specimen was transited.

After the saturation stage under the 20 kPa cell pressure, the cell pressure and the back pressure were manually simultaneously increased up to the respective values of 320 kPa and 300 kPa using the pressure regulators R1 and R2 in Fig.3.2. The isotropic consolidation stage of the specimen was then performed by increasing the cell pressure using pressure regulator R1.

The degree of saturation has been monitored in terms of Skempton's pressure coefficient B (Skempton, 1954). The coefficient B can be calculated as the ratio between the pore pressure change and the variation of the total mean stress during undrained isotropic loading. A value B equal to unity is typical of a fully saturated soil, while a partially saturated soil would show a coefficient B less than one. The measurement of this coefficient was performed after the consolidation stage of each test and a B value of 0.97 was considered the lower bound threshold for satisfactory saturation degree in both drained and undrained tests.

3.5 Error from the measurements

The advent and the widespread use of electrical transducers have consistently enhanced the precision and the facility of the measurements and have enabled automated data logging with consistent improvement in the quality of the results. However there are many potential sources of errors for the measurement of the stresses and the deformations of the specimens in a triaxial apparatus and the principal ones are summarised below:

- *flexibility of the system for measuring the interstitial pressure;*
- non-uniformity of deformations;
- deformability of the axial loading system and edge effects;
- membrane effects.

These sources will be discussed in the remainder of this section and the expedients taken for their elimination or quantification as well as their incidence on the test results will be analysed.

a) Volumetric flexibility

The connection system between the pore pressure transducer, the volume gauge and the specimen is not completely rigid. Especially in undrained tests, the development of pore pressure inside the specimen can be affected by the volumetric flexibility of the back pressure line and by the compressibility of the water itself. The recommendations by Lade and Hernandez (1977) have been taken to minimise the effect of the volumetric flexibility and they are listed in the following:

- the diameter and the length of the pipes has been reduced to the minimum;
- pipes and connections are very rigid and taps have no variation of volume;
- de-aired water has been used.

Therefore, because of the adoption of these precautions, the influence of the flexibility of the system on the measurement of the pore pressure and volume of the specimen has been considered negligible.

b) Non –uniformity of deformations

The use of conventional end platens in triaxial tests produces frictional forces at specimen ends preventing the achievement of a good homogeneity of deformation and stress distribution throughout the whole specimen. Rough ends produces a rigid zone at the bottom and the top of the sample causing the localisation of deformation in one or more failure surface (Rowe and Barden, 1964; Kirkpatrick and Belshaw, 1968). The effects of the restraints are negligible in the mid part of the sample only if a length to diameter ratio of two is used (Bishop and Green, 1965; Colliat-Dangus et al., 1988).

Lubricated platens can be used to minimise the lateral restraint on the specimen caused by the friction with the end platen and to obtain an acceptable uniformity of deformation and stresses throughout the specimen. Description of the antifrictional system has been given in paragraph 3.4.1. However the use of the antifrictional system may induce errors on the measurement of the axial deformation of the specimen when its measurement is performed externally to the triaxial cell as in this research. The axial deformations are overestimated and obviously the stiffness of the specimen is underestimated. This problem will be discussed in the following paragraph.

c) Deformability of the axial loading system and edge effects

The measurement of the axial deformations made externally to the triaxial cell is subjected to several sources of error (Jardine et al., 1984; Costa Filho, 1985; Baldi et al. 1988).Typical errors comprise:

- compressibility of the equipment, including the internal load cell, the top cap and especially the lubricated ends;
- the effects of the end restraints on the stress and strain distribution in the specimen. This effect has been minimised by using lubricated ends;
- problems of contact between the specimen and the top cap. These errors are in general caused by lack of fit or surface irregularities at the interface between the specimen and the loading surface;

- seating errors between different elements.

Most of the sources of these errors can be eliminated if a local measurement system for the axial deformations is adopted but this was not possible in this research. However, the determination of the small strain stiffness for which these errors may have a remarkable effect is beyond the scope of this research. Nonetheless, particular attention has been paid to minimising any inaccuracy due to the previous listed elements.

d) Membrane effects

Membrane penetration

Laboratory tests on granular soils are often performed enclosing the specimen in a flexible membrane. When the stresses are applied by gaseous or liquid media, the membrane enclosing the soil is pressed into the peripheral voids of the specimen and it partially penetrates into the specimen. In any drained triaxial test, the cell pressure increase during the consolidation stage involves a change on the amount of membrane penetration into the sample. This means that the prediction of the sample volume change based on the measurement of water leaving or entering the specimen needs to be corrected in order to account for this phenomenon. Similar error occurs in an undrained triaxial test: during testing, pore pressure changes are accompanied with changes in membrane penetration inducing a partially drained state.

The membrane penetration effects was first recognized by Newland and Alley (1957, 1959) in drained triaxial tests and they proposed a method of correction based on the assumption of material isotropy under hydrostatic loading increment. Since then, numerous researches (Kiekbusch and Schuppener, 1977; Martin et al., 1978 Baldi and Nova, 1984 Frydman et al., 1973; Ramana and Raju, 1982; Nicholson et al., 1993) have investigated the membrane penetration effect and the change of peripheral volume was found to be linked to:

- mean grain size of the soil;
- confining pressure;
- sample dimensions connected with the ratio between sample volume and lateral area.

Baldi and Nova (1984) proposed the following relationship for estimating the parasitic volume (ΔV_m) due to the penetration of the membrane:

$$\Delta V_m = \frac{d_g}{2D} V_0 \left[\frac{d_g}{E_m t_m}\right]^{1/3} \left[(\sigma'_3)^{1/3} - (\sigma'_{30})^{1/3}\right] \qquad (3.3)$$

where d_g is the mean grain size of the soil (D_{50}), D is the diameter of the specimen, V_0 is the volume of the specimen, E_m and t_m are respectively the elastic modulus and the thickness of the membrane, σ'_{30} and σ'_3 are respectively the initial and final confining pressures applied. Estimation of the parasitic volume has been performed here for the loosest specimen with an initial volume $V_0 = 270 cm^3$, mean grain size $d_g = D_{50} = 0.32$, elastic modulus of the membrane $E_m = 2MPa$, thickness of the membrane $t_m = 0.25mm$ and a diameter of the specimen $D = 70mm$. A variation of the pressure from an initial confining pressure $\sigma'_{30} = 20kPa$ to a confining pressure of $\sigma'_3 = 200kPa$ induces a variation of parasitic volume $\Delta V_m = 0.31cm^3$ which corresponds to a variation of volume of 0.11%.

Alternatively Sivathayalan and Vaid (1998) proposed another relationship for assessing the amount of membrane penetration:

$$\Delta V_m = 0.115 \cdot D_{50} \cdot A_L \cdot [\log(\sigma'_3) - \log(\sigma'_{30})] \qquad (3.4)$$

where A_L is the lateral surface of the specimen. According to this method a slightly larger amount of variation of parasitic volume $\Delta V_m = 0.57 cm^3$ was found which corresponds to a variation of volume of 0.21%. For the loosest specimens tested in this research, this change of volume approximately corresponds to a change in void ratio $\Delta e = 0.004$. The error in the calculation of the initial void ratio (that will be discussed in the following paragraph) is much larger than this value, therefore, the correction due to membrane penetration has been considered negligible and no correction has been applied in this study. The same conclusion was achieved by Ibraim (1998) in testing similar specimens.

Membrane stiffness

The rigidity of the membrane may influence the magnitude of axial and radial stresses during loading. Two main methods for calculating the stresses applied to the soil have been proposed following the findings of Henkel and Gilbert (1952). The former is based on the compression shell theory in which the membrane is assumed to maintain the shape of a thin wall cylindrical shell. The latter is based on the hoop stress theory: the resistance of the membrane to axial stresses is negligible due to its buckling and the membrane may apply only "hoop" radial stresses. The first method is generally preferred (Kuerbis and Vaid, 1990; Fukushima and Tatsuoka, 1984) and it is proposed by ASTM D4767-04 for considering the effect of membrane strength even if some authors (Kolymbas and Wu, 1990) have preferred the hoop stress theory for correcting test results. Generally, the employment of the compression shell theory is considered more appropriate for following conditions (Kuerbis and Vaid, 1990 among others):

- loose sandy materials which are susceptible to liquefaction;
- low effective stress;
- specimen loaded in both compression and extension;
- consolidation strains which may increase the susceptibility to buckling are small.

These conditions are encountered in the tests performed in this research and the compression shell theory has been adopted for correcting the tests results. According to the ASTM D4767-04, the measured axial and radial stresses on the specimens ($\sigma_{a,mes}$ and $\sigma_{r,mes}$, respectively) can be corrected by the quantities ($\Delta\sigma_{a,corr}$ and $\Delta\sigma_{r,corr}$) to obtain the corrected value of the axial and radial stresses (σ_a and σ_r):

$$\sigma_a = \sigma_{a,mes} + \Delta\sigma_{a,corr} \tag{3.5}$$

$$\sigma_r = \sigma_{r,mes} + \Delta\sigma_{r,corr} \tag{3.6}$$

with

$$\Delta\sigma_{a,corr} = \frac{-4t_m E_m}{d_i}\left(\varepsilon_a + \frac{\varepsilon_v}{3}\right) \tag{3.7}$$

$$\Delta\sigma_{r,corr} = \frac{-4t_m E_m}{3d_i}\varepsilon_v \tag{3.8}$$

where E_m and t_m are respectively the elastic modulus at 10% strain and the thickness of the membrane and d_i is the initial diameter of the membrane. The corrections have been applied to all the tests even if it was found considerable only for the unreinforced specimens tested at low pressures or subjected to liquefaction.

e) Initial void ratio correction

When dealing with very loose specimens, particular attention is required for the estimation of the initial void ratio of the specimens. In this research it will be referred to as initial void ratio (e_c), the void ratio at the end of the isotropic consolidation stage prior to shearing.

The void ratio after fabrication (e_0) is subjected to many variations before the test starts after the consolidation stage. The main problems on estimating these variations arise from the stages in which it is not possible to record the variation of volume of the specimen. In the experimental campaign performed here, the modifications of the void ratio between fabrication and testing occur in the following stages:

a) cell placement;
b) filling the cell with water;
c) removal of the vacuum and application of 20 kPa cell pressure;
d) saturation of the specimen;
e) consolidation stage;
f) eventual phase of attachment of the extension system.

The variation of the volume during the last two stages (e and f) can be directly recorded through the volume gauge, since the specimen is fully saturated. However, estimation should be performed for assessing the variation in void ratio during the other stages (a to d).

Castro (1969) proposed a procedure to account for the densification of the specimen on the saturation stage based on the hypothesis of isotropic deformation of the sample. The same

procedure was adopted by Sladen et al.(1985) who remarked that the densification was increased by the percentage of fines in the specimen. Konrad (1990) proposed a method to maintain constant the diameter of the specimen during saturation; this implies that volumetric changes depend only on the axial deformation of the specimen. Verdugo and Ishihara (1996) used two different methods for estimating the variation of volume; the former based on measure of height and diameter of the specimen and the latter based on the quantity of water at the end of the test. Vaid and Syvathayalan (1996) assessed that the errors on the initial void ratio are directly proportional to the height and diameter of the specimen but inversely proportional to its size.

Ibraim (1998) investigated the variation of the void ratio before the consolidation stage in specimens fabricated with the same sand type and with the same size of the ones used in this investigation. The axial deformation of the specimens during phase (a) to (d) was measured and the volumetric variation was extrapolated supposing that the ratio between the volumetric and axial deformation is similar to the one measured during the isotropic consolidation. Ibraim (1998) found that for very loose specimen (e_0=1.019) the variation of void ratio during stages (a) – (d) was $\Delta e_{corr} = -0.034$. Due to the similarity of the tested specimens, the findings by Ibraim (1998) have been used in this research and his results have been considered applicable to the loosest specimens, while for the densest specimens it was supposed that no collapse of the void ratio took place in phases (a)–(d). For simplicity it was assumed that for the intermediate fabrication void ratios, the correction of the void ratio could be expressed by a linear relationship to give:

$$\Delta e_{corr} = -0.15(e_0 - 0.8) \text{ if } e_0 \geq 0.8 \qquad (3.9)$$

$$\Delta e_{corr} = 0 \text{ if } e_0 < 0.8 \qquad (3.10)$$

The application of this correction permits the determination of a unique critical state line in the υ-ln p' plane for unreinforced specimens as it will be shown in paragraph 5.4.1. This was not possible if the proposed correction was not applied. For the sake of simplicity and lack of experimental data the same correction will be applied to both unreinforced and reinforced specimens

CHAPTER 4

FIBRE ORIENTATION AND INITIAL TEST RESULTS

4.1 Introduction

Mixing sands with random discrete flexible fibres increases their strength and influences their deformation characteristics. However, fibres offer their contribution only when pulled in tension and it is not surprising that the orientation of the fibres within a specimen is found to be particularly important for the strength of reinforced soils (Jewell and Wroth, 1987; Palmeira and Milligan, 1989; Michałowski and Čermák, 2002): fibres are in general most influential when orientated in the same direction as tensile strains.

Since the domain of tensile strains varies with the loading conditions, it is impossible to universally define a most effective or optimum sought fibre orientation; the desirable fibre orientation is related to the particular geotechnical application and the future working conditions. However, it would be of particular interest to find a procedure for controlling or, at least, for assessing the distribution fibre orientation induced by the adopted mixing and sample formation procedure.

A new procedure for determining the fibre orientation distribution in reinforced sand specimens is outlined in this chapter. The procedure is applied to specimens similar to those used in the triaxial experimental investigation. They are prepared using the moist tamping technique which produces a soil-fibre fabric which might reproduce the soil structure resulting from compaction of reinforced soils in the field by dynamic compactor plates (Michalowsky, 2008). The orientation of fibres is found particularly anisotropic with a preferred near horizontal orientation. Since the method of sample fabrication procedure is expected to control the orientation of fibre distribution, the procedure is then applied to reinforced specimens prepared by moist vibration technique and a preferred horizontal fibre orientation is again found. However, small differences in the induced distribution of fibre orientation can be observed.

Performances of the specimens prepared with the two different techniques are compared with a series of conventional triaxial tests.

4.2 Distribution of fibre orientation

The non-uniformity of fibre orientations can affect sample stress-strain behaviour because of the consequent anisotropy. A fibre orientation distribution function may be used to describe this non-uniformity and also used as a modelling tool to explain some of the anisotropic constitutive features of reinforced samples when loaded (Michalowski and Čermák, 2002). One possible form for the fibre orientation distribution function is based on the notion that the distribution is axisymmetric with respect to the axis normal to the compacted layers, which for most practical cases is the vertical axis. Using the spherical coordinates shown in Fig.4.1, a generalised fibre orientation distribution function $\rho(\theta)$, which represents the volumetric concentration of fibres in an infinitesimal volume dV (Fig.4.1) having an orientation of angle θ above the horizontal, is of the form (Michalowski and Čermák, 2002):

$$\rho(\theta) = \overline{\rho}\left(A + C\left|\cos^n \theta\right|\right) \tag{4.1}$$

where $\overline{\rho}$ is the average volumetric concentration of the fibres and is defined as the total volume of fibres (V_f) per sample volume (V):

$$\overline{\rho} = V_f / V \tag{4.2}$$

and A, C and n are constants linked by the relationship:

$$C = \frac{1 - A}{\int_0^{\pi/2} \cos^{n+1}(\theta) \mathrm{d}\theta} \tag{4.3}$$

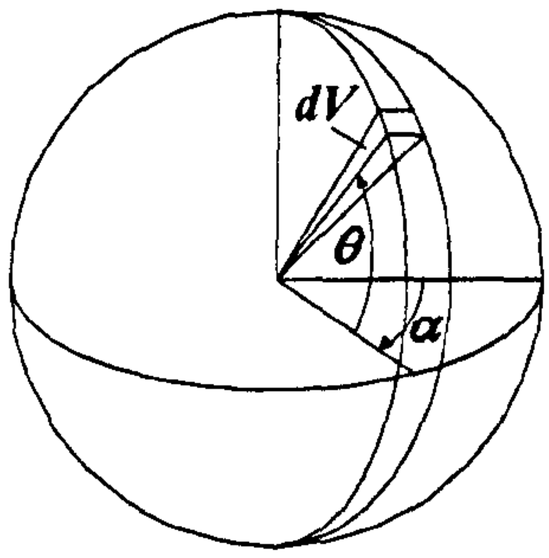

Fig. 4.1 Sphere and coordinates used to define the orientation distribution function

However, there are no particular restrictions on the choice of the $\rho(\theta)$ function as long as the following Eq. (4.4) is fulfilled:

$$\overline{\rho} = \frac{1}{V}\int_{V} \rho(\theta)\mathrm{d}V \tag{4.4}$$

A reference sphere, which has a radius R equal to half the fibre length ($l_f/2$) and contains only fibres which have a mid-point coinciding with the centre of the sphere, can be now defined. Eq.(4.4) can be expanded for this reference sphere by introducing $V = 4\pi R^3/3$ and $\mathrm{d}V = R^3\cos(\theta)\mathrm{d}\alpha\mathrm{d}\theta/3$ to show that the average volumetric concentration of fibres in the reference sphere is:

$$\overline{\rho} = \frac{1}{\frac{4}{3}\pi R^3}\int_{-\pi/2}^{\pi/2}\int_{0}^{2\pi} \rho(\theta)\frac{R^3}{3}\cos(\theta)\mathrm{d}\alpha\mathrm{d}\theta \tag{4.5}$$

Within this reference sphere, or in a sample of any shape with fibre orientation distribution described using Eq. (4.1), the ratio (P) of the volume of fibres having orientations within an angle $\pm\beta$ from the horizontal to the total volume of fibres is:

$$P = \frac{1}{2\overline{\rho}}\int_{-\beta}^{\beta} \rho(\theta)\cos(\theta)\mathrm{d}\theta \tag{4.6}$$

4.3 Analytical solution for number of fibres intersecting a plane

For a sample with dimensions much larger than the fibre length it is reasonable to assume that the mid-points of all fibres are uniformly distributed throughout the sample. It is also assumed that the fibres themselves have an orientation distribution defined by $\rho(\theta)$ in Eq. (4.1) - that is axisymmetric with respect to the vertical axis. Outlined below is the analytical procedure for determining the number of fibres intersecting finite areas on both vertical and horizontal planes cut through the sample.

To use a procedure similar to that outlined in this work to define a fibre orientation distribution function other than Eq. (4.1), or to check the validity of Eq. (4.1), it would be necessary to obtain analytical solutions for the number of fibres intersecting planes in addition to those orientated vertically and horizontally. This is not the objective of this investigation. Rather, Eq. (4.1) is assumed to be applicable and the focus is on the analytical procedure.

The first part of the procedure involves determining the volumes of fibres intersecting both vertical and horizontal planes cut through the reference sphere and dividing these by the total volume of the sphere. The procedure is then extended through integration by considering all the points within a sample for which a fibre (and therefore the reference sphere that models the presence of this fibre) can potentially intersect a finite area on the plane cut through the sample.

4.3.1 Vertical plane

Consider first the reference sphere described above when its centre is located at a distance b from a vertical plane (Fig.4.2a). The volume of the fibres belonging to the parts of the sphere which are cut by the vertical plane divided by the total volume of the sphere is:

$$\hat{\rho} = \frac{1}{V_{sphere}} \int_{V_1} \rho(\theta) \mathrm{d}V \qquad \text{or} \tag{4.7}$$

$$\hat{\rho} = \frac{1}{V_{sphere}} \left(\int_{-\arccos(b/R)}^{\arccos(b/R)} \int_{-\arccos(b/(R\cos(\theta))}^{\arccos(b/(R\cos(\theta))} \rho(\theta) \frac{R^3}{3} \cos(\theta) \mathrm{d}\alpha \mathrm{d}\theta + \int_{-\arccos(b/R)}^{\arccos(b/R)} \int_{\pi-\arccos(b/(R\cos(\theta))}^{\pi+\arccos(b/(R\cos(\theta))} \rho(\theta) \frac{R^3}{3} \cos(\theta) \mathrm{d}\alpha \mathrm{d}\theta \right)$$

where V_1 is the volume of the two cones plus the two spherical segments (Fig.4.2a) contained within the angle defined by the intersection between the plane and the sphere, and $V_{sphere} = 4\pi R^3/3 = \pi l_f{}^3/6$ is the volume of the sphere. From the symmetry of the cones and spherical segments, the terms between brackets in the expanded part of Eq.(4.7) can be condensed and $\hat{\rho}$ can be expressed as:

$$\hat{\rho} = 2\frac{1}{V_{sphere}} \int_{-\arccos(b/R)}^{\arccos(b/R)} \int_{-\arccos(b/(R\cos(\theta)))}^{\arccos(b/(R\cos(\theta)))} \rho(\theta)\frac{R^3}{3}\cos(\theta)\mathrm{d}\alpha\mathrm{d}\theta \tag{4.8}$$

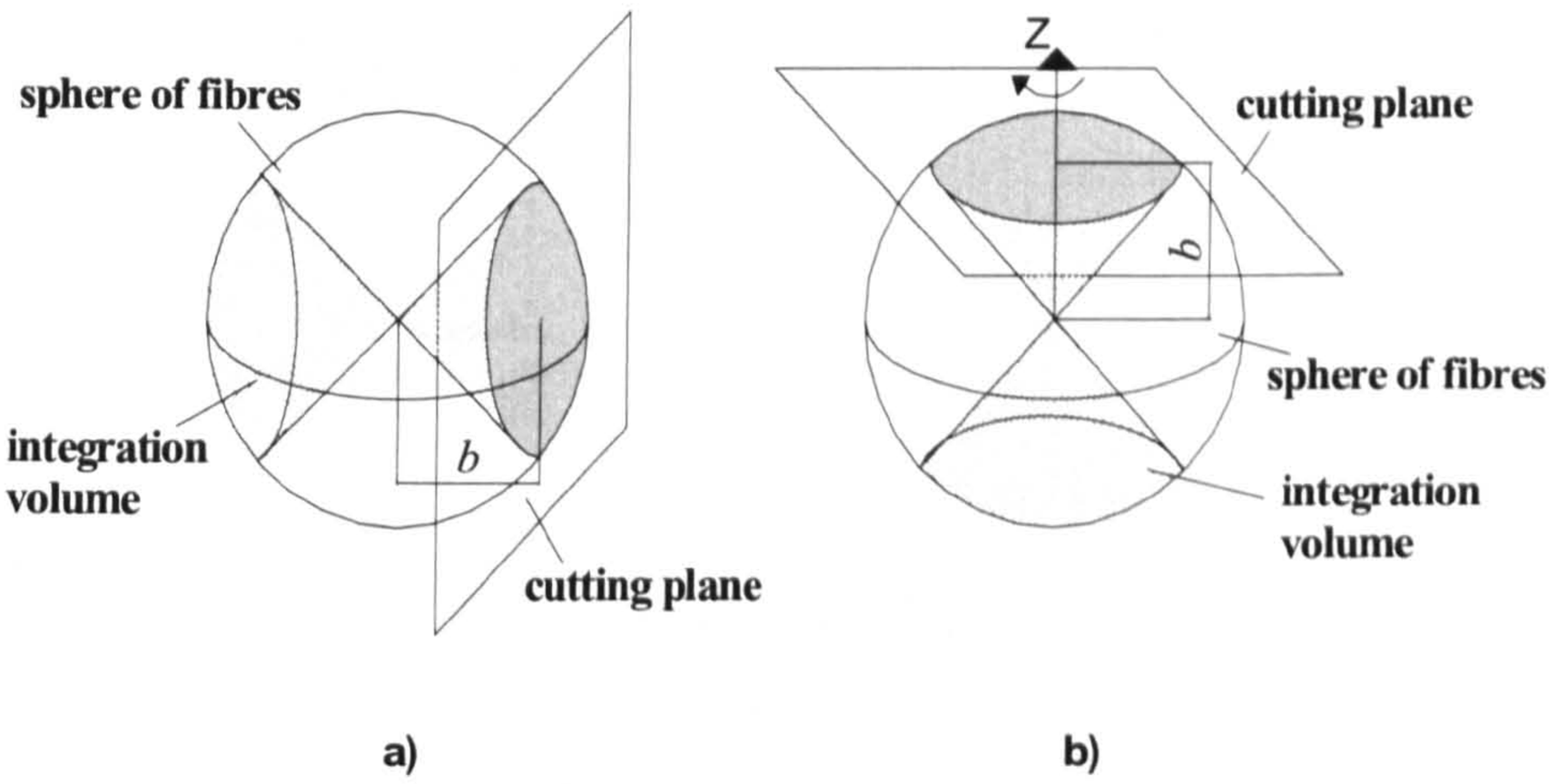

Fig. 4.2 Partial volume of sphere containing fibres intersecting (a) a vertical plane and (b) a horizontal plane at a distance b from the sphere centre

Consider next a rectangular area with edge lengths l_1 and l_2 that is located on a vertical plane that cuts a sample (of any shape) in which fibre midpoints are distributed uniformly throughout the sample and orientated according to Eq.(4.1). The total volume of fibres $\left(V^V{}_{tot}\right)$ intersecting this area is calculated by integrating $\hat{\rho}$ given in Eq.(4.8) over a volume with the shape of the parallelepiped with edges l_1 and l_2 and width $l_f/2$ (Fig.4.3a), and doubling it to account for fibres on both sides of the plane, to give:

$$V^{V}{}_{tot} = 4l_1 l_2 \int_0^{l_f/2} \left(\frac{1}{V_{sphere}} \int_{-\arccos(b/R)}^{\arccos(b/R)} \int_{-\arccos(b/(R\cos(\theta)))}^{\arccos(b/(R\cos(\theta)))} \rho(\theta) \frac{R^3}{3} \cos(\theta) \mathrm{d}\alpha \mathrm{d}\theta \right) \mathrm{d}b \qquad (4.9)$$

b values between 0 and $-l_f/2$ are not considered in the integration in order to avoid the inclusion of each fibre twice. This integration effectively accounts for all the points within the sample for which a fibre can potentially intersect the finite area on a plane cut through the sample.

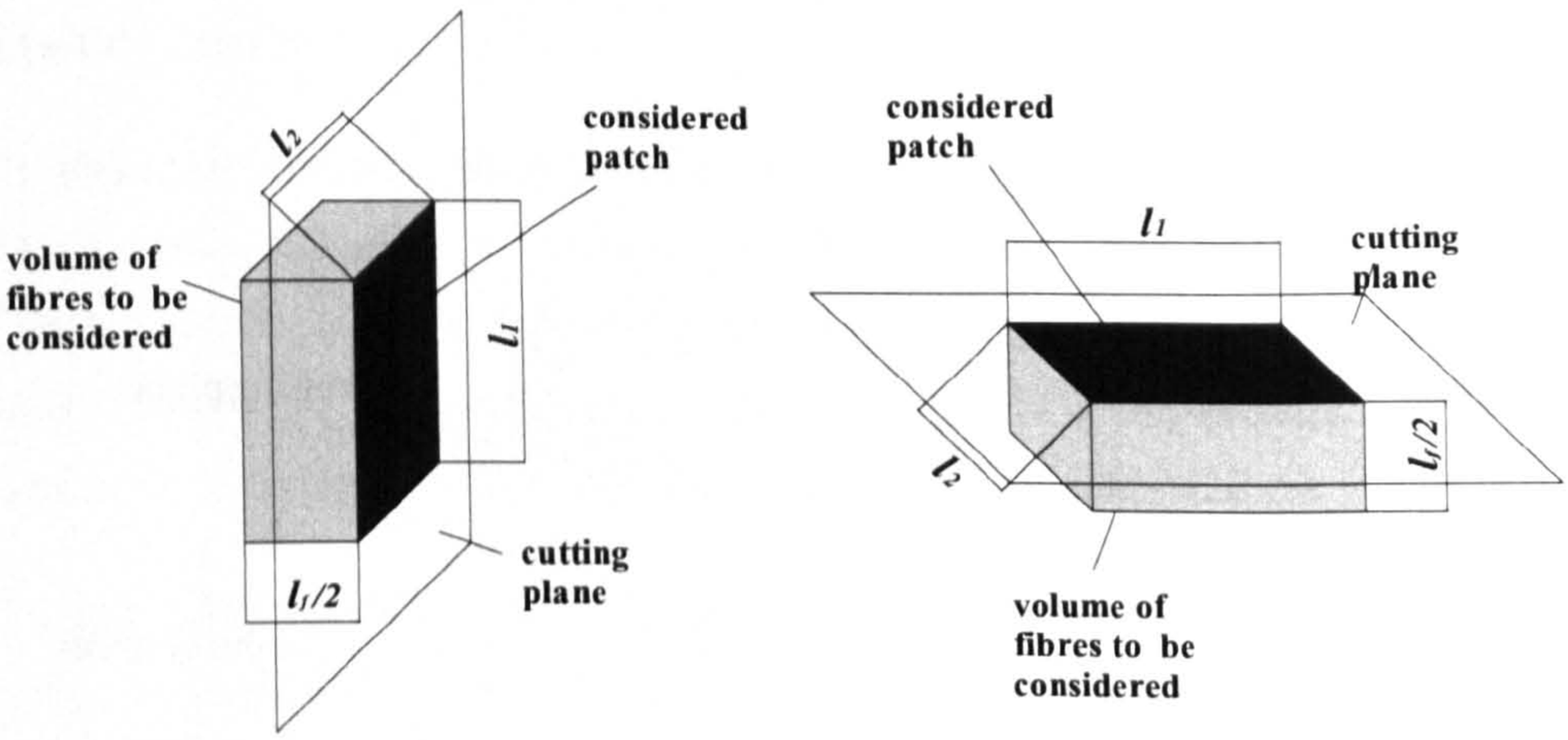

Fig. 4.3 Parallelepiped used to determine the number of fibres intersecting (a) a vertical plane and (b) a horizontal plane cut through a sample

The total number of fibres $\left(N^{V}{}_{tot}\right)$ can be calculated by dividing $V^{V}{}_{tot}$ by the volume of a single fibre $\left(V_{1f}\right)$:

$$N^{V}{}_{tot} = \frac{V^{V}{}_{tot}}{V_{1f}} \qquad (4.10)$$

Note that it is impossible to go beyond the first step of the integral in Eq.(4.9) once the limit $\alpha = \arccos\left(b/\left(R\cos\left(\theta\right)\right)\right)$ is introduced into the function to be integrated. However, α can be very closely approximated (for $0 \le \theta \le \pi/2$ and $0 \le b/R \le 1$) by α^* (Fig. 4.4) defined as:

$$\alpha^* = \frac{c_1}{\theta - c_2} + c_2 \tag{4.11}$$

where $c_1 = 0.53\frac{b}{R}\left(1-\frac{b}{R}\right)$ and $c_2 = \left(\arccos\left(\frac{b}{R}\right) + \left(\arccos^2\left(\frac{b}{R}\right) + 4c_1\right)^{1/2}\right)\Big/2$.

α^* can be substituted into Eq.(4.9) in place of $\arccos(b/(R\cos(\theta)))$, although it is necessary to take advantage of symmetry to avoid using Eq.(4.11) outside the range of θ values for which it is valid, to give:

$$N^V{}_{tot} = \frac{16 l_1 l_2}{V_{1f}} \int_0^{l_f/2} \left(\frac{1}{V_{sphere}} \int_0^{\arccos(b/R)} \int_0^{\alpha^*} \rho(\theta) \frac{R^3}{3} \cos(\theta) \, d\alpha \, d\theta \right) db \tag{4.12}$$

which can be readily evaluated.

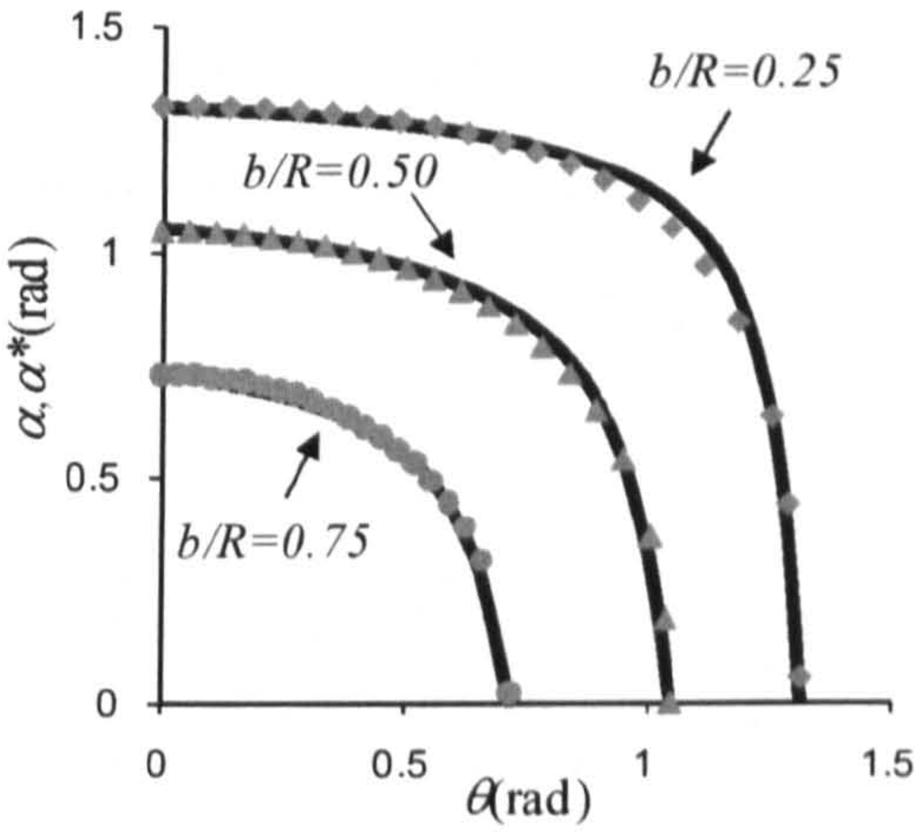

Fig. 4.4 Approximation of the function $\alpha = \arccos(b/(r\cos(\theta))$ for different values of b/R. Open symbols represents the exact relationship and the solid lines represent approximation with Eq.(4.11)

4.3.2 Horizontal plane

The determination of the number of fibres intersecting a finite area on a horizontal plane is much simpler. For a horizontal plane cut through the reference sphere the volume of the cones plus spherical segments can be treated as a rotational solid around the vertical axis of symmetry (Fig. 4.2b). It follows that the integral required to calculate the volume of fibres intersecting the finite area on a horizontal plane cut through a sample $\left(V^H{}_{tot}\right)$ is of the form:

$$V^H{}_{tot} = 4l_1 l_2 \int_0^{l_f/2} \left(\frac{1}{V_{sphere}} \int_{\frac{\pi}{2}-\arccos(b/R)}^{\frac{\pi}{2}} \int_0^{2\pi} \rho(\theta) \frac{R^3}{3} \cos(\theta) \mathrm{d}\alpha \mathrm{d}\theta \right) \mathrm{d}b \tag{4.13}$$

which can be readily evaluated. The total number of fibres is:

$$N^H{}_{tot} = \frac{V^H{}_{tot}}{V_{1f}} = 4\frac{l_1 l_2}{V_{1f}} \int_0^{l_f/2} \left(\frac{1}{V_{sphere}} \int_{\frac{\pi}{2}-\arccos(b/R)}^{\frac{\pi}{2}} \int_0^{2\pi} \rho(\theta) \frac{R^3}{3} \cos(\theta) \mathrm{d}\alpha \mathrm{d}\theta \right) \mathrm{d}b \tag{4.14}$$

For a given value of average volumetric concentration of fibres $\bar{\rho}$, it can be shown using Eq.(4.14) and (4.12) that $N^H{}_{tot}$ and $N^V{}_{tot}$ depend on l_f and therefore d_f. However, the ratio $N^H{}_{tot}/N^V{}_{tot}$ is independent of l_f and d_f.

4.3.3 Verification

Verification of Eq.(4.12) and Eq.(4.14) can be performed by considering a very simple case. Imposing $A = 1.0$ in Eq.(4.1) makes the fibre orientation distribution function constant (isotropic) for all θ:

$$\rho(\theta) = \bar{\rho} \tag{4.15}$$

For this case, from symmetry, the numbers of fibres intersecting finite areas of equal size on horizontal and vertical planes should be the same.

Substituting $\overline{\rho} = 0.0275\%$ (that is 1 fibre per 1000 mm^3 of sample) and choosing dimensions $l_1 = 10$ mm and $l_2 = 10$ mm for the areas on the cutting planes in Eq. (4.12) and Eq. (4.14), the number of fibres intersecting the area on the plane, whether it be vertical or horizontal, is 1.75, as expected. As an analytical solution for the number of fibres crossing a finite area it is not necessarily an integer. The *potential* number of fibres intersecting the area on the plane from only one of its sides is 1.75 (that is the number of fibres having their mid-points in the parallelepiped with edges $l_1 = 10$ mm, $l_2 = 10$ mm and width $l_f/2 = 17.5$ mm). As demonstrated by Maher and Gray (1990), the *actual* number of fibres that intersect the area on the plane is half the *potential* number of fibres belonging to this parallelepiped. Therefore, considering both sides of the plane, the number of intersecting fibres is 1.75. This result is equivalent to the one obtained using Maher and Gray's Eq.(5):

$$N_s = N_v \frac{L}{2} \qquad \text{(Maher and Gray's Eq.(5))}$$

where N_s is the average number of fibres crossing a unit area, N_v is the average number of fibres per unit volume and L is the length of the fibres.

4.4 Application to moist tamped specimen

4.4.1 Sample preparation for fibre orientation study

Specimens have been prepared in three equal layers according to the procedure illustrated in paragraph 3.5.1. but a cylindrical Perspex mould with diameter 92 mm and height 75 mm has been used. The counting process, which will be introduced later on in this chapter, was found extremely difficult for fibrillated fibres (type 2) due to their small diameter, therefore only type (1) and type (3) fibres have been used for the preparation of the reinforced specimens. For fibre type (1), a further two samples of 70 mm height were prepared using a similar procedure but in two equal layers. Sand void ratios e equal to 0.90 and 0.92 were achieved, considering the volume of the fibres to be part of the volume of the voids, corresponding to a loose condition (relative density index I_D of 21% and 26% respectively).

The amounts of fibres added as a percentage of dry mass of sand were 0.05 %, 0.15 % and 0.25 % for fibre type (1) and 0.15 %, 0.25 % and 0.50 % for fibre type (3) as listed in Tab. 4.1. The corresponding values of the average volumetric concentration of the fibres $\overline{\rho}$, determined using a sand particle density of 2.65 x 10^{-3} g/mm^3 and a fibre density of 0.91 x 10^{-3} g/mm^3, are also reported. Since the counting of fibres was visually performed without using any scanning microscope, smaller amounts for fibres type (1) were employed because some difficulties arose in the counting procedure when a consistent amount of fibres was mixed.

After preparation the samples were saturated by immersing them (in their mould) in de-aired water. A connection at the base of the mould with a metal plate was not watertight so that water could seep slowly upwards through the sample without disturbing it. The mould and sample were then gently lifted out of the water and placed on a bench. Most of the water inside the samples then leaked back out of the non-watertight mould. However, because of the existence of some modest capillary suction inside the samples, helped by the reinforcing effect of the fibres, it was possible to lift the mould off the samples without affecting their shape. The samples were then placed in a freezer for 24 hours. The freezing process caused some of the samples to swell locally at their top, but measurements along the rest of the sample length confirmed that the bulk of the sample was undisturbed.

The frozen samples were then cut in vertical and horizontal directions using a bench-saw. It was necessary to remove a thin layer of sand from the cut plane using a rasp in order to remove the residues of the cutting process. Vertical cuts passed through the vertical axis of symmetry, horizontal cuts were made through the centres of the horizontal layers.

Fig. 4.5 Image of the cut surface on a specimen reinforced with fibre type (1)

For specimen reinforced with fibre type (1), the fibres intersecting an area 20 mm x 20 mm on the cut plane were counted. This was made easier by staining the fibres prior to mixing. Counting was repeated for different area locations on each cut plane, ensuring the areas did not overlap. Moving the areas ensured that a large part of cut plane was covered. However, the area locations were kept away from the sample edges as sample dimensions were only about twice the fibre length and there may have been localised non uniformities in the fibre mid-point distributions near the edges. The fibre counting procedure for each area was performed visually with the help of digital images (Fig.4.5). For the unavailability of any electronic image analysis tool which could automatically perform the counting of fibres, difficulties in visual counting arose when the fibre content by dry mass was 0.25 %, as fibres tended to accumulate into groups. It is clear that the counting procedure can be improved by employing the use of microscope or particular digital image analysis software.

Because of their bigger dimension, the counting process for fibre type (3) did not revealed any difficulty and it was done over the whole cut section of the specimen (Fig. 4.6). However the results shown in the Table 4.1 have been converted to an equivalent area of 20mm x 20mm for ease of comparison.

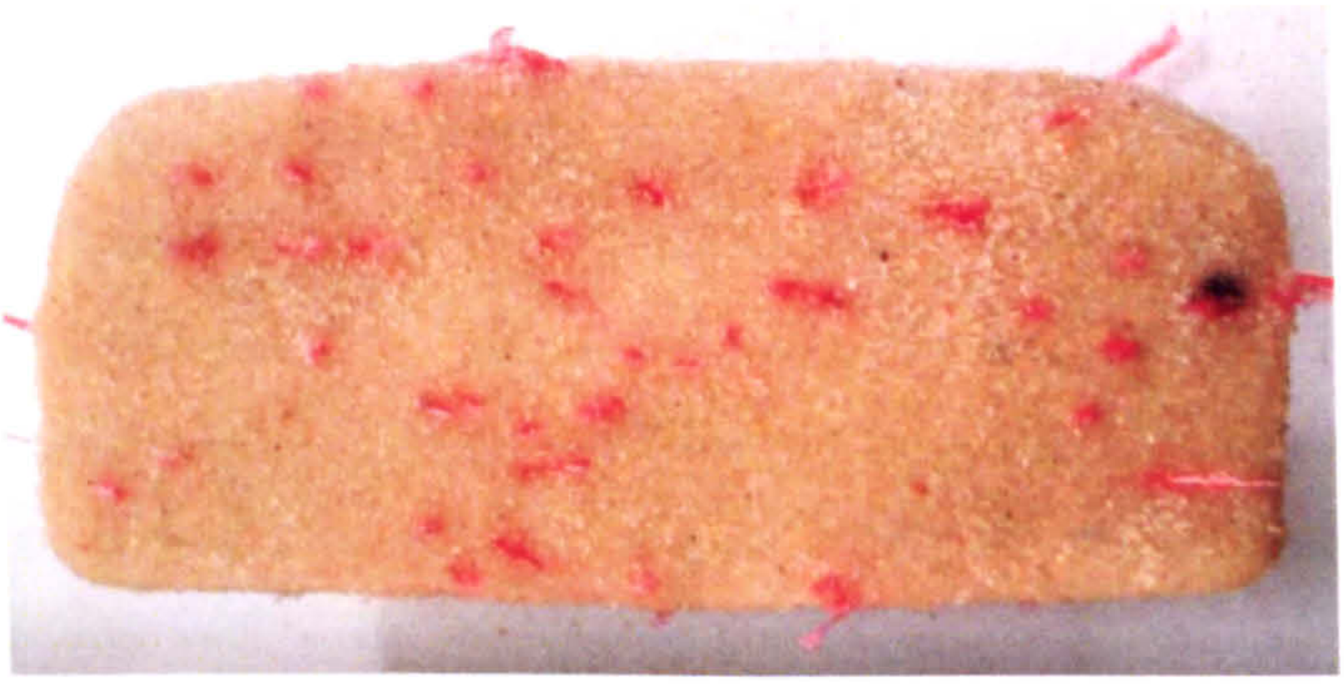

Fig. 4.6 Image of the cut surface on a specimen reinforced with fibre type (3)

4.4.2 Results

The fibre orientation distribution in Eq.(4.1) requires two of the constants A, C and n to be specified. This can be done by adjusting A and n (C is automatically evaluated using Eq.(4.3)) such that the solutions of Eq.(4.12) and Eq.(4.14) closely match the actual number of fibres intersecting vertical and horizontal planes cut through a sample. A perfect fit may not be possible as it is necessary for n to be an integer in the integration. The procedure can be simplified even further by assuming $A = 0$, meaning that no fibres have a vertical orientation, so that only n needs to be adjusted.

Tab. 4.1 presents the results for eight samples reinforced with fibre type (1) and six samples reinforced with fibre type (3), vertical and horizontal planes, and a range of $\bar{\rho}$ values. Also listed are the parameters n and C (for $A = 0$) that provide a reasonable fit between Eq. (4.12) and Eq. (4.14) and the average number of fibres counted per 20 mm x 20 mm area. The values of $N^{V}{}_{tot}$ and $N^{H}{}_{tot}$ measured for samples with identical $\bar{\rho}$ and same fibre type are very similar despite the slight errors expected during the counting procedure. However, subtle differences in $N^{V}{}_{tot}$ and $N^{H}{}_{tot}$ measurements lead to larger differences in $N^{V}{}_{tot}/N^{H}{}_{tot}$ ratios.

For samples reinforced with fibre type (1), the ratio $N^{V}{}_{tot}/N^{H}{}_{tot}$ varies from 1.90 to 2.63 which correspond to values of n from 4 to 8. The best-fit integer n values correspond to reasonably similar fibre orientation distributions, as can be seen in Fig. 4.7 where curves of $\rho(\theta)/\bar{\rho}$ versus θ are presented for $n = 4$, 5, 6, 7 and 8. Considering the results for all samples, the moist

tamping technique appears to produce a N^V_{tot}/N^H_{tot} ratio of about 2.11, which is independent of $\bar{\rho}$ for the range of fibre contents considered. Only the results for sample MT05F1b differed from the average N^V_{tot}/N^H_{tot} ratio of 2.11 by more than 10%. Therefore for specimen reinforced with fibre type (1), the values $A = 0$ and $n = 6$ (corresponding to $N^V_{tot}/N^H_{tot} = 2.17$, closest to the average value for the samples prepared here) have been adopted.

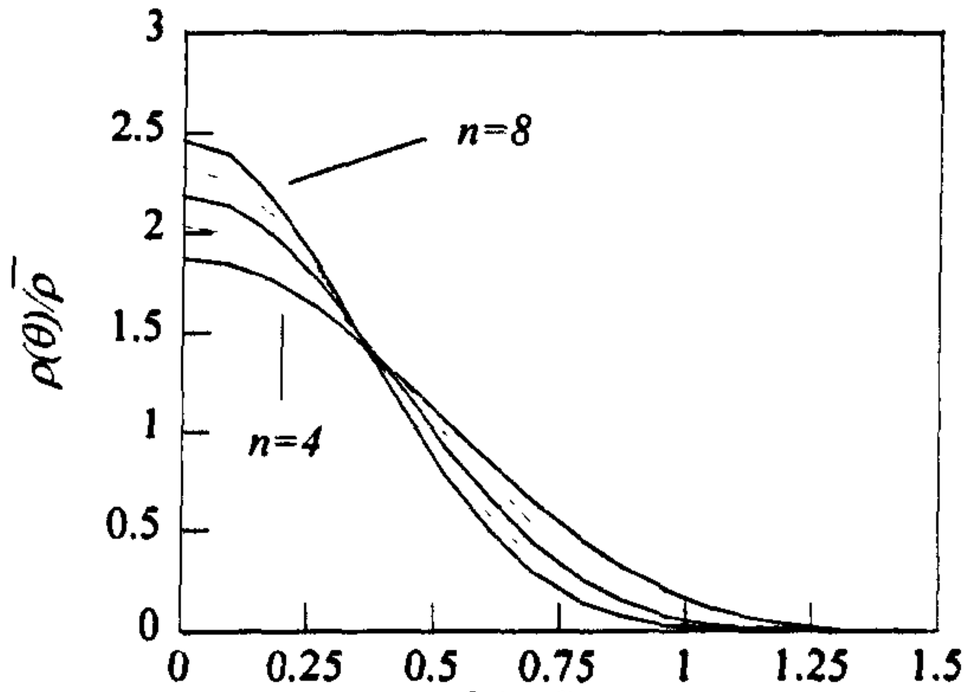

Fig. 4.7 Fibre orientation distribution according to Eq.(4.1) for $A = 0$ and a range of best-fit integer n values (n= 4, 5, 6, 7 and 8) determined for the samples reinforced with fibre (1)

Tab. 4.1 Sample details, average numbers of fibres intersecting vertical and horizontal planes and the fitting parameters used in the analytical prediction of the fibre orientation distributions for reinforced specimens prepared with MT

Sample	Fibre type	Height spec.	Diam. spec.	Void ratio **	Fibre content (w_f)	Average volumetric concentration of fibres $(\bar{\rho})$	Ave. no. fibres intersecting a 20 mm x 20 mm area			Orientation parameters			Analytical prediction		
		mm	mm				$N^V{}_{tot}$	$N^H{}_{tot}$	$\frac{N^V{}_{tot}}{N^H{}_{tot}}$	A	n	C	$N^V{}_{tot}$	$N^H{}_{tot}$	$\frac{N^V{}_{tot}}{N^H{}_{tot}}$
MT05F1a	1	75	92	0.90	0.05 %	0.077 %	20.61	10.88	1.90	0.0	4.0	1.88	22.71	12.19	1.86
MT05F1b	1	75	92	0.90	0.05 %	0.077 %	24.56	9.33	2.63	0.0	8.0	2.46	23.43	9.60	2.45
MT15F1a *	1	70	92	0.92	0.15 %	0.228 %	65.69	31.88	2.06	0.0	5.0	2.04	68.20	33.72	2.03
MT15F1b*	1	70	92	0.92	0.15 %	0.228 %	63.33	28.75	2.28	0.0	7.0	2.33	68.78	31.68	2.31
MT15F1c	1	75	92	0.92	0.15 %	0.228 %	62.11	32.19	1.93	0.0	4.0	1.88	67.44	36.20	1.87
MT15F1d	1	75	92	0.92	0.15 %	0.228 %	57.5	29.89	1.92	0.0	4.0	1.88	67.44	36.20	1.87
MT15F1e	1	75	92	0.90	0.15 %	0.230 %	60.83	30.00	2.03	0.0	5.0	2.04	68.92	34.07	2.03
MT25F1a	1	75	92	0.90	0.25 %	0.383 %	99.31	46.95	2.12	0.0	5.0	2.04	114.88	56.79	2.03
MT15F3a	3	75	92	0.90	0.15 %	0.230 %	3.97	0.95	4.20	0.0	27	4.26	4.35	1.03	4.22
MT15F3b	3	75	92	0.90	0.15 %	0.230 %	4.13	1.25	3.30	0.0	16	3.34	4.31	1.30	3.31
MT25F3a	3	75	92	0.90	0.25 %	0.383 %	3.80	1.11	3.42	0.0	17	3.43	7.18	2.12	3.40
MT25F3b	3	75	92	0.90	0.25 %	0.383 %	6.52	1.51	4.30	0.0	28	4.33	7.26	1.69	4.30
MT50F3a	3	75	92	0.90	0.50 %	0.766 %	11.69	2.69	4.35	0.0	29	4.41	14.64	3.35	4.37
MT50F3b	3	75	92	0.90	0.50 %	0.766 %	12.46	3.29	3.78	0.0	21	3.79	14.55	3.88	3.75

* samples prepared in two equal layers and less than eight areas were used in the counting procedure

** fibres are considered as part of the voids.

For specimen reinforced with fibre type (3), the ratio $N^V{}_{tot}/N^H{}_{tot}$ is quite similar for all the samples. The ratio varies from 3.30 to 4.35 which correspond to values of n from 16 to 29. The variability of the results for these fibres is greater than for fibres type (1) and this can be explained by the much smaller number of fibres (3) in specimen reinforced with the same fibre content. However, the best-fit integer n values still correspond to reasonably similar fibre orientation distributions as shown in Fig. 4.8. Considering the results, an average ratio $N^V{}_{tot}/N^H{}_{tot}$ of 3.89 was chosen. Therefore, for specimen reinforced with fibre type (3), the values $A = 0$ and $n = 23$ (corresponding to $N^V{}_{tot}/N^H{}_{tot} = 3.92$, closest to the average value for the samples prepared here) have been adopted.

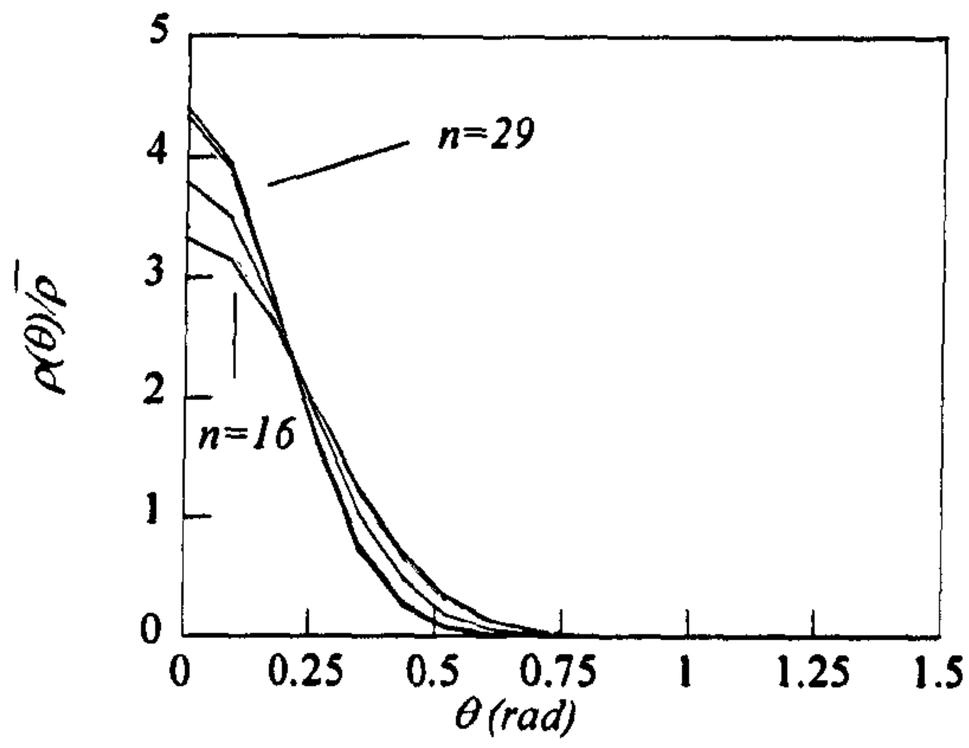

Fig. 4.8 Fibre orientation distribution according to Eq.(4.1) for $A = 0$ and a range of best-fit integer n values (n= 16, 17, 21, 27, 28, 29) determined for the samples reinforced with fibre (3)

Graphical representation of the determined fibre orientation distributions for the analysed reinforced specimens is given in Fig. 4.9. The function $\rho(\theta)/\bar{\rho}$ has been used for the vertical axis while the orientation θ from the horizontal is plotted on the horizontal axes. An assumed isotropic orientation distribution (A=1.0) is also plotted as a reference. Substantial differences are observed. The orientation distribution for both type of fibres are far from isotropic, showing both a clear preferred horizontal orientation of fibres. Specimens reinforced with platy fibres presented a more pronounced near horizontal distribution. Employing Eq.(4.6), it can be calculated that 86% of fibres type (1) and even 99% of fibres type (3) rest between $\pm 30°$ of the

horizontal. The higher fibre length/layer height ratio for the platy fibres may probably explain these differences in orientation. Figure 4.9 presents the distributions for A = 1.0 (isotropic), A = 0 and n = 6 and A = 0 and n= 23 in another plane where substantial differences are also observed.

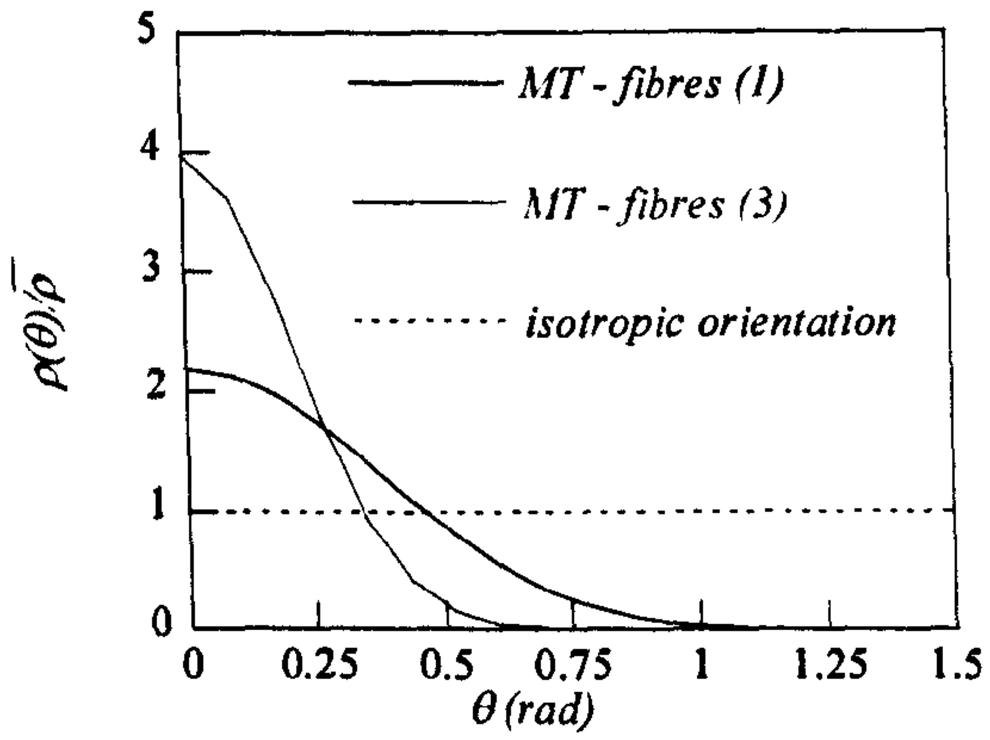

Fig. 4.9 Fibre orientation distribution according to Eq.(4.1) determined for samples reinforced with fibre (1) (A = 0 and n = 6) and with fibre (3) (A = 0 and n = 23) prepared with MT technique, compared with an isotropic orientation distribution

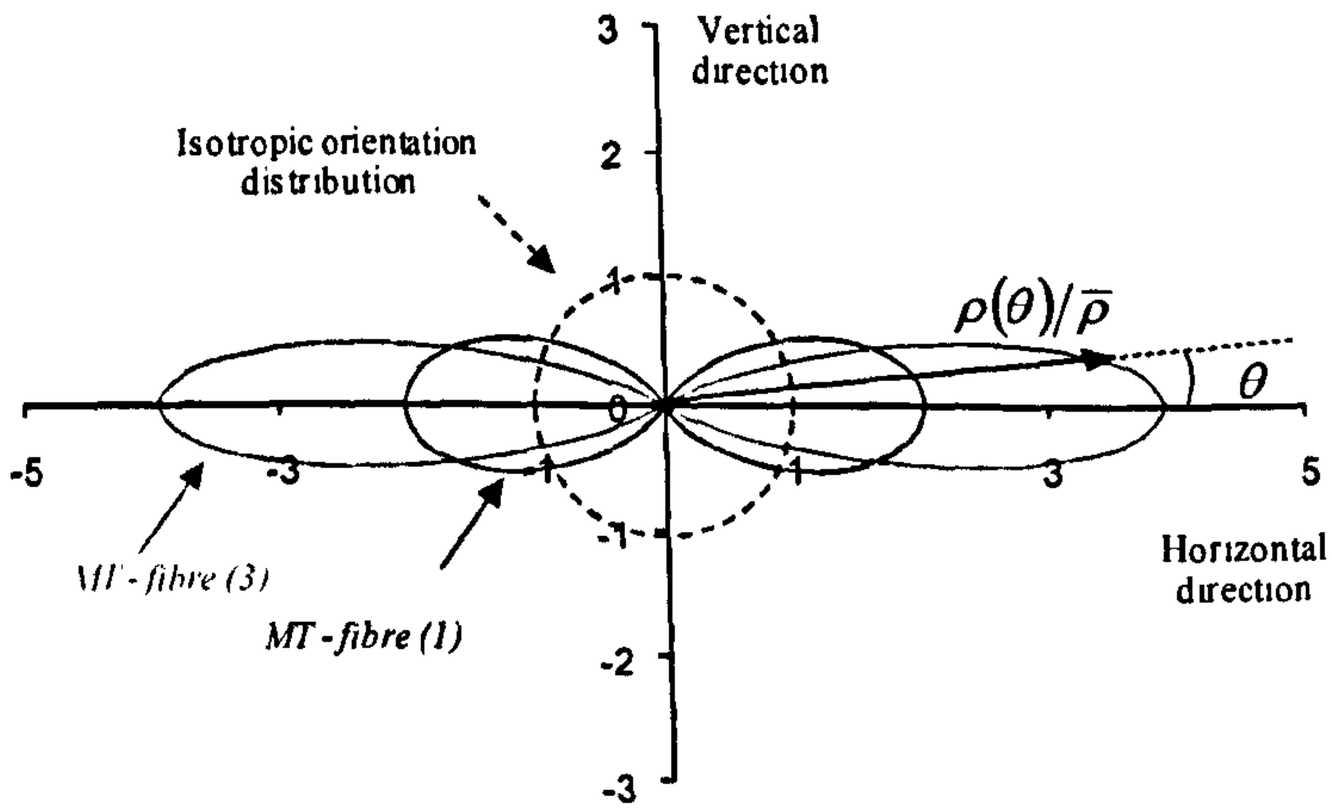

Fig. 4.10 Fibre orientation distribution according to (1) for A = 0 and n = 6 compared with an isotropic orientation distribution

4.5 Application to moist vibrated specimens

4.5.1 Motivations

A strongly anisotropic orientation of fibres such as the one produced by moist tamping may result in a pronounced anisotropy of strength for the composite materials. However, considering that the stress state within a soil mass is rarely axisymmetric and continuous rotations of principal axes are expected to occur along a potential failure surface of an embankment or throughout the soil during changes of loading, particularly if a geotechnical structure is subjected to seismic excitation, there may be a real concern about the suitability of the MT technique for certain applications. A more isotropic distribution orientation of fibre orientation (and maybe a resultant isotropy of strength for the composite material) may be the more desirable for such loading conditions. Therefore, a new fabrication procedure based on the moist vibration (MV), that may resemble the compaction in the field by vibration, is proposed here and its influence on the orientation of fibres is investigated.

4.5.2 Specimen preparation

As for the moist tamping technique, in the proposed moist vibrated technique there are two critical stages when fibre-reinforced specimens are prepared in the laboratory: mixing and formation. The mixing requires the addition of some amount of water to mix more efficiently the sand with the fibres and to prevent the segregation of fibres. The amount of water used was chosen following the experimental determination of water content (w) - void ratio (e) relationships for Hostun RF sand. Unreinforced specimens were investigated as were reinforced specimens with fibre contents (w_f) of 0.3% and 0.5% by dry weight of soil (fibre type 1). All the specimens had the same amount of dry sand and were subjected to identical amounts of vertical vibration energy using a vibratory sieve shaker with a frequency between 50 and 60Hz. The obtained relationships are presented in Figure 4.11. The densest state is achieved for dry specimens but segregation of fibres was observed during the tests. For moist specimens, the achievable soil density does not change when the water content varies between about 10% and 20% as also observed by Bement and Selby (1997). The relationships show that a less dense

packing is obtained as the quantity of fibres is increased. It was considered reasonable to use a water content (w) of 10% for the mixing of fibres and sand when using the MV technique.

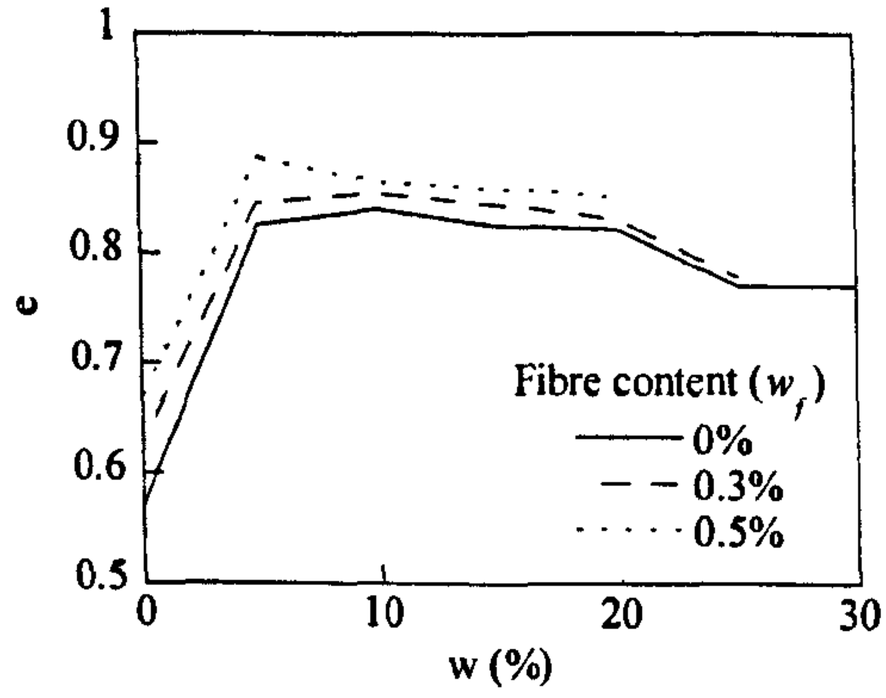

Fig. 4.11 Maximum void ratio (e) versus water content (w) using vertical vibration for unreinforced and reinforced specimens (0.3% and 0.5% of fibres by dry unit weight of sand).

The mixed material was delicately placed into a transparent cylindrical mould (inner diameter 92 mm). Then, the mould was placed into the vibratory device and the material was vibrated in the mould until the soil reached a height of 70mm. Visual inspection through the transparent mould ensured that no macro voids were created by the vibration process (Fig.4.12). Particular attention was given to the achievement of an even and flat top surface. To do this a guided light-weight cap was placed on the top of the specimen prior to vibration (Fig. 4.12).

Because some difficulties arose on the counting process of the thinnest fibres, only specimen reinforced with fibre type (1) and (3) have been prepared as for the moist tamping technique. Three specimens have been prepared for each type of reinforcement and the fibres contents have been chosen consistently with the specimen described in section 4.4 to enable the comparison of the results between the two different fabrication methods. A list of the investigated samples is given in Table 4.2.

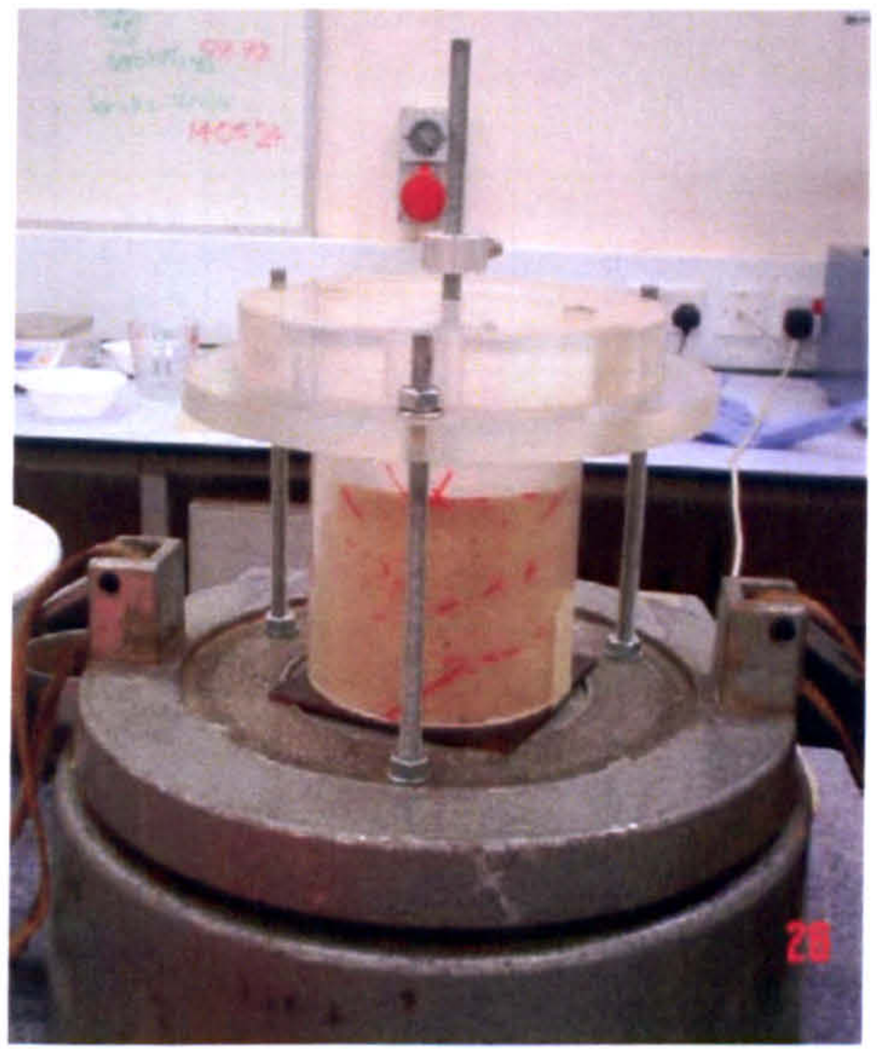

Fig. 4.12 Vibration phase for fabricating specimens reinforced with fibre type (3)

4.5.3 Results

Similar to specimens prepared with the moist tamping technique, 8 different non-overlapping areas (dimensions 20mm x 20mm) were considered for each section of specimens reinforced with fibres (1). Measured average values are reported in Table 4.2. For fibres (3), the counting was performed over the whole cut section but the results shown in the Table 4.2 have been converted to an equivalent area of 20mm x 20mm for ease of comparison.

The same form of the orientation distribution as described in Eq.(4.1) has been adopted. Again, the parameter A in Eq.(4.1) has been set equal to zero and only the parameter n has been calibrated against the experimental values (C can be easily obtained using Eq. (4.4)). The values of n and C are listed in Table 4.2.

Tab. 4.2 Sample details, average numbers of fibres intersecting vertical and horizontal planes and the fitting parameters used in the analytical prediction of the fibre orientation distributions for reinforced specimens prepared with MV

Sample	Fibre type	Height spec.	Diam. spec.	Void ratio*	Fibre content (w_f)	Average volumetric concentration of fibres $(\bar{\rho})$	Ave. no. fibres intersecting a 20 mm x 20 mm area			Orientation parameters			Analytical prediction		
		mm	mm				$N^V{}_{tot}$	$N^H{}_{tot}$	$\frac{N^V{}_{tot}}{N^H{}_{tot}}$	A	n	C	$N^V{}_{tot}$	$N^H{}_{tot}$	$\frac{N^V{}_{tot}}{N^H{}_{tot}}$
MV05F1a	1	75	92	0.90	0.05 %	0.077 %	20.45	8.70	2.35	0.0	7.0	2.33	22.93	10.56	2.31
MV15F1a	1	75	92	0.90	0.15 %	0.230 %	70.30	37.30	1.88	0.0	4.0	1.88	68.13	36.57	1.86
MV25F1a	1	75	92	0.90	0.25 %	0.383 %	104.40	54.60	1.91	0.0	4.0	1.88	113.55	60.95	1.86
MV15F3a	3	75	92	0.90	0.15 %	0.230 %	2.78	1.38	2.01	0.0	5.0	2.04	4.13	2.04	2.03
MV25F3a	3	75	92	0.90	0.25 %	0.383 %	4.35	2.05	2.13	0.0	6.0	2.19	7.00	3.22	2.17
MV50F3a	3	75	92	0.90	0.50 %	0.766 %	6.28	3.34	1.88	0.0	4.0	1.88	13.73	7.37	1.86

* fibres are considered as part of the voids

For samples reinforced with fibre type (1), the ratio $N^V{}_{tot}/N^H{}_{tot}$ varies from 1.88 to 2.33 which correspond to values of n from 4 to 7. The average value of the ratio $N^V{}_{tot}/N^H{}_{tot}$ is 2.04. Results of the orientation distribution are very similar to those obtained on specimens prepared with the MT, although the orientation of fibres seems slightly less anisotropic. Therefore, the values $A = 0$ and $n = 5$ (corresponding to $N^V{}_{tot}/N^H{}_{tot} = 2.03$, closest to the average value for the samples prepared here) have been adopted for MV specimens reinforced with fibres (1).

For samples reinforced with fibres type (3), the ratios $N^V{}_{tot}/N^H{}_{tot}$ show different values from the results on tamped specimens. An average value $N^V{}_{tot}/N^H{}_{tot}$ of 2.04 can be selected and the values $A = 0$ and $n = 5$ can be adopted for defining the orientation of this specimens. It can be noted that the vibration technique induces a more uniform orientation of platy fibres. Also the MV technique leads to virtually identical results for both types of fibres with the same parameters defining the orientation distribution.

Irrespective of the fabrication technique used and fibre reinforcement type, the fibre content does not seem to have any effect on the fibre orientation distribution. MV technique causes a less anisotropic orientation distribution compared with that induced by the MT technique, especially for platy fibres, even though there is still a strong near-horizontal preference. Employing Eq.(4.6), it can be calculated that, identically, 83% of fibres type (1) and type (3) rest between $\pm 30°$ of the horizontal. Graphical representations of the fibre orientation distributions $\rho(\theta)/\bar{\rho}$ for reinforced specimens prepared with both the fabrication techniques are given in Figure 4.13; as is the result for an isotropic orientation distribution. As can be observed, both fabrication methods generate fibre orientation which is still far from isotropic.

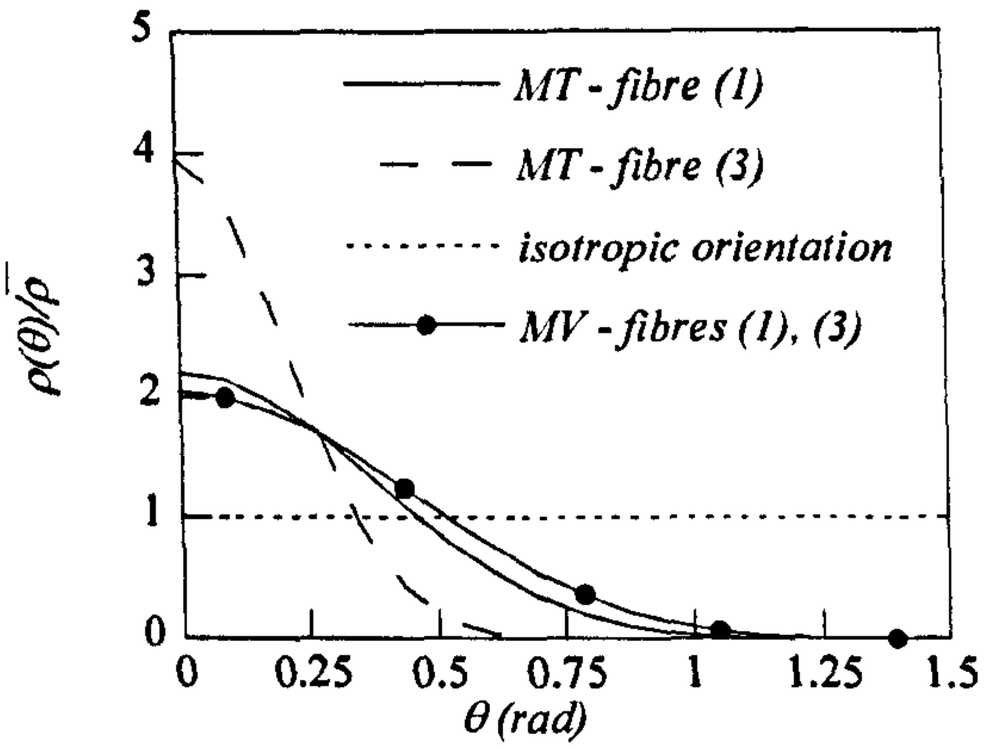

Fig. 4.13 Fibre orientation distribution according to Eq.(4.1) determined for samples reinforced with fibre (1) (A = 0 and n = 5) and with fibre (3) (A = 0 and n = 23) prepared with MV technique, compared with an isotropic orientation distribution

4.6 Comparison of triaxial performances on the investigated specimens

4.6.1 Test programme

Drained triaxial tests, including conventional compression tests as well as a few conventional extension tests, were conducted on specimens formed using both MT and MV techniques. The test results and the rotation of principal axes from compression to extension should complement the conclusions on the fibre orientation distributions induced by the different fabrication techniques.

The triaxial tests have been performed using the apparatus described in Chapter 3. A cell confining pressure of 100 kPa has been adopted for all the tests that have been performed in fully saturated conditions. Satisfactory saturation was monitored by ensuring a Skempton's B parameter of at least 0.97 and a back pressure of 300 kPa was adopted for all the tests. Table 4.3 presents a list of all the triaxial tests performed in this study, including information about reinforcement type, the initial void ratio after consolidation (e_c) (fibres are now considered as part of the solids as in the remainder of this study), the fibre content (w_f) and the type of tests (*C/E* represents compression/extension loading). The influence of fabrication procedure has

been investigated for all the three type of reinforcement, even if the orientation distribution could not be determined for the fibres type (2).

Tab. 4.3 List of triaxial tests performed for investigating the influence of fabrication

	Test	Fibres	C/E	e_c	w_f(%)
MT	T00	-	C	0.960	0.00
	-	-	-	-	-
	T03f1	1	C	0.935	0.30
	-	-	-	-	-
	T06f1	1	C	0.915	0.60
	T09f1	1	C	0.905	0.90
	T03f2	2	C	0.934	0.30
	T045f2	2	C	0.929	0.45
	T06f2	2	C	0.916	0.60
	T03f3	3	C	0.947	0.30
	T06f3	3	C	0.925	0.60
	T09f3	3	C	0.915	0.90
	ExT00	-	E	0.958	0.00
	ExT03f1	1	E	0.937	0.30
	ExT06f1	1	E	0.934	0.60

	Test	Fibres	C/E	e_c	w_f(%)
MV	V00a	-	C	0.957	0.00
	V00b	-	C	0.953	0.00
	V03f1a	1	C	0.938	0.30
	V03bf1b	1	C	0.919	0.30
	Vf06f1	1	C	0.919	0.60
	Vf09f1	1	C	0.894	0.90
	Vf03f2	2	C	0.934	0.30
	V045f2	2	C	0.923	0.45
	V06f2	2	C	0.890	0.60
	V03f3	3	C	0.941	0.30
	V06f3	3	C	0.922	0.60
	V09f3	3	C	0.901	0.90
	ExV00	-	E	0.951	0.00
	ExV03f1	1	E	0.933	0.30
	ExV06f1	1	E	0.905	0.60

4.6.2 Results

The triaxial tests results for unreinforced specimens prepared with the two different techniques are shown in Fig. 4.14 where the variations of the deviatoric stress (q) and volumetric strain (ε_v) are plotted against axial strain (ε_a). Two specimens prepared with MV have been tested to check the repeatability of the results which seem quite well confirmed in both the deviatoric and volumetric plane. The repeatability of the results for moist tamped specimens will be investigated in the following paragraph 5.3.

The stress responses of two unreinforced specimens do not seem to be highly influenced by the fabrication methods employed. The moist vibrated specimens show a higher strength between 0.05 and 0.15 axial strains but the strength of the specimen becomes very similar at larger strains. However, differences are clearly observed in the volumetric responses with a more

dilative behaviour for the MV fabricated specimen. Similar results have also been observed by De Gregorio (1990).

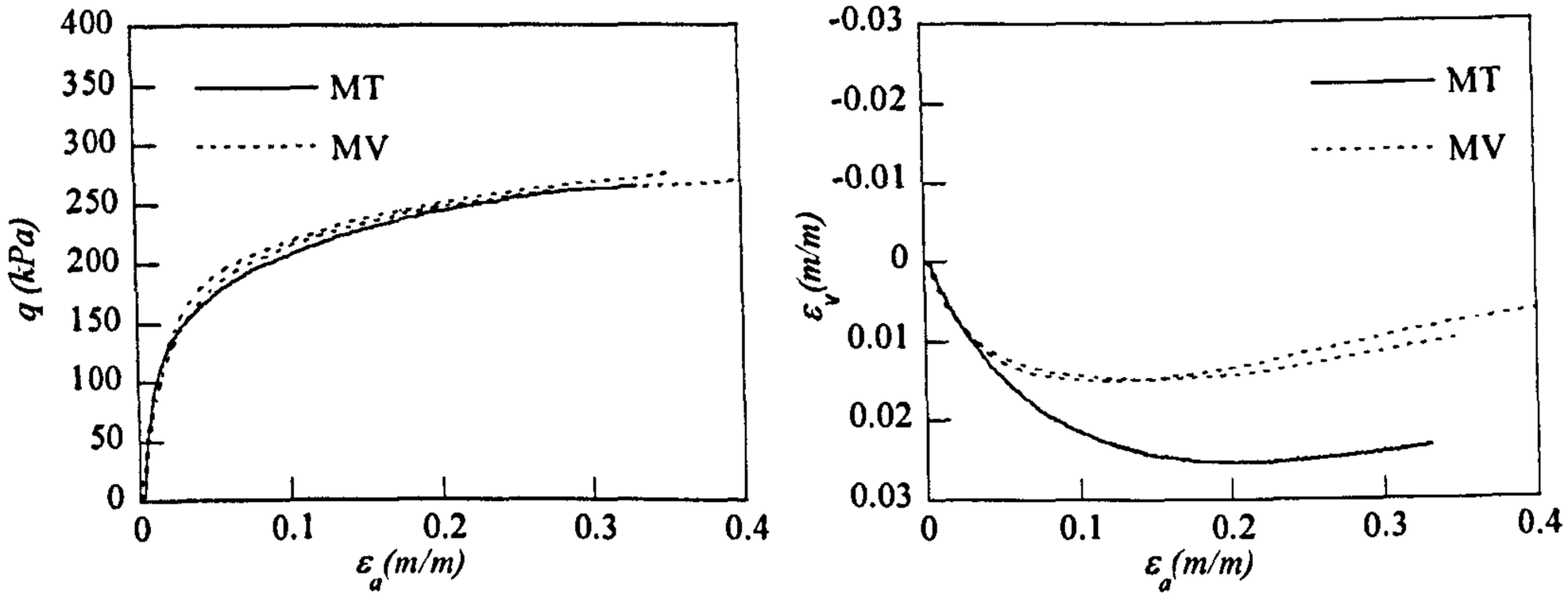

Fig. 4.14 Triaxial compression tests performed on unreinforced samples prepared with MT and MV techniques

Figure 4.15 shows the results of triaxial compression tests on specimens unreinforced and reinforced with Loksand^{TM} fibres (type 1), fabricated using both MT and MV techniques. The test results for the unreinforced specimens are also reported for comparison. Two specimens prepared with MV and reinforced with 0.3% fibre content have been tested to ensure the repeatability of test results. The repeatability for reinforced tamped specimens will be further investigated in paragraph 5.3.

The stress responses for unreinforced and reinforced sand seem to be similar at low axial displacements (Heineck et al., 2005), after which the stress responses of the composites exhibit clearly different behaviours with the increasing axial strain. For all the fibre contents the stress-strain relationships appear to be linear even for very large levels of axial strain. This pattern may suggest that the interaction mechanism between the fibres and the sand matrix is not weakened by the deformation process, the Loksand^{TM} fibres are not pulled out and they do not break either. In the volumetric plane (Fig. 4.15b), the addition of fibres results in a more dilative behaviour.

The specimens prepared with the MT technique show a slightly higher compressive strength than the MV prepared specimens, except for that of 0.6% reinforcement where the responses are almost identical. In general these results confirm the conclusions generated by the fibre orientation distribution study. A greater percentage of fibres are orientated near the horizontal for the MT technique than the MV technique, therefore offering greater resistance to tensile strains in the horizontal direction and a corresponding greater increase in strength. As also observed for unreinforced specimens, MV fabricated specimens exhibit a more dilative response compared with the MT fabricated specimens.

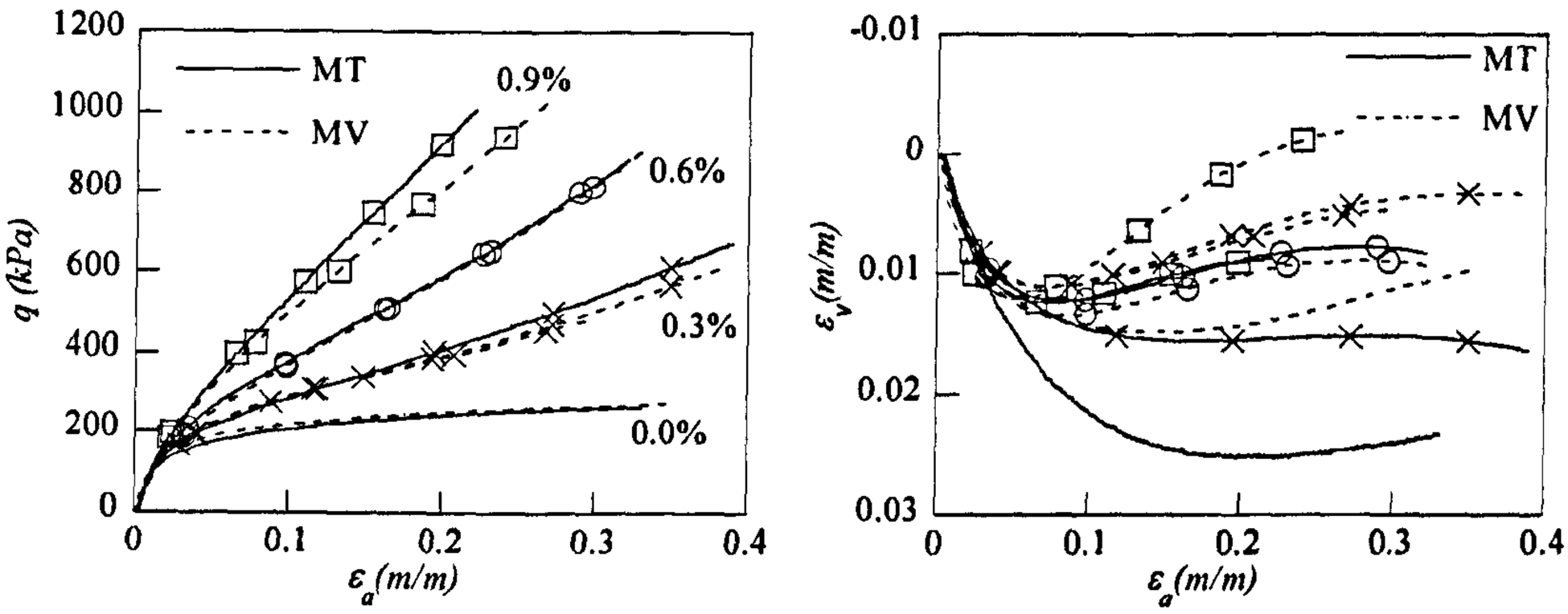

Fig. 4.15 Triaxial compression tests performed on reinforced specimens with fibre type 1 and prepared with MT and MV techniques

Similar stress-strain response patterns are observed for the sand specimens reinforced with the fibres (2), with an exception at large strains where a flattening of the stress-strain curve is noticeable (Figure 4.16). The flattening is not shown for the specimens reinforced with 0.6% of fibres because the test had to be stopped at an earlier stage in order to avoid exceeding the capacity of the load cell. Analysis of exhumed samples did not reveal breakages of the fibres - it is believed that failure of the interaction mechanism and therefore flattening of the curves is caused by sliding between fibres and sand grains. As for the fibre type 1, the specimens prepared using the MT technique show a higher stress increase in triaxial compression than those for the MV technique, but still the strength increase is limited. Again, the presence of fibres generates a more dilative behaviour on both MT and MV specimens when compared to unreinforced specimens, with it being slightly more pronounced for the MV specimens.

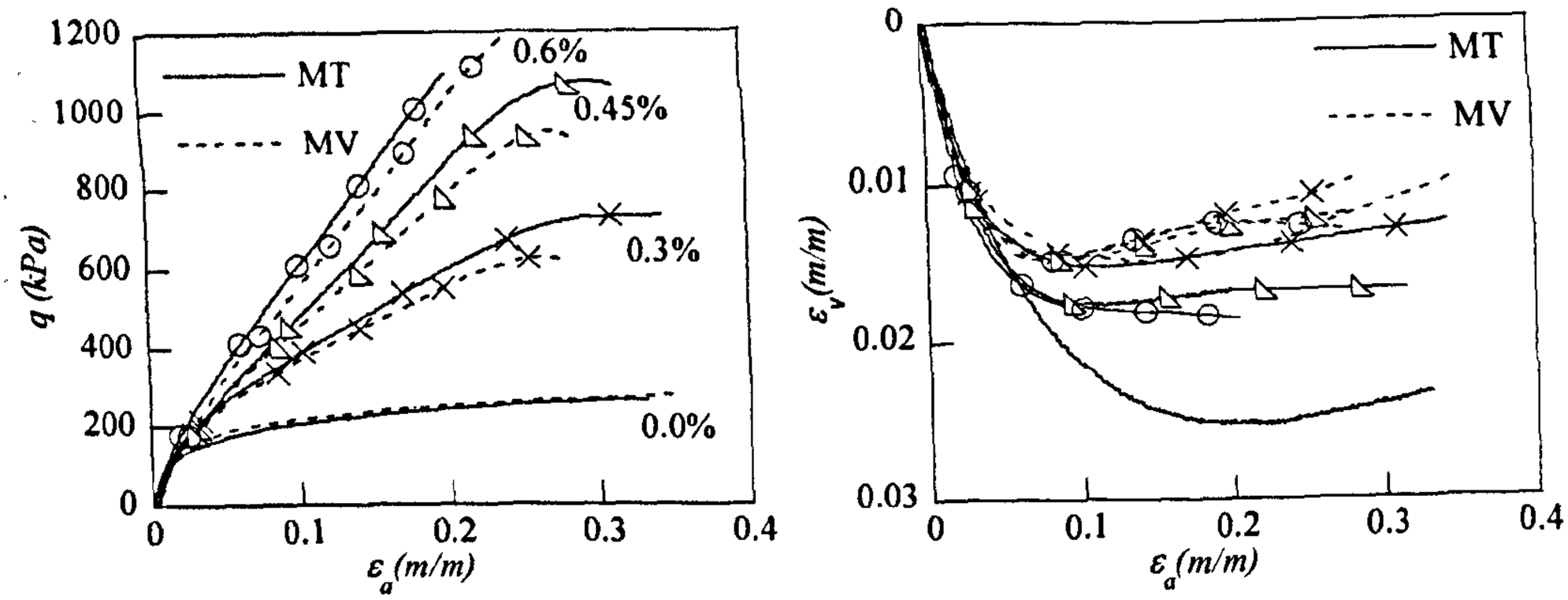

Fig. 4.16 Triaxial compression tests performed on specimens reinforced with fibres type 2 and prepared with MT and MV techniques

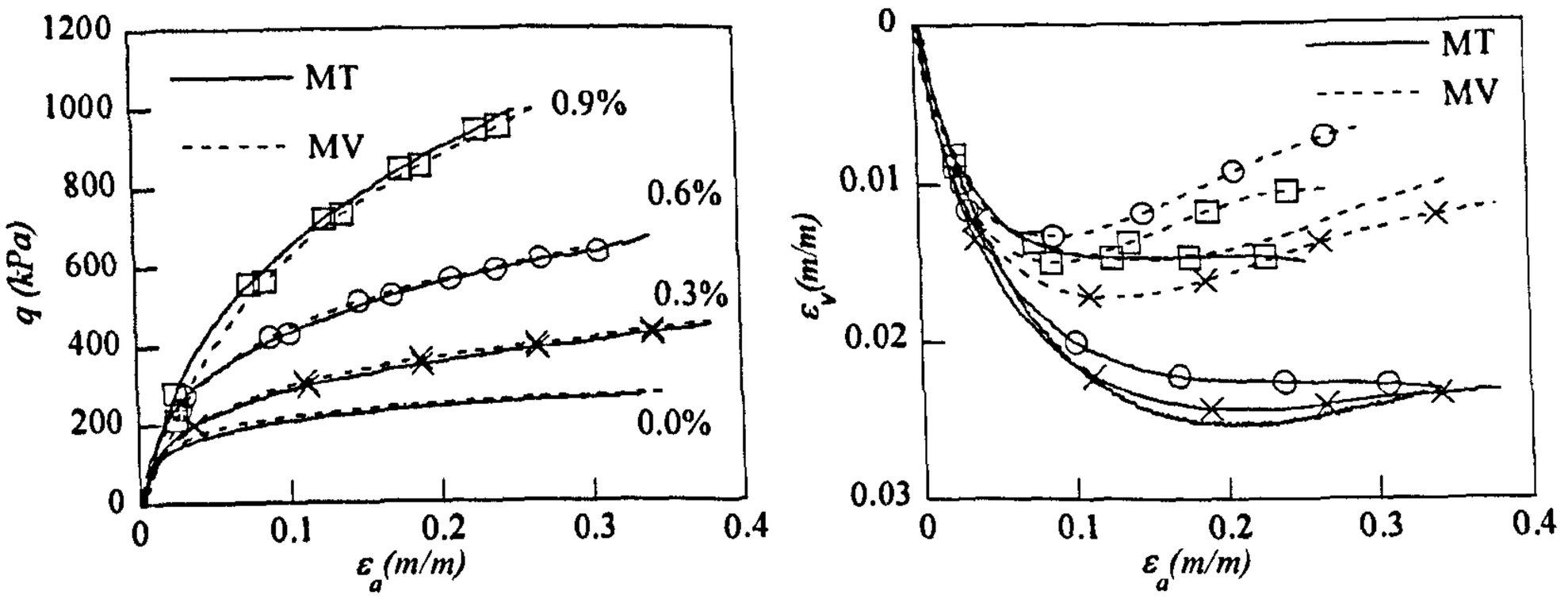

Fig. 4.17 Triaxial compression tests performed on specimens reinforced with fibres type 3 and prepared with MT and MV

The triaxial compression test results for the platy fibres (type 3) are presented in Fig. 4.17. For this case, the stress-strain curves are rather parabolic and a flattening of the response in large strains can not be observed. For this type of fibres, the stress-strain responses seem to be independent on the specimen preparation technique. For the same fabrication procedure, clear trends in the volumetric behaviours of the reinforced specimens can not be easily detected - the volumetric curves locate in a very narrow zone. However, a clear distinction is made between the volumetric curves of the specimens reconstituted by the two methods with MV being more dilative than MT.

Extension tests have also been performed on specimens reinforced with Loksand^{TM} fibres (Fig. 4.18). The benefit of fibre reinforcement seems to be quite limited for this loading condition; the net strength increase for 0.6% of fibre reinforcement is only about 8 to 10% compared with 180% to 200% for the compression tests at 20% axial strain. The percentage of fibres oriented in the vertical direction (tensile strain direction in an extension triaxial test) is very limited. These results confirm the importance of fibre orientation on the performances of reinforced sands. Even if the strength increase is almost negligible, the volumetric behaviour is still clearly affected when fibres are added: dilation increases with the fibre content. Similarly, the MV specimens dilate more than MT ones.

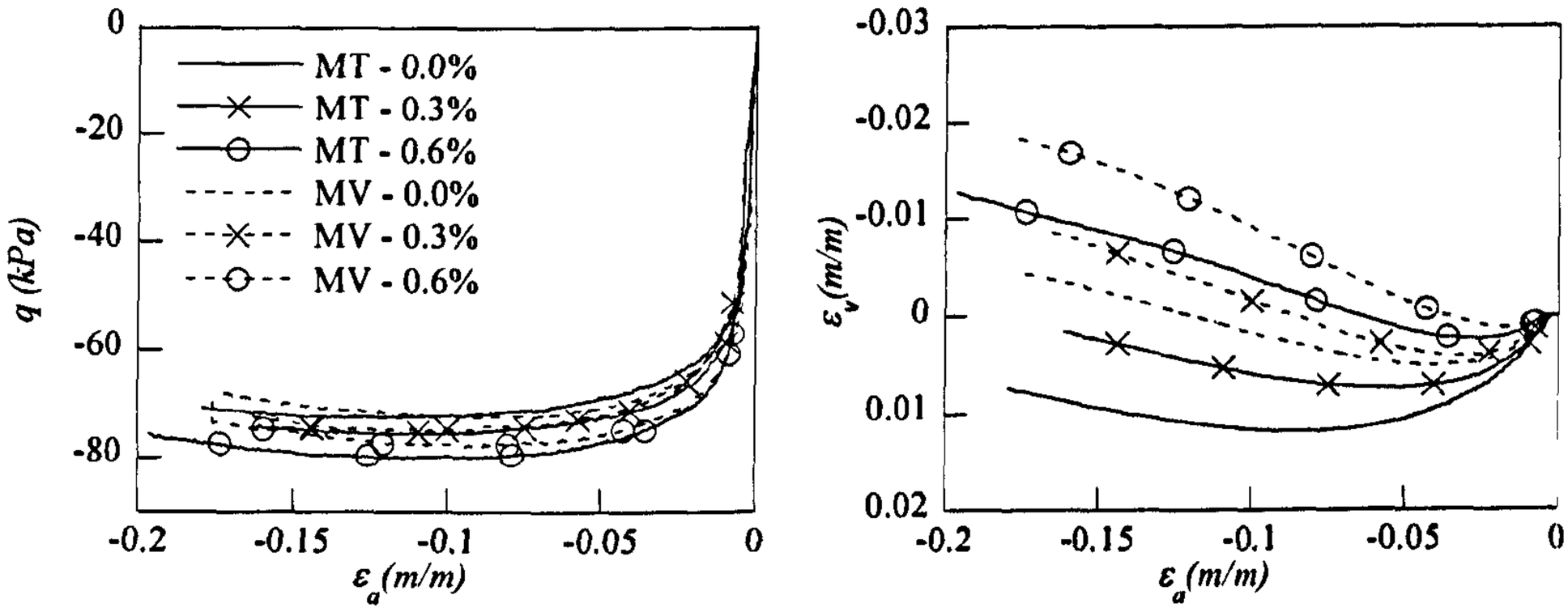

Fig. 4.18 Extension triaxial tests performed on specimens reinforced with fibres type 1 and prepared with MT and MV

4.7 Conclusions

A procedure for determining the distribution of fibre orientations in sand reinforced with flexible fibres has been presented. It has been applied to cylindrical samples prepared using moist tamping and moist vibration so that the fibre orientations have a vertical axis of symmetry. However, it may be applied to samples of any shape as long as the axis of symmetry of the distribution of fibre orientation is known: it will typically be normal to the layering in a compacted sample. The procedure for determining the orientation of fibres has been applied to

specimens reinforced with fibres type (1) and (3) as it was impossible to apply the technique to fibre (2) without the use of a scanning microscopy. However, the performances of the specimens prepared with the two different fabrication techniques have been compared with a series of conventional triaxial tests for all three types of reinforcement. Conclusions from the investigation are summarised below:

- For moist tamped specimen, the orientation distribution was found to be far from isotropic: typically 86 % of fibres type (1) and even 99% of fibres type (3) have an orientation that lies within $\pm 30°$ of the horizontal plane.

- The MV technique leads to virtually identical results for both types of fibres with 83% being oriented within $\pm 30°$ of the horizontal.

- The MV technique causes a less anisotropic orientation distribution compared with that induced by the MT, especially for platy fibres, although there is still a strong near-horizontal preferred. One may conclude that both compacting and vibrating the sand-fibre mixture during sample preparation leads to a preferred near horizontal orientation for the fibres.

- Both the procedures were found to produce a distribution of fibre orientations that was largely independent of the average volumetric concentration of fibres for the range of values considered.

- Compression triaxial tests results seem to confirm the results from orientation distribution for fibre (1) with moist tamped specimen slightly stronger than vibrated one. The same trend has been observed for specimens reinforced with fibre (2). The deviatoric stress-strain response seems independent from the preparation technique for specimens reinforced with fibre (3).

- Comparison between triaxial compression and extension test results corroborate the conclusions given by the analysis of the fibre orientation. The fibres seem to be more effective in triaxial compression than in extension loading and the experimental results

confirm the importance of the fibre orientation distribution as a key parameter which has to be considered for the design of the fibre reinforced geotechnical structures.

CHAPTER 5

TRIAXIAL TEST: DRAINED CONDITIONS

5.1 General

The effect of the addition of polypropylene fibres on the mechanical behaviour of the reinforced sand has been investigated by conducting conventional triaxial tests in both drained and undrained conditions. Three different types of polypropylene fibres have been used as reinforcement and the tests have been performed employing different confining pressures, specimen densities and fibre contents. Results of the drained tests are reported and analysed in this chapter while the undrained test results will be presented in chapter 6.

To the author's knowledge, fibre reinforced specimens have only been tested under compressive loading and investigation of the effect of rotating principal stresses has not been yet reported in literature. Therefore, even if the apparatus employed here does not allow a continuous rotation of principal axes but only a jump of the principal stresses direction by 90 degrees is permitted, the investigation of the performances of reinforced specimens has been performed under both compressive and extensive loading. The highly anisotropic orientation of fibres and the preliminary triaxial test results mentioned in Chapter 4 further encouraged the attempt of this investigation.

In the remainder of this chapter, the analysis of the tests results is divided according to reinforcement type to investigate the influence of each type of reinforcement on the strength and deformation characteristic of the sand. A comparison between the contributions of the fibres is then performed to understand the governing parameter of the interaction mechanism between fibres and sand grains. The observations and remarks exposed in this chapter will be helpful in the development of a constitutive model proposed in Chapter 7. The proposed constitutive model will be calibrated by using the experimental results presented here.

5.2 Testing programme

The apparatus described in Chapter 3 has been used for investigating the triaxial behaviour of reinforced sands. Tests have been performed on specimens reinforced with three different types of fibres described in paragraph 3.4. Different confining cell pressures, relative densities and fibre contents have been employed in both compression and extension loading conditions.

In the following, test results will be first analysed separately according to type of reinforcement and then the contribution of different types of fibres will be compared in paragraph 5.4.4. A complete list of the performed drained triaxial tests is given in Tables 5.1-5.3 respectively for the tests on specimens reinforced with fibres type (1), (2) and (3). The following information is supplied in the tables: test name, fibre content (w_f), confining pressure (σ_r), void ratio at the end of consolidation (e_c) and the corresponding density index, $I_{Dc} = (e_{max} - e_c)/(e_{max} - e_{min})$, after the consolidation stage. As previously discussed in paragraph 3.5, the void ratio is determined by considering fibres as part of the solids.

A total of 45 tests have been performed on specimens reinforced with fibre type (1). Tests cover a range of cell confining pressure from 30 to 300 kPa that may reproduce the low stress level of near surface soil layers. Density of the specimens ranges from very loose specimens ($I_D \approx 0\%$) to medium dense specimens ($I_D \approx 50\%$). The employed fibre content varies from 0.0% to 0.9% for the loosest specimens and from 0.0% to only 0.3% for the medium dense specimens. The maximum amount of fibres that can be used for preparing reinforced specimen decreases when the density of the specimen increases (Ibraim and Fourmont, 2006), therefore it was not considered appropriate to test denser reinforced specimens. Tests will be sometimes grouped according to their relative density and they will be referred to as series *(L)*, *(M)* and *(D)* that respectively correspond to a nominal density index $I_D \approx 0\%$, $I_D \approx 25\%$ and $I_D \approx 50\%$ for the unreinforced specimens before consolidation. This is different from the value in Tables 5.1-5.3 where the relative density indexes after the consolidation stage are reported. For this type of fibres the investigation has been expanded to include extension tests. However, because of the

less significant contribution of fibres for this particular loading condition, only 14 tests have been performed in extension while 31 tests have been performed in compression.

A number of 15 tests have been performed on specimens reinforced with each fibres type (2) and (3). Most of the tests have been performed on very loose (series *(L)*) specimens which permitted the adoption of a wider range of fibre content. A different range of fibre content (w_f=0.3%, 0.45% and 0.6% instead of 0.3%, 0.6% and 0.9%) has been selected for specimens reinforced with fibre type (2) in order to pursue a more accurate investigation of the failure strength of the reinforced soil. In fact, as it will be shown in section 5.4.3, a proper failure was only reached by specimens reinforced with this type of fibres and the adoption of greater fibre content would have led to more resistant specimens and in turn the capacity of the load cell would have been overcome before reaching the failure of the specimens. Cell pressures varying from 30 to 100 kPa and a few tests on series *(M)* specimens have also been executed to expand the investigation of the performance of this type of reinforcement.

Tab. 5.1 List of tests on specimens reinforced with fibre type (1)

COMPRESSION TESTS				
Test	w_f (%)	σ_r (kPa)	e_c	I_{Dc} (%)
L030-00-D-1	0.00	30	0.970	7.89
L030-03-D-1	0.30	30	0.953	12.38
L030-06-D-1	0.60	30	0.928	18.87
L030-09-D-1	0.90	30	0.925	19.85
L060-00-D-1	0.00	60	0.967	8.68
L060-03-D-1	0.30	60	0.950	13.17
L060-06-D-1	0.60	60	0.937	16.54
L060-09-D-1	0.90	60	0.917	21.90
L100-00-D-1	0.00	100	0.960	10.53
L100-03-D-1	0.30	100	0.935	17.08
L100-06-D-1	0.60	100	0.915	22.49
L100-09-D-1	0.90	100	0.906	24.73
L200-00-D-1	0.00	200	0.947	13.95
L200-03-D-1	0.30	200	0.916	22.04
L200-06-D-1	0.60	200	0.904	25.33
L200-09-D-1	0.90	200	0.881	31.39
M030-00-D-1	0.00	30	0.884	30.53
M030-03-D-1	0.30	30	0.876	32.73
M030-06-D-1	0.60	30	0.863	35.94
M100-00-D-1	0.00	100	0.909	23.95
M100-03-D-1	0.30	100	0.876	32.73
M100-06-D-1	0.60	100	0.866	35.16
M200-00-D-1	0.00	200	0.894	27.89
M200-03-D-1	0.30	200	0.881	31.43
M200-06-D-1	0.60	200	0.855	38.26
M300-00-D-1	0.00	300	0.904	25.26
M300-03-D-1	0.30	300	0.886	30.12
M300-06-D-1	0.60	300	0.870	34.13
D030-00-D-1	0.00	30	0.804	51.58
D030-03-D-1	0.30	30	0.799	52.82
D100-00-D-1	0.00	100	0.801	52.37
D100-03-D-1	0.30	100	0.789	55.43
D200-00-D-1	0.00	200	0.796	53.68
D200-03-D-1	0.30	200	0.778	58.30

EXTENSION TESTS				
Test	w_f (%)	σ_r (kPa)	e_c	I_{Dc} (%)
EL100-00-D-1	0.00	100	0.958	0.11
EL100-03-D-1	0.30	100	0.937	0.17
EL100-06-D-1	0.60	100	0.934	0.17
EL200-00-D-1	0.00	200	0.929	0.19
EL200-03-D-1	0.30	200	0.923	0.20
EL200-06-D-1	0.60	200	0.914	0.23
EM100-00-D-1	0.00	100	0.861	0.37
EM100-03-D-1	0.30	100	0.864	0.36
EM100-06-D-1	0.60	100	0.861	0.37
ED100-00-D-1	0.00	100	0.797	0.53
ED100-03-D-1	0.30	100	0.791	0.55

Tab. 5.2 List of tests on specimens reinforced with fibre type (2)

Test	w_f (%)	σ_r (kPa)	e_c	I_{Dc} (%)
L030-00-D-2	0.00	30	0.970	7.89
L030-03-D-2	0.30	30	0.956	11.60
L030-045-D-2	0.45	30	0.948	13.56
L030-06-D-2	0.60	30	0.937	16.54
L060-00-D-2	0.00	60	0.967	8.68
L060-03-D-2	0.30	60	0.952	12.65
L060-045-D-2	0.45	60	0.944	14.86
L060-06-D-2	0.60	60	0.930	18.35
L100-00-D-2	0.00	100	0.960	10.53
L100-03-D-2	0.30	100	0.934	17.34
L100-045-D-2	0.45	100	0.929	18.76
L100-06-D-2	0.60	100	0.916	22.23
M100-00-D-2	0.00	200	0.909	23.95
M100-03-D-2	0.30	200	0.865	35.60
M100-045-D-2	0.45	200	0.859	37.20

Tab. 5.3 List of tests on specimens reinforced with fibre type (3)

Test	w_f (%)	σ_r (kPa)	e_c	I_{Dc} (%)
L030-00-D-3	0.00	30	0.970	7.89
L030-03-D-3	0.30	30	0.954	12.12
L030-06-D-3	0.60	30	0.946	14.21
L030-09-D-3	0.90	30	0.929	18.57
L060-00-D-3	0.00	60	0.967	8.68
L060-03-D-3	0.30	60	0.947	13.95
L060-06-D-3	0.60	60	0.935	17.06
L060-09-D-3	0.90	60	0.920	21.13
L100-00-D-3	0.00	100	0.960	10.53
L100-03-D-3	0.30	100	0.947	13.95
L100-06-D-3	0.60	100	0.925	19.64
L100-09-D-3	0.90	100	0.915	22.42
M100-00-D-3	0.00	200	0.909	23.95
M100-03-D-3	0.30	200	0.864	35.86
M100-06-D-3	0.60	200	0.849	39.82

5.3 Repeatability of results

The assessment of the repeatability of the experimental results is fundamental when the behaviour of soil is investigated. It concerns the study of tests performed in the same laboratory, at the same condition, by the same operator, using the same apparatus and measuring system and on specimens fabricated with the same procedure. Indeed results on similar specimens usually show variability due to the materials, measuring system and the operator.

The study of the repeatability performed here involved the testing of five unreinforced and five reinforced specimens in drained compression triaxial conditions. All the specimens have been isotropically consolidated up to 100 kPa effective cell pressure with a nominal fabrication void ratio e_0=0.9 that correspond to $I_D \approx 25\%$. The reinforced specimens were fabricated by using fibre type (1) with 0.6% fibre content. A summary of the tests performed is given in Table 5.4, where the data about specimen preparation are reported including the fabrication void ratio (e_0) , the consolidation void ratio (e_c) corrected for the initial collapse of the specimens due to saturation and cell placement (paragraph 3.5) and their respective density index I_{D0} and I_{Dc}.

A serviceability failure criterion has been defined at 20% axial strain (ε_a) and the results of the tests *at failure* are also reported in the Table 5.4. The value of the deviatoric stress ($q_{20\%}$), effective stress ratio ($M_{20\%}$), the mobilised angle of friction ($\phi_{20\%}$) and the maximum angle of dilatancy (ψ_{max}) are shown. The mobilised angle of dilatancy for triaxial conditions is defined as the inverse tangent of the ratio of incremental volumetric and axial strains, and for simplicity it has been assumed that the elastic components of the strain increments are small compared with the plastic components (denoted with the superscript ^{p}), to give:

$$\tan\psi = -\frac{\dot{\varepsilon}_v^p}{\left|\dot{\varepsilon}_a^p\right|} \approx -\frac{\dot{\varepsilon}_v}{\left|\dot{\varepsilon}_a\right|} \qquad (5.1)$$

Tab. 5.4 Results from repeatability tests in drained compression for unreinforced and reinforced specimens

Test	w_f (%)	e_0	I_{D0} (%)	e_f	I_{Dc} (%)	$q_{20\%}$ (kPa)	$M_{20\%}$	$\phi_{20\%}$ (°)	ψ_{max} (°)
UR1	0.0	0.922	20.53	0.890	28.95	272.44	1.417	34.97	4.11
UR2		0.922	20.53	0.892	28.42	274.51	1.433	35.34	3.79
UR3		0.927	19.21	0.895	27.63	278.38	1.422	35.08	4.19
UR4		0.927	19.21	0.896	27.37	274.41	1.407	34.74	3 87
UR5		0.933	17.63	0.900	26.32	268.56	1.413	34.88	3.73
Average value		0.926	19.421	0.895	27.74	273.66	1.418	35.00	3.94
Standard deviation		0.005	1.197	0.004	1.01	3.57	0.010	0.23	0.20
R1	0.6	0.892	28.44	0.857	37.75	751.90	2.119	51.53	10.10
R2		0.897	27 14	0.860	36.71	766.95	2.134	51.91	9.39
R3		0.892	28.44	0.855	38.26	760.98	2.128	51.76	10.43
R4		0.900	26.37	0.863	35.94	781.40	2.160	52.57	8.37
R5		0.894	27.92	0.860	36.97	761.19	2.124	51.66	11.06
Average value		0.895	27.660	0.859	37.13	764.48	2.133	51.89	9.87
Standard deviation		0.003	0.896	0.003	0.91	10.88	0.016	0.41	1.03

The experimental results for both the reinforced and unreinforced specimens are presented in Fig. 5.1 where the variations of the stress ratio (q/p), the volumetric strain (ε_v) and the angle of dilatancy (ψ) are presented with the axial displacement (ε_a). Unreinforced specimens show the typical behaviour of loose sand: the initial void ratio after the isotropic consolidation stage is very similar for all the specimens with an average value of 0.895 (which corresponds to 27.74% relative density) and a standard deviation of 0.004. The stress-strain behaviour shows a very repeatable trend with a continuous increase of the deviatoric stress towards a limit condition (Fig. 5.1a). The failure deviatoric stress ($q_{20\%}$) is 273.66 kPa with a standard deviation of 3.57 kPa and this corresponds to a very low coefficient of variation of about 1.31%. The mobilised

friction angle at failure is 35° with a standard deviation of 0.23°. These results are in accord with the experimental results on Hostun sand already published by Lancelot et al. (2006).

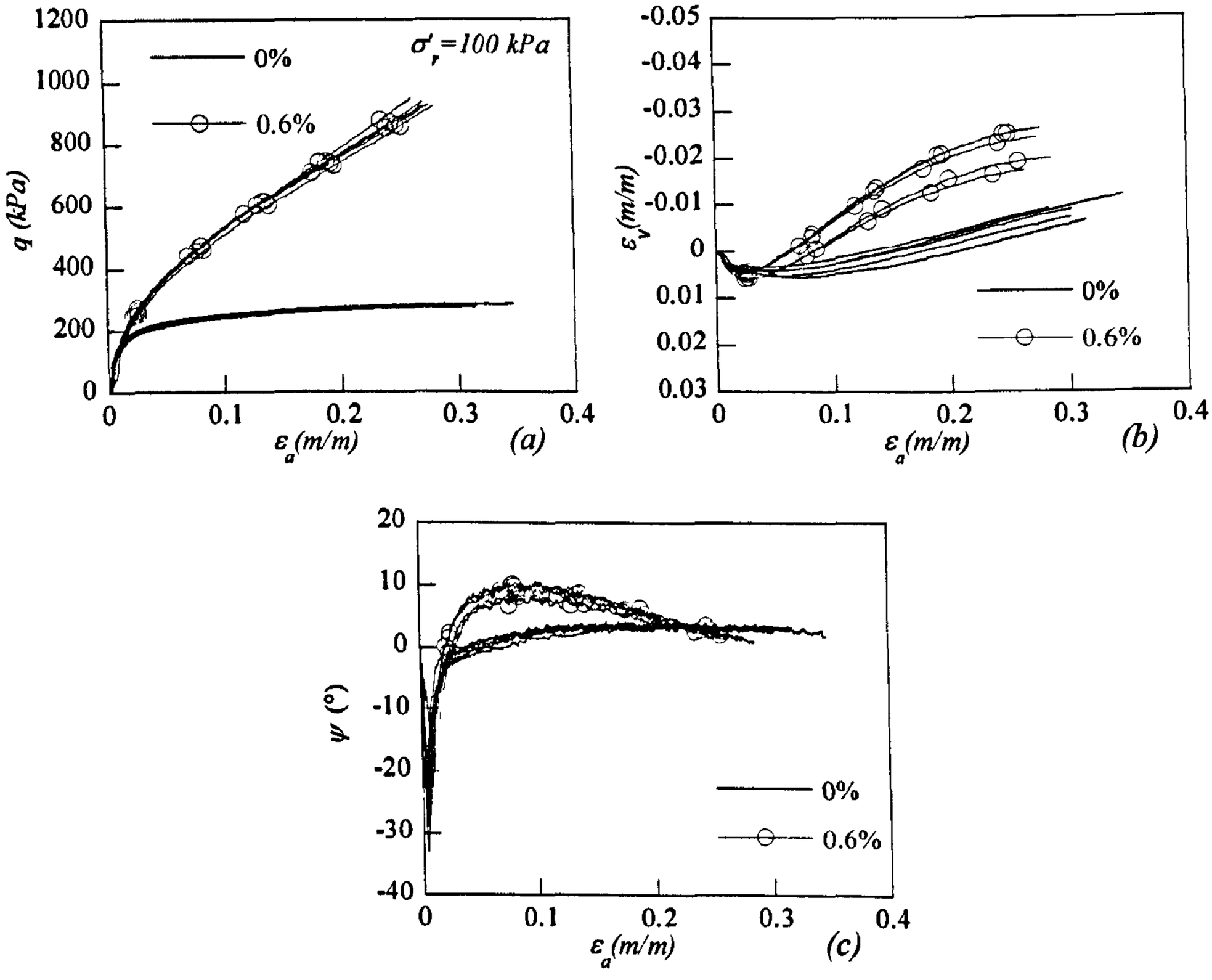

Fig. 5.1Set of experimental results for repeatability assessment: *(a)* deviatoric stress - axial strain; *(b)* volumetric strain - axial strain; *(c)* dilatancy angle - axial strain (legend indicates fibre content)

The scatter in the volumetric behaviour is more pronounced than that observed in the stress-strain behaviour (Fig. 5.1b), however all the tests can still be grouped in a unique band of qualitative similar trend. The differences in the volumetric behaviour can be attributed to the variation of the relative density between the tested specimens but a correspondence between the volumetric behaviour and the relative density after consolidation has been observed (e.g. to the slightly denser specimens correspond the more dilative behaviour). This draws attention to the influence of small variations of void ratio on the volumetric performance of the specimens. However, if the volumetric behaviour is studied through the evolution of the dilatancy angle,

the results can be grouped in a narrower band (Fig. 5.1c). The average maximum dilation angle is 3.94°with a standard deviation of 0.20°.

Reinforced specimens have been prepared using the same amount of sand as for unreinforced specimens and 0.6% of fibres by dry weight of sand have been added. This results in an initial relative density slightly greater than for unreinforced specimens with an average value of 37.13%. The average initial void ratio of the specimen was 0.859 with a deviation standard of 0.003. The stress-strain behaviour shows a good reproducibility of results with a scatter increasing at large strains when the deformation of the specimen may not be very uniform. It is clear that fibres largely improve the strength characteristic of the sand increasing the failure deviatoric stress ($q_{20\%}$) by about 3 times to an average value of 764.48 kPa. The standard deviation from the mean value is 10.88 kPa which corresponds to a coefficient of variation of only 1.42%, demonstrating the satisfactory reproducibility of results. The presence of fibres increases the friction angle of the material up to an average value of 51.89°.

The presence of fibres induces also a more dilative behaviour when compared with unreinforced specimens (Fig 5.1b). Again the volumetric trends show a more pronounced scatter than the stress-strain ones but they can still be grouped in a quite narrow band which is evidently distanced from the one of unreinforced specimens. Also for reinforced specimens, there is still a correspondence between the relative density and the volumetric behaviour of the specimens: as expected the two less dilative behaviours correspond to the two loosest specimens. However, the trend of the dilation angle is very similar for all the specimens (Fig. 5.1c) with an average maximum value of 9.87° and a standard deviation of 0.92°

In conclusion, a satisfactory reproducibility of results has been shown by this investigation. A variation of the initial void ratio after consolidation (e_c) of 0.43% for unreinforced specimens and 0.40% for reinforced specimens was found. The behaviour of both unreinforced and reinforced specimens is well repeatable in similar tests with a very good reproducibility in the stress-strain plane (q - ε_a) and some more scatters but still acceptable repeatability in the volumetric plane (ε_v - ε_a). This means that a small variation of the initial void ratio slightly influences the deviatoric behaviour of the sample while it has a more pronounced effect on the

volumetric behaviour. However, if the volumetric behaviour is analysed through the evolution of the mobilised dilatancy angle, test results fall in a quite narrow band (Fig. 5.1c).

5.4 Results

5.4.1 Unreinforced specimens

5.4.1.1 General

Experimental tests for unreinforced specimens have been performed to check the reliability of the apparatus and as a reference point for understanding the effectiveness of the contribution of the fibres in the tests performed. Experimental results for unreinforced specimen are in accord with the already published results on identical sand specimens (Ibraim 1998). Typical test results for unreinforced specimens (series *(M)*) at different cell confining pressures are reported in Fig. 5.2 where the variations of the stress ratio (q/p'), the volumetric strain (ε_v) and the angle of dilatancy (ψ) are presented with the axial displacement (ε_a). The trends show the typical behaviour of a loose specimen with absence of peak condition in compression and a very slight peak for extensive loading. Stress ratios increase with the cell confining pressure (Fig. 5.2.a) and they tend to a critical state value ranging between 1.36 and 1.48 which correspond to a critical friction angle (ϕ'_{cr}) between 33.6° and 36.4° . As usual the critical state is referred here as the ultimate and asymptotic condition for a soil when sheared: at critical state, the plastic shearing could continue indefinitely without changes in volume or effective stress.

The volumetric behaviour is dilative when the low cell pressures are employed but the propensity to dilate almost disappears at the highest cell confining pressure (Fig 5.2b). However, irrespective of the cell confining pressure and under compressive loading, the trends of the dilatancy angle seem convergent at large strains (Fig. 5.2c): critical dilatancy angles (ψ_{cr}) vary between 1° and 3.4°. At the same confining stress the dilatancy seems more pronounced for extensive loading (Fig 5.2b and c).

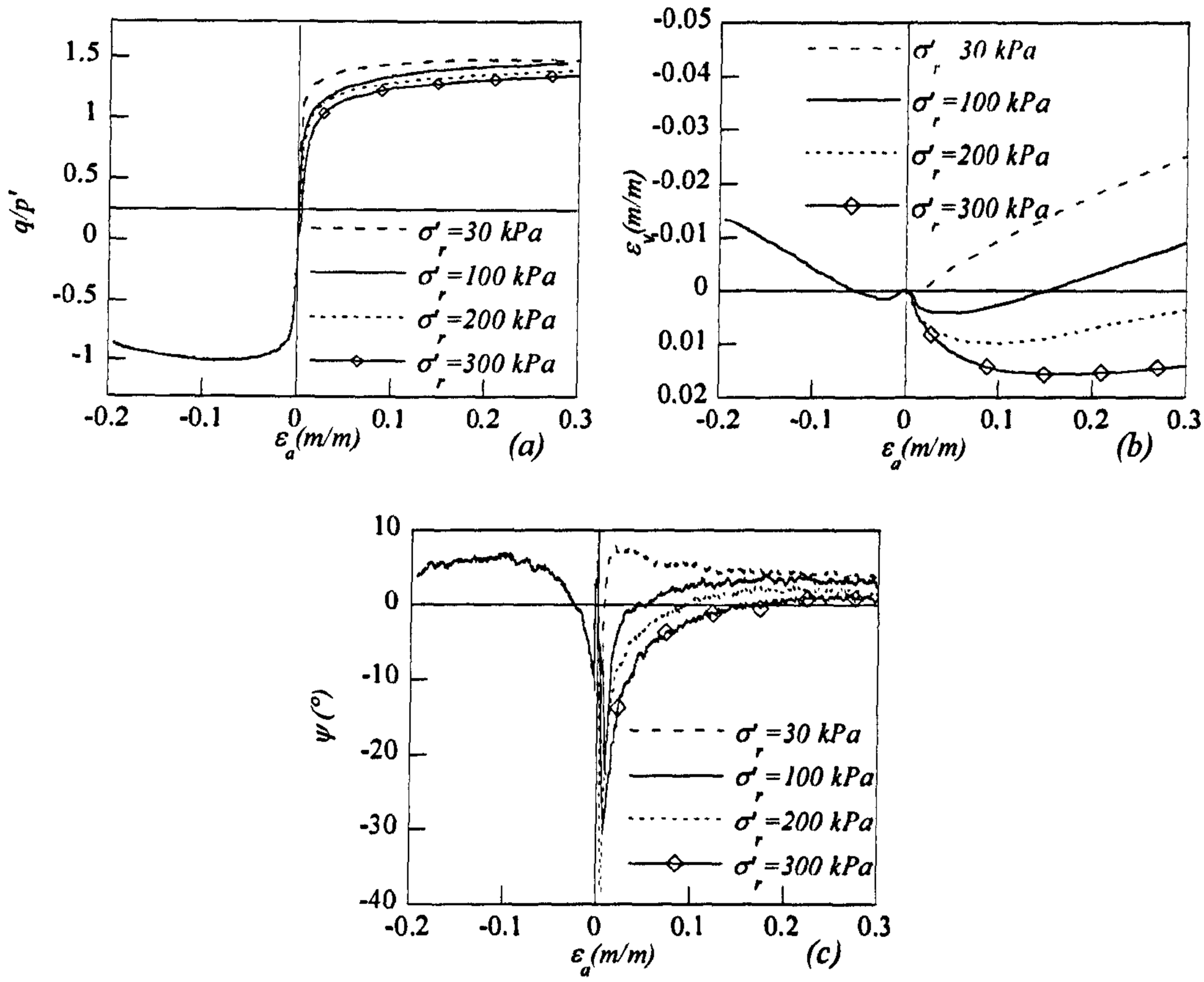

Fig. 5.2 Typical experimental results from triaxial tests on *(M)* series specimen: *(a)* deviatoric stress - axial strain; *(b)* volumetric strain - axial strain; *(c)* dilatancy angle - axial strain (legend indicates cell confining pressure)

The influence of the density of the specimen is explored in Fig.5.3 where series *(L)*, *(M)* and *(D)* are compared when tested at 100 kPa cell confining pressure. All the specimens tend towards the same critical stress ratio (Fig 5.3a) corresponding to a value $q/p' = 1.43$ (ϕ'_{cr}=35.3°) in compression. The critical stress ratio value could not be defined in extension for the consistent necking of the specimens after 15% axial strain, however, all the specimens showed the same stress ratio at that strain. As expected the strength and the dilatancy increase with the relative density of the specimens. Values of critical dilatancy angles (ψ_{cr}) vary between 1.5° and 3.2° for compressive loading while they approach approximately 3.5° in extension.

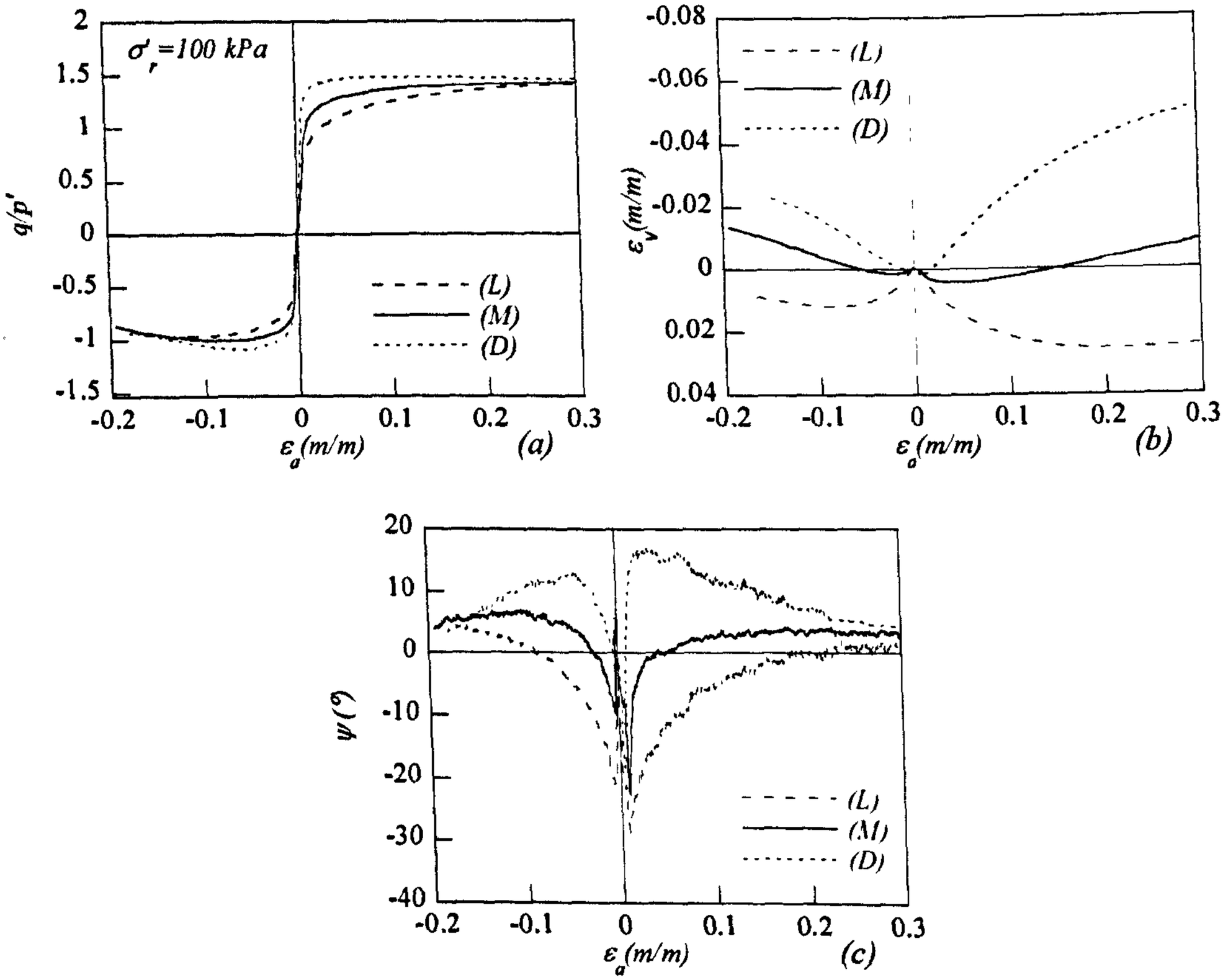

Fig. 5.3 Experimental results on specimens tested at 100 kPa cell confining pressure: *(a)* deviatoric stress - axial strain; *(b)* volumetric strain - axial strain; *(c)* dilatancy angle - axial strain (legend indicates relative density)

5.4.1.2 Strength

A peak or steady value for the friction angle was not detectable for the loosest specimens, even if the test was carried to further than 20% of axial strain. For those specimens a serviceability limit was applied to determine the strength for compressive loading. For extensive loading a peak was instead detectable in the tests, however a serviceability limit was set at 10% axial strain. As generally found in the literature the maximum angle of friction was found to be dependent on the relative density and on the confining pressure. The angle of friction strongly increases when low pressures are employed (Ponce and Bell, 1971 and Fukushima and

Tatsuoka, 1984) and the relationship found from experimental data (Fig. 5.4) is in accord with the results obtained by Lancelot et al. (2006) on Hostun sand specimens with a void ratio prior to shearing e_c=0.877 (which corresponds to a relative index $I_D \approx 34\%$). The trend seen by Lancelot et al. (2006) lies between series *(M)* and *(D)* as expected.

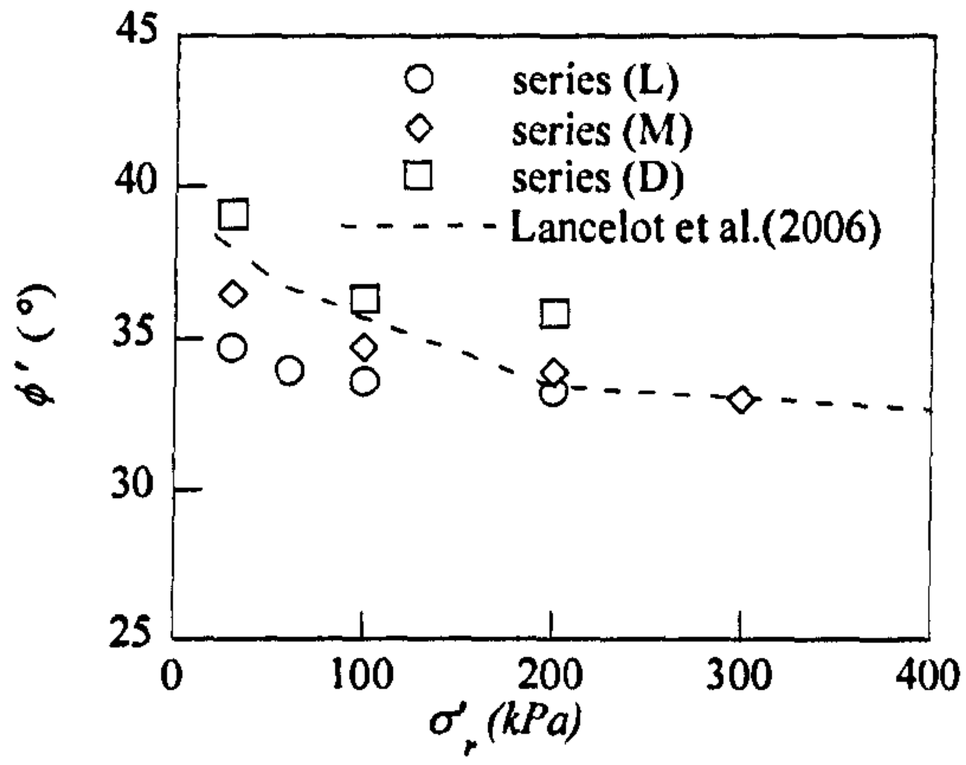

Fig. 5.4 Dependency of the peak friction angle on the confining cell pressure and on specimen density for compressive loading - results from Lancelot et al. (2006) on specimen with similar density are also reported

5.4.1.3 Critical state line

The determination of the critical state line (CSL) in the *v-ln p'* plane can not be directly determined from these tests, since a clear state when shearing occurs with no change in volume and no change in the principal stress ratio is not detectable. However the procedure proposed by Parry (1958) may be applied here to locate the CSL. Parry (1958) defined p'_f as the mean effective stress recorded at the end of the test and p'_{cs} as the mean stress on the critical state line at the same value of specific volume (v) that the sample had at the end of the test. Following a trial and error procedure the CSL can be determined in order to find a linear relationship between the rate of the volume change at the end of the test $(d\varepsilon_v/d\varepsilon_q)_f$ and the logarithm of the ratio p'_f/p'_{cs} (Fig.5.5).

A straight critical state line has been defined using the conventional equation:

$$\upsilon = \Gamma - \lambda \ln(p') \qquad (5.2)$$

where $\Gamma = 3.08$ and $\lambda = 0.031$. The location of the CSL and the final points of the drained tests on unreinforced specimens are shown in Fig. 5.6. The parameters defining the CSL are in accord with the already published data on Hostun sand (Ibraim, 1998; Sadek, 2006).

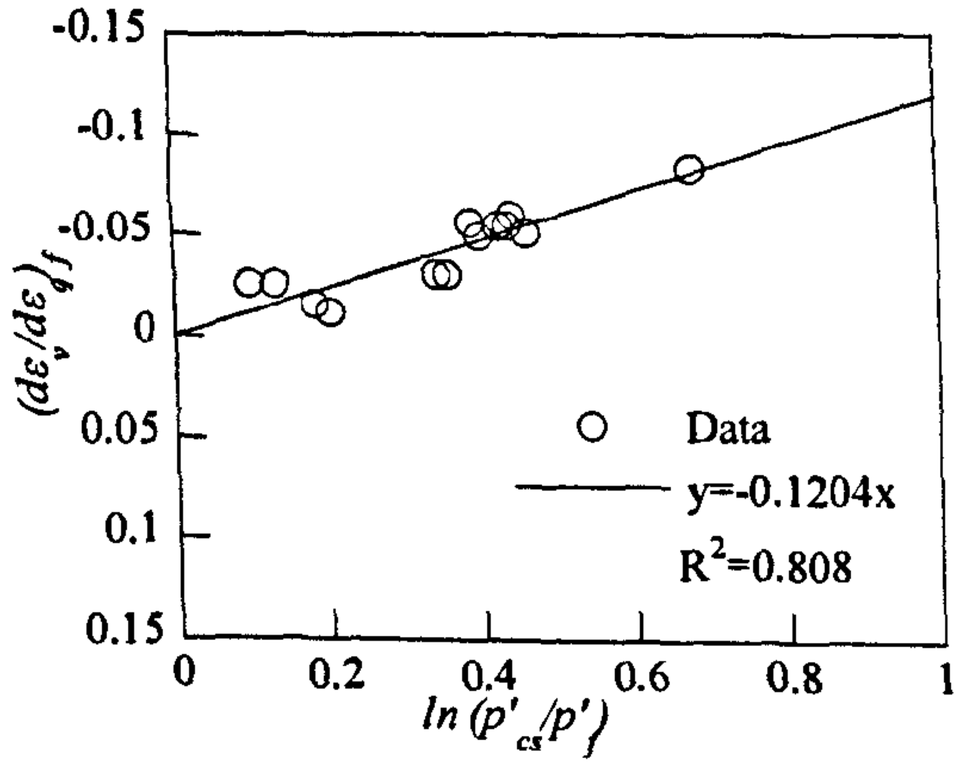

Fig. 5.5 End points of drained conventional triaxial tests: rate of volume change versus logarithm of the ratio p'_f/p'_{cs}. Linear regression through origin is reported as suggested by Parry (1958)

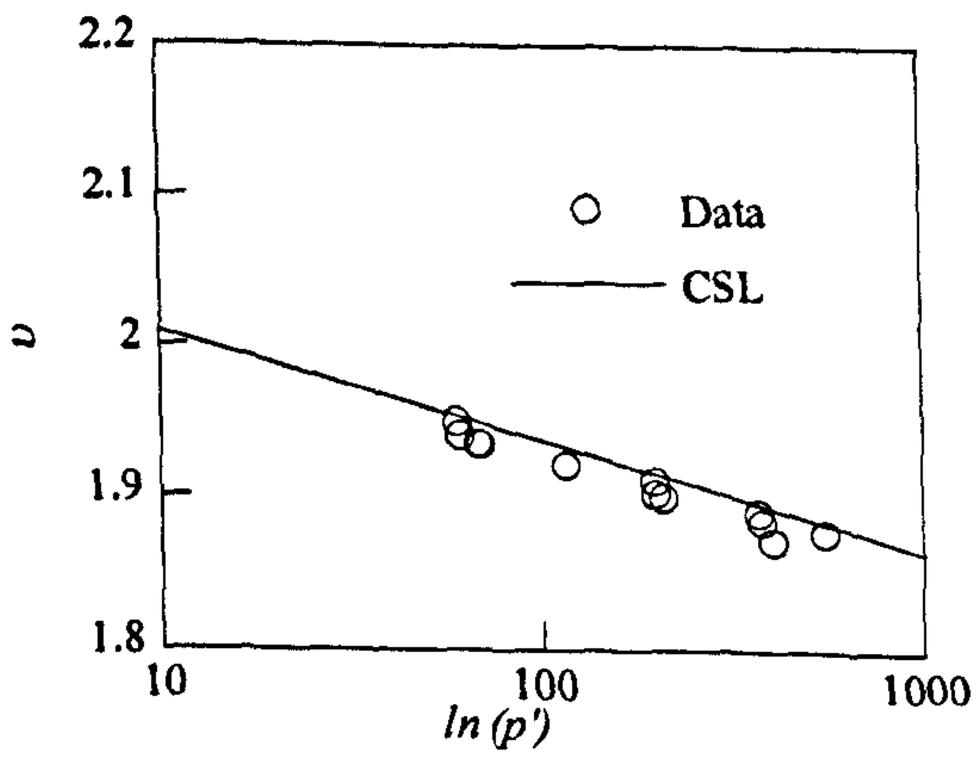

Fig. 5.6 Critical state line on the v-$ln(p')$ plane and end points of the drained conventional triaxial tests.

5.4.2 Specimens reinforced with fibre type 1

5.4.2.1 General

Typical results of drained triaxial tests on specimen reinforced with fibre type (1) are presented in Figures 5.7-5.9 where the variations of the deviatoric stress (q), the volumetric strain (ε_v) and the dilatancy angle (ψ) are presented with the axial displacement (ε_a). Respectively series *(L)*, *(M)* and *(D)* are shown when tested at 100 kPa confining pressure. Serviceability strength, peak strength (for extension tests only) and maximum dilatancy determined from the experimental tests are also summarised in Table 5.5.

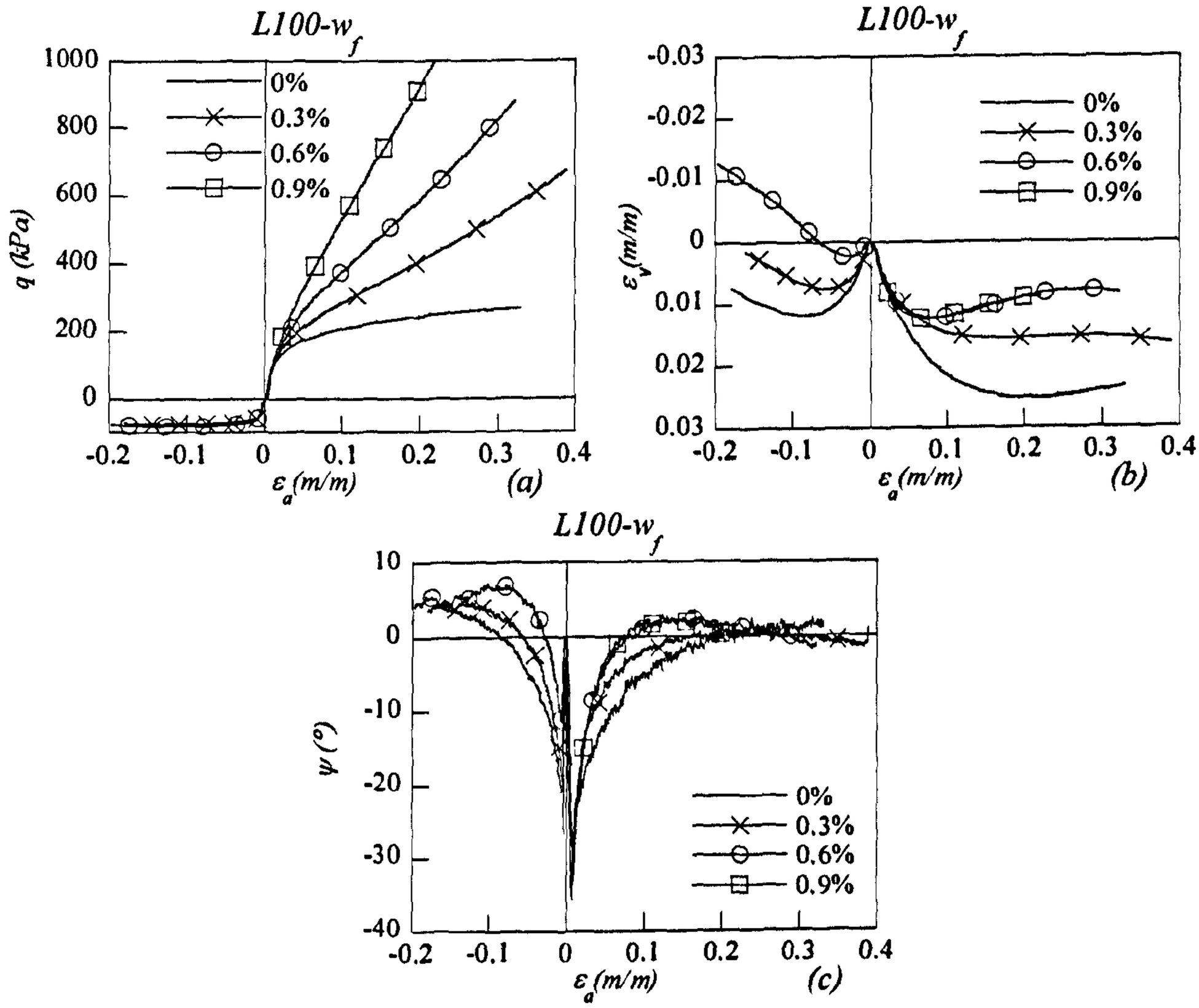

Fig. 5.7 Experimental results on *(L)* series specimens tested at 100 kPa cell confining pressure: *(a)* deviatoric stress - axial strain; *(b)* volumetric strain - axial strain; *(c)* dilatancy angle - axial strain (legend indicates fibre content)

It is evident that the contribution of fibres to the deviatoric response differs from compression to extension conditions. The deviatoric response is appreciably enhanced by the addition of fibres in compression while the contribution of fibres appears to be limited in extension: for example specimens reinforced with 0.6% fibres content and tested at 100 kPa cell confining pressure show a net strength increase (at serviceability failure) up to 135% in compression but only 10.5% net strength increase is recorded for the extension tests. In term of friction angles, it corresponds to an increase from 33.7° to 48.2° in compression and from 35.2° to 41.5° in extension. It is well known that fibres are most influential when oriented with the tensile strains (Jewell and Wroth, 1987, Palmeira and Milligan, 1989 and Michalowski and Čermák, 2002) and it has been demonstrated that the adopted method of fabrication induces a preferred orientation of fibres that is somewhat coincident with the horizontal direction of the tensile strains for compressive loading. On the other hand only very few fibres are oriented in the vertical direction, which is the direction of tensile strains for extensive loading.

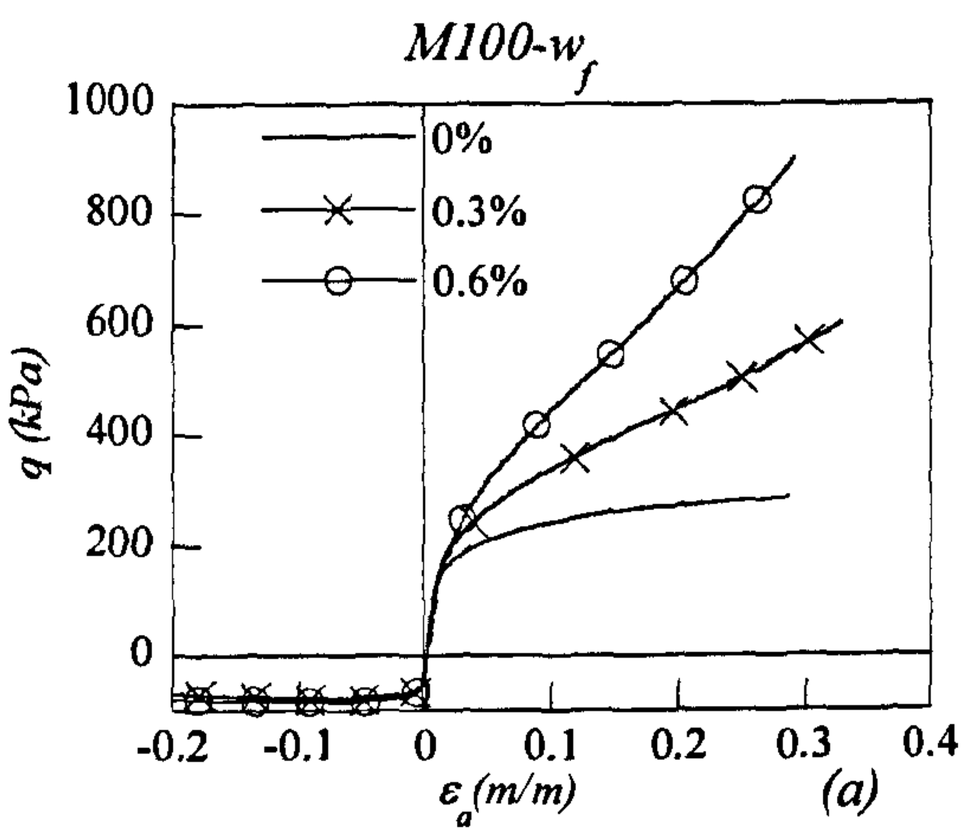

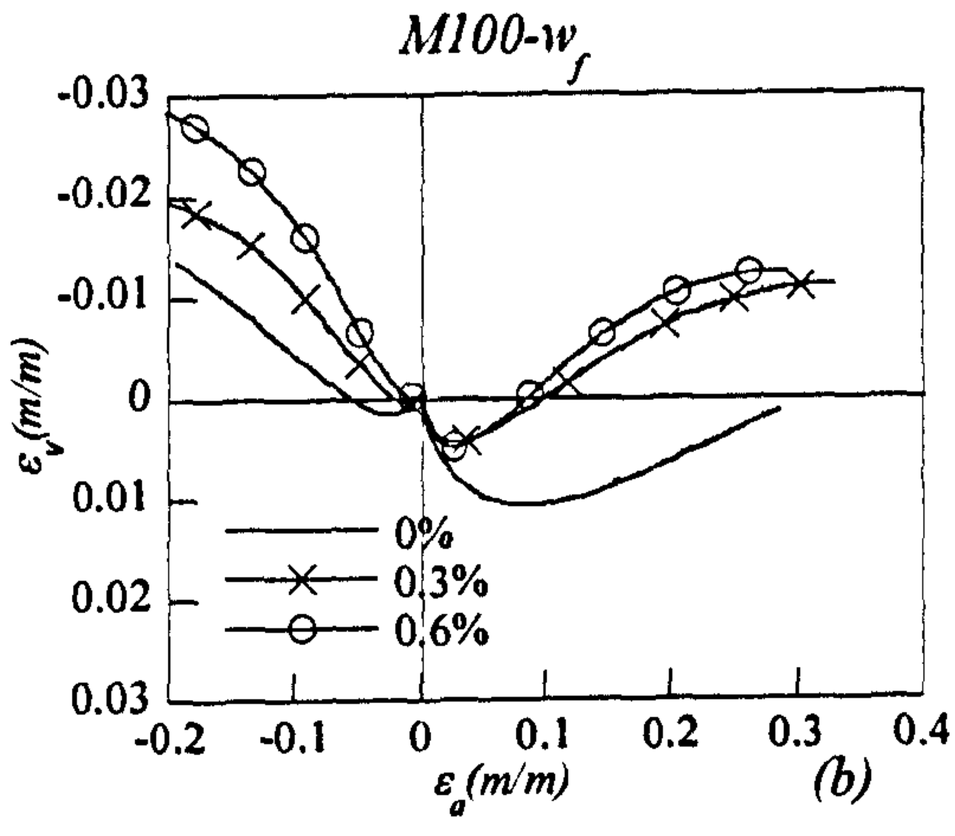

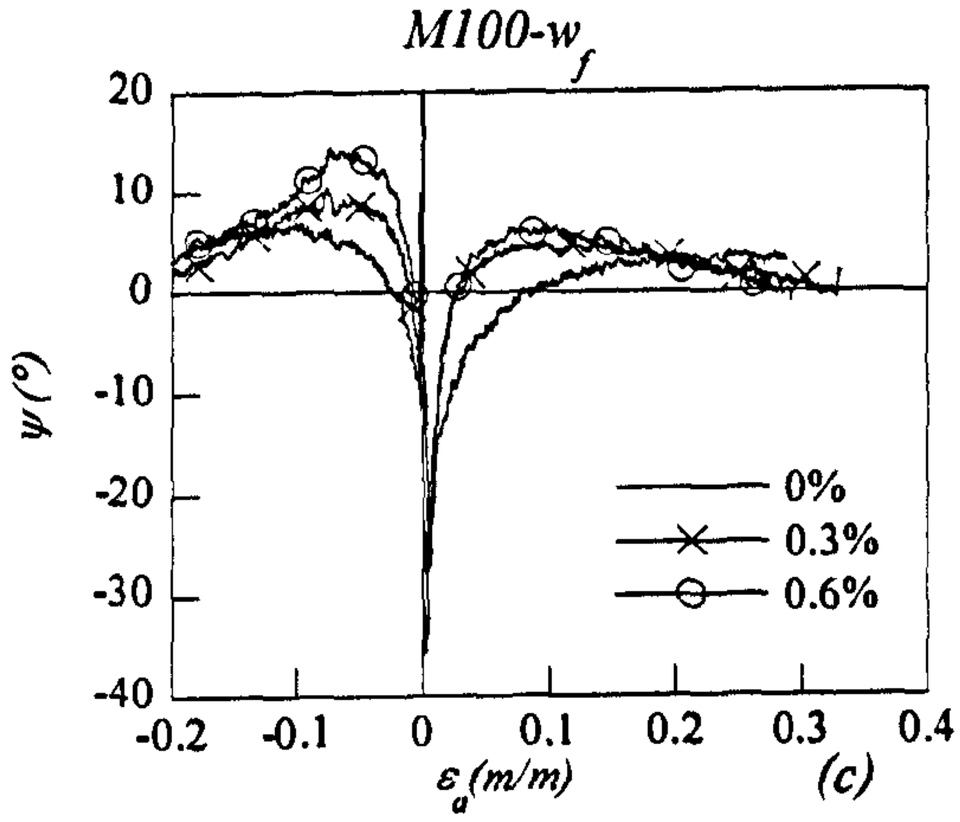

Fig. 5.8 Experimental results on *(M)* series specimens tested at 100 kPa cell confining pressure: *(a)* deviatoric stress - axial strain; *(b)* volumetric strain - axial strain; *(c)* dilatancy angle - axial strain (legend indicates fibre content)

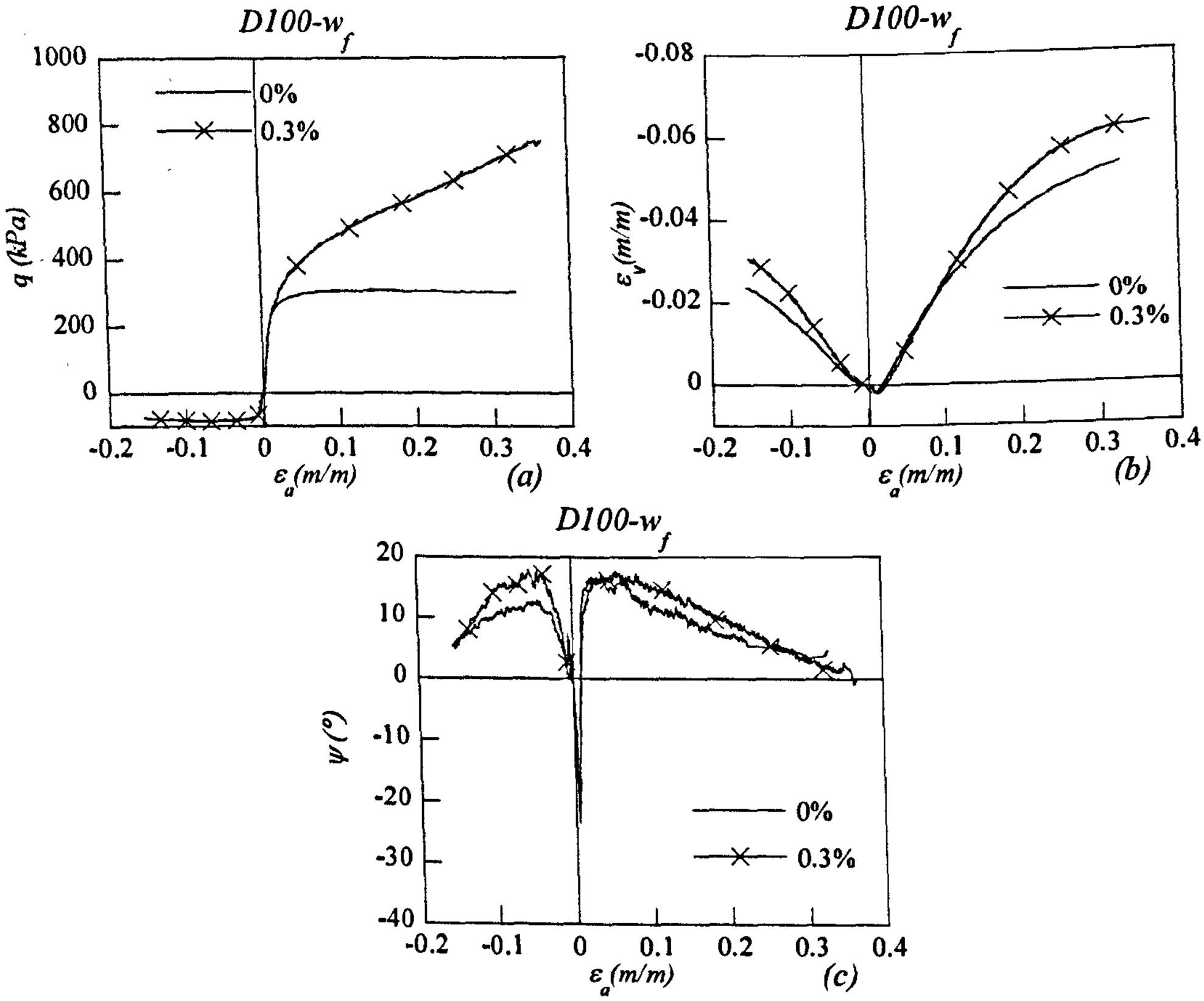

Fig. 5.9 Experimental results on *(D)* series specimens tested at 100 kPa cell confining pressure: *(a)* deviatoric stress - axial strain; *(b)* volumetric strain - axial strain; *(c)* dilatancy angle - axial strain (legend indicates fibre content)

Heineck et al. (2005) suggest that the initial stiffness of the composite soil is not influenced by the presence of fibres. Fibres become more effective under medium and large strains and this seems to be clearly shown by the triaxial compression results: the net strength increase induced by the fibre addition increases with the axial displacement. However, although some tests were taken to 30% to 40% axial strain, the deviatoric stress appears as though it would continually increase even beyond the values reached at these large axial strains. Similar patterns in triaxial compression tests and for polypropylene fibres have been presented by Ranjan et al. (1996) and Sway and Bang (2007). These macro results indicate that these particular fibres maintain an

ability to withstand tension within the sand matrix. Furthermore, exhumed specimens revealed that no appreciable plastic deformations (or breakage) of the fibres took place during the tests. The bonding between fibres and sand grains is unlikely to be complete: partial slippage will occur even though bonding remains sufficient for fibres to continue to work in tension. The stress transfer mechanism between sand and fibres is expected to be governed by friction but adhesion between fibres and sand grains may also be relevant.

A clearer representation of the contribution of fibres to the deviatoric response for extension loading is given in Fig. 5.10 where the deviatoric responses for *(M)* series specimens reinforced with different fibre contents are reported. The stress-strain relationships for reinforced specimens are almost identical to those for unreinforced specimens, showing a peak condition followed by a softening behaviour. This trend is qualitatively different from the one observed under compressive loading where a steady increase of the deviatoric strength with the axial strain was recorded for the whole duration of the tests. The contribution of fibres under extensive loading is limited and the response is mostly controlled by the sand matrix. However, even if not as consistent as for compressive loading, an increase of the peak friction angle from 37.1° for the unreinforced specimen to 40.1° and 44.4° for respectively 0.3% and 0.6% fibre content has been recorded.

No fibres damaged by the deformation process were observed after the tests. Therefore, the limit of the resistance afforded by the reinforcement seems to be due to pull-out between fibres and sand grains. This seems reasonable for the low confining pressures adopted in the tests.

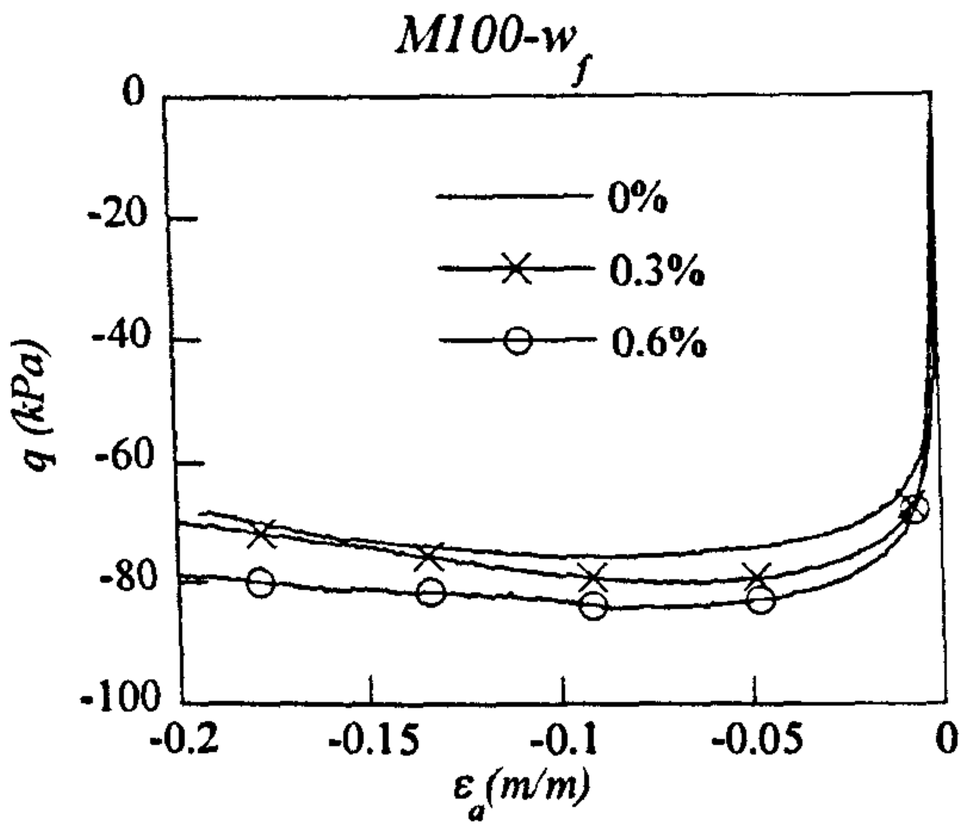

Fig. 5.10 Deviatoric stress-strain response for extension triaxial tests on *(M)* series specimens confined at 100 kPa cell pressure and reinforced with different fibre content as given in the legend

In both compression and extension loading, the volumetric response for reinforced sand, as for the unreinforced sand, showed an initial compression followed by dilation. The addition of fibres resulted in a decrease to the amount of compression followed by a tendency to exhibit more dilation, as also observed in the direct shear tests performed by Ibraim and Fourmont (2006) on similar specimens. This may be in contrast with the idea that fibres provide an extra confinement to the sand matrix and that their addition should result in a more compressive behaviour for reinforced specimens. However, it should be remarked that fibres also occupy a portion of the volume and they may be entangled enough to prevent the sand grains from using some of the available voids. This may result in an apparent densification effect for the sand matrix which in turn induces a more dilative behaviour for reinforced specimens. This suggested new interaction mechanism between sand and fibres will be further discussed in Chapter 7.

Tab. 5.5 Summary of results from triaxial tests in drained conditions for specimens unreinforced and reinforced with fibre type (1)

Test	$q_{20\%}$ (kPa)	$q / p_{20\%}$	$\phi_{20\%}$ (°)	ψ_{max} (°)
L030-00-D-1	83.2	1.44	35.5	2.5
L030-03-D-1	183.8	2.01	48.9	1.5
L030-06-D-1	316.6	2.34	57.2	3.5
L030-09-D-1	523.6	2.56	63.8	3.0
L060-00-D-1	155.2	1.39	34.3	1.8
L060-03-D-1	279.6	1.83	44.4	2.0
L060-06-D-1	458.3	2.15	52.4	2.4
L060-09-D-1	645.7	2.35	57.5	4.5
L100-00-D-1	248.8	1.36	33.7	1.5
L100-03-D-1	412.0	1.74	42.3	0.5
L100-06-D-1	585.8	1.98	48.2	2.0
L100-09-D-1	916.2	2.26	55.2	2.1
L200-00-D-1	477.2	1.33	33.0	1.0
L200-03-D-1	549.4	1.43	35.4	0.6
L200-06-D-1	910.1	1.81	44.0	0.7
L200-09-D-1	1236.7	2.02	49.1	--
M030-00-D-1	92.8	1.52	37.4	7.0
M030-03-D-1	208.0	2.09	50.9	9.4
M030-06-D-1	427.2	2.48	61.3	10.4
M100-00-D-1	275.1	1.44	35.4	3.5
M100-03-D-1	436.5	1.78	43.3	4.5
M100-06-D-1	648.4	2.05	49.8	6.0
M200-00-D-1	497.6	1.36	33.7	2.1
M200-03-D-1	699.6	1.62	39.5	3.5
M200-06-D-1	1010.0	1.88	45.8	4.4
M300-00-D-1	702.4	1.32	32.6	1.1
M300-03-D-1	934.2	1.53	37.5	2.0
M300-06-D-1	1300.5	1.77	43.2	3.5
D030-00-D-1	103.1	1.60	39.2	23.5
D030-03-D-1	265.7	2.24	54.7	21.5
D100-00-D-1	173.6	1.47	36.3	16.0
D100-03-D-1	332.8	1.95	47.3	17.1
D200-00-D-1	285.6	1.46	36.0	11.2
D200-03-D-1	427.0	1.76	42.9	14.4

Test	$q_{10\%}$ (kPa)	$q / p_{10\%}$	$\phi_{10\%}$ (°)	q_{peak} (kPa)	q / p_{peak}	ϕ_{peak} (°)	ψ_{max} (°)
ExL100-00-D-1	-72.1	-0.967	35.2	-73.3	-0.97	35.3	4.0
ExL100-03-D-1	-75.3	-1.028	38.3	-76.5	-1.027	38.3	4.5
ExL100-06-D-1	-79.8	-1 086	41.5	-79.7	-1.085	41.5	6 8
ExL200-00-D-1	-141.8	-0.947	34 2	-144.6	-0.953	34.5	2.2
ExL200-03-D-1	-148.3	-0.979	35.8	-148.3	-0,979	35,8	4.1
ExL200-06-D-1	-154 2	-1 032	38.5	-154 2	-1.032	38 5	6 0
ExM100-00-D-1	-75.5	-0.996	36.7	-75.2	-1.004	37.1	6.3
ExM100-03-D-1	-78.5	-1.036	38.7	-78.4	-1.061	40.1	8.8
ExM100-06-D-1	-82.8	-1.106	42.7	-82.3	-1.135	44.4	13.8
ExD100-00-D-1	-75.4	-0.995	36.6	-79.7	-1.086	41.5	12.6
ExD100-03-D-1	-81 9	- .078	41 1	-81.9	-1.127	43.9	17.2

The influence of the density of the sand matrix on the performance of reinforced specimens is evident as dense specimens are generally stronger than loose ones (Fig. 5.11-5.13). As a matter of fact, dense specimens tend to dilate more than loose ones, inducing a greater desire for *radial* strain and therefore greater potential tensile stresses in the fibres which results in a much larger strength increase than observed for loose specimens. However, it seems that specimens tested at the same confining pressure may converge towards the same deviatoric strength irrespective of their density as normally occurs for unreinforced specimens.

As for unreinforced specimens, the behaviour of the reinforced specimens is less compressive and more dilative when lower confining pressures and higher density are employed (Figs 5.11b-5.13b). The loosest specimens show a very compressive behaviour with a negligible tendency to dilate while the densest specimen tested with 30 kPa cell confining pressure shows clearly a very dilative behaviour.

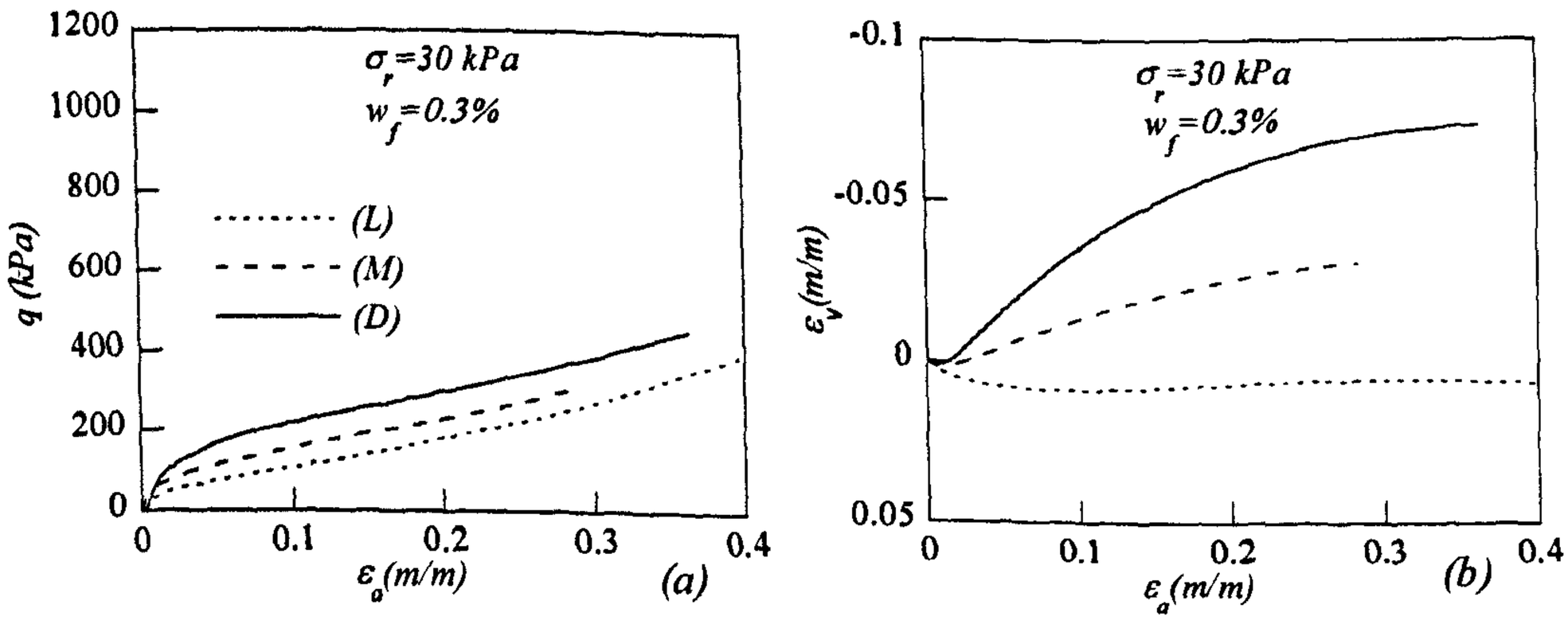

Fig. 5.11 Influence of relative density on compressive behaviour for specimens reinforced with 0.3% of fibres under 30 kPa cell confining pressure: *(a)* deviatoric stress-strain behvaiour ; *(b)* volumetric behaviour

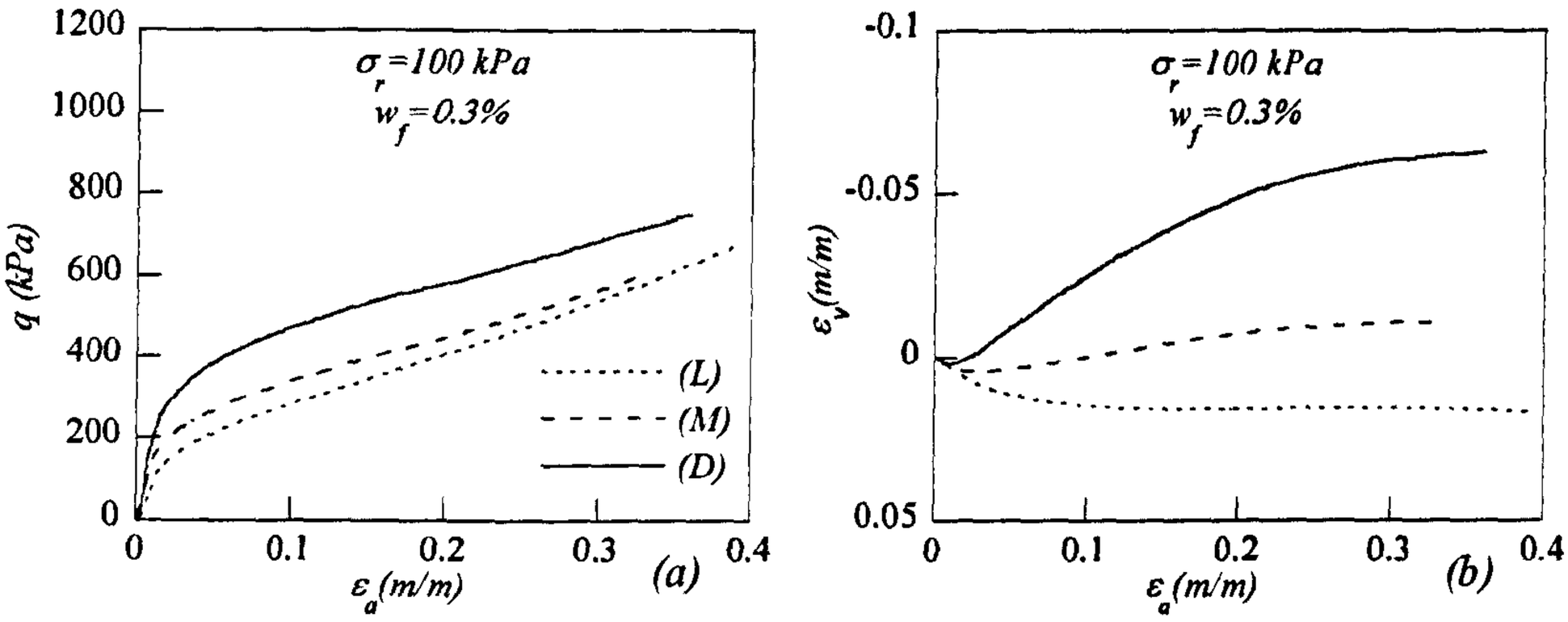

Fig. 5.12 Influence of relative density on compressive behaviour for specimens reinforced with 0.3% of fibres under 100 kPa cell confining pressure: *(a)* deviatoric stress-strain behvaiour ; *(b)* volumetric behaviour

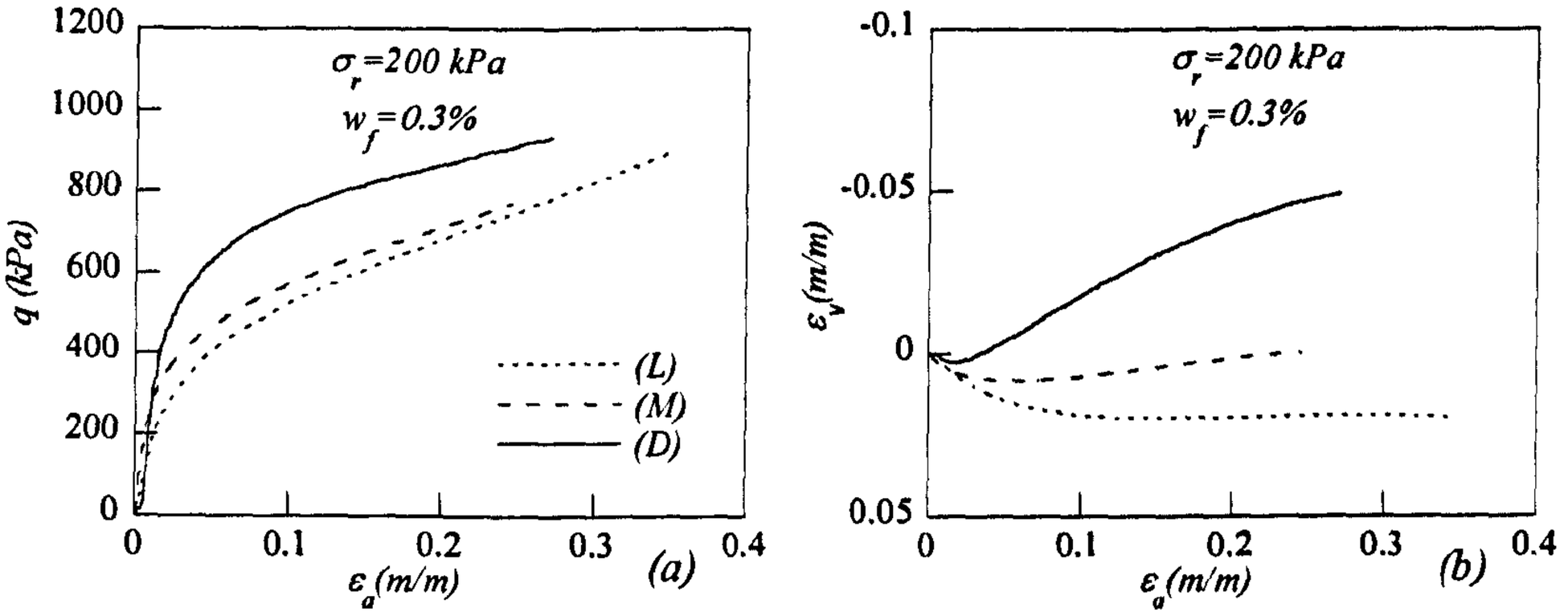

Fig. 5.13 Influence of relative density on compressive behaviour for specimens reinforced with 0.3% of fibres under 100 kPa cell confining pressure: *(a)* deviatoric stress-strain behvaiour ; *(b)* volumetric behaviour

The influence of the cell confining pressure for compressive loading is also highlighted in Figs. 5.11-5.13 where the deviatoric stress supported by the reinforced specimens increases with the confining stress. A common feature among the plots is the somewhat bilinear trend of the deviatoric response for all the specimen densities and cell confining pressures. However, the second part of the bilinear trend of the deviatoric response becomes rather parabolic for the lower cell confining pressures (Fig.5.11a): the tangent modulus ($E_{tg} = dq/d\varepsilon_a$) of the stress-strain seems to increase with the axial strain as the bonding between fibres and sand grains is improved during loading. It has already been discussed that the bonding between fibres and

sand grains may not be perfect and it seems reasonable that the bonding can be enhanced by the stress level. During shearing the stresses in the specimens increase and in turn fibres and sand grains may be more efficiently bonded together: this may decrease their relative slippage and indeed increase the slope of the stress-strain trend. This feature becomes more evident if the evolution of the tangential modulus (E_{tg}) is plotted versus the axial strains (ε_a) as shown in Fig. 5.14 for *(L)* series specimens reinforced with different amounts of fibres. For low confining pressure, the tangential modulus does not reach a constant value but it increases as shearing continues. It seems also that for all the specimens with the same density and fibre content the tangential modulus of the deviatoric response converges towards a unique value.

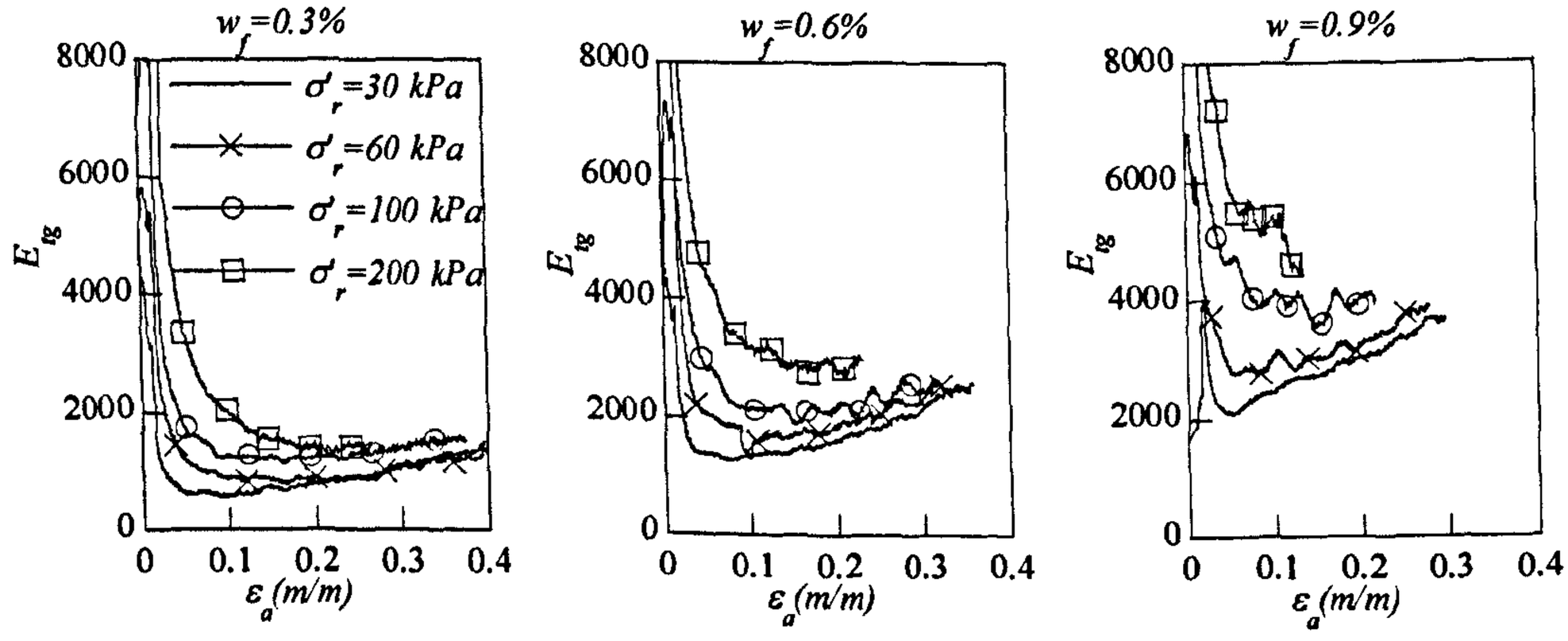

Fig. 5.14 Tangential modulus (E_{tg}) of the deviatoric stress-strain behaviour during test for *(L)* series specimens reinforced with different fibre content and tested at different cell pressures

5.4.2.2 Strength envelopes

The serviceability failure criterion was previously defined as 20% axial strain for compressive loading or as 10% for extensive loading. The *at failure* deviatoric strength envelopes for specimens reinforced with different fibre contents and at the same initial relative density are reported in Fig. 5.15, where the strength envelope for the unreinforced sand is also reported for comparison. Because of the limited number of tests in extension, the failure envelopes for this loading condition are shown only for the *(L)* series specimens (Fig. 5.15a). The strength

envelopes are almost linear for a given fibre content irrespective of the relative density and the dependence of the effectiveness of fibres on the load condition is again clear. It should be noted that these strength envelopes are different from the typical bilinear or curved-linear failure envelope for fibre reinforced sand (Gray and Ohashi, 1983; Maher and Gray, 1990; Bailey, 2000 among others) but this may be due to the absence of a limit on the resistance afforded by the reinforcement or by the low confining pressure applied that does not permit a tension failure of the reinforcement.

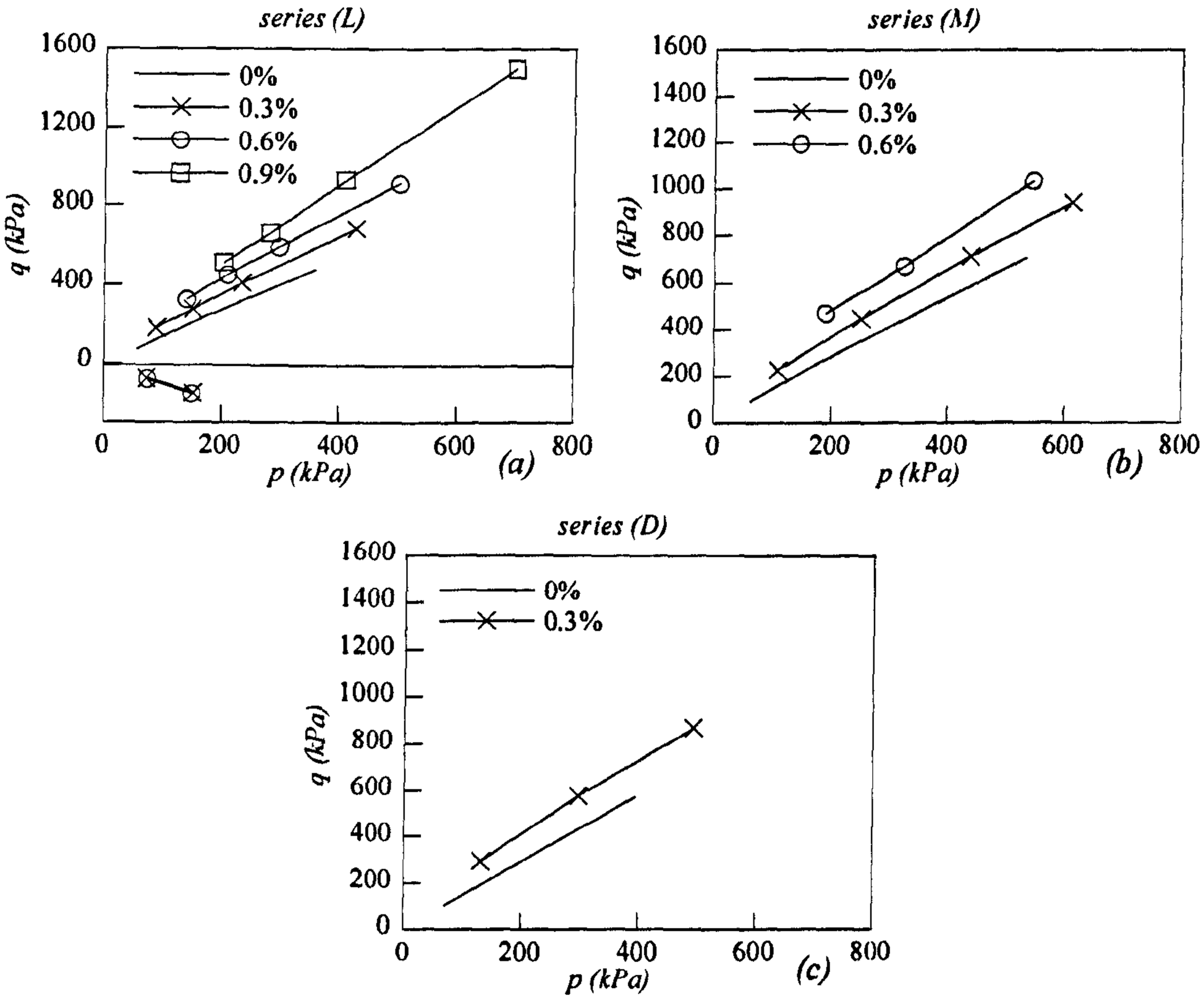

Fig. 5.15 Deviatoric strength envelopes at 20% of axial strain: *(a) (L)* tests series, *(b)* (M) tests series and *(c)* (D) tests series, (legend gives the fibre content used)

The friction angle for soils is generally dependent on the test confining pressure and the failure envelope is expected to be non-linear. However for the limited range of confining pressure employed here and for a simpler quantification of the reinforcing effect of the fibres, a linear envelope has been considered satisfactory enough to describe the strength of the specimens. The shear strength parameters for all series of tests have been derived assuming a Mohr-Coulomb failure criterion and the strength parameters are summarised in Table 5.6. In compression the addition of fibres results in a significant increase of the friction angle and cohesion intercept while in extension the increase is very limited for both the parameters. The Mohr circles at failure for unreinforced and reinforced specimens are compared in Fig.5.16a for the loosest specimens tested with a cell confining pressure of 100 kPa. As expected the size of the circle increases with the fibre content. A typical strength envelope for a reinforced specimen is reported in Fig 5.16*b*.

Tab. 5.6 Angle of friction and cohesion intercept of all series of tests in compression at failure (ε_a=20%)

Compression tests - FIBRE 1 - at failure $\varepsilon_a = 20\%$								
Test Series	Fibre content (%)							
	0		0.3		0.6		0.9	
	c (kPa)	ϕ(°)	c (kPa)	ϕ(°)	c (kPa)	ϕ(°)	c (kPa)	ϕ(°)
(L) tests	0.0	33.5	25.0	36.5	48.0	40.0	72	47
(M) tests	6 0	33.0	38 0	36.0	83 0	39.0	-	-
(D) tests	6 0	35.5	45.0	39 0	-	-	-	-
Extension tests - FIBRE 1 - at failure								
(L) tests	2.0	34.0	3.0	35 0	6 0	36.0	-	-

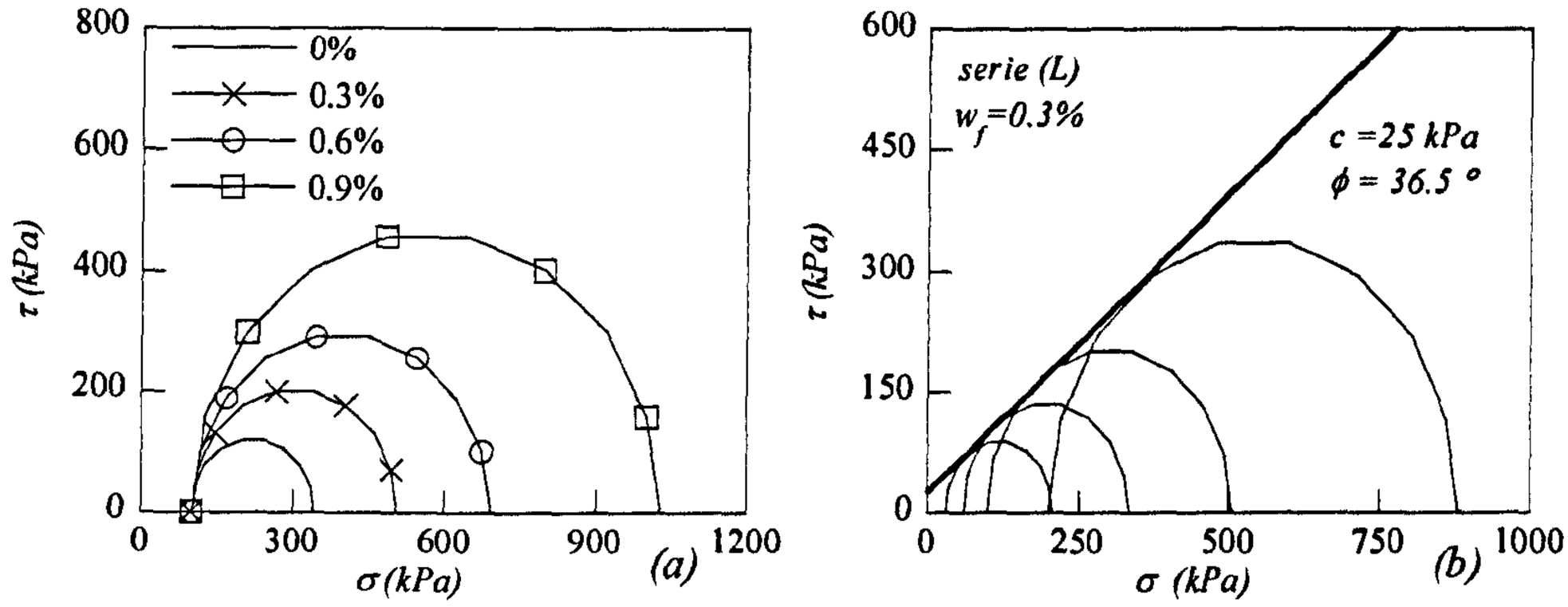

Fig. 5.16 Influence of specimen density on the size of Mohr-circle at failure for compressive loading: *(a)* tests performed at 100 Kpa cell pressure, *(b)* summary of test on specimens reinforced with 0.3% fibre content

The variation of the deviatoric stress at the serviceability failure (ε_a=20% in compression and ε_a=-10% in extension) with the amounts of fibres is presented in Fig. 5.17 for both compressive and extensive loading conditions. In compression (Fig. 5.17a), the trend of the deviatoric stress seems parabolic with the fibres content for all the reported specimen densities. However, the deviatoric stress is also dependent on the density of the specimen: for example a loose specimen *(L)* reinforced with 0.6% fibre content has the same deviatoric strength as a denser specimen *(D)* with 0.3% fibre content. As already explained, this particular feature is related to the deformation patterns of the specimens: dense specimens tend to dilate more than loose ones inducing greater tensile strain (and in turn stresses) in the fibres. This plot (Fig. 5.17) reports also the following similarities with the results obtained by Ibraim and Fourmont (2006) on similar reinforced specimens tested with the direct shear apparatus:

- the envelopes of test series *(L)* and *(M)* show a much closer trend than the others;
- the difference of the envelopes for different densities increases with the confining pressure;
- the slope of the envelopes increase with the confining pressure.

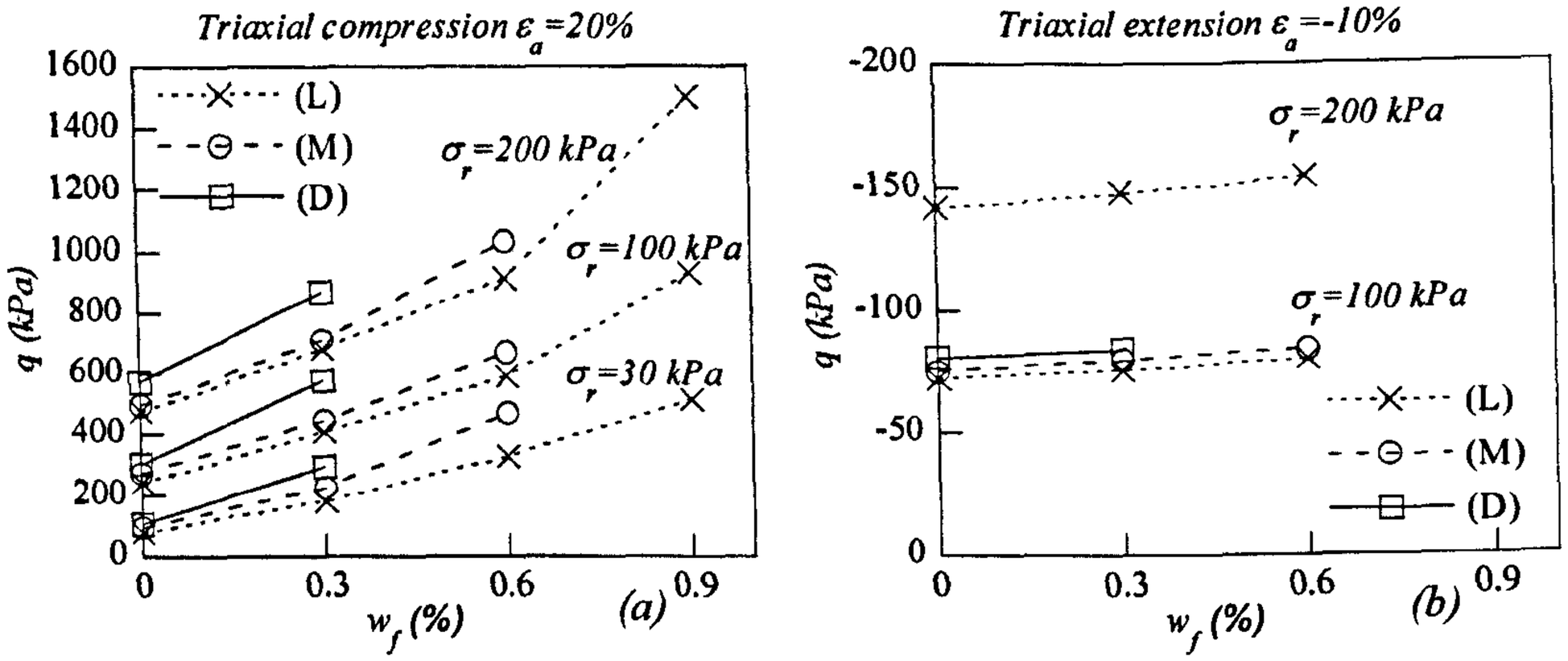

Fig. 5.17 Deviatoric strength at 20% axial strain in triaxial compression *(a)* and extension *(b)* for ensemble of specimen densities and three different confining stresses, 30, 100 and 200 kPa

It can be noted that for all confining pressures, the loosest specimen *(L)* reinforced with 0.3% of fibres give much higher shear strength than the densest but unreinforced specimen *(D)*. However this is not the case in extension (Fig. 5.17b) where for 100 kPa of cell pressure, the performance typical of a dense specimen can be obtained by reinforcing a loose one with approximately 0.6% of fibres. For this load condition the trend of the deviatoric strength is nearly linear with the fibre content.

Since the contribution of the fibres is dependent on the loading condition, it is interesting to make a wider comparison of the strength envelopes by introducing the results of direct shear tests performed by Ibraim and Fourmont (2006) on the same type of reinforced material. Failure criteria for both reinforced and unreinforced material in all test conditions can be described according to Mohr Coulomb theory:

$$\tau = c + \sigma \tan(\phi) \tag{5.2}$$

and the extra strength $\Delta\tau$ provided by the reinforcement can be measured as the difference between the strength of the reinforced specimen τ_R and the unreinforced specimen τ_{UNR}:

$$\Delta\tau = \tau_R - \tau_{UNR} \tag{5.3}$$

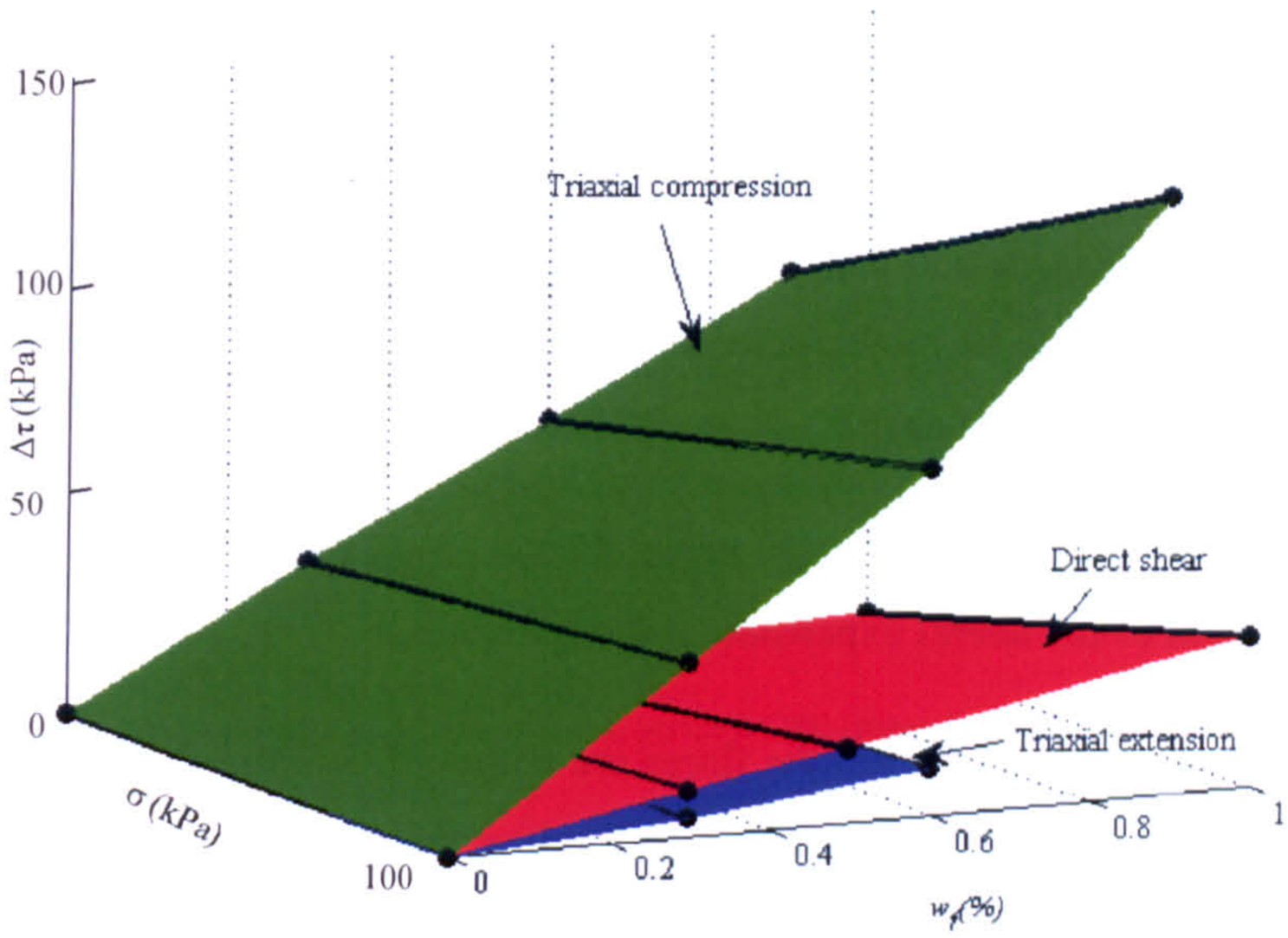

Fig. 5.18 Extra strength provided by fibres reinforcement for different loading conditions

A comparison between the contributions of the fibres for the different loading conditions (triaxial compression, triaxial extension and direct shear) is reported in Fig.5.18 in terms of the extra strength envelope $\Delta\tau$ as a function of the effective stress σ and the fibre content w_f. The strength envelope for triaxial compression is much higher than the ones in triaxial extension and direct shear test which are comparable. However the reinforcement seems to be more effective for direct shear tests than for extension tests: the direction of the tensile strains for direct shear test is between the ones for compression and extension, therefore fibres stresses are more mobilised in direct shear than in triaxial extension. The trend shown in Fig. 5.18 demonstrates again that the effectiveness of fibres is dependent on the fibre orientation relative to the tensile strain direction.

5.4.2.3 Dilatancy

The volumetric response for reinforced sand, as for the unreinforced sand, showed an initial compression followed by dilation. The addition of fibres resulted in a decrease to the amount of compression followed by a tendency to exhibit more dilation, as also observed in the direct shear tests performed by Ibraim and Fourmont (2006) on similar specimens. However, at large

strains the unreinforced specimens continue to dilate while the reinforced ones reach a constant volume condition or start to recompress again (Figs. 5.7, 5.8 and 5.9). This may be explained by a double interaction mechanism between fibres and the sand matrix:

- fibres occupy volume and their addition results in an increase of relative density of the specimens (it should be remembered that in this research the fibres are added on the top of a constant amount of sand);

- fibres provide extra confining stress to the sand matrix which may result in a containment of the lateral expansion of the specimens.

At small strains, when the stresses in the fibres are not much mobilized, the increase of density may have a bigger effect on the volumetric behaviour than the confinement effect while the extra confinement of the fibres may become more important at larger strains as more tensile stresses are developed in the fibres.

The trend of the dilatancy ratio evolution with the stress ratio (q/p) is reported in Fig. 5.19 for both unreinforced and reinforced specimens. The trend for the unreinforced specimen (black dots in Fig.5.19) shows a linear trend with the dilatancy ratio approaching zero at the critical state condition which is in general agreement with the common formulation of the dilatancy relationship (Rowe, 1962; Roscoe et al., 1963). For a reinforced specimen, when the density has ceased to change further, there is still an increase in the supported deviatoric stress leading to a vertical trend on the stress-dilatancy plane and the data diverge from Rowe's relationship. Further discussion on the dilatancy for reinforced soil will be given in section 5.4.5.3 and it will be further analysed when a modelling approach will be proposed in Chapter 7.

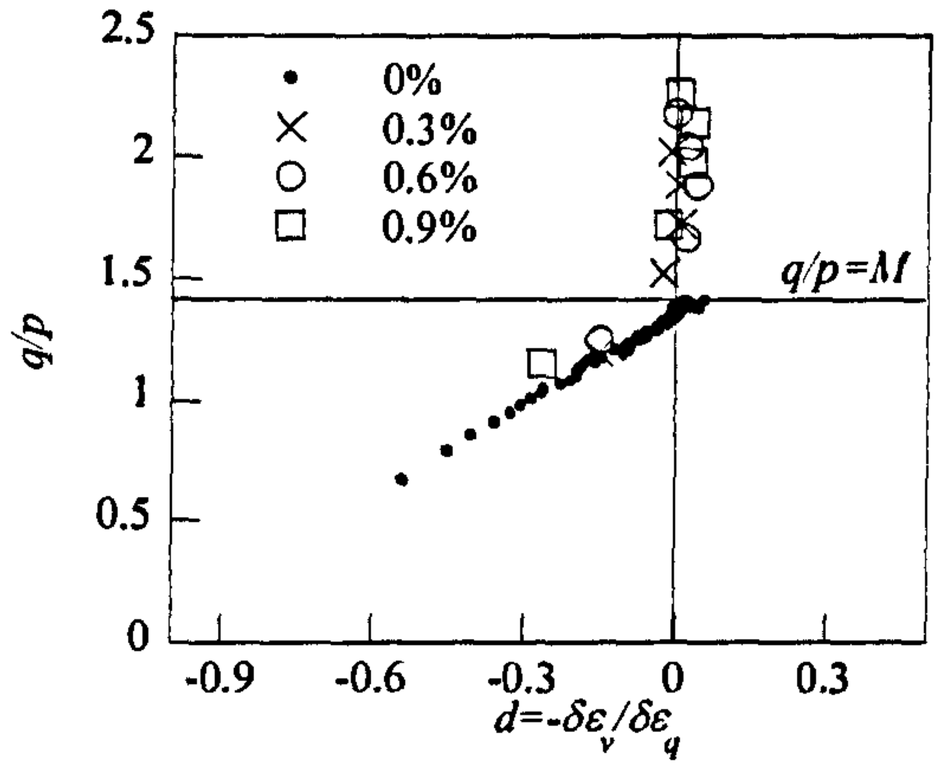

Fig. 5.19 Stress-dilatancy ratio for the test series M200 (legend express fibre content)

5.4.3 Specimens reinforced with fibre type 2

5.4.3.1 General

Specimens reinforced with fibre (2) have been tested only under compressive loading where the contribution of fibres is more remarkable. Most of the tests have been performed on loose specimens *(L)* under confining pressures ranging from 30 kPa to 100 kPa. Details of the test performed have been given in paragraph 5.2. Typical results from the triaxial tests are presented in Figs. 5.20 where the variations of the deviatoric stress (q), the volumetric strain (ε_v) and the angle of dilatancy (ψ) are presented with the axial displacement (ε_a). Performances of *(L)* and *(M)* series specimen tested at 100 kPa cell confining pressure are shown.

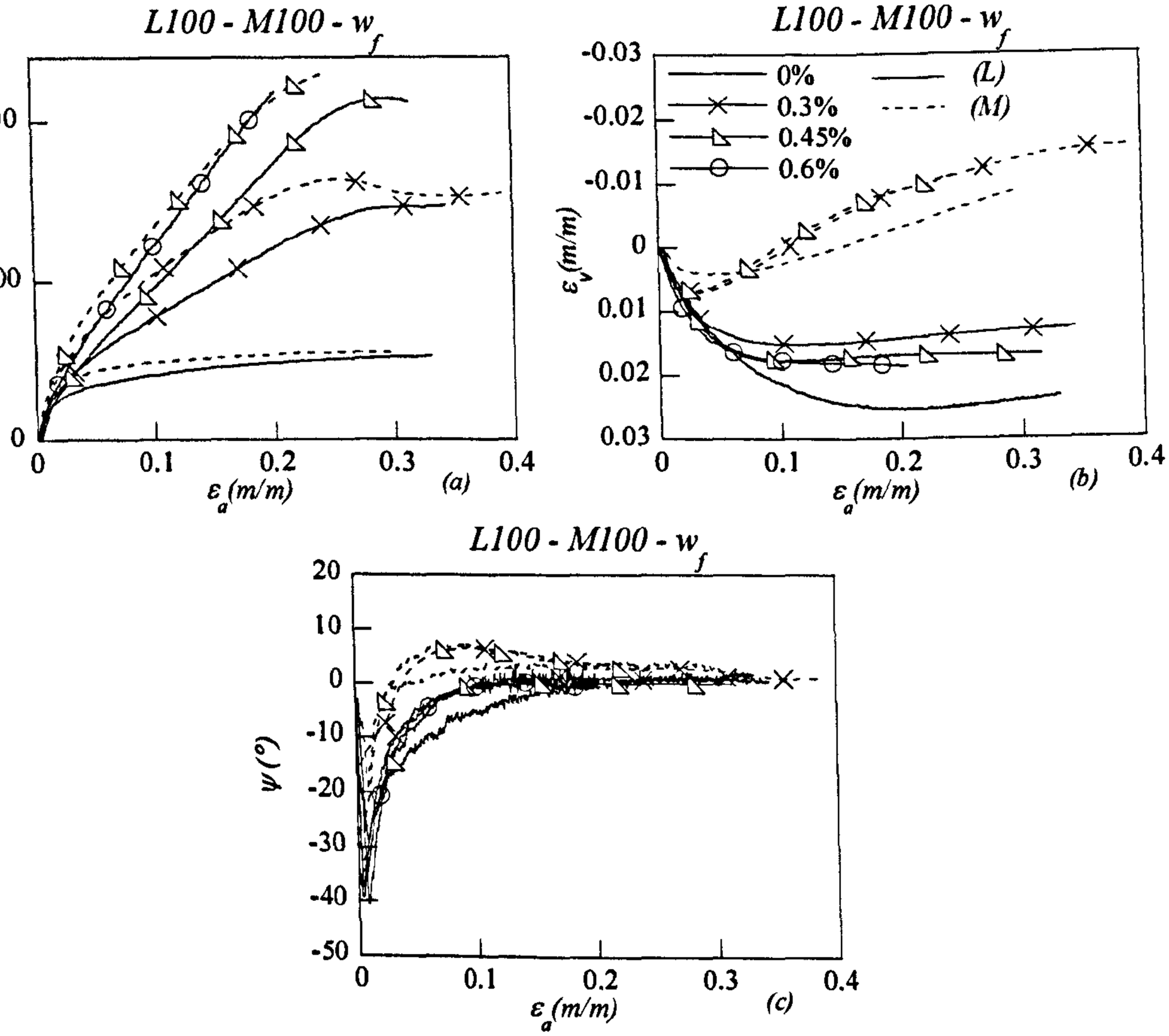

Fig. 5.20 Experimental results on *(L)* and *(M)* series specimens tested at 100 kPa cell confining pressure: *(a)* deviatoric stress - axial strain; *(b)* volumetric strain - axial strain; *(c)* dilatancy angle - axial strain

The deviatoric stress-axial strain curves in Fig. 5.20 show again that the reinforced sand exhibits a greater strength than the unreinforced sand. The stress-strain pattern is very similar to that observed for fibre type (1) with an exception at large strains where a flattening of the curve is noticeable: a limit of the resistance afforded by this type of reinforcement has been reached during the tests. The flattening is not shown for the specimens reinforced with 0.6% of fibres because the test had to be stopped at an earlier stage in order to avoid exceeding the capacity of the load cell. The analysis of exhumed samples did not reveal breakages of the fibres and it is believed that failure of the interaction mechanism and therefore flattening of the curves is caused by sliding between fibres and sand grains. This is in accord with some models and

observations already published (Zornberg, 2002; Michalowski and Čermák 2003) which implies the use of higher cell confining pressure to cause the breakage of such resistant fibres.

The deviatoric strength at failure does not seem to be much influenced by the density of the specimen. *(L)* and *(M)* specimens reinforced with 0.3% of fibres reach a similar deviatoric strength at failure, while specimens reinforced with 0.45% might do the same if the *(M)* test was carried out further (the test was stopped because the maxima allowance of the load cell was reached). Instead, the stiffness of the reinforced specimen is indeed influenced by the relative density and denser specimens reach the failure state before looser specimens. Series *(L)* specimens reach failure at about 30% of axial strain while series *(M)* ones fail at about 25%: dense specimens dilate more than loose ones, inducing greater tensile strains in the fibres which reach the slippage threshold in advance.

As for fibres (1), the presence of fibres generates a more dilative behaviour when compared with unreinforced specimens (Fig. 5.20 b and c). This may again be explained by the increase of relative density when fibres are added, however a general trend of the volumetric behaviour with the fibre content can not be recognised. For *(M)* series specimens, the increase in dilation is also accompanied by a more compressive behaviour at the very early stage of the test.

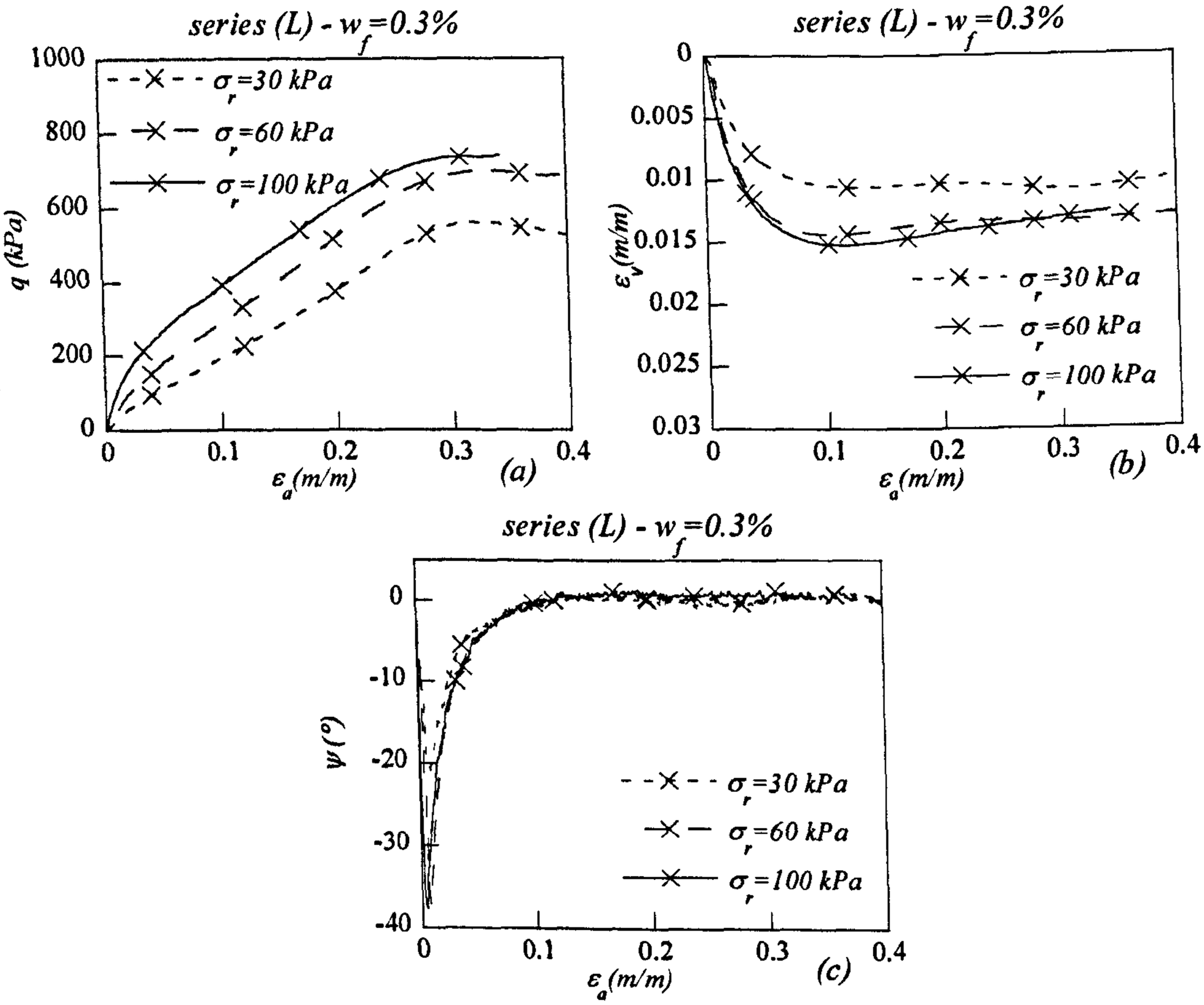

Fig. 5.21 Set of experimental results on specimens reinforced with 0,3% of fibres. Influence of relative density (given in the legend): *(a)* deviatoric stress - axial strain; *(b)* volumetric strain - axial strain; *(c)* dilatancy angle - axial strain

The influence of the cell confining pressure on the behaviour of reinforced specimen is reported in Fig. 5.21 where *(L)* specimens reinforced with 0.3% of fibres are compared when tested at different pressures. Again at low cell pressures, the second portion of the deviatoric trend seems not linear with a slope increasing during the test (Fig. 5.21a). This may prove the enhancement of the bonding between fibres and sand as the stresses in the composite increase. The adoption of lower cell pressure results in less compressive behaviour of the specimens (Fig. 5.21b).

Tab. 5.7 Summary of results from triaxial tests in drained conditions for specimens unreinforced and reinforced with fibre type (2)

Test	$q_{20\%}$ (kPa)	$q / p_{20\%}$	$\phi_{20\%}$ (°)	$q_{failure}$ (kPa)	q / p_{failur}	$\phi_{failure}$ (°)	ψ_{max} (°)
L030-00-D-2	402.7	2.45	60.5	585.0	2 60	65.1	4.6
L030-03-D-2	560.6	2.59	64 6	795.2	2.70	68.4	1.7
L030-045-D-2	704.1	2.66	67.1	1049.2	2.76	71.1	2.6
L030-06-D-2	541.0	2.25	54.9	715.5	2.40	58.9	0.9
L060-00-D-2	645.7	2 35	57.5	954 5	2.52	62.7	0 8
L060-03-D-2	902.2	2.50	62.0	1197.6	2.61	65.4	1 3
L060-045-D-2	610 9	2.01	48.9	740.5	2.14	51.9	1.0
L060-06-D-2	884 2	2.24	54.6	1106.3	2.36	57.9	0.5
L100-00-D-2	1084.6	2.35	57.6	n.a	n a	n.a	0.5
L100-03-D-2	749.0	2.14	52.1	747.7	2.14	52.1	6.8
L100-045-D-2	1055.4	2.34	57.2	1133.1	2.37	58.2	7.4
L100-06-D-2	402.7	2.45	60.5	585.0	2.60	65.1	4 6
M100-00-D-2	560.6	2.59	64.6	795.2	2.70	68 4	1.7
M100-03-D-2	704 1	2 66	67.1	1049.2	2.76	71.1	2.6
M100-045-D-2	541 0	2 25	54.9	715.5	2.40	58.9	0.9

5.4.3.2 Strength envelopes

The strength envelopes for the reinforced specimens are reported in Fig. 5.22 for the serviceability failure condition (previously defined at 20% of axial strain) and for the proper failure of the specimen. The contribution of the reinforcement to the strength of the sand is remarkable and the strength parameters for different fibre concentrations are reported in Table 5.8 for both failure conditions. Both the friction angle and the cohesion of the material increase with the fibres content. The strength parameters for medium dense specimens could not be calculated because they were tested only at 100 kPa cell pressure and the failure envelope could not be determined.

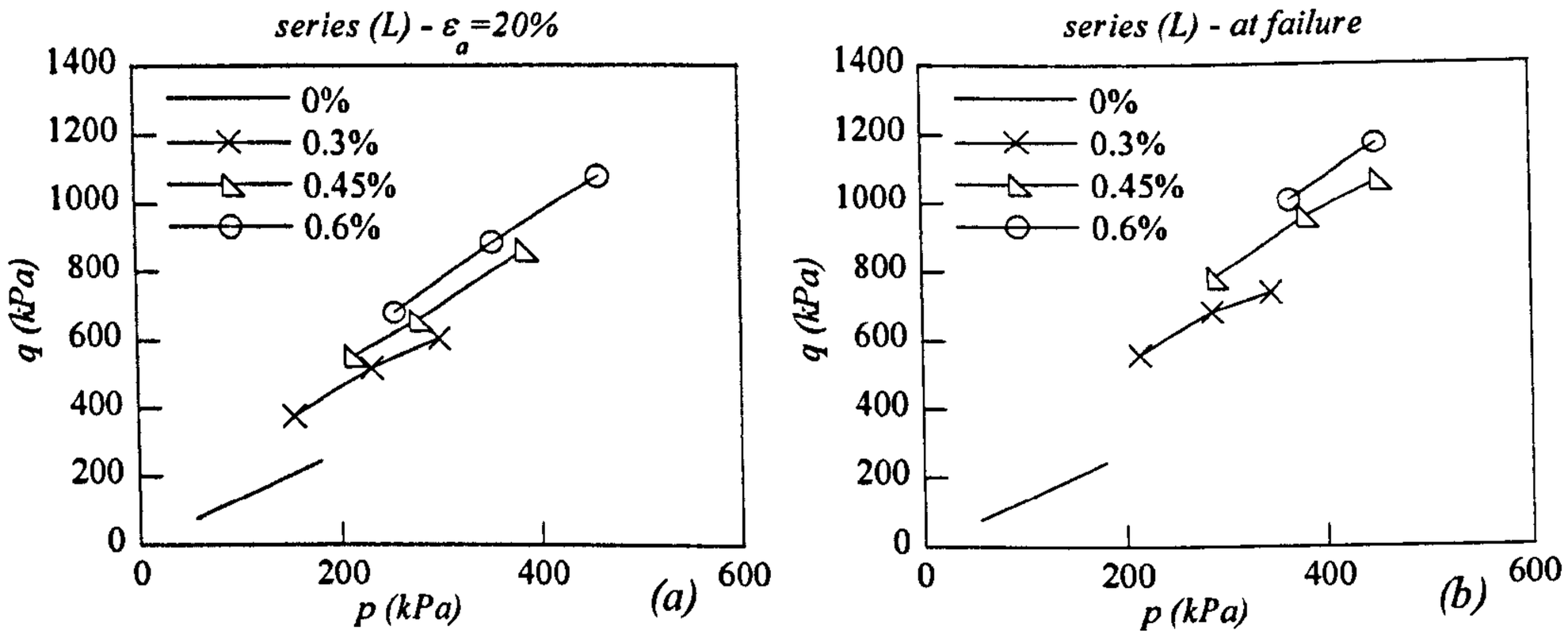

Fig. 5.22 Deviatoric strength envelopes: *(a)* at ε_a=*20%* and *(b)* at failure for (L) tests series (legend gives the fibre content used)

Tab. 5.8 Angle of friction and cohesion intercept for *(L)* series of tests at serviceability failure (ε_a=20%) and at the reinforcement failure for fibre type (2)

FIBRE (2) - (L) tests								
	Fibre content (%)							
	0		0.3		0 45		0.6	
	c (kPa)	ϕ(°)	c (kPa)	ϕ(°)	c (kPa)	ϕ(°)	c (kPa)	ϕ(°)
At failure	0.0	33.5	125 0	35.0	150 0	43.0	170.0	47.0
ε_a = 20%	0.0	33.5	70	39.0	100	43.0	115	47

The variation of the deviatoric strength with the quantity of fibres is presented in Fig.5.23 for both failure conditions. The lines are almost linear for all the relative densities and cell pressures, particularly for proper failure conditions (Fig.5.23b). The effectiveness of the fibres is immediately noticeable as the deviatoric strength at failure is enhanced by about 300% in the lowest case (w_f=*0.3%* - σ_r=*100kPa*)

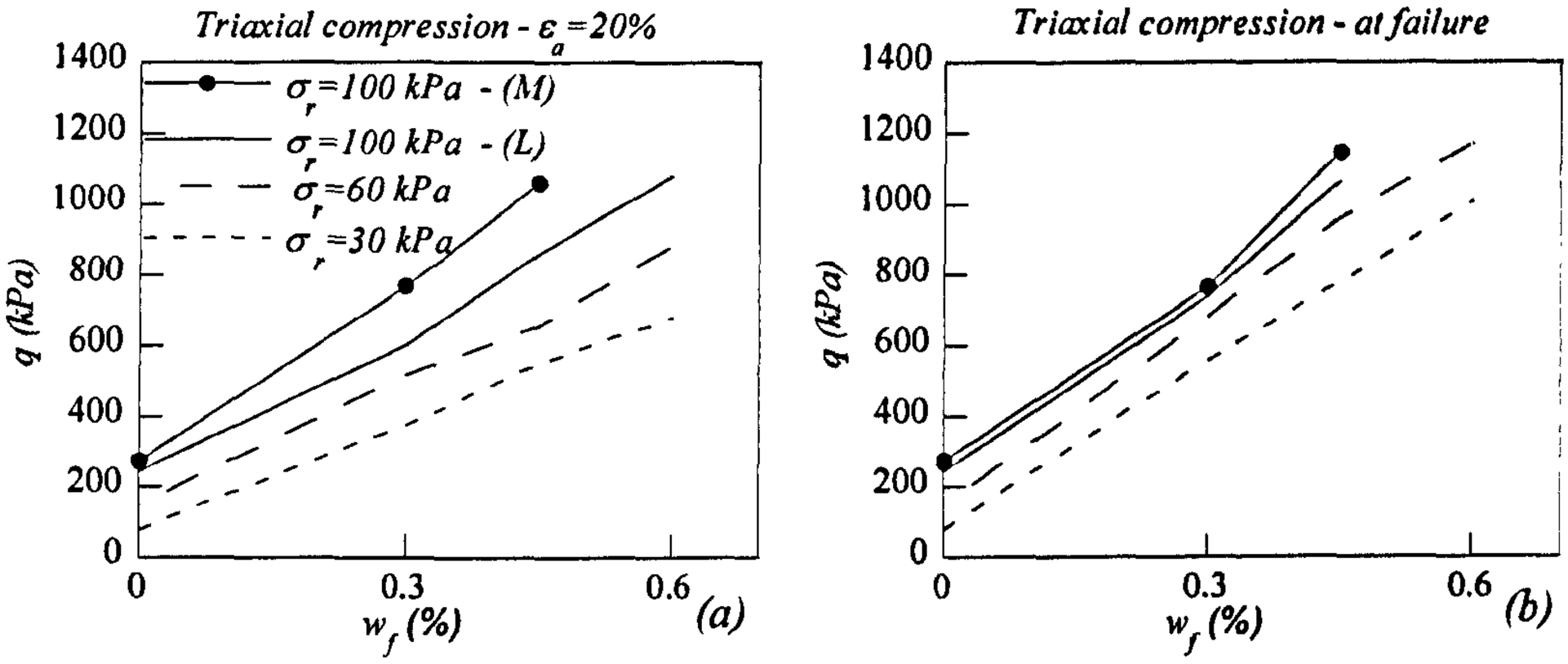

Fig. 5.23 Deviatoric strength at 20% axial strain and at failure in for ensemble of specimen densities and three different confining stresses, 30, 60, and 100 kPa

5.4.4 Specimens reinforced with fibre type (3)

5.4.4.1 General

The experimental campaign on specimens reinforced with fibre type (3) comprises the same tests as performed for fibre type (2) (see Table 5.3). The triaxial compression test results for the platy fibres (3) are presented in Fig. 5.24 where performances of *(L)* and *(M)* series specimen tested at 100 kPa cell confining pressure are shown. For this case, the stress-strain curves are rather parabolic and a gradual flattening of the response can be observed at large strains (Fig. 5.24*a*). However a complete flattening of the stress-strain trend is not detectable and definitive conclusions about the failure of the reinforcement can not be drawn. It should be mentioned that fibres type (3) are very stiff when compared with the other types and no plastic deformations were observed on exhumed specimens after the test. This means that if there is a failure mechanism of the reinforcement, this is certainly governed by the sliding between fibres and sand grains. However, if the sliding is not complete, it is thought to be very much developed.

The relative density influences the stress-strain behaviour of both unreinforced and reinforced specimens, even if the critical state deviatoric strength seems only to be dependent on the fibre content and not on the density of the specimen (Fig. 5.24*a*): stress-strain response for *(L)* and

(M) unreinforced and reinforced (0.3% and 0.6% fibre content) specimens seem to converge towards the same critical state deviatoric stress.

As for the previously employed fibres (type (1) and (2)), the addition of fibres generates a more dilative behaviour when compared to unreinforced specimens (Fig. 5.24*b* and *c*) but a clear trend of the volumetric behaviour with fibre content is not detectable. It should be remarked that for this type of reinforcement, the increase of the dilative behaviour accompanying fibre addition is not as evident as for the previously used reinforcements.

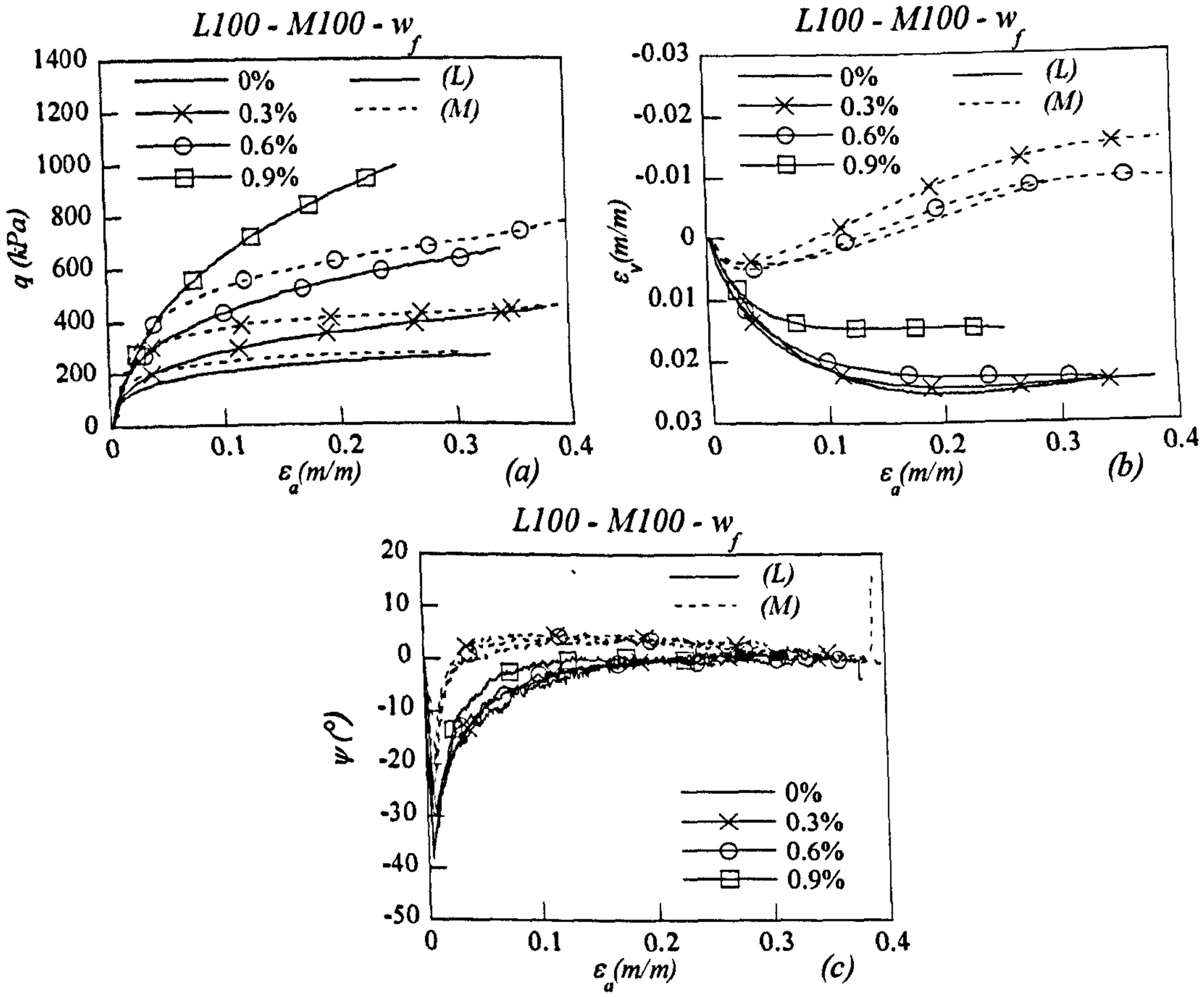

Fig. 5.24 Experimental results on (L) and (M) series specimens tested at 100 kPa cell confining pressure: *(a)* deviatoric stress - axial strain; *(b)* volumetric strain - axial strain; *(c)* dilatancy angle - axial strain (legend indicates fibre content)

Experimental results shown in Fig.5.25 highlight the influence of cell confining pressure on the deviatoric, volumetric and dilatancy behaviour of loose specimens reinforced with 0.6% of fibres. Trends are as generally expected: the deviatoric strength increases with confining pressure while dilatancy decreases.

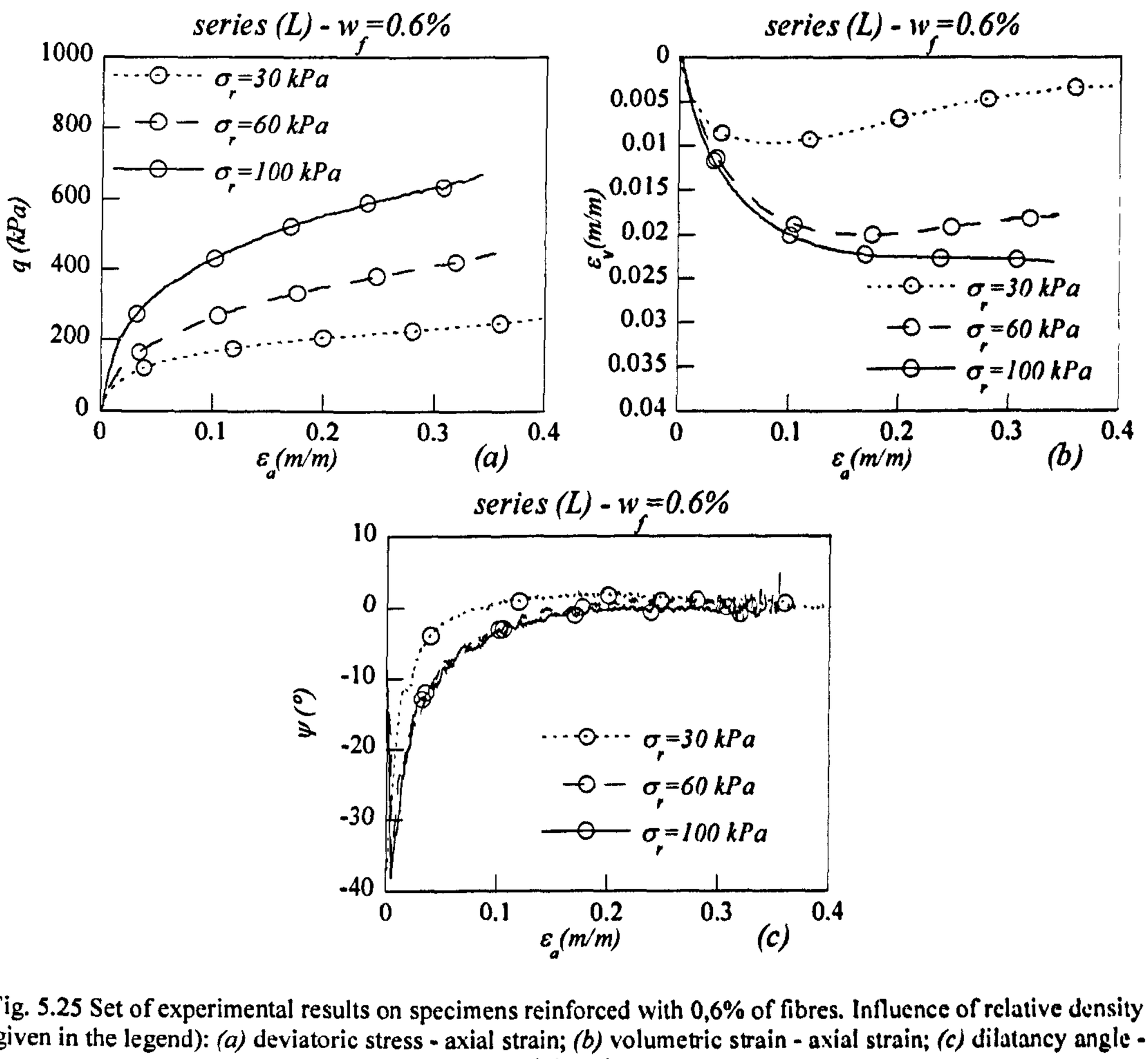

Fig. 5.25 Set of experimental results on specimens reinforced with 0,6% of fibres. Influence of relative density (given in the legend): *(a)* deviatoric stress - axial strain; *(b)* volumetric strain - axial strain; *(c)* dilatancy angle - axial strain

Tab. 5.9 Summary of results from triaxial tests in drained conditions for specimens unreinforced and reinforced with fibre type (3)

Test	$q_{20\%}$ (kPa)	$q / p_{20\%}$	$\phi_{20\%}$ (°)	ψ_{max} (°)
L030-00-D-3	140.4	1 83	44 5	1.8
L030-03-D-3	216.1	2.12	51.5	2.2
L030-06-D-3	289.2	2.29	55.9	2.9
L030-09-D-3	233 8	1.70	41.4	1.5
L060-00-D-3	363 3	2 01	48 7	1 5
L060-03-D-3	595.9	2.30	56.3	1.0
L060-06-D-3	373.1	1.66	40.6	0.9
L060-09-D-3	568.7	1.96	47.7	0.1
L100-00-D-3	917.9	2.26	55.2	0.4
L100-03-D-3	409.8	1.73	42.2	4.9
L100-06-D-3	622 1	2 02	49.2	4.4
L100-09-D-3	140.4	1 83	44 5	1.8
M100-00-D-3	216.1	2.12	51.5	2.2
M100-03-D-3	289.2	2.29	55.9	2.9
M100-06-D-3	233.8	1.70	41.4	1 5

5.4.4.2 Strength envelopes

Since the failure of the composite material is not as clear as for fibre (2), the failure is again referred to a serviceability limit here. The strength envelopes for *(L)* series specimens reinforced with different amount of fibres are shown in Fig. 5.26, where the strength envelope for unreinforced sand is also plotted for comparison. The strength envelope may be described with a linear trend for all the fibre contents employed.

The contribution of the reinforcement to the strength of the sand is consistent even if not as remarkable as for previous reinforcements. The strength parameters, determined assuming a linear Mohr-Coulomb failure criterion, are reported in Table 5.10. The addition of fibres slightly increases the cohesion intercept (intended as the intercept of the failure envelope with the shear stress axis) but it highly affects the friction angle of the fibres. According to the recent failure theories for fibre reinforced soils (Zornberg, 2002; Michalowski and Čermák 2003), this confirms that the eventual failure mechanism is governed by relative slippage between the components.

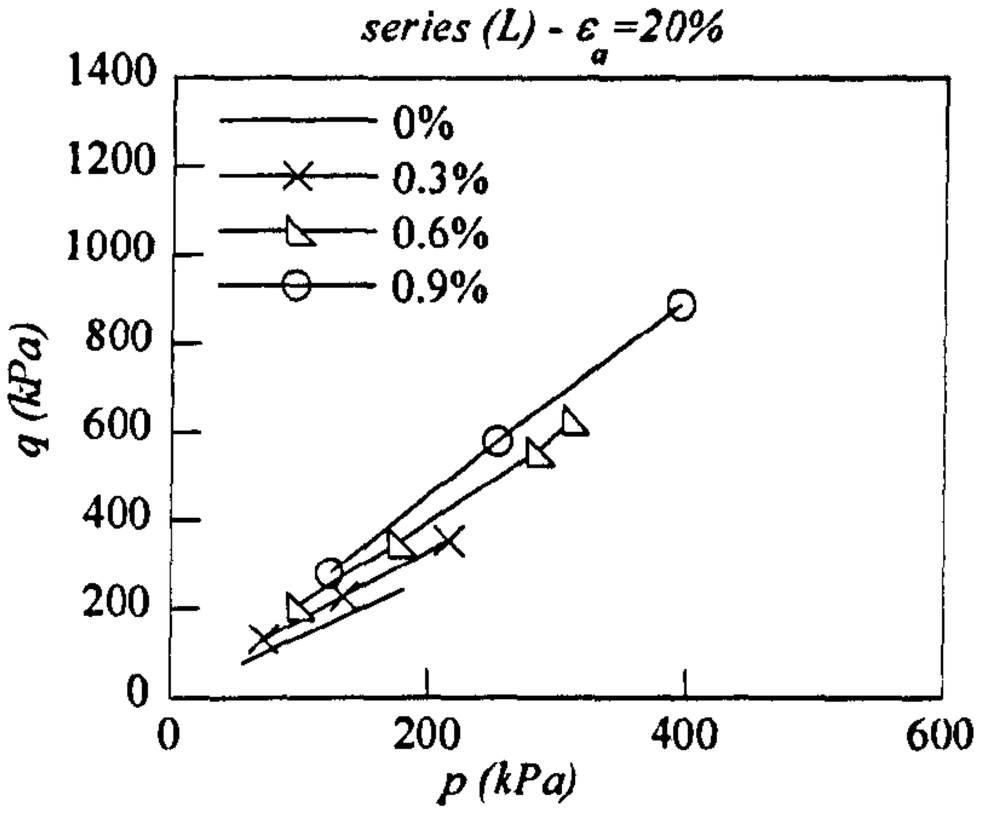

Fig. 5.26 Deviatoric strength envelopes at failure for *(L)* tests series (legend gives the fibre content used)

Tab. 5.10 Angle of friction and cohesion intercept for *(L)* series of tests at serviceability failure (ε_a=20%) for fibre type (3)

FIBRE 3 at failure $\varepsilon_a = 20\%$								
	Fibre content (%)							
	0		0.3		0.6		0.9	
	c (kPa)	ϕ(°)	c (kPa)	ϕ(°)	c (kPa)	ϕ(°)	c (kPa)	ϕ(°)
ε_a = 20%	0.0	33.5	7.0	39 0	10.0	46.0	5.0	55.0

The deviatoric strength variation with the amounts of fibres is presented in Fig. 5.27, where the evolution of the deviatoric strength seems parabolic with the fibre content. The trend is similar to the one presented for fibre (1), while for fibre type (2) the variation for the deviatoric strength was rather linear. The slope of the lines increases with the fibre content, proving that higher confining pressures may improve the interaction mechanism between sand and fibres.

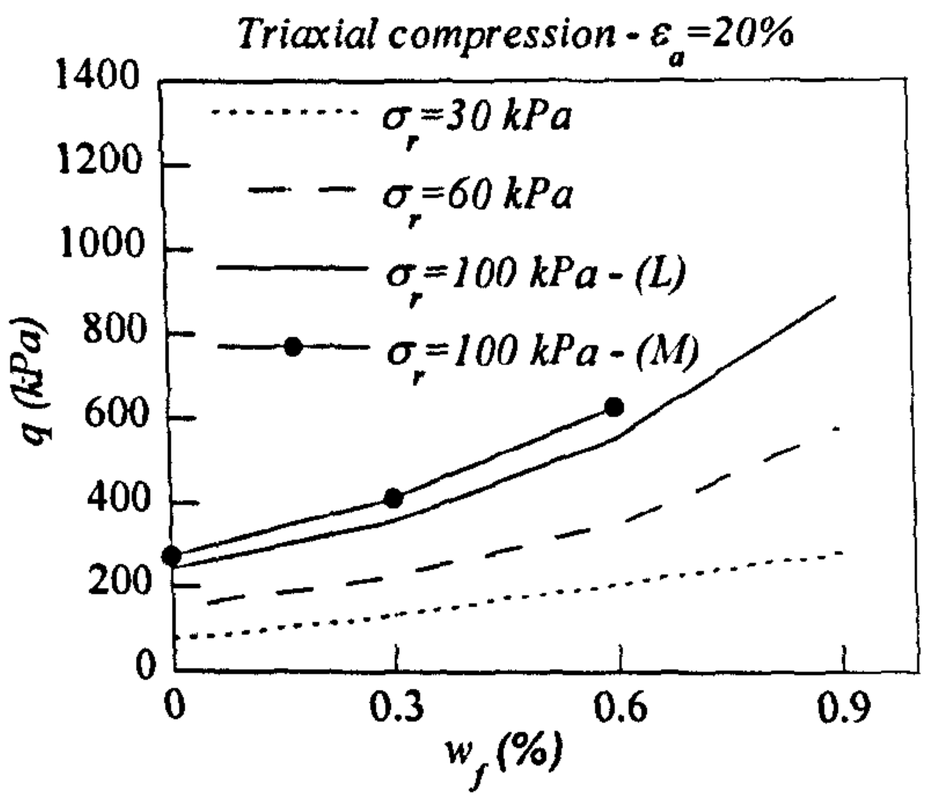

Fig. 5.27 Deviatoric strength at 20% axial strain in triaxial compression for ensemble of specimen densities and three different confining stresses, 30, 60 and 100 kPa

5.4.5 Comparison between the different types of fibres in drained compression

5.4.5.1 General

Comparison of the stress-strain behaviour of reinforced specimens is reported in Figs. 5.28 and 5.29 for *(L)* and *(M)* specimen reinforced respectively with 0.6% and 0.3% of fibres and tested at 100 kPa cell confining pressure. The performances of unreinforced specimens are also shown for comparison. Specimens reinforced with fibrillated fibres (type (2)) clearly show the highest strength. These fibres have an aspect ratio larger than the other fibres and, having more lateral surface per unit volume of fibres, it is possible that their effectiveness depends on the capacity of transferring more tangential stresses between sand grains and fibres. It should be remarked that the two most commonly used approaches for predicting the strength of reinforced soils (Zornberg (2002); Michalowsy and Čermák (2003)) consider the aspect ratio of the fibres as a fundamental factor. For both approaches the resistance of the soil increases with the aspect ratio of the fibres and this is respected by the experimental results performed in this research.

The stress-strain behaviour at small strain seems instead quite similar and differences increase with the continuation of the test. The stresses developed in the fibres increase and the contribution of the fibres becomes predominant relative to the contribution of the sand matrix.

Even if the platy fibres are less effective in increasing the strength at failure, at lower strains (ε_a<5%) they often show the highest strength or at least higher than the fibre type (1). Platy fibres are the stiffest and when equally stretched they develop more stresses than the others. Probably the contact between the sand and the fibres degrades soon and sharply and they lose the ability to keep the sand matrix confined.

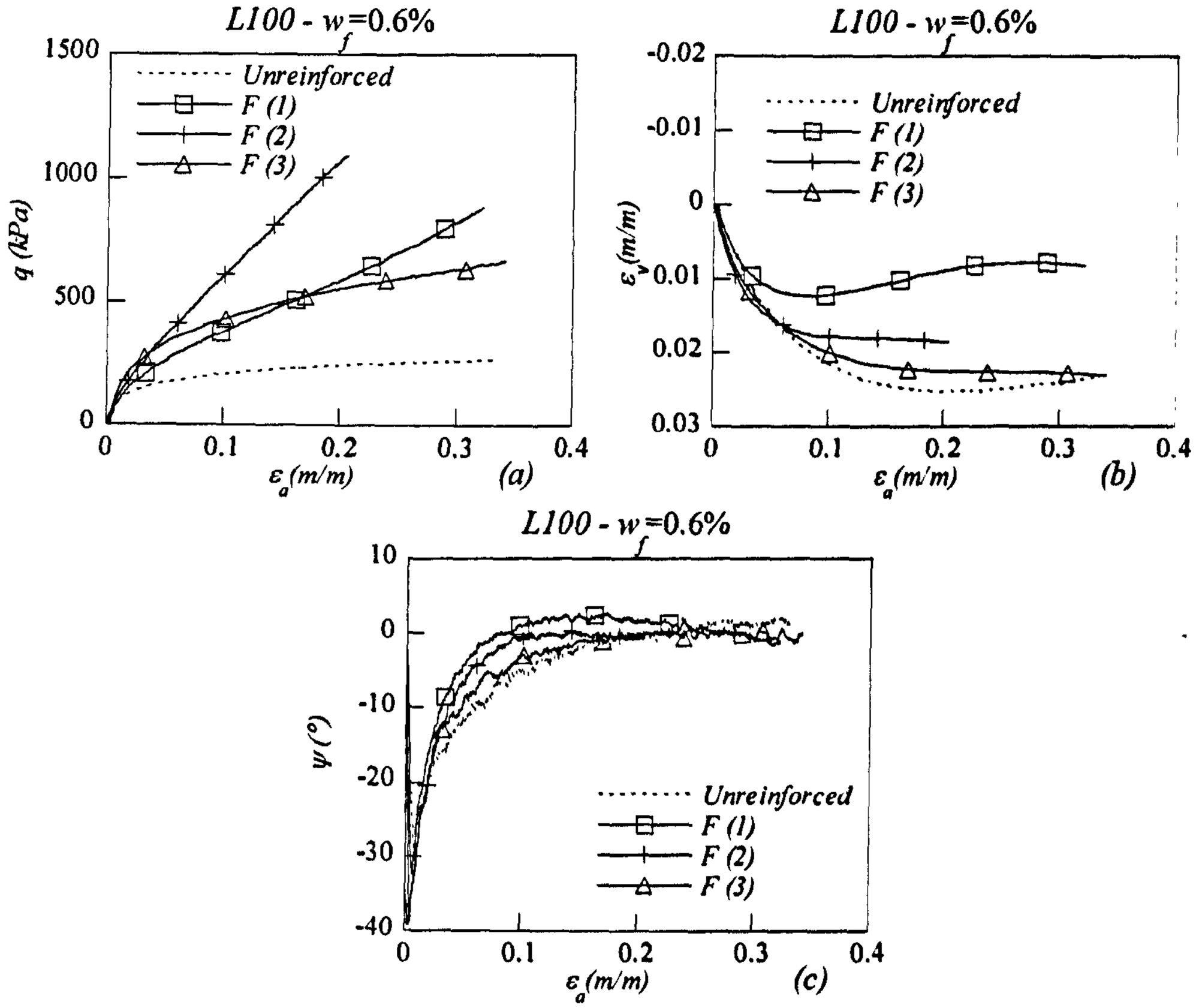

Fig. 5.28 Comparison of the performances of *(L)* specimen reinforced with 0.6% content of different types of fibres (given in the legend): *(a)* deviatoric stress - axial strain; *(b)* volumetric strain - axial strain; *(c)* dilatancy angle - axial strain

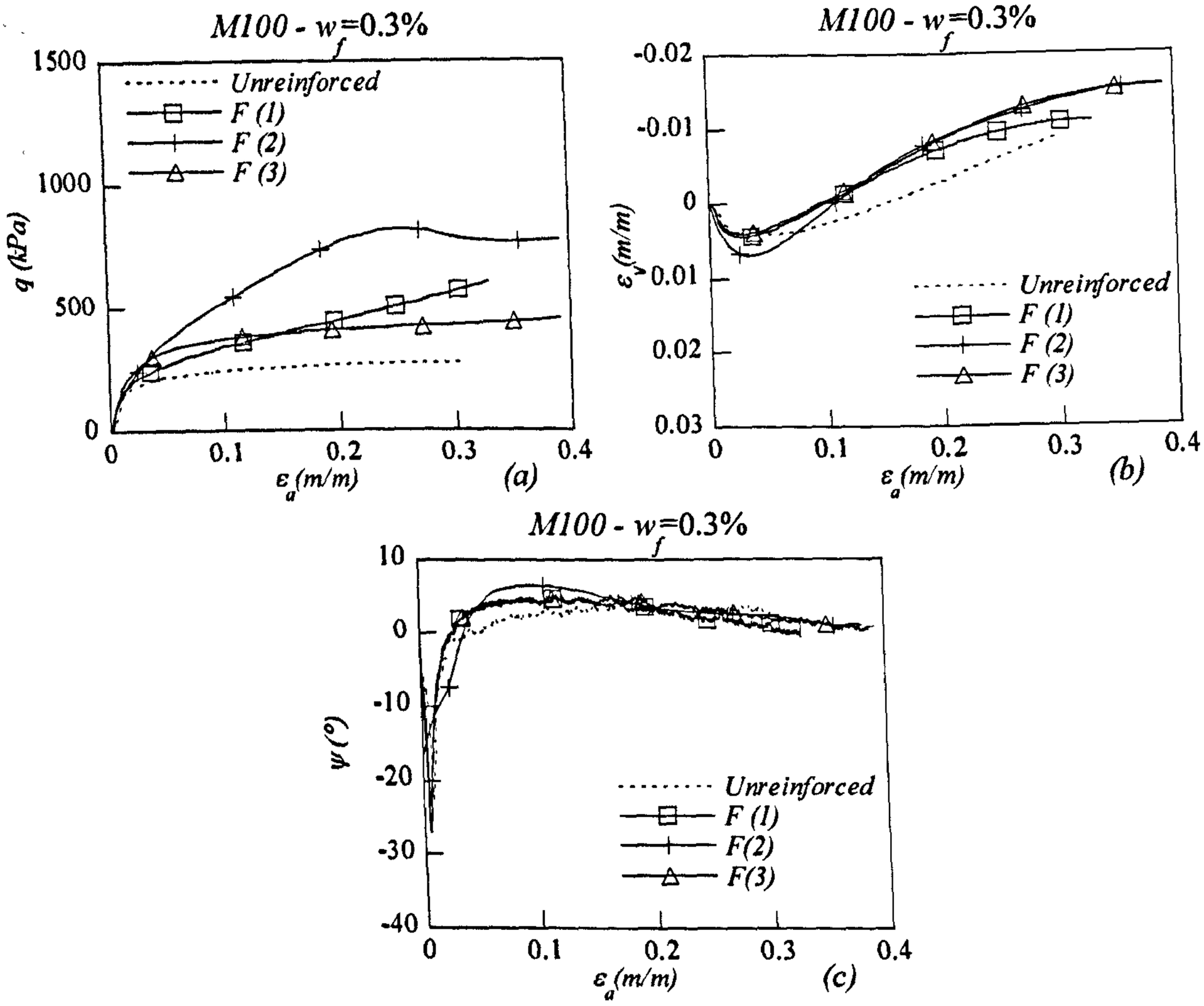

Fig. 5.29 Comparison of the performances of *(M)* specimen reinforced with 0.3% content of different types of fibres (given in the legend): *(a)* deviatoric stress - axial strain; *(b)* volumetric strain - axial strain; *(c)* dilatancy angle - axial strain

The effect of all the fibres on the volumetric behaviour is very similar with a common increase of dilation for all the types of reinforcement. A general trend to distinguish between the influences of different types of fibre is not so clear and this may be due to the appreciable influence of a small variation in the void ratio on the volumetric behaviour of the specimens as already discussed in paragraph 5.3.

5.4.5.2 Strength

Proper failure conditions were reached only by specimens reinforced with fibre type (2), while for specimens reinforced with fibre type (1) and (3) the strength has been defined only according to a serviceability failure criterion. However, even if specimens reinforced with fibre (3) did not show an unequivocal flattening of the curve, it is believed that failure of the reinforcement may have been reached or at least the slippage between the phases was very much developed. It is believed that the stress transfer mechanism between sand grains and fibres is mainly governed by friction but the presence of an adhesive component was also suggested by Zornberg (2002).

The extra strength $\Delta\tau$ provided by the three different types of reinforcement (defined in Eq. (5.3)) are compared in Fig.5.30. The envelopes are reported for the *(L)* series specimens and it is evident that the contribution of fibre (2) is greater than the others and fibres (3) are the less effective.

A comparison of the strength parameters for the loosest specimens is reported in Fig.5.31 where lines are drawn to link points with the same quantity of reinforcement. For all the fibres, both the apparent cohesion intercept and the friction angle increase with the fibre content while only the apparent cohesion intercept shows a clear correlation with the aspect ratio of the fibres. In support of this observation it should be recalled that Zornberg (2002) has proposed a model where the cohesion intercept of the reinforced soil is dependent on the adhesive component of the interface shear strength between the soil and the fibre and it increases linearly with the aspect ratio of the fibres themselves (Eq.(28) in Zornberg 2002). Fig. 5.31*a* shows a similar trend with the cohesion intercept increasing with the aspect ratio of the fibres. Moreover, the aspect ratio represents the slenderness of the fibres and if fibres are slender, they are also more flexible and they may be more prone to interlock together which may result in an apparent cohesion for the reinforced specimen strength envelope.

The trend of the friction angle versus the aspect ratio of the fibres is not very clear (Fig.5.31*b*). The friction angles for fibre (2) and (3) are very similar, while the value is much lower for fibres type (1) that have an intermediate aspect ratio compared with the other fibres. However,

it should be noted that the employed fibres are different for many characteristics such as shape, diameter and stiffness, therefore definite conclusions can not be drawn on the influence of a single characteristic on the strength parameters for reinforced soils.

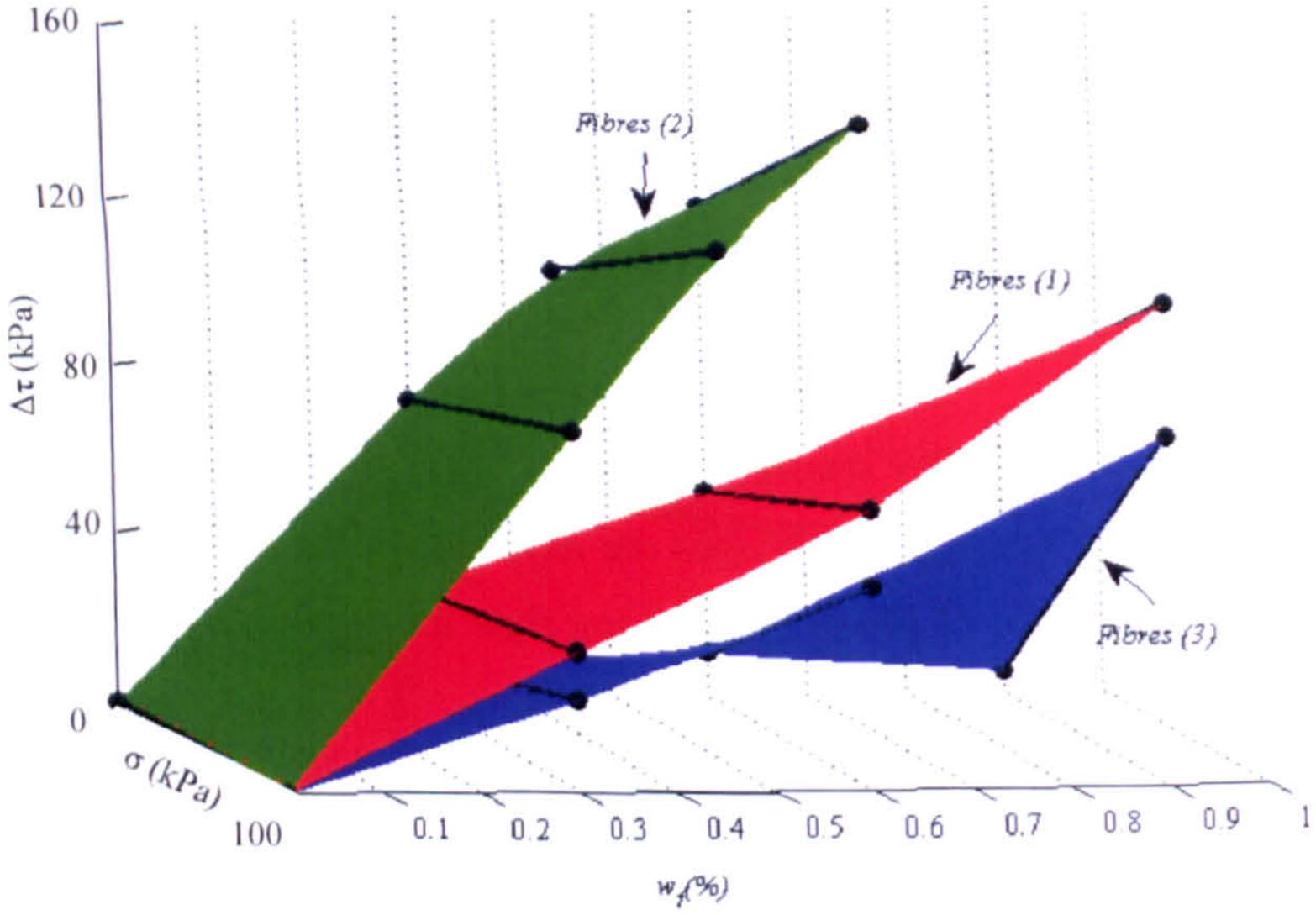

Fig. 5.30 Extra strength provided by different fibres reinforcement for triaxial compressive loading

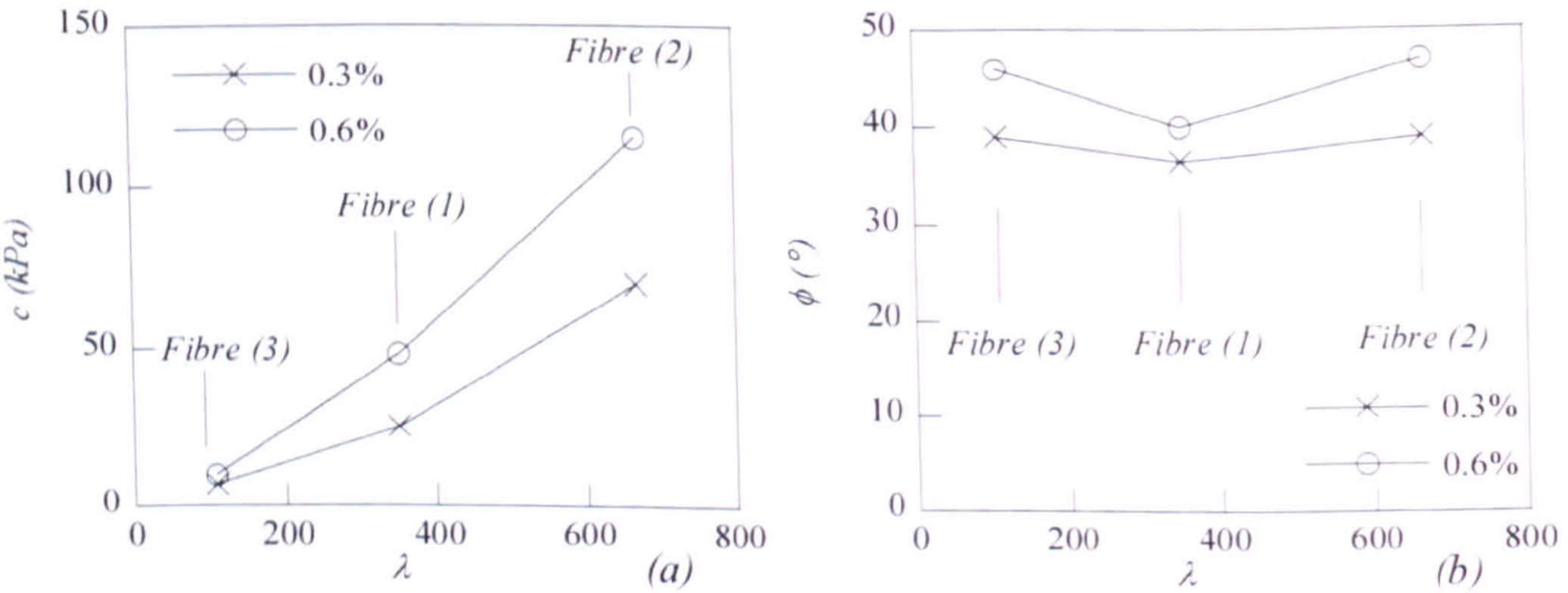

Fig. 5.31 Trend of the cohesion intercept *(a)* and friction angle *(b)* with the aspect ratio for the different reinforcement types

5.4.5.3 Dilatancy

It has been already discussed that the relationship between stress and dilatancy for specimen reinforced with fibre type (1) does not follow the general diltancy rule proposed by Rowe (1962): the deviatoric stress increased even when the density of the specimen had reached a steady state resulting in a vertical trend on the stress-dilatancy (see section 5.4.2.3). This applies also to specimens reinforced with fibre type (2) and (3) since the same increase of deviatoric stress was recorded after the volume had stopped changing. Instead, a modification to the equation proposed by Bolton (1986) for the maximum angle of dilatancy (ψ_{max}) was found to fit the data quite well:

$$\tan\psi_{max} = a_0\left(I_D\left(Q - \ln(p_c)\right) - \gamma\right) \qquad (5.4)$$

where I_D and p_c are respectively the density index and the mean stress at the end of the consolidation, and a_0, Q and γ are three material parameters. The maximum angle of dilatancy (ψ_{max}) is defined up to an axial strain of 20% in compression and 10% in extension because after those axial strains the uniformity of deformation of the specimen was not guaranteed by the enlarged lubricated ends. The use of the consolidation mean stress p_c (rather than mean stress at critical state p_{cri}) was necessary as a distinct failure is not detectable before the imposed limit. However, it is recognised that the stress state, in which the angle of dilatancy is calculated, is quite different from the initial stress state and the deviation from Bolton's equation is considered acceptable provided that only one stress path case $(\dot{q}/\dot{p} = 3)$ is analysed. Further experimental research including a range of stress paths is needed for a more general maximum dilatancy relationship for reinforced sands. The values which give the best fit with experimental data were obtained using the least square method and results are reported in the following Table 5.11 for the three types of fibres. A Three-dimensional view of the surface defined by Eq. (5.4) for the three types of reinforcement is given in Figs. 5.20, 5.21 and 5.22.

Tab. 5.11 Best fit parameters for Eq. 5.4 for the three types of reinforcement

Fibre type	a_0	Q	γ	R^2
(1)	0.175	8.414	0.512	0 921
(2)	0.147	7.741	0 396	0.841
(3)	0.140	6 495	0.197	0.872

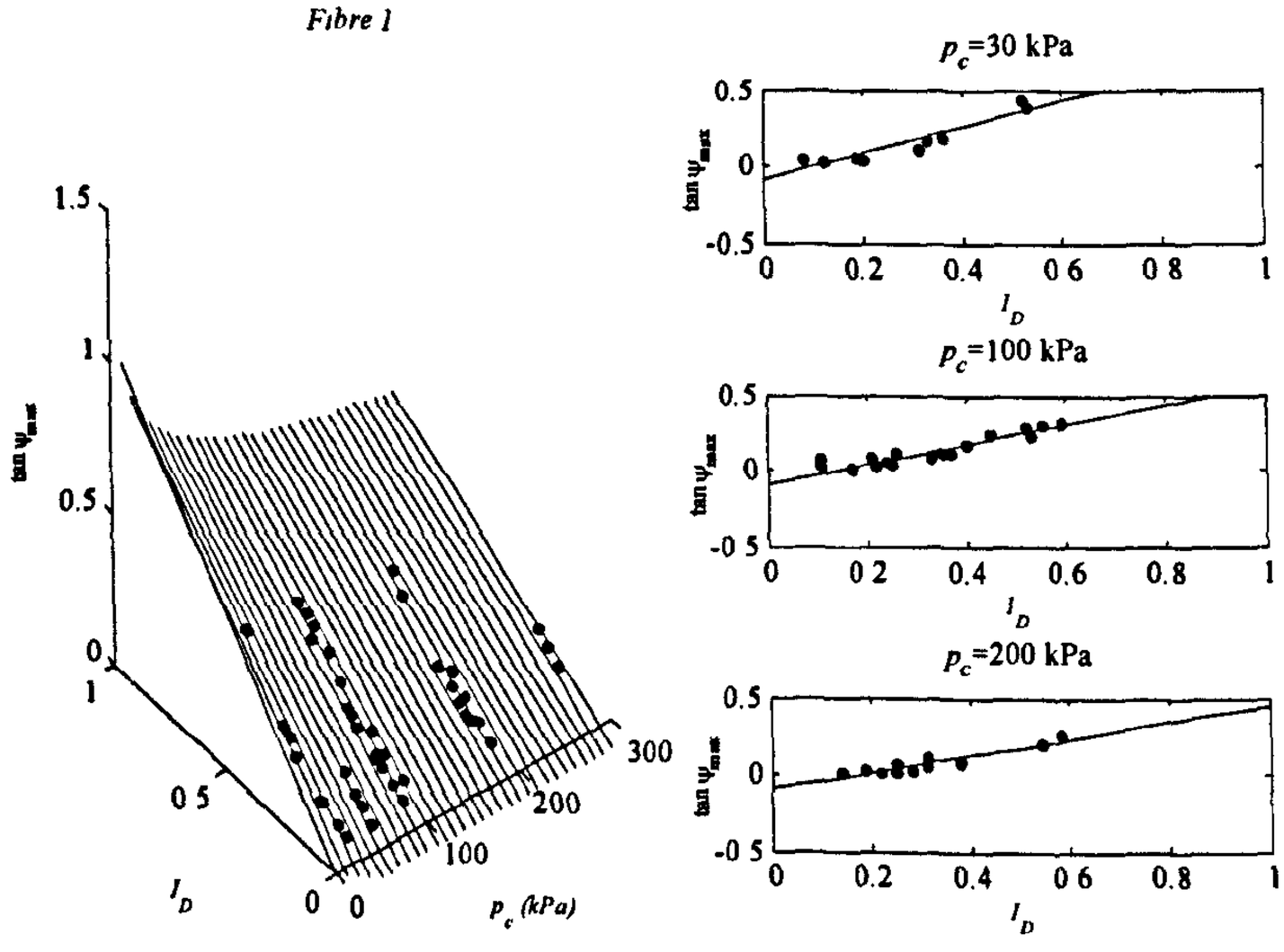

Fig. 5.32 Three-dimensional representation of the experimental flow rule and plane sections at three constant consolidation pressures, 30, 100 and 200 kPa for specimen reinforced with fibre type (1)

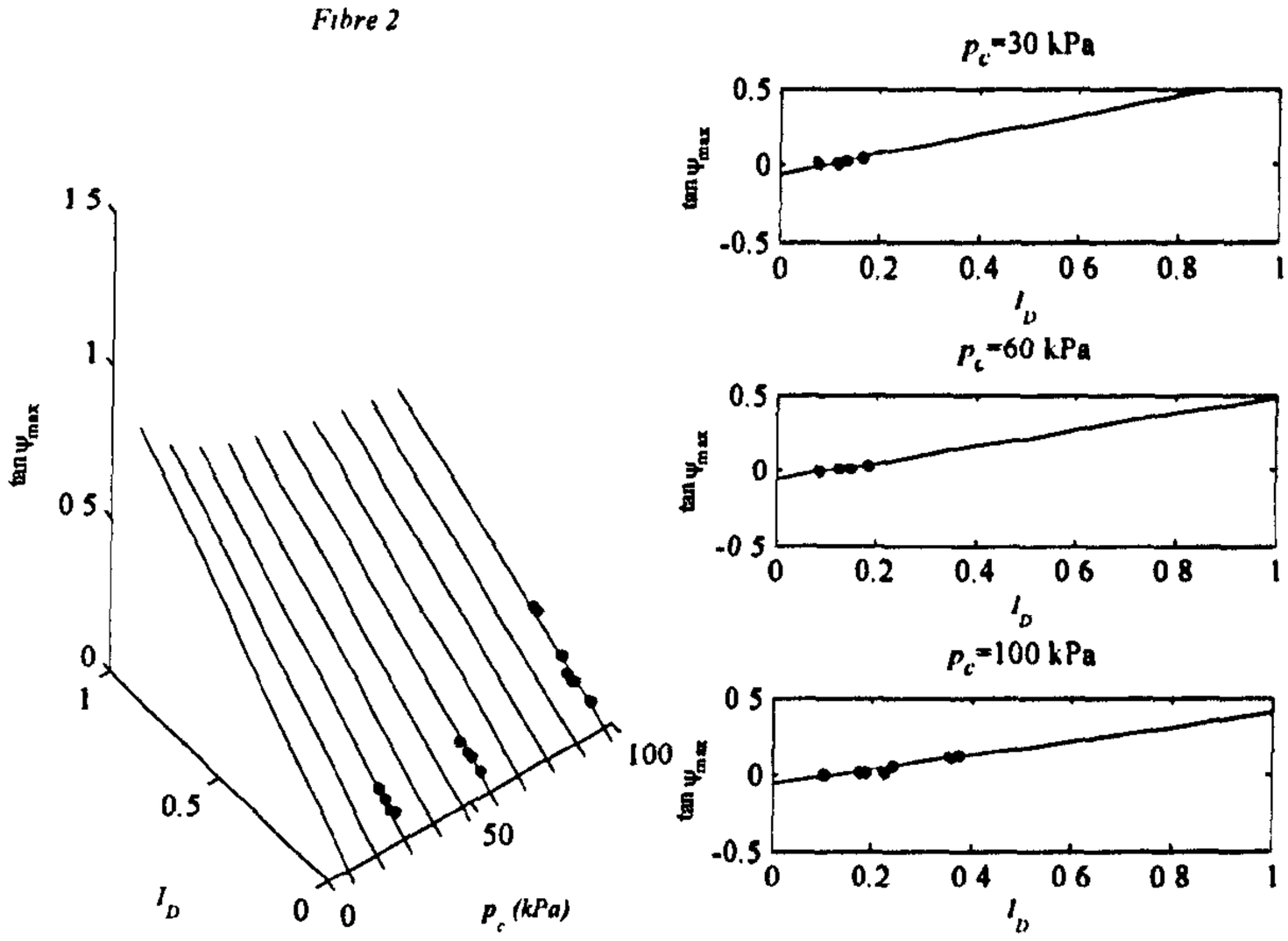

Fig. 5.33 Three-dimensional representation of the experimental flow rule and plane sections at three constant consolidation pressures, 30, 60 and 100 kPa for specimen reinforced with fibre type (2)

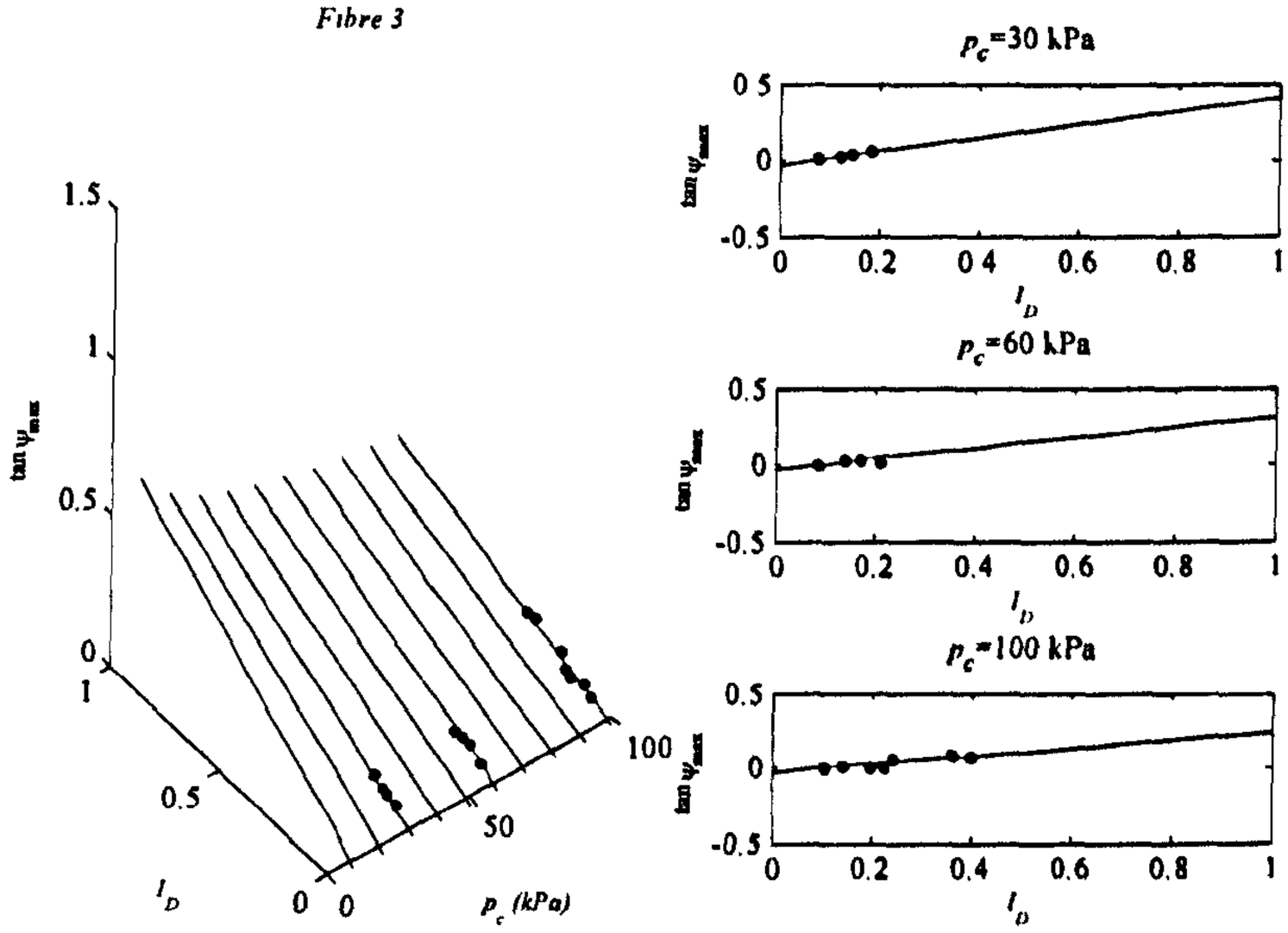

Fig. 5.34 Three-dimensional representation of the experimental flow rule and plane sections at three constant consolidation pressures, 30, 100 and 200 kPa for specimen reinforced with fibre type (3)

5.5 Conclusions

The results of the drained triaxial tests performed in this research on specimens reinforced with three different types of fibres have been presented here. The repeatability of the experimental results has been investigated for both unreinforced and reinforced specimens. The experimental results for unreinforced specimens confirm the results already published in the literature and demonstrate the reliability of the experimental investigation that has been performed.

The main conclusions deriving from the experimental campaign are as follows:

- The shear strength characteristics of the soil in triaxial compression loading are appreciably enhanced by all the three types of reinforcement. Addition of fibres increases both the apparent cohesion intercept and the friction angle of the material. The increase of the apparent cohesion intercept seems proportional to the aspect ratio of the fibres, while a trend of the friction with the aspect ratio is not well defined.

- The contribution of the fibres to the strength of the soil is proportional to the fibre content. Increase in relative density of the specimens has a positive effect on the contribution of fibres: dense specimens dilate more than loose ones and this induces more tensile stresses in the fibres. The adoption of higher confining pressure may result in a better bonding between fibres and sand grains. At low pressures the bonding seems to improve during the test as the stresses in the specimens increases.

- Fibres type (2) are the most effective, then fibres type (1) while fibres type (3) are the least effective. Specimens reinforced with fibre type (2) are the only ones that clearly show a limit of the resistance afforded by the reinforcement and the failure mechanism is governed by relative sliding between the constituents. The sliding mechanism seems to occur even for fibre type (3) but it is not clear if the relative sliding is complete. Specimens reinforced with fibres type (1) did not show a strength limit even if the test was carried out to very large strains.

- The effectiveness of the fibres is dependent on the loading condition and it was found remarkable in triaxial compression and limited in triaxial extension. Comparison of the contribution of fibres in compression tests, extension test and direct shear tests (performed by Ibraim (1998)) confirms that the effectiveness of fibres is dependent on their orientation in respect to tensile strain directions.

- The volumetric behaviour is in general more dilative when fibres are added for both compressive and extensive loading. However, fibres affect the volumetric behaviour for two main reasons with contrasting effects: by their presence they increase the relative density of the specimen but they also provide extra confinement to the sand matrix.

- Experimental results on reinforced specimens demonstrate that the usual dilatancy rule can not be applied to the composite materials. However, the maximum dilation angle could be quite well reproduced with slight modification of an existing model taken from the literature.

CHAPTER 6

TRIAXIAL TEST: UNDRAINED CONDITIONS

6.1 Introduction

Since the pioneering work of Bjerrum et al. (1961) and Castro (1969), static liquefaction phenomena of granular soils have been intensively studied especially in the laboratory (Castro and Christian, 1976; Vaid and Chern, 1983; Konrad, 1990; Chu, 1991; Lade, 1992; Hyodo et al., 1994; Doanh et al., 1997; Doanh and Ibraim, 2000, among others). Static liquefaction, typically associated with loose and very loose saturated sands and sand-silt mixtures while in situ and under relatively low stress conditions, may be defined as a large reduction of mean effective pressure under monotonic undrained loading induced by a persistent generation of pore pressures. Large strains develop with a significant drop of the undrained shear strength which eventually stabilises around a steady state condition (Poulos, 1981). Several failures of natural loose saturated sandy slopes, earth dams or hydraulically filled submarine berms have been attributed to the static liquefaction of soil (Castro and Poulos, 1977; Lindenberg and Koning, 1981; Sladen et al., 1985; Kramer and Seed, 1988). In some cases, a trigger mechanism such as a minor disturbance in the form of vibrations due to man-made activities or earthquakes of small intensities, local erosion, tidal variations or overloading imposed by additional fill, has been proposed as the origin of the sudden increase of pore-water pressures (Lade, 1993).

The present chapter explores through a series of laboratory experiments the prospect of altering the undrained response of a loose clean sand to reduce its liquefaction potential by mixing the sand with short flexible fibres. As a matter of facts, no study has been reported concerning the undrained monotonic behaviour of fibre reinforced sands or on the effect of fibre inclusions on the static liquefaction response of sand.

6.2 Test programme

The apparatus that has been used to investigate the undrained triaxial behaviour of reinforced sand has been already described in section 3. Because of shortage of time the investigation of the liquefaction properties has only been performed on specimens reinforced with fibre type (1). It is evidently desirable that a future research programme should include the study of the liquefaction properties of specimens reinforced with other types of fibres.

The conventional undrained triaxial compression and extension tests were conducted on unreinforced and reinforced isotropically consolidated specimens. Three different consolidation pressures - 30, 100 and 200 kPa - were used. A complete list of tests including test name, fibre content (w_f), confining pressure (σ_r), void ratio at the end of consolidation (e_c) and the corresponding density index, $I_{Dc} = (e_{max} - e_c)/(e_{max} - e_{min})$, after the consolidation stage is given in Table 6.1.

Tab. 6.1 List of the undrained triaxial tests performed

Test	w_f (%)	σ_r (kPa)	e_c	I_{Dc} (%)
L030-00-U-1	0.00	30	0.982	4.74
L030-03-U-1	0.30	30	0.958	11.08
L030-06-U-1	0.60	30	0.945	14.47
L030-09-U-1	0.90	30	0.933	17.54
L100-00-U-1	0.00	100	0.966	8.95
L100-03-U-1	0.30	100	0.934	17.34
L100-06-U-1	0.60	100	0.917	21.71
L100-09-U-1	0.90	100	0.912	23.19
L200-00-U-1	0.00	200	0.952	12.63
L200-03-U-1	0.30	200	0.921	20.73
L200-06-U-1	0.60	200	0.903	25.59
L200-09-U-1	0.90	200	0.894	27.80

Test	w_f (%)	σ_r (kPa)	e_c	I_{Dc} (%)
EL030-00-U-1	0.00	30	0.965	9.21
EL030-03-U-1	0.30	30	0.940	15.78
EL030-06-U-1	0.60	30	0.928	18.87
EL030-09-U-1	0.00	100	0.936	16.84
EL100-00-U-1	0.30	100	0.909	23.86
EL100-03-U-1	0.60	100	0.901	26.11
EL100-06-U-1	0.00	200	0.939	16.05
EL100-09-U-1	0.30	200	0.907	24.38
EL200-00-U-1	0.60	200	0.899	26.63

6.3 Experimental results

The test results for reinforced and unreinforced specimens, and their dependence on the consolidation pressures are shown in Figs 6.1, 6.2 and 6.3 for consolidation pressures of 30, 100 and 200 kPa respectively. Each of these figures shows: (a) the stress – strain response in terms of q^*:ε_a; (b) the effective stress path for the composite in the q^*~p^* plane; and the evolution with the shear strain of: (c) the effective stress part of the excess pore pressure $(\Delta u)'$, with $(\Delta u)' = \Delta u - \Delta p$ normalised by the effective mean consolidation stress, p_c^*, and (d) the composite effective mobilised angle of friction, ϕ_m^*. The use of $(\Delta u)'$ is instructive because it shows only the pore pressure resulting from the suppressed volume change of the soil, and subtracts the pore pressure change resulting from the imposed changes in total stress (which has nothing to do with the response of the soil).

6.3.1 Unreinforced specimens

In compression, as well as in extension, the specimens show a progressive generation of pore pressure and continuous decrease of effective mean stress acting on the sand. After a peak reached rapidly near the start of the test there is a sharp drop of deviator stress and stabilisation around a steady state as deformation continues: behaviour typical of static liquefaction. The static liquefaction phenomenon is reached even for specimens consolidated at the very low stress level of 30kPa. The effective stress part of the excess pore pressure $(\Delta u)'$ developed progressively and reached a constant value at a shear strain of about 10% in compression and -5% in extension. The highest pore pressure increase in extension as well as in compression is about 85% of p_c^*.

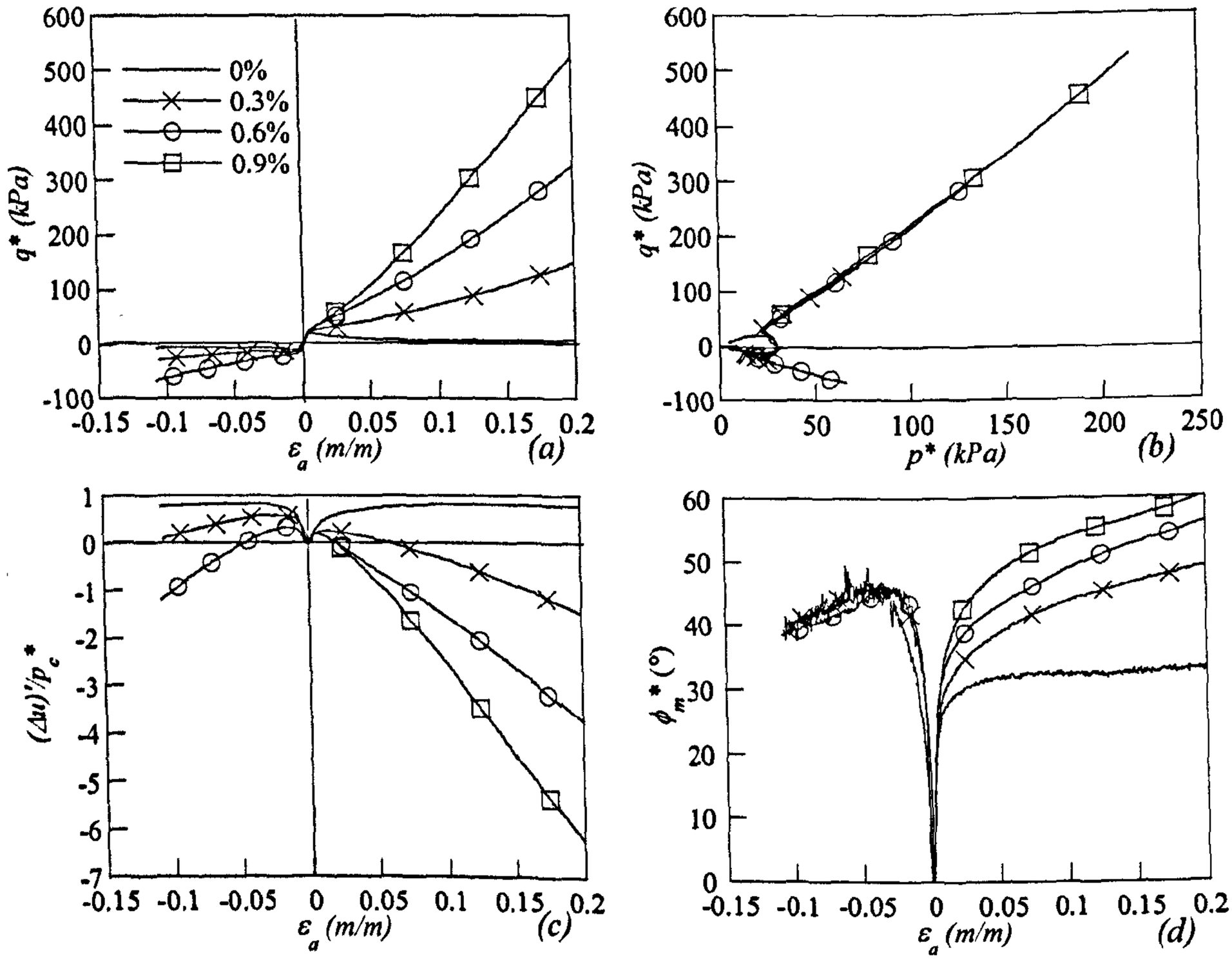

Fig. 6.1 Triaxial undrained compression and extension tests at 30 kPa initial consolidation pressure

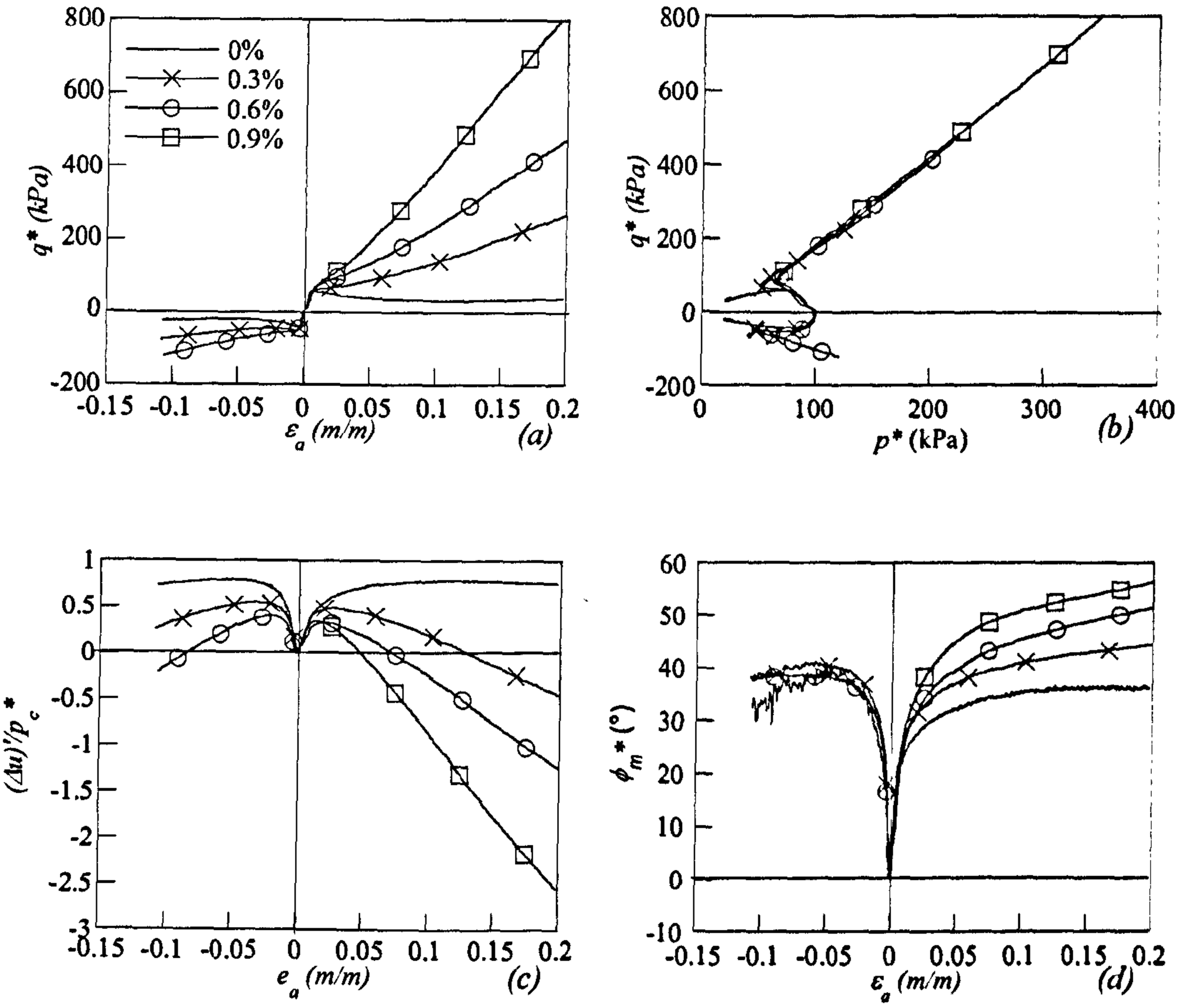

Fig. 6.2 Triaxial undrained compression and extension tests at 100 kPa initial consolidation pressure

The mobilised angle of friction at the peak deviator stress for the extension tests shows some dependency on the effective confining pressure with 19.8°, 19.6° and 18.2° for 30, 100 and 200 kPa respectively and this pattern is equally shown by the compression tests with 22.6°, 21.9° and 20.2° for the same successive effective consolidation pressures. However, both series of angles appear much higher than those obtained by Doanh et al. (1997) where an average of 12.7° for extension and 16.8° for compression for effective confining pressures ranging from 50 to 300 kPa were obtained: possibly, the present study has used slightly higher specimen densities.

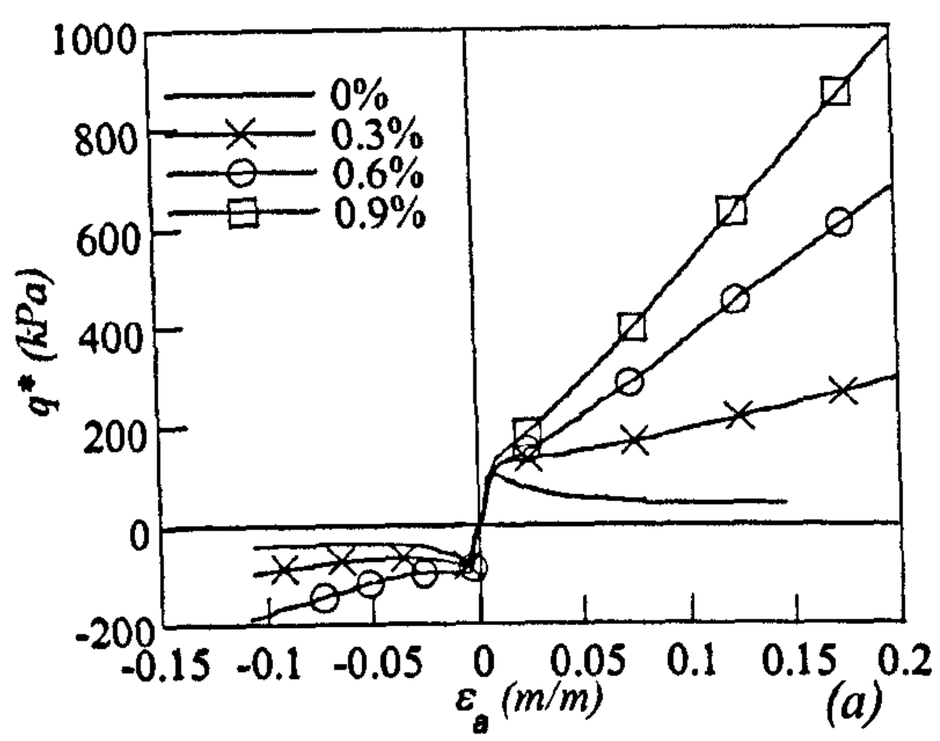

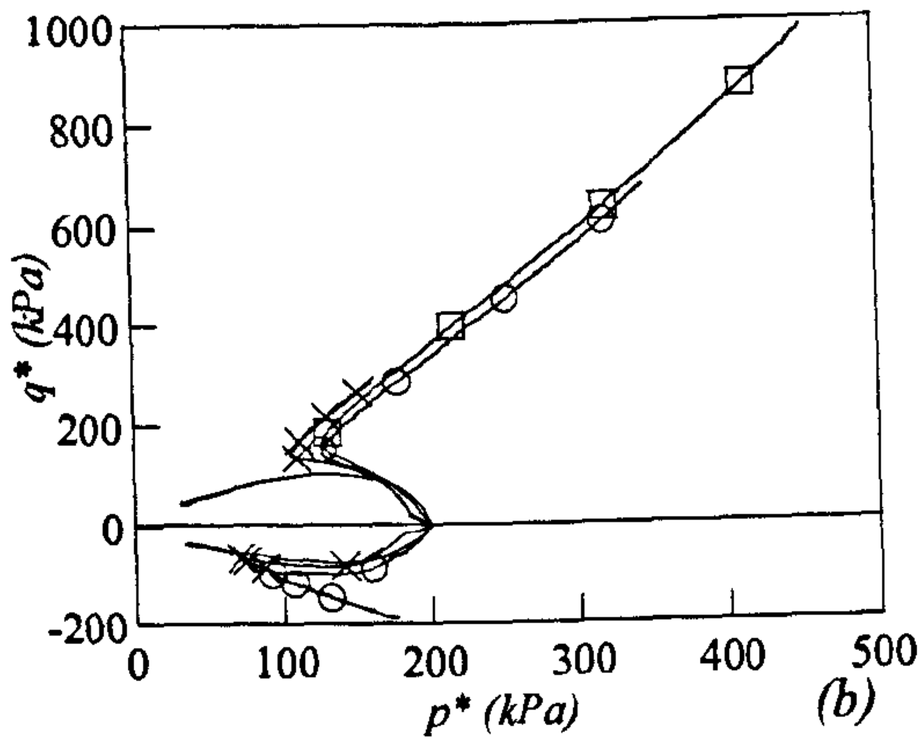

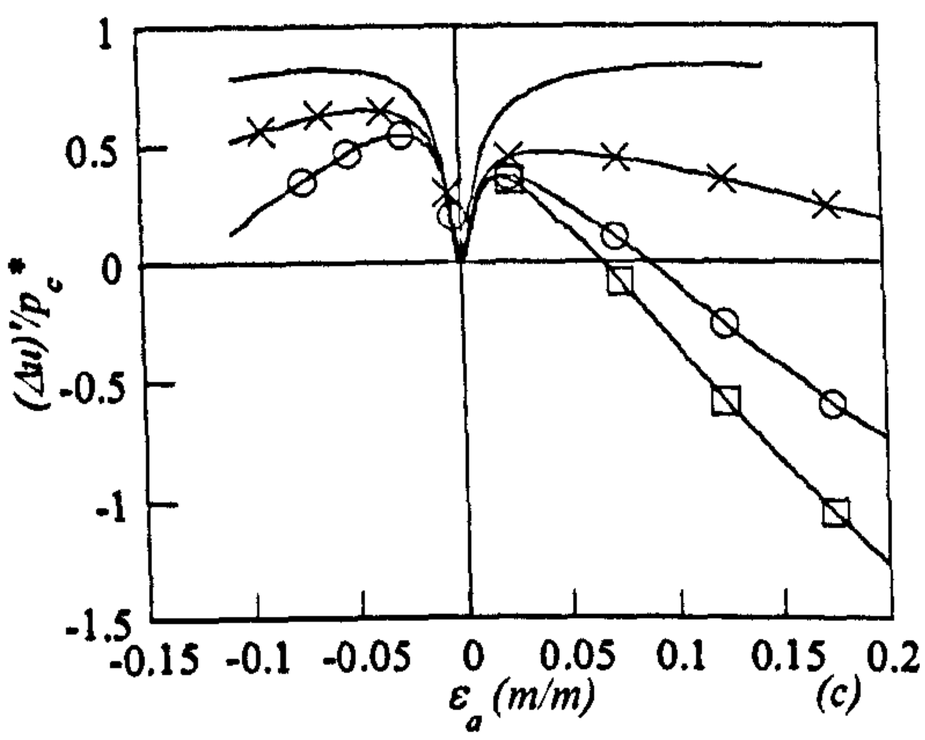

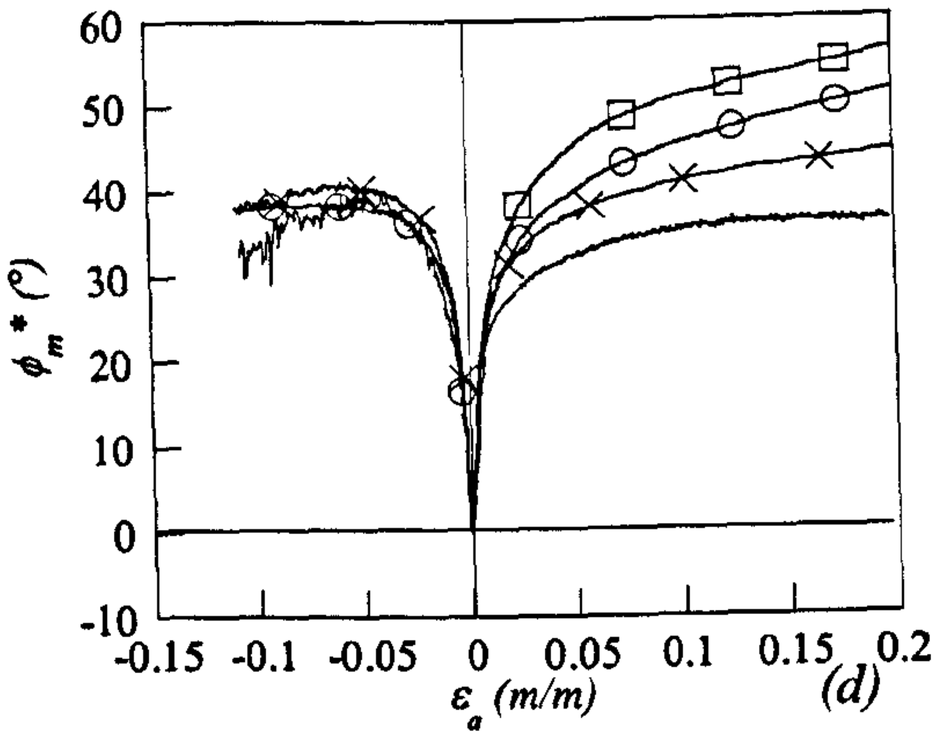

Fig. 6.3 Triaxial undrained compression and extension tests at 200 kPa initial consolidation pressure

The slope of the steady state $M_c^{ss}=q^*/p^*$ line in compression is about 1.38 and the corresponding maximum mobilised angle of friction is around 34° (close to that found by Doanh et al. 1997). In extension, the stress ratio $M_e^{ss}=q^*/p^*$ at the steady state of deformation is around -0.97 and the corresponding mobilised angle of friction tends towards 35° which is slightly higher than in compression. However, the difference of friction angles between compression and extension may be considered in the range of experimental scatter.

6.3.2 Fibre reinforced specimens

When different concentrations of fibres are used as inclusions, the undrained behaviour of the reinforced specimens appears qualitatively very coherent from one group of tests to another. The presence of fibres – irrespective of the amount employed and the initial consolidation pressure – strongly affects the undrained response. Static liquefaction is fully prevented in compression with a behaviour comparable to that of a dense unreinforced sand. In extension there is a clear increase of both undrained peak and steady state shear strength response for low fibre concentrations and a strain hardening response for higher values of w_f (Figs. 6.1 -6.3).

Any initial effects of imperfect contacts between loading ram and top specimen platen are quickly erased as loading continues. The responses observed for both compression and extension loadings are very similar and follow quite closely the responses of the unreinforced specimens over the small strain domain in all planes (Figs. 6.1-6.3). This suggests that the initial behaviour of the composite is to a certain extent solely controlled by the sand matrix (Heineck et al., 2004; Yetimoglu et al., 2005; Ibraim and Maeda, 2007). For a given consolidation pressure, further shearing in compression induces a monotonic increase of the undrained deviator stress that is highly dependent on the amount of the fibres employed, while in extension, for a fibre content w_f = 0.3%, the deviator stress still exhibits a softening behaviour after reaching a peak (although the peak is slightly higher than that of an unreinforced specimen), followed then by hardening (Figs 6.1a, 6.2a, 6.3a). The undrained deviator peak observed in extension for the unreinforced and reinforced specimens (w_f= 0.3%) vanishes for a fibre content of 0.6% and the deviator stress increases monotonically similar to the compressive response.

In compression as well as in extension, the undrained stress paths of the composite specimens in the q^*~p^* plane initially follow closely the stress path of the unreinforced one but at certain points the stress paths change direction sharply and show rapid increase in p^* following somewhat straight trajectories (Figs. 6.1b, 6.2b, 6.3b). For the same confining pressure, these trajectories appear to have the same slope independent of fibre concentration. However, straight lines that best fit each trajectory do not intersect the origin of axes either in compression or

extension: a negative q^* axis offset intercept (much higher in absolute value in compression) is found systematically for all the consolidation pressures.

Tab. 6.2 Summary of undrained test results

Test	$q^* / p^*_{20\%}$	$\phi_m{}^*_{20\%}$ (°)
L030-00-U-1	1.35	33.4
L030-03-U-1	2.02	49.1
L030-06-U-1	2.30	56.2
L030-09-U-1	2.44	60.1
L100-00-U-1	1.46	36.0
L100-03-U-1	1.82	44.3
L100-06-U-1	2.11	51.3
L100-09-U-1	2.30	56.2
L200-00-U-1	1.34	33.2
L200-03-U-1	1.82	44.3
L200-06-U-1	1.96	47.6
L200-09-U-1	2.16	52.6
EL030-00-U-1	-1.00	36.9
EL030-03-U-1	-1.11	42.9
EL030-06-U-1	-1.03	38.4
EL030-09-U-1	-0.92	32.9
EL100-00-U-1	-1.02	37.9
EL100-03-U-1	-1.02	37.9
EL100-06-U-1	-0.99	36.4
EL100-09-U-1	-1.00	36.9
EL200-00-U-1	-1.08	41.2
L200-03-U-1	1.35	33.4
L200-06-U-1	2.02	49.1
L200-09-U-1	2.30	56.2

The pore pressure response of the reinforced specimens (effective stress part of the excess pore pressure (Δu)'normalised by the effective mean consolidation stress, $p_c{}^*$) in compression as well as in extension typically shows an initial increase in $(\Delta u)'/p_c{}^*$ ratio up to a peak level (significantly affected by the presence of fibres) followed by a decrease which, for some

amounts of fibres, can even become negative (Figs 6.2c, 6.2c, 6.3c), indicating a switch from suppressed contraction to suppressed dilation. For a given consolidation pressure, the rate at which $(\Delta u)'$ decreases with continued straining is lower in extension than in compression and higher for higher fibre concentrations. For a given fibre content, the rate at which $(\Delta u)'/p_c^*$ decreases following the peak is lower for higher consolidation pressures.

The mobilised angle of friction, ϕ_m^*, of the specimens reinforced with 0.3 to 0.9% of fibres in compression increases monotonically with the shearing and, at 20% of shear strain, respectively ranges from 49° to 60° for 30 kPa consolidation pressure, from 44° to 56° for 100 kPa and from 44° to 52° for 200 kPa (Figs 6.1d-6.3d and Table 6.2). It can be observed that for a given fibre concentration, the mobilised angle of friction is higher for lower values of the consolidation pressure. In extension, for all fibre contents and consolidation pressures, the range of the mobilised angle of frictions at 10% of shear strain presents a narrow variation with values around 40±3°.

6.3.3 Characteristic states

The undrained effective stress paths for medium dense and dense sands typically include a point of vertical tangency, $dp'/dq' = 0$, which corresponds to the switch from suppressed contraction to suppressed dilation. This is similar to the so-called characteristic state (Luong, 1980) which also refers to a stress state corresponding to the transition from a contractive response to a dilative one. However, Luong originally defined the characteristic state (stress state corresponding to a volumetric strain increment $d\varepsilon_v$=0) based on conventional drained compression triaxial tests which certainly implies that there might be some stress path dependency. There may be some similarity between the characteristic stress state that we are deducing from the shape of the undrained effective stress path and the so-called 'phase transformation' stress ratio introduced by Ishihara et al. (1975). This particular state can be identified in a $q' \sim p'$ undrained effective stress path as the point where the effective mean stress reaches a minimum value and the tangent is parallel to the q' axis. The definition of the characteristic state (in the $q^* \sim p^*$ plane for reinforced specimens) in the in this way is therefore independent of the total stress path.

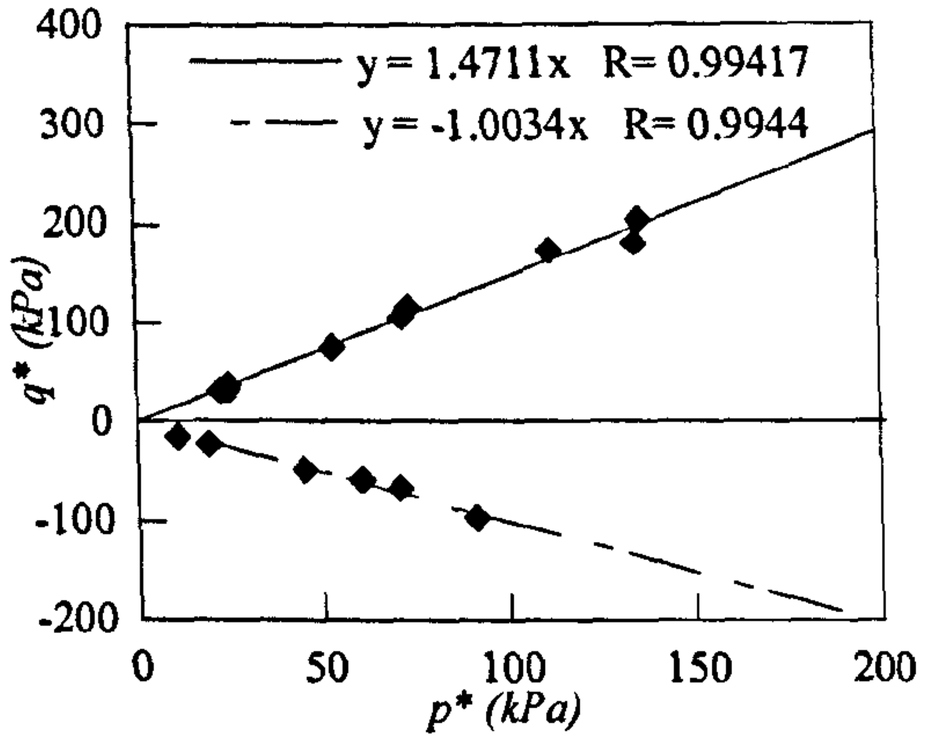

Fig. 6.4 Position of the point of phase transformation/characteristic states in the q^*~p^* stress plane for all the triaxial tests in compression and extension on reinforced specimens

The positions of these characteristic state points for all the reinforced specimens in compression and in extension in the q^*~p^* stress plane are shown in Fig. 6.4. Irrespective of the fibre contents and initial consolidation pressures used in this study, the characteristic states can be well fitted in compression as well as in extension by two straight lines (with good regression coefficients) passing through the origin of the q^*~p^* axes with slopes of 1.27 in compression and -1.01 in extension. The corresponding mobilised angles of friction are 31.6° in compression and 37.3° in extension.

6.3.4 Normalised stress paths

The stress paths in the q^*~p^* plane for tests on specimens reinforced with identical amounts of fibres but consolidated to different values of effective mean stress, p_c *, are shown in Fig. 6.5. On the compression side, and for one fibre content, the linear effective stress paths developed after the characteristic state run practically parallel to each other, with a higher intercept on the positive p^* axis (or lower intercept on the negative q^* axis) for higher consolidation pressures. In extension, Figs. 6.6a and b, a close examination of the stress paths may show a similar pattern but the distances between these parallel lines and the differences between the values of the negative q^* axis intercept are both extremely small: therefore a common line passing through the origin of q^*~p^* axes could well approximate these linear stress paths. When these

effective stress paths are normalised with p_c * (Fig. 6.6) it appears that all the linear paths fall onto an identical straight line, unaffected by the proportion of fibres: Fig. 6.7 groups all the normalised stress paths of all the undrained tests performed in this study. In compression, its slope is approximately 2.75 (corresponding to friction angle of about 70.5°) and its intercept with the p^*/p_c^* axis occurs at a value of around 0.3 while in extension the slope is around -0.84 (corresponding to friction angle of about 30.6°).

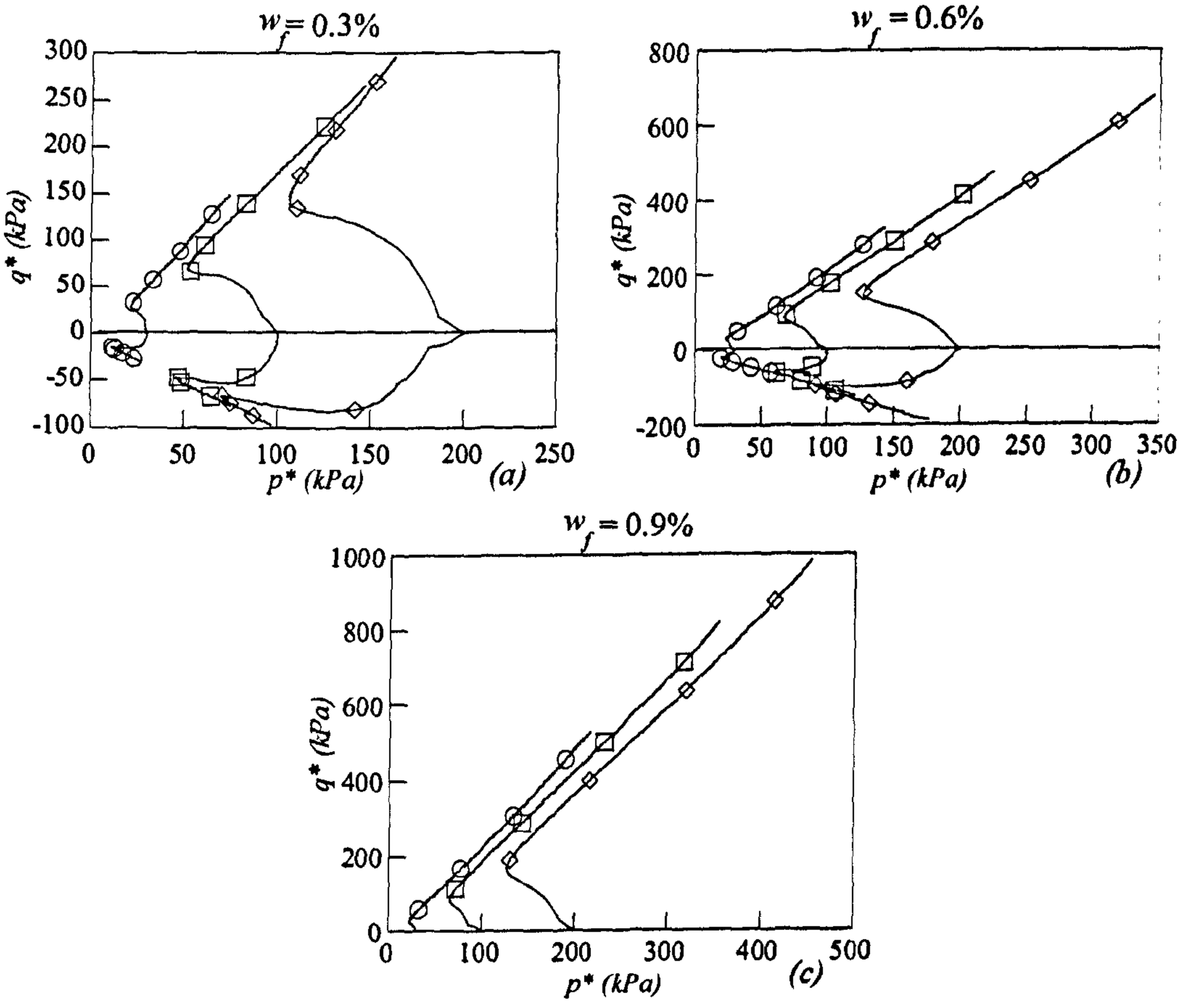

Fig. 6.5 Triaxial undrained compression and extension stress paths of tests on isotropically consolidated specimens to different consolidation pressures, p_c*: *(a)* w_f=0.3%; *(b)* w_f=0.6%; *(c)* w_f=0.9%

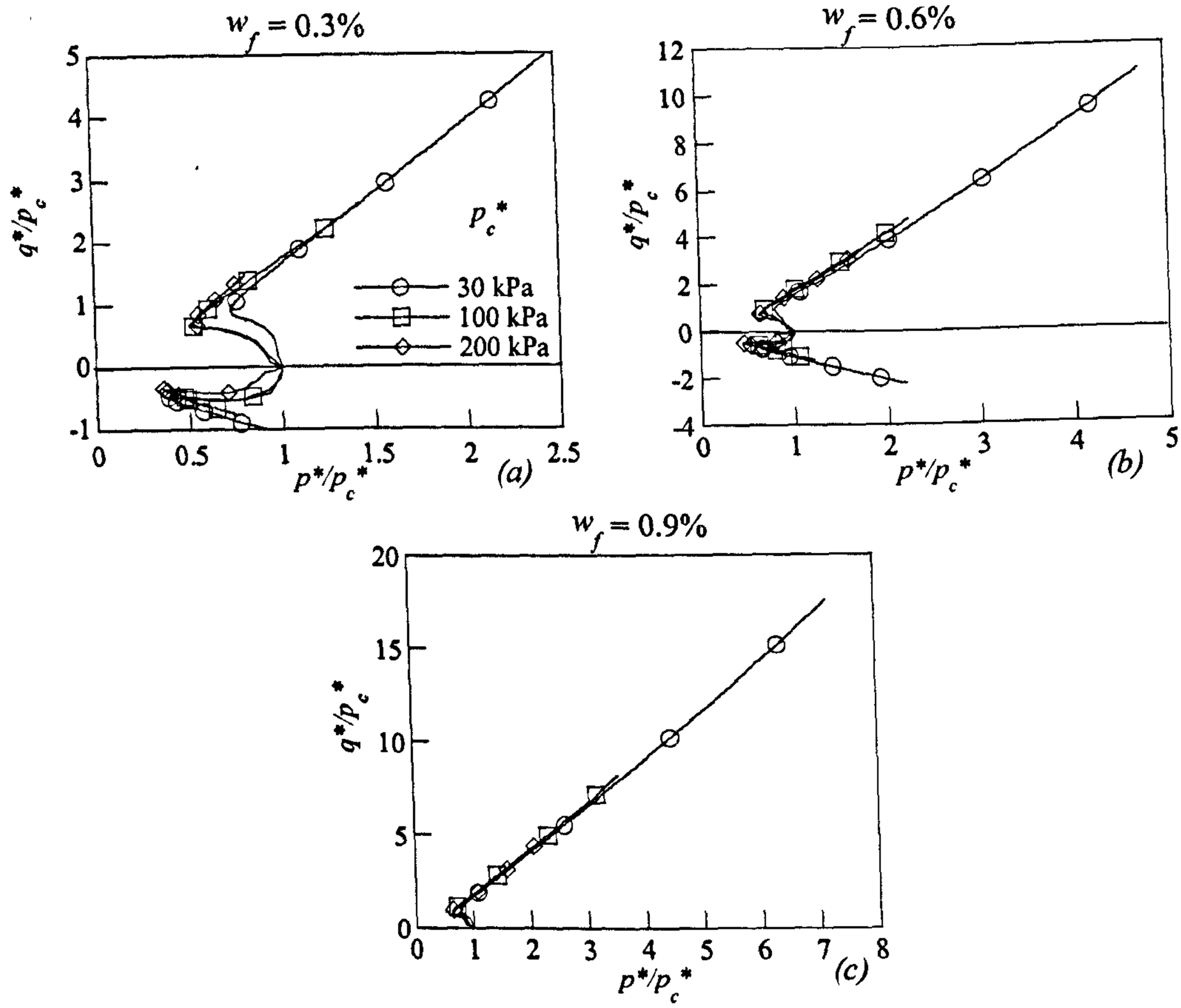

Fig. 6.6 Effective stress paths q^*~p^* normalised with the effective mean consolidation pressure, p_c^*

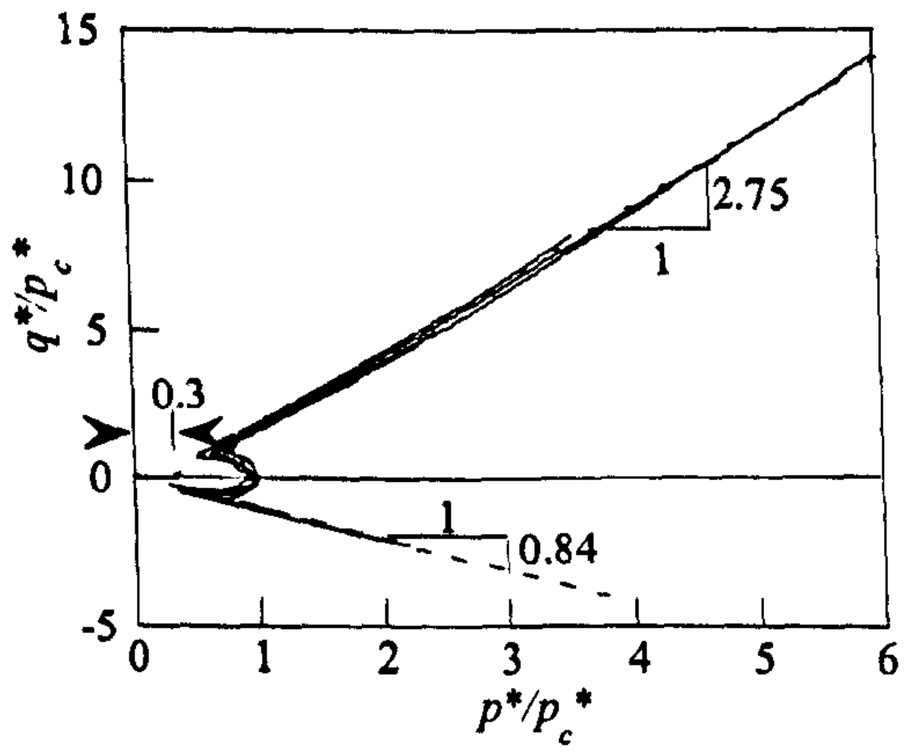

Fig. 6.7 Effective stress path q^*~p^* normalised with the effective mean consolidation pressure, pc*, of all tests on reinforced specimens

6.3.5 Additional observation

Given the strict definition of liquefaction, a complete static liquefaction was not attained for any of the unreinforced specimens tested in this study, either in compression or in extension. Full liquefaction is possible, however, for unreinforced and reinforced specimens by applying a strain reversal (implying a sudden 90° rotation of principal strain axes) at the end of the monotonic loading. Fig. 6.8 shows pictures of the fully liquefied specimens: the unreinforced specimen (Fig. 6.8a) clearly shows a completely collapsed structure, while the reinforced one (Fig. 6.8b) is still able to maintain some structural stability even after the removal of the membrane. Considering that one of the consequences of the liquefaction is the lateral spreading of the soil, it seems that the presence of fibres can limit or even prevent the occurrence of this phenomenon.

6.4 Summary and conclusions

The analysis of the undrained triaxial compression and extension tests on fibre reinforced and unreinforced sand specimens has revealed a number of points of interest. The presence of fibres clearly affects the undrained behaviour in compression as well as in extension and converts a strain softening response (typical for a loose unreinforced sand) into a strain hardening response. Static liquefaction appears to be prevented for both loading conditions but a higher concentration of fibres is needed for the prevention of liquefaction in extension. Normalisation of the stress paths with the mean effective stress at the end of consolidation shows a common path once the characteristic state is reached irrespective of the fibre concentration. The mobilised angles of friction coming from the slopes of the stress paths at large strains are vastly different for compression and extension and this is a consequence of the anisotropic nature of the distribution of fibre orientations. The angle of friction of reinforced specimens mobilised at the characteristic state appears independent of the fibre contents and initial consolidation pressure conditions used in this study but dependent on the loading conditions (compression/extension).

The addition of fibres was also found to be beneficial in avoiding the full liquefaction that was noticed for unreinforced specimens by applying a strain reversal at the end of the monotonic loading. Considering that one of the consequences of the liquefaction is the lateral spreading of the soil, it seems that the presence of fibres can limit or even prevent the occurrence of this phenomenon.

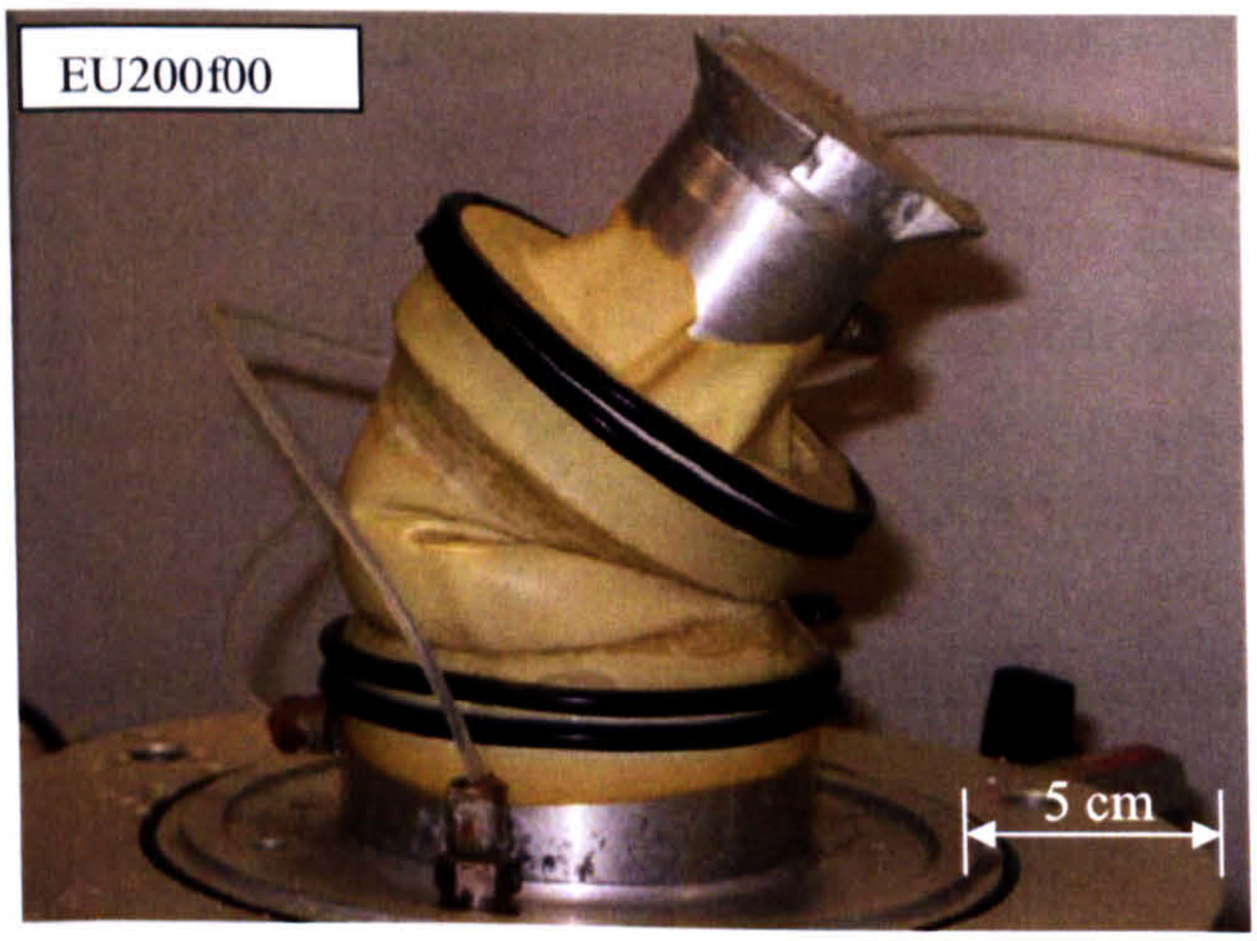

Fig. 6.8 Two photos of fully liquefied specimens due to a reversal axial straining at the end of the unloading extension tests: *(a)* unreinforced specimen; *(b)* reinforced specimen 0.3% fibre content

CHAPTER 7

CONSTITUTIVE MODELLING OF FIBRE REINFORCED SANDS

7.1 Introduction

Most of the modelling approaches proposed so far in literature have concentrated on the contribution of fibres to shear strength increase of soils and only a few authors have tried to propose a general constitutive law for fibre reinforced soils. The difficulties behind the development of a reliable constitutive model are also evident from the fact that the proposed constitutive models have been applied only to drained triaxial compression loading and they have been mainly developed for soil reinforced with continuous thread. A feeling of the complexity of the behaviour of this composite material is given by the experimental test results presented in the previous chapters which have highlighted the considerable number of factors which influence the response of the material. In fact, not only both the constituents play a central role in the behaviour of the composite material but also the sample preparation technique and test conditions affect the interaction between the constituents and influence the material performances. The aim of this chapter is to present a model which is able to capture the main factors governing the behaviour of reinforced sands and to try to reproduce the main features of their mechanical behaviour.

The model is based on the well known rule of mixtures of composite materials which allows us to adopt separate constitutive laws for each constituent and to combine their effects to characterise the behaviour of the composite. The approach is firstly applied by adopting a linear elastic – perfectly plastic model for the sand and a linear elastic law for the fibres. The model is calibrated and tested using results from a series of triaxial drained compression and extension tests which have been presented in Chapter 5. The versatility of the model is highlighted by its ability to accommodate any eventual fibre orientation distribution so that the anisotropy of

strength observed experimentally between compression and extension triaxial conditions can be reproduced.

The modelling of the fibre reinforced mixture is then repeated adopting the more complex Severn-Trent model for the sand matrix (Gajo and Muir Wood, 1999a). The model is successfully challenged to reproduce the test results of specimens reinforced with all three types of fibres in both drained and undrained conditions for compressive and extensive loading (experimental test results have been presented in Chapters 5 and 6). The versatility of the model is further highlighted by introducing small adjustments to the constitutive laws of each constituent to obtain particular features of the behaviour of the composite material. To obtain an accurate simulation of the volumetric or undrained behaviour it is necessary to attribute some of the voids in the sand to the fibres so that not all the voids are available to the sand for deforming. The importance of considering the real orientation distribution of fibres and the allocation of the voids between the two constituents will be highlighted in the following of this chapter.

7.2 General constitutive models for fibre reinforced composites

The determination of the physical properties of a composite material is a complex task because it is strongly influenced by several parameters such as shape, size, properties and spatial distribution of the different phases. In the literature two main alternatives have been employed to determine the mechanical behaviour of composite materials: micro or macro models. Micro-models focus on the micro-mechanical level of bonding between the phases. They usually generate discrete elements that accurately represent the microstructure of the materials and the macroscopic behaviour of the composite can be predicted in a reasonable time with current computational systems. Macro-models express the whole composite behaviour as that of a single material. They usually involve a homogenisation technique that is employed to obtain a constitutive model that can be inserted at the macroscopic level.

The simplest homogenisation technique is certainly the rule of mixtures (or mixing theory). The overall properties of the composite are calculated from the single properties of the constituents weighted by their volumetric fraction. This approach is justified only for linear

material constants (e.g. elastic moduli) but it has been widely used also in elasto-plastic conditions as explained later in paragraph 7.3.

Another class of homogenisation techniques is based on energetic considerations. Among them can be mentioned the method employed by Michalowski and Zhao (1996), Michalowski (1997) and Michalowski and Čermák (2002) for reinforced soils based on the work dissipation rate. The strength of the reinforced soils was determined by requiring that the rate of the dissipated work in the composite was equal to the sum of the work dissipated in its constituents. The approach was not applied for the description of the whole stress-strain behaviour of reinforced soils, probably because of the difficulties of determining the work of the constituents during stages of partial sliding between them or partial breakage of fibres. In other types of composite materials, approaches based on the strain energy density function are quite popular. They relate the strain of the materials with the energy developed by its deformation but they have the main disadvantage of being applicable only to hyper-elastic materials. The most famous applications are the Neo-Hookean and Ogden models. Examples of these models are Merodio and Ogden (2004) for incompressible non-linear elastic solids, or Peng et al. (2006) for human annulus fibrosus among others.

Other more complex homogenisation techniques such as the self consistent or effective medium approximation introduced by Eshelby (1957) or the asymptotic homogenisation theory (Bensoussan et al., 1978) are restricted to structures with simple or regular geometries (Kouznetsova et al., 2001). Models in which the overall properties of the composites are determined by fitting theoretical and experimental data are also common in the literature. This type of model belongs to the continuum theory and it has been widely explored by Spencer (1984).

The rule of mixtures has been chosen here for its simplicity and versatility. The accuracy required for predicting the behaviour of soils is generally lower than that required for other materials such as metals, therefore the adoption of more complex and sophisticated approaches has been considered pointless in the first instance. Time and temperature effects have been neglected in this formulation.

7.3 Rule of mixtures

The usual axioms of the rule of mixtures are:

- each component of a composite satisfies its own constitutive law,
- each component is homogeneously distributed throughout the composite,
- the individual contributions of each component to the overall composite behaviour are scaled according to their volumetric fractions.

Even if the rule of mixtures has been developed for elastic material, it has also been applied for predicting the elastic–plastic behaviour of a wide variety of composites, including a reinforced metal-matrix (Dvorak and Bahei-El-Din, 1982; Dvorak and Bahei-El-Din, 1987 and Voyaiadjis and Thiagarajan, 1995), anisotropically fibre reinforced materials at large strains (Car et al., 2000), fibre-reinforced laminates (Luccioni, 2006), concrete when treated as a composite of mortar and aggregates (Ortiz and Popov, 1982), municipal soil waste (Machado et al., 2002), cemented sands (Abdulla and Kiousis, 1997) and fibre reinforced soils (Villard et al., 1990 and di Prisco and Nova, 1993).

The total volume of the composite is made up of sand, fibres and voids. Fibres and sand grains are discrete materials whose behaviour is linked to the volume of voids (V_v) of the specimen. The fibres may create a network within the soil matrix and they may prevent the soil skeleton from using some of the voids of the specimen (Fig. 7.1).In the most general case, it is therefore assumed that some voids are "attached" to the grains (V_{vs}) and some others are attached to the fibres (V_{vf}) with:

$$V_v = V_{vs} + V_{vf} \qquad (7.1).$$

The components of the reinforced and unreinforced specimens are represented in the phase diagram shown in Fig. 7.2.

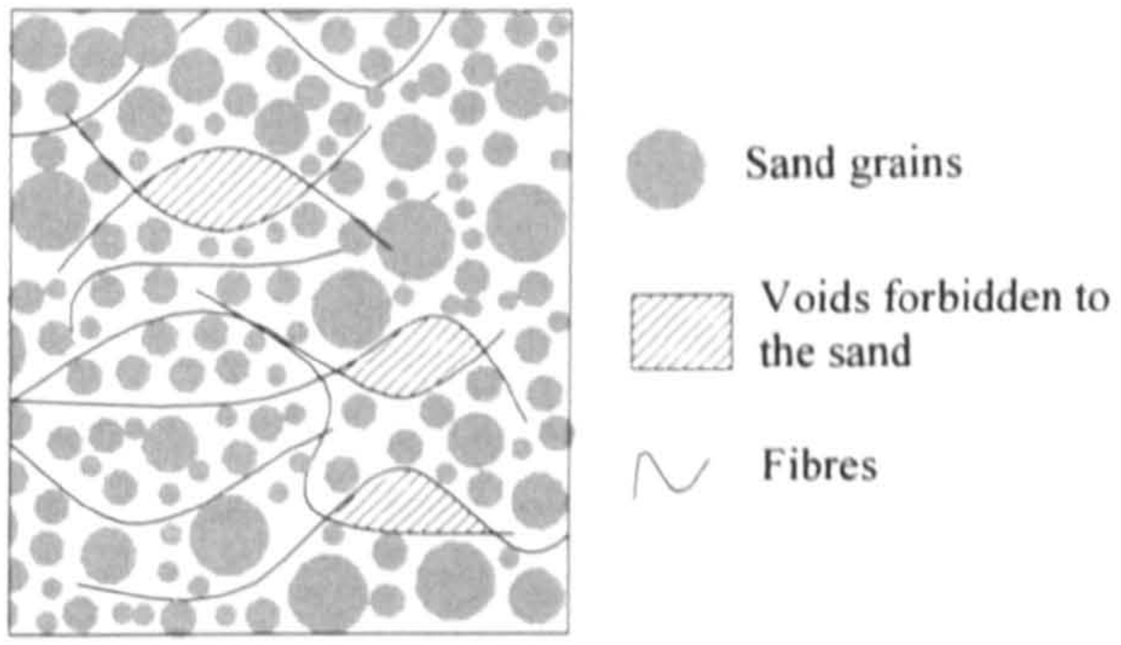

Fig. 7.1 Schematic illustration of the voids forbidden to the sand grains when rearranging

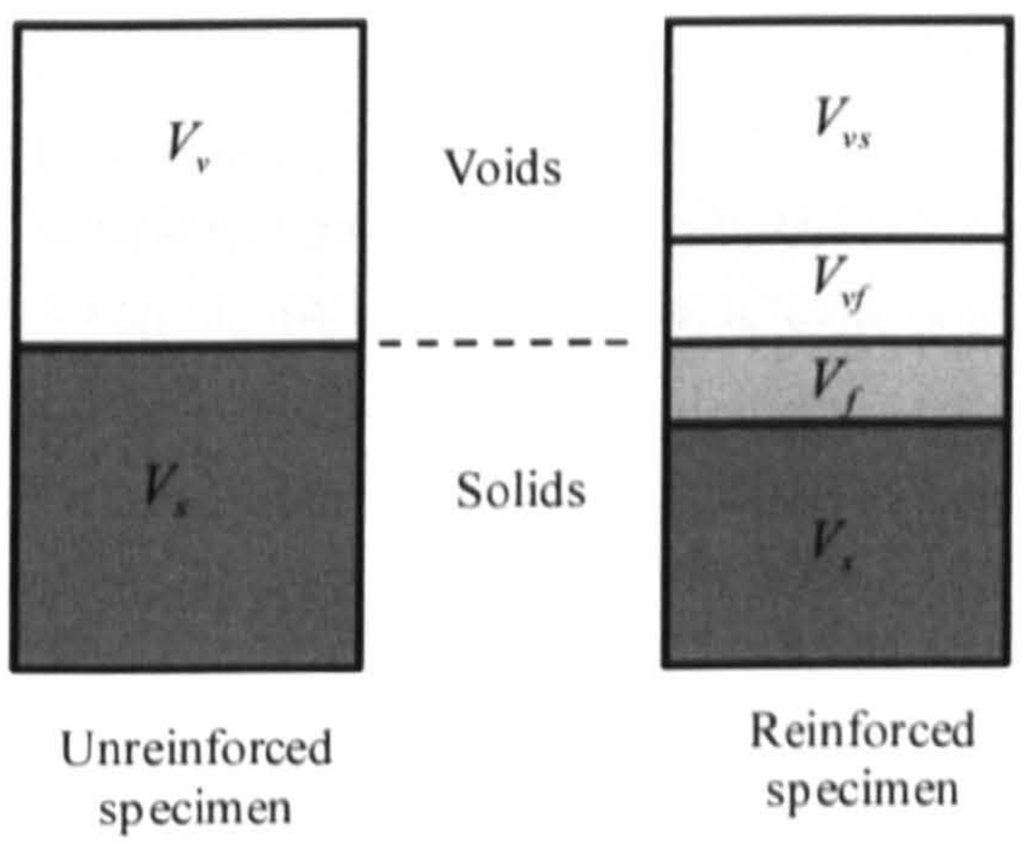

Fig. 7.2 Phase diagram for both unreinforced and reinforced specimens

The specific volumes of the composite, sand and fibres are defined as follows in order:

$$\upsilon = \frac{V}{V_s + V_f} \qquad \upsilon_m = \frac{V_{vs} + V_s}{V_s} \qquad \upsilon_f = \frac{V_{vf} + V_f}{V_f} \tag{7.2}$$

and they are linked by the relationship:

$$\upsilon = \left(\upsilon_m + \upsilon_f \frac{G_s w_f}{G_f} \right) \frac{G_f}{G_f + G_s w_f} \tag{7.3}$$

Substituting Eqs.(7.1) and (7.2) in Eq.(1.2) ($\dot{\varepsilon}_\upsilon = -\dot{\upsilon}/\upsilon$), the relationship between the incremental volumetric strains of the composite and its constituents ($\dot{\varepsilon}_{m\upsilon}$, $\dot{\varepsilon}_{f\upsilon}$ for the sand and fibres respectively) can be defined:

$$\dot{\varepsilon}_\upsilon = \dot{\varepsilon}_{m\upsilon}\mu_m + \dot{\varepsilon}_{f\upsilon}\mu_f \tag{7.4}$$

where μ_m and μ_f are the volumetric contents of sand and fibres with their specific "attached" voids:

$$\mu_m = \frac{(V_s + V_{vs})}{V} \tag{7.5}$$

$$\mu_f = \frac{(V_f + V_{vf})}{V} \tag{7.6}$$

Consistently with Eq. (7.4), the relationship between the incremental vector of strains of the composite and its constituents can be defined as:

$$\dot{\boldsymbol{\varepsilon}} = \dot{\boldsymbol{\varepsilon}}_m\mu_m + \dot{\boldsymbol{\varepsilon}}_f\mu_f \tag{7.7}$$

The stress state of a composite, $\boldsymbol{\sigma}$, is expressed in terms of the stress states of the soil matrix $\boldsymbol{\sigma}' = [p', q']^T$ and fibres $\boldsymbol{\sigma}_f = [p_f, q_f]^T$:

$$\boldsymbol{\sigma} = \boldsymbol{\sigma}'\mu_m + \boldsymbol{\sigma}_f\mu_f \tag{7.8}$$

The incremental form of the rule of mixtures for stresses can be expressed as:

$$\dot{\boldsymbol{\sigma}} = \mu_m\dot{\boldsymbol{\sigma}}' + \dot{\mu}_m\boldsymbol{\sigma}' + \mu_f\dot{\boldsymbol{\sigma}}_f + \dot{\mu}_f\boldsymbol{\sigma}_f \tag{7.9}$$

A basic assumption of this model is that the fibres do not act in compression and they offer no resistance to flexion: they only develop stresses when pulled in tension. However, the deformation process may induce changes of the voids attached to the fibres but these changes of V_{vf} has not be linked to the stresses developed in the fibres. Therefore the stresses mobilised in the fibres are only linked to their stretching and therefore to the deformation of the fibre skeleton $\tilde{\boldsymbol{\varepsilon}}_f$.

The stress-strain relationship for each constituent can be introduced to express the incremental stresses for both sand and fibres:

$$\dot{\boldsymbol{\sigma}}' = [M_m]\dot{\boldsymbol{\varepsilon}}_m \qquad (7.10)$$

$$\dot{\boldsymbol{\sigma}}_f = [M_f]\dot{\tilde{\boldsymbol{\varepsilon}}}_f \qquad (7.11)$$

where M_m is the stiffness matrix for the sand and M_f is the stiffness matrix for the fibres.

The final form of the stress-strain relationship for the reinforced soil, when Eqs.(7.10) and (7.11) are substituted in Eq. (7.9), is:

$$\dot{\boldsymbol{\sigma}} = \mu_m\dot{\boldsymbol{\sigma}}' + \dot{\mu}_m\boldsymbol{\sigma}' + \mu_f\dot{\boldsymbol{\sigma}}_f + \dot{\mu}_f\boldsymbol{\sigma}_f = \mu_m[M_m]\dot{\boldsymbol{\varepsilon}}_m + \dot{\mu}_m\boldsymbol{\sigma}' + \mu_f[M_f]\dot{\tilde{\boldsymbol{\varepsilon}}}_f + \dot{\mu}_f\boldsymbol{\sigma}_f \qquad (7.12).$$

7.4 Modelling stiffness matrix for fibres

In reinforced composites fibres are embedded in the sand matrix and their deformation follows the deformation of the specimen. In the first instance the coincidence between the deformation of the fibre skeleton and the composite material (Voigt's assumption) can be assumed. Thus the magnitude of deformation in a single fibre depends on its orientation. Also, assuming an elastic behaviour for the fibres, even the magnitude of the stress in the fibre depends on fibre orientation as will now be shown. Considering conventional triaxial conditions, the following relationship between the incremental strains at any angle θ from the horizontal ($\dot{\varepsilon}_\theta$) and the principal incremental strains ($\dot{\varepsilon}_a$ in vertical direction and $\dot{\varepsilon}_r$ in horizontal direction) can be easily obtained:

$$\dot{\varepsilon}_\theta = \dot{\varepsilon}_a \sin^2(\theta) + \dot{\varepsilon}_r \cos^2(\theta) \qquad (7.13)$$

The stress carried by an elastic fibre oriented at an angle θ from the horizontal is then:

$$\dot{\sigma}_{\theta f} = E_f \dot{\varepsilon}_\theta \qquad (7.14)$$

It is possible to derive the contribution of a single fibre to the principal stresses, $\sigma_{af}(\theta)$ and $\sigma_{rf}(\theta)$, by decomposing $\sigma_{\theta f}$ requiring the conservation of the generated work on the conventional triaxial space:

$$\sigma_{af}\dot{\varepsilon}_a + 2\sigma_{rf}\dot{\varepsilon}_r = \sigma_{\theta f}\dot{\varepsilon}_\theta = \sigma_{\theta f}\sin^2(\theta)\dot{\varepsilon}_a + \sigma_{\theta f}\cos^2(\theta)\dot{\varepsilon}_r \tag{7.15}$$

which gives the following relationship between incremental strains:

$$\dot{\sigma}_{af}(\theta) = \dot{\sigma}_\theta \sin^2(\theta) \tag{7.16}$$

$$\dot{\sigma}_{rf}(\theta) = \dot{\sigma}_\theta \cos^2(\theta)/2 \tag{7.17}$$

In expanded form these can be rewritten as:

$$\dot{\sigma}_{af}(\theta) = E_f\left(\dot{\varepsilon}_a \sin^4(\theta) + \dot{\varepsilon}_r \cos^2(\theta)\sin^2(\theta)\right) \tag{7.18}$$

$$\dot{\sigma}_{rf}(\theta) = E_f \frac{\left(\dot{\varepsilon}_a \sin^2(\theta)\cos^2(\theta) + \dot{\varepsilon}_r \cos^4(\theta)\right)}{2} \tag{7.19}$$

7.4.1 Agglomerate of fibres

A procedure similar to the one proposed by Zhu et al. (1994) for the determination of the strength of short-fibre reinforced metal-matrix has been used here. Fibres have a non-uniform orientation distribution, and using the spherical coordinates shown in Fig. (7.3), the general fibre orientation distribution function $\rho(\theta)$ introduced in paragraph 4.2 may be used to describe the fibre orientation. It is worth recalling that $\rho(\theta)$ represents the volumetric concentration of fibres in an infinitesimal volume dV (Fig. 7.3) having an orientation of angle θ above the horizontal and its main property has to be:

$$\overline{\rho} = \frac{1}{V}\int_V \rho(\theta)\,\mathrm{d}V \tag{7.20}$$

where V is the volume of the reference sphere (made of the composite material) shown in Fig. (7.3) and $\overline{\rho}$ is the average fibre concentration defined by:

$$\overline{\rho} = V_f / V \tag{7.21}$$

According to its definition, $\rho(\theta)$ is the concentration factor of the fibre skeleton within the composite which has an orientation of θ above the horizontal plane. Expressions for the overall contribution of fibres within the composite in the directions of the principal stresses can then be obtained by integration using the two expressions:

$$\dot{\sigma}_{fa} = \frac{1}{V}\int_V \frac{\rho(\theta)}{\mu_f}\dot{\sigma}_{af}(\theta)\mathrm{d}V \tag{7.22}$$

$$\dot{\sigma}_{fr} = \frac{1}{V}\int_V \frac{\rho(\theta)}{\mu_f}\dot{\sigma}_{rf}(\theta)\mathrm{d}V \tag{7.23}$$

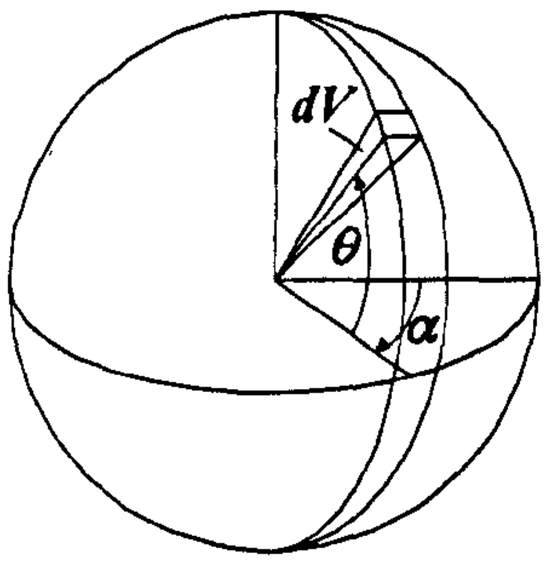

Fig. 7.3 Spherical coordinates used for the definition of the fibre orientation distribution

If the orientation distribution is symmetrical with respect to the horizontal plane, (7.22) and (7.23) can be expanded and rearranged to give:

$$\dot{\sigma}_{fa} = \frac{E_f}{2}\left(\dot{\varepsilon}_a\int\frac{\rho(\theta)}{\mu_f}\sin^4(\theta)\cos(\theta)\mathrm{d}\theta + \dot{\varepsilon}_r\int\frac{\rho(\theta)}{\mu_f}\cos^3(\theta)\sin^2(\theta)\mathrm{d}\theta\right) \tag{7.24}$$

$$\dot{\sigma}_{fr} = \frac{E_f}{4}\left(\dot{\varepsilon}_a\int\frac{\rho(\theta)}{\mu_f}\sin^2(\theta)\cos^3(\theta)\mathrm{d}\theta + \dot{\varepsilon}_r\int\frac{\rho(\theta)}{\mu_f}\cos^5(\theta)\mathrm{d}\theta\right) \tag{7.25}$$

For flexible fibres, only those fibres acting in tension contribute to the stresses of the composite. Therefore the integrations of (7.24) and (7.25) should be performed within those

limits of θ for which $\dot{\varepsilon}_\theta < 0$. If θ_0 is the direction of zero incremental strains which, according to Mohr's circle for strain increment, is:

$$\theta_0 = \arctan\sqrt{-\frac{\dot{\varepsilon}_r}{\dot{\varepsilon}_a}} \tag{7.26}$$

and due to the symmetry of the deformation pattern, the limits of the integration in Eqs. (7.24) and (7.25) must correspond to $0 \le \theta \le \theta_0$ for triaxial compression and $\theta_0 \le \theta \le \pi/2$ for triaxial extension, as illustrated in Fig. 7.4.

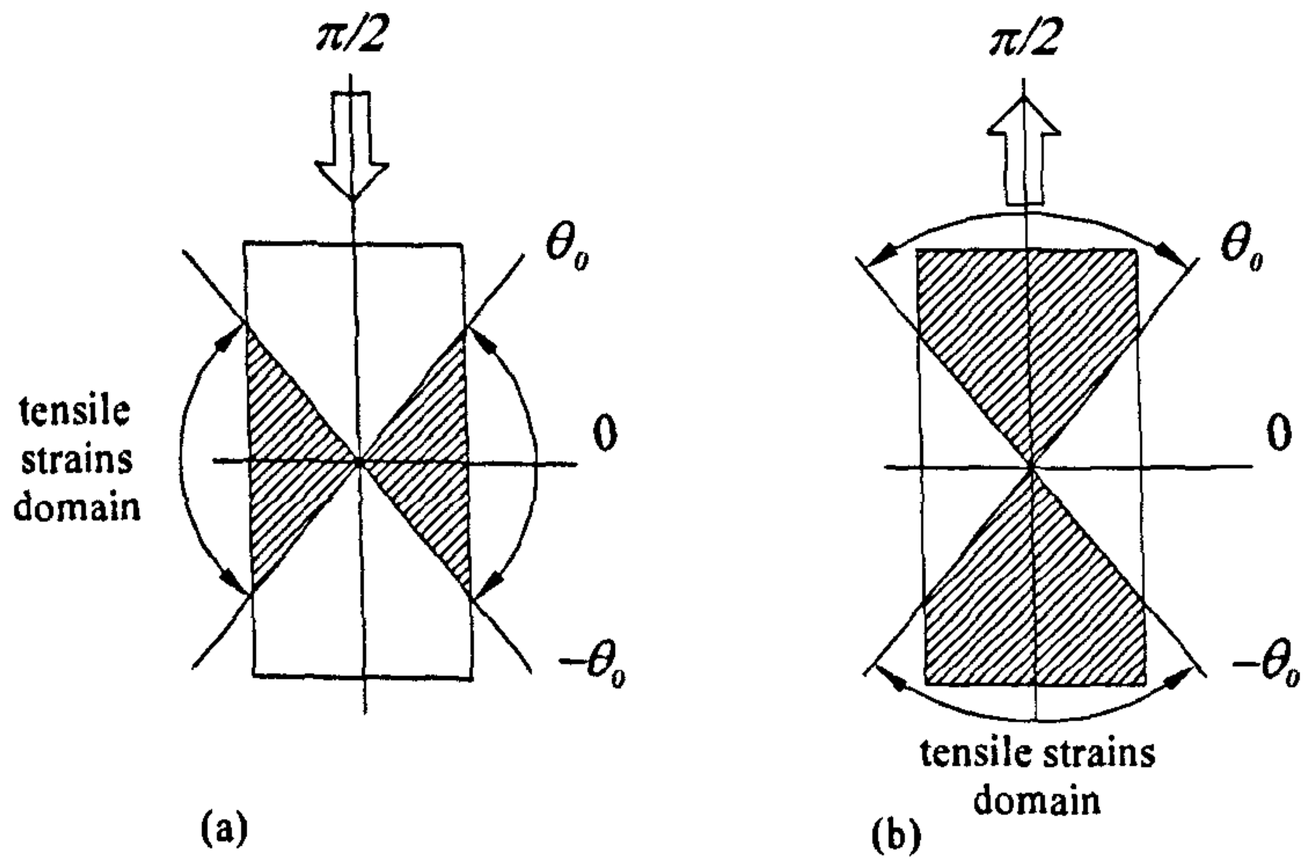

Fig. 7.4 Domains of tensile strain orientations for (a) compression and (b) extension loading

The mechanical response of the composite depends not only on the individual characteristics of its components but also on the interaction between them. The magnitude of the interfacial bond between fibres and sand grains affects the transfer of stresses between the two components. The stress in a single fibre is not constant along its length – it must reduce to zero at its end – and assuming that a uniform mobilised tensile stress exists is therefore an approximation. The bonding between fibres and sand grains is not perfect as some amount of relative sliding between the two constituents will almost certainly occur, with the amount of sliding being

dependent on the mobilised stress along the length of individual fibres. The imperfect interfacial bond can be accounted for in the model with the introduction of a dimensionless sliding function (f_b), similar to that used by Machado et al. (2002) and Brighenti (2004). f_b can vary between 0 and 1 with f_b =1 for perfect bonding and f_b =0 for full sliding. Introducing f_b means that the deformation of the fibres is not coincident with the deformation of the specimen but is instead given by:

$$\dot{\tilde{\boldsymbol{\varepsilon}}}_f = f_b \dot{\boldsymbol{\varepsilon}} \tag{7.27}$$

If the orientation distribution is symmetrical with respect to the horizontal plane, Eqs. (7.24) and (7.25) may now be expanded and rearranged and Eq. (7.27) introduced to give:

$$\begin{bmatrix} \dot{\sigma}_{af} \\ \dot{\sigma}_{rf} \end{bmatrix} = E_f \begin{bmatrix} \int_{l_1}^{l_2} \frac{\rho(\theta)}{\mu_f} \cos(\theta)\sin^4(\theta)\mathrm{d}\theta & \int_{l_1}^{l_2} \frac{\rho(\theta)}{\mu_f} \cos^3(\theta)\sin^2(\theta)\mathrm{d}\theta \\ \frac{1}{2}\int_{l_1}^{l_2} \frac{\rho(\theta)}{\mu_f} \cos^3(\theta)\sin^2(\theta)\mathrm{d}\theta & \frac{1}{2}\int_{l_1}^{l_2} \frac{\rho(\theta)}{\mu_f} \cos^5(\theta)\mathrm{d}\theta \end{bmatrix} \begin{bmatrix} f_b \dot{\varepsilon}_a \\ f_b \dot{\varepsilon}_r \end{bmatrix} \tag{7.28}$$

where the integration limits are $l_1 = 0$ and $l_2 = \theta_0$ for compression loading and $l_1 = \theta_0$ and $l_2 = \pi / 2$ for extension loading. The stiffness matrix for the fibres is therefore defined as:

$$[M_f] = \frac{E_f}{\mu_f} \begin{bmatrix} \int_{l_1}^{l_2} \rho(\theta)\cos(\theta)\sin^4(\theta)\mathrm{d}\theta & \int_{l_1}^{l_2} \rho(\theta)\cos^3(\theta)\sin^2(\theta)\mathrm{d}\theta \\ \frac{1}{2}\int_{l_1}^{l_2} \rho(\theta)\cos^3(\theta)\sin^2(\theta)\mathrm{d}\theta & \frac{1}{2}\int_{l_1}^{l_2} \rho(\theta)\cos^5(\theta)\mathrm{d}\theta \end{bmatrix} \tag{7.29}$$

Returning to the conventional p and q triaxial notations, the contribution of fibres to the stresses in the composite can be expressed as:

$$\dot{\boldsymbol{\sigma}}_f = [M_f] f_b \begin{bmatrix} \dot{\varepsilon}_v \\ \dot{\varepsilon}_q \end{bmatrix} = \frac{E_f}{\mu_f} \begin{bmatrix} A_{11} & A_{12} \\ A_{21} & A_{22} \end{bmatrix} f_b \begin{bmatrix} \dot{\varepsilon}_v \\ \dot{\varepsilon}_q \end{bmatrix} \tag{7.30}$$

where:

$$\left.\begin{aligned} A_{11} &= \frac{1}{9}(F_{11} + F_{12} + 2F_{21} + 2F_{22}) \\ A_{12} &= \frac{1}{3}\left(F_{11} - \frac{F_{12}}{2} + 2F_{21} - F_{22}\right) \\ A_{21} &= \frac{1}{3}(F_{11} + F_{12} - F_{21} - F_{22}) \\ A_{22} &= \frac{1}{2}(2F_{11} - F_{12} - 2F_{21} + F_{22}) \end{aligned}\right\} \qquad (7.31)$$

and the F_{ij} terms represent the components of the matrix of Eq. (7.29) with the first subscript being the column number and the second subscript being the line number.

7.5 Application 1: classical elastic-plastic Mohr-Coulomb model for sand

An appealing feature of the modelling framework presented here is that any constitutive model for describing the stress-strain behaviour of the sand may be used to obtain the stiffness matrix for an unreinforced sand. In the first instance the modelling framework will be challenged by adopting a simple linear elastic-perfectly plastic constitutive law for the sand matrix. The failure of the soil is predicted following the Mohr-Coulomb failure criterion.

For the first application of the modelling framework, since the volume of fibres is very small compared to the volume of the composite, the following minor modifications have been made:

- the volume of voids "attached" to the fibres (V_{vf}) is negligible;
- the matrix volumetric concentration factor $\mu_m \approx 1$;
- the variation of the fibres concentration factor $\dot{\mu}_f \approx 0$.

This leads to a very simplified formulation of the rule of mixtures for stresses:

$$\dot{\boldsymbol{\sigma}} = \dot{\boldsymbol{\sigma}}' + \mu_f \dot{\boldsymbol{\sigma}}_f \qquad (7.32)$$

and to the following simplified relationship between strains:

$$\dot{\boldsymbol{\varepsilon}} = \dot{\boldsymbol{\varepsilon}}_m \qquad (7.33).$$

7.5.1 The sand stiffness matrix

In the elastic domain the increments of stresses are related to the increments of strains through the bulk modulus K and the shear modulus G:

$$\begin{bmatrix} \dot{p}' \\ \dot{q}' \end{bmatrix} = \begin{bmatrix} K & 0 \\ 0 & 3G \end{bmatrix} \begin{bmatrix} \dot{\varepsilon}_v \\ \dot{\varepsilon}_q \end{bmatrix} \tag{7.34}$$

The elastic parameters are a function of the Young's modulus, E, and Poisson's ratio, ν, through:

$$K = \frac{E}{2(1-\nu)} \tag{7.35}$$

$$G = \frac{E}{2(1+\nu)} \tag{7.36}$$

Yielding occurs when the following relation is satisfied:

$$q' = Mp' \tag{7.37}$$

where M represents one of two properties M_c or M_e, depending on whether triaxial compression or triaxial extension is occurring, linked to the friction angle ϕ' of the sand by the relationships:

$$M_c = \frac{6\sin\phi'}{3-\sin\phi'} \tag{7.38}$$

$$M_e = -\frac{6\sin\phi'}{3+\sin\phi'} \tag{7.39}$$

When the soil yields the relationship between incremental plastic strains is controlled by:

$$\frac{\dot{\varepsilon}_v^p}{\dot{\varepsilon}_q^p} = -M^* \tag{7.40}$$

where M^* represents one of two properties M_c^* or M_e^*, depending on whether triaxial compression or triaxial extension is occurring, linked to the pseudo dilation angle ψ of the sand:

$$M_c^* = \frac{3\tan\psi}{3+\tan\psi} \tag{7.41}$$

$$M_e^* = \frac{3\tan\psi}{\tan\psi-3} \tag{7.42}$$

The dilation is formally expressed in terms of plastic increments of strain as defined in Eq. (5.1).

7.5.2 Model calibration

7.5.2.1 Input parameters

The model is calibrated using results of drained triaxial tests performed on both unreinforced and reinforced specimens while the undrained tests have not been considered in this section because of the inability of the model for the sand matrix to accurately simulate the volumetric behaviour of soils. Because the model is based on the superposition of the effects of sand and fibres, the two stiffness matrices can be calibrated independently.

Parameters governing the behaviour of the sand matrix were determined from the results of tests performed on unreinforced specimens. The Mohr-Coulomb model requires the definition of two elastic and two plastic parameters. Here a typical value for Poisson's ratio v= 0.3 was adopted and the elastic modulus, E, is assumed to depend on the consolidation effective mean stress:

$$E \approx kp'_c \tag{7.43}$$

where the scaling parameter k=36 was defined by fitting the experimental results . It is acknowledged that the mobilised peak angle of friction is stress level dependent, especially when confining stress is low, less than 100 kPa. However, for the sake of simplicity a constant value of ϕ'=34.5° was used here.

To obtain a reasonable simulation of the volumetric behaviour, the dilatancy angle for the unreinforced specimen has been taken as being equal to the maximum dilatancy angle ψ_{max} as defined in Eq. (5.4). However, M^* represents a ratio between increments of plastic strains while tan ψ_{max} was computed from increments of total strain. A correction is therefore needed to allow for the occurrence of elastic strains in reinforced specimen and details are given in Appendix 1 in Diambra et al. (2010). The corrected relationships are as follows:

$$M_c^* = \frac{3}{2}\frac{m_c^* + 2}{m_c^* - 1}\ ,\ M_e^* = \frac{3}{2}\frac{m_e^* + 2}{m_e^* - 1} \tag{7.44}$$

where

$$m_c^* = \frac{1 + \frac{E_f \cdot f_b}{E}\left(\frac{1+\sin\phi'}{1-\sin\phi'} - 2\mu\right)\left(F_{21} + F_{22}\frac{\tan\psi_{max}+1}{2}\right)}{\frac{\tan\psi_{max}+1}{2} + \frac{E_f \cdot f_b}{E}\left(-\nu\frac{1+\sin\phi'}{1-\sin\phi'} + (1-\mu)\right)\left(F_{21} + F_{22}\frac{\tan\psi_{max}+1}{2}\right)} \tag{7.45}$$

and

$$m_e^* = \frac{1 + \frac{E_f \cdot f_b}{E}\left(\frac{1-\sin\phi'}{1+\sin\phi'} - 2\mu\right)\left(F_{21} + F_{22}\frac{\tan\psi_{max}-1}{2}\right)}{\frac{\tan\psi_{max}-1}{2} + \frac{E_f \cdot f_b}{E}\left(-\mu\frac{1-\sin\phi'}{1+\sin\phi'} + (1-\mu)\right)\left(F_{21} + F_{22}\frac{\tan\psi_{max}-1}{2}\right)} \tag{7.46}$$

The definition of the stiffness matrix for the fibres requires only the definition of the elastic modulus of the fibres, the sliding function and the fibre orientation distribution. The fibre orientation distribution for the tested specimen has been determined in Chapter 4. The orientation distribution of fibres is axisymmetric with respect to the vertical axis and, according to the spherical coordinate defined in Fig.7.3, it was defined as:

$$\rho(\theta) = \bar{\rho}\left(A + C\left|\cos^n\theta\right|\right) \tag{7.47}$$

where $A=0$, $C=2.19$ and $n=6$ for tamped specimens reinforced with fibre (1). Difficulties were encountered in the integration of the fibre stiffness matrix if the orientation distribution as expressed in Eq. (7.46) is adopted; therefore a slightly modified orientation distribution

function $\rho(\theta)$ as proposed by Diambra et al. (2007) was used in this research. The new function for $\rho(\theta)$ is:

$$\rho(\theta) = \overline{\rho}\frac{2ab^2|\cos(\theta)|}{\cos(\theta)^2(b^2-a^2)+a^2} \tag{7.48}$$

where $a = 1.095$ and $b = 0.449$ were determined by forcing equality in (7.47) and (7.48) at $\theta = 0$ and by satisfying (7.20). The similarity between the two orientation distribution functions is illustrated in Fig.7.5.

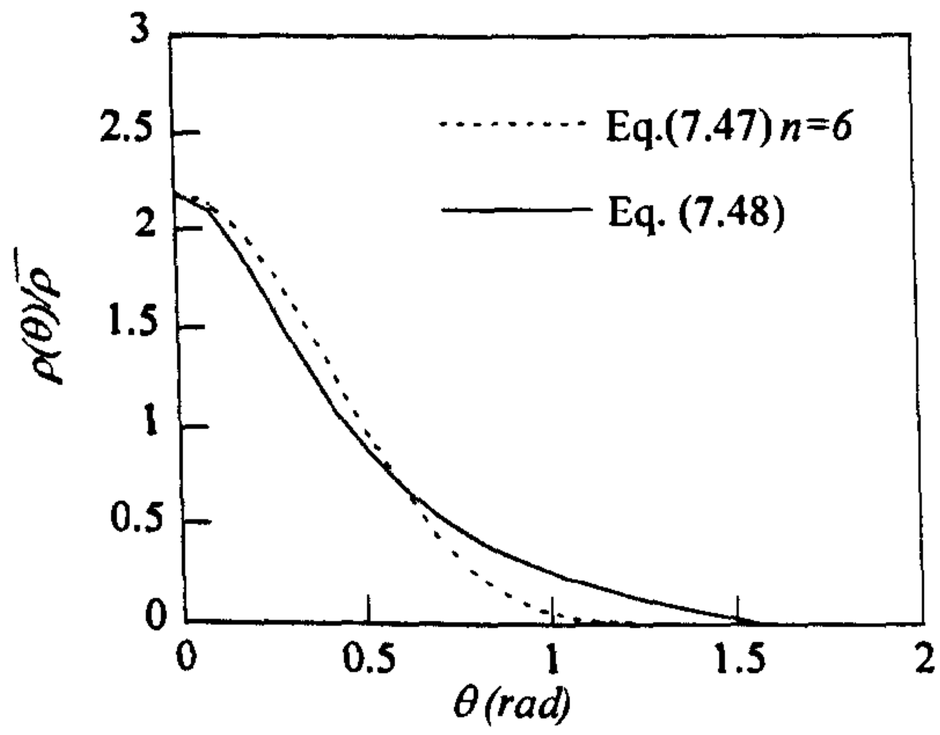

Fig. 7.5 Comparison between the assumed orientation distribution functions in Eq. (7.47) and Eq. (7.48) for fibres type (1)

The elastic modulus for the fibres has been determined by means of the results of tension tests performed on single fibres. As shown in Fig. 3.9 in paragraph 3.3.2, a reasonable fit of the initial part of the tensile stress-strain response of a fibre can be obtained by adopting $E_f = 900$ MPa.

The sliding function, f_b, which indirectly accounts for the imperfect interfacial contact between fibres and sand grains is one of the most difficult model ingredients to establish. A procedure based on a back analysis of the experimental results was used here. The extra strength of a composite is attributed to the artificial confinement provided by the reinforcement, which in turn affects the stress path of the sand matrix within the composite. The stress path of the sand matrix is different from a conventional triaxial one - only the stress path of the composite obeys

$\dot{q} / \dot{p} = 3$. The fibre stresses are subtracted from the stresses in the composite, and the resulting stresses, which represent those of the sand matrix, are then adjusted using f_b so that they ultimately approach the failure surface, as schematically shown in Fig. 7.6.

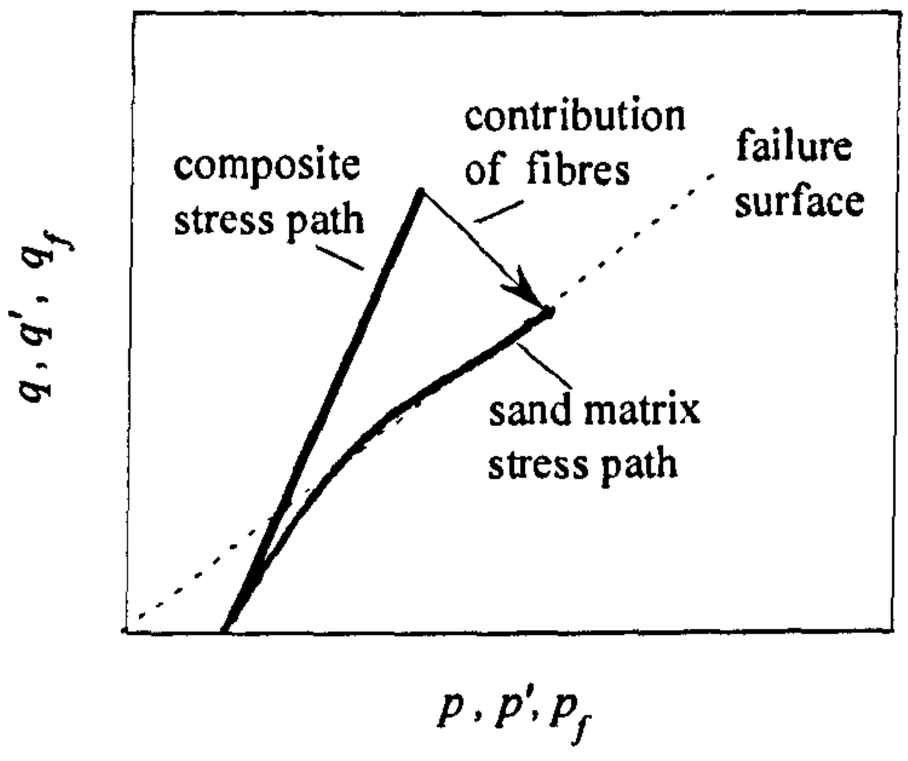

Fig. 7.6 Procedure for determination of the sliding function f_b

A function for f_b of the following form:

$$f_b = K_e\left(1-\exp\left(-c_s \cdot \frac{p}{p_{ref}}\right)\right) \tag{7.49}$$

was introduced, where K_e is an efficiency coefficient of the fibre-sand bonding and the bracketed component, which includes the mean stress of the sand matrix p' normalised with a reference pressure, p_{ref} of 0.1MPa, accounts for a confining pressure effect. Values of K_e=0.6 and c_s=0.75 have been determined with the previous procedure. The dependency of f_b on p allows the simulation of an enhanced bonding between fibres and sand matrix at higher confining stresses as observed in the experiments.

7.5.2.2 Model Simulation

Figs. (7.7) - (7.10) compare typical results of model simulations with experimental results for conventional drained triaxial tests in the $q \sim \varepsilon_q$ and $\varepsilon_v \sim \varepsilon_q$ planes. Each figure shows tests with a range of fibre contents but a single confining pressure and specimen density. The model simulations are represented by the thick continuous lines whereas the experimental data are represented with thin lines. Despite the simplicity of the model adopted for the sand matrix, the model generally reproduces the main features of the behaviour of unreinforced and reinforced specimens.

For compressive loading (Figs. 7.7-7.9), the model captures well the somewhat bilinear nature of the reinforced soil response irrespective of fibre content, density and confining stress. The initial stress-strain responses generated by the model are not affected by the presence of fibres. In these initial parts the fibre contribution to the composite behaviour is quite small, which is not surprising as ε_r is also small, preventing the fibres from elongating and mobilising large tensile forces. At larger shear strains, the shear stress supported by the composite increases, apparently without limit, and this can be successfully reproduced by adopting a simple elastic model for the fibres and an anisotropic fibre orientation distribution. The presence of the fibres acts to increase the confinement of the sand matrix as the shear strain increases, allowing the sand to support greater deviatoric stresses. The assumption that the fibres are working within their elastic range seems correct for these fibres and these test conditions. In fact, careful examination of the fibres at the end of the triaxial tests showed no signs of fibre breakage or plastic deformation.

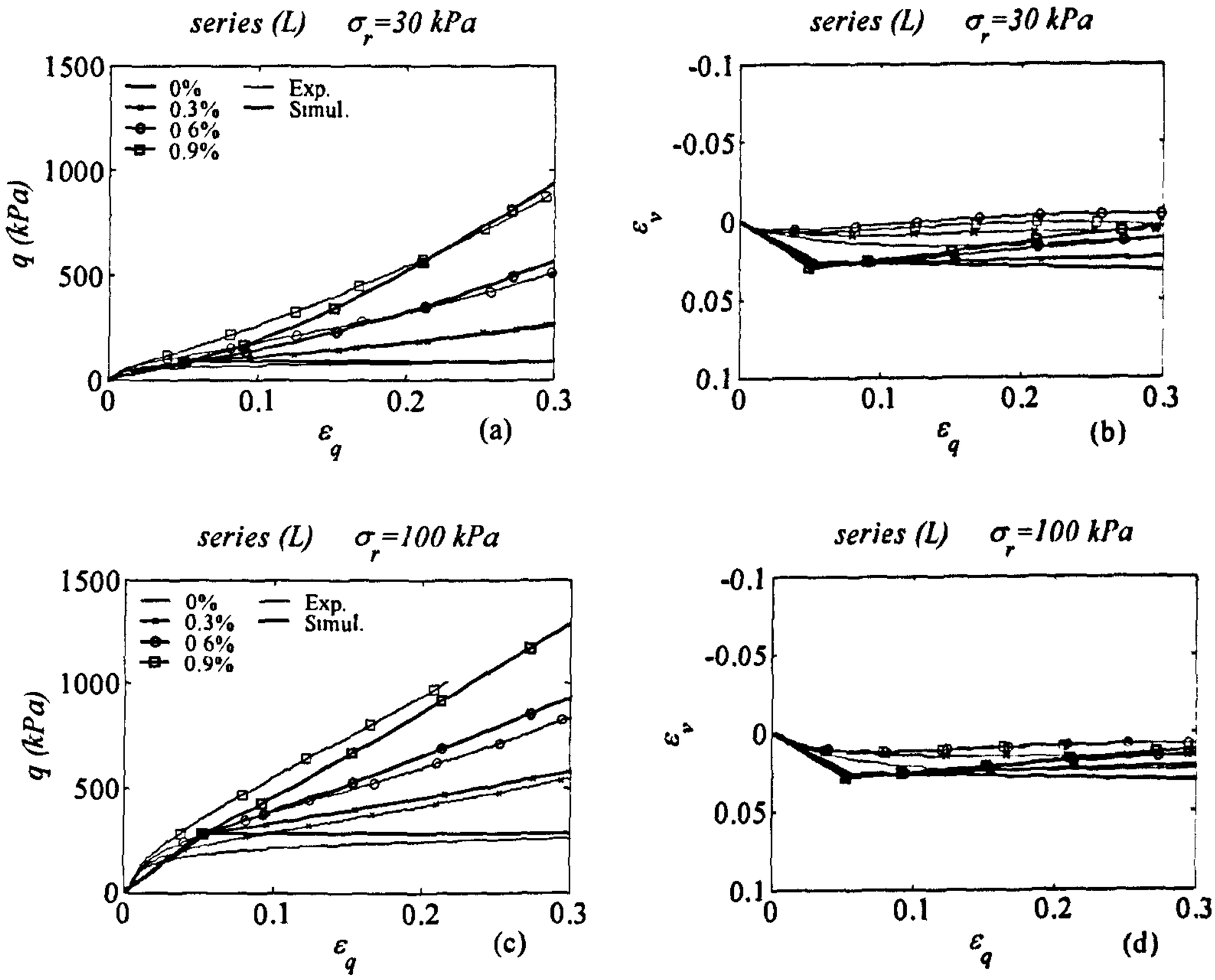

Fig. 7.7 Compression triaxial test results and model simulations for reinforced and unreinforced specimens of *(L)* test series (legend indicates the fibre content)

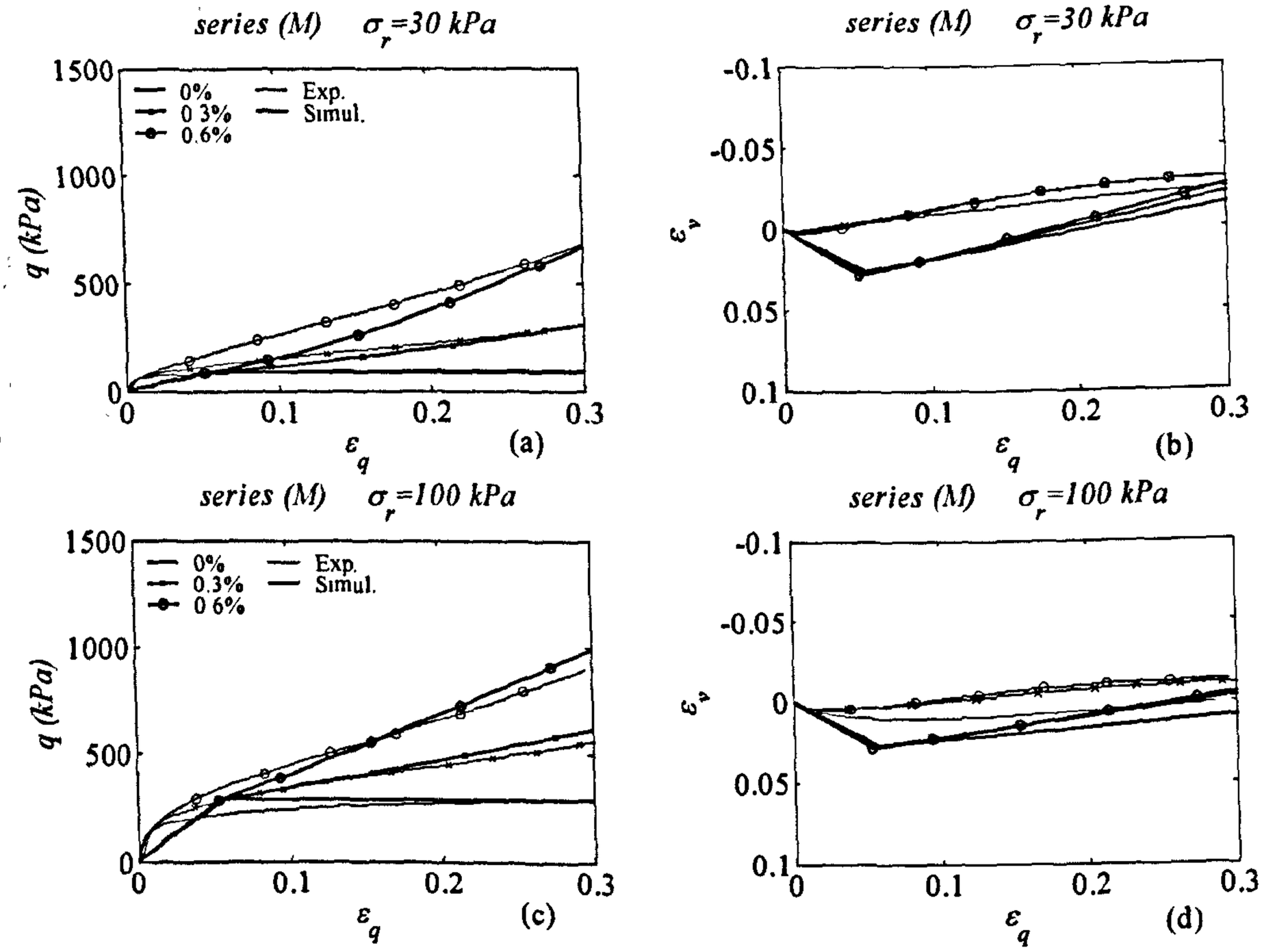

Fig. 7.8 Compression triaxial test results and model simulations for reinforced and unreinforced specimens of *(M)* test series (legend indicates the fibre content)

The slightly curved shape of the experimentally measured stress-strain curves at low confining pressures (Figs. 7.7a-7.8a-7.9a) is also well reproduced by the model and this is attributed to the dependency of the sliding function f_b on the mean stress in the composite.

The limited contribution of fibres observed for extension loading is very satisfactorily simulated by the model (Figs. 7.10). Results are reported in the deviatoric stress-strain and on the volumetric plane for two different specimen densities. In extension only very few fibres are orientated in the direction of tensile strains and this is taken into account by the fibre orientation distribution adopted.

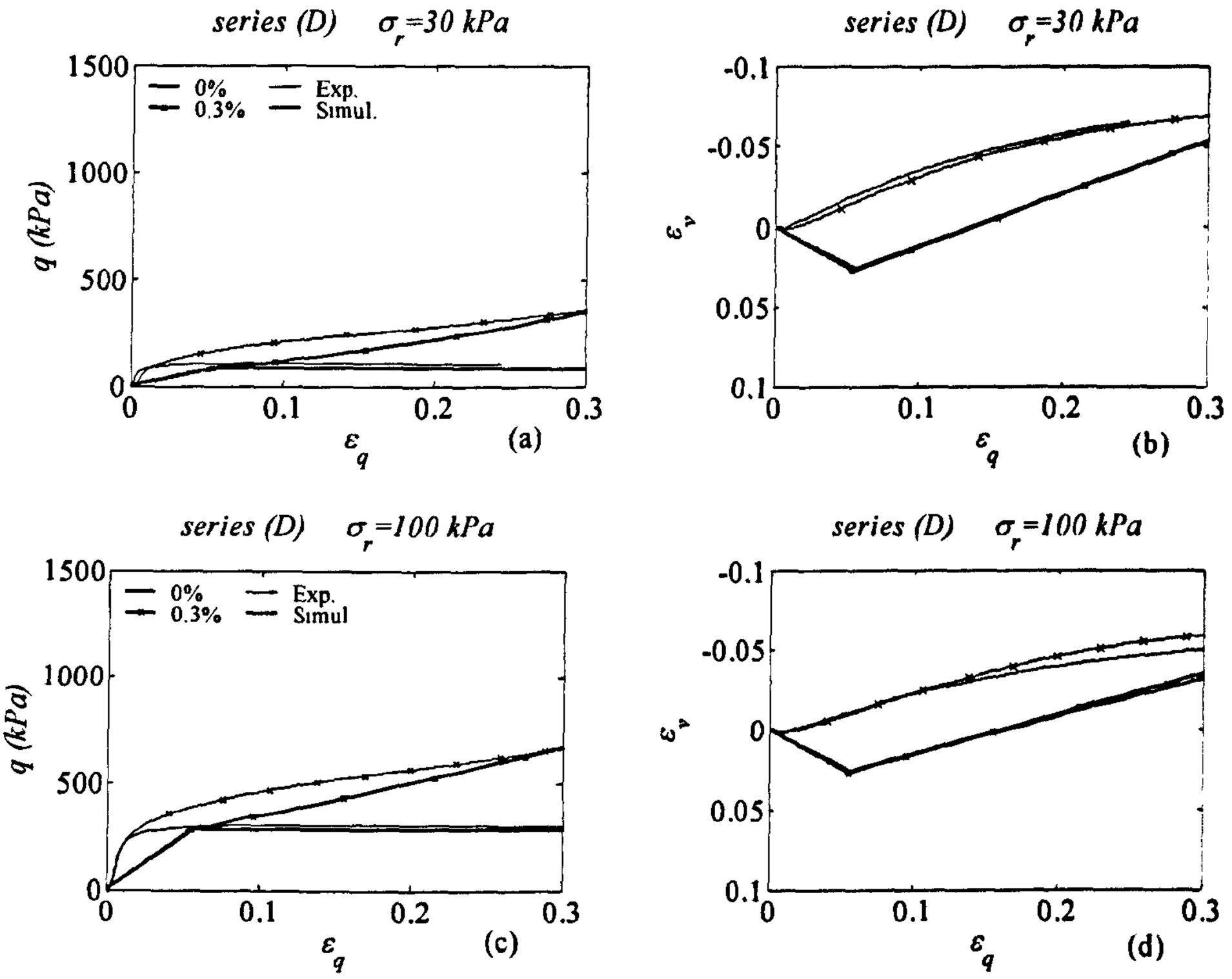

Fig. 7.9 *Compression triaxial test results and model simulations for reinforced and unreinforced specimens of (D)* test series (legend indicates the fibre content)

The volumetric behaviour is, in general, well simulated. The addition of fibres affects the deformation behaviour of the assembly of sand grains, whose movements are influenced by the physical presence of fibres. In the extension tests, the volumetric behaviour is not simulated as well as that for the compression tests because the initial plastic volumetric strains have opposite magnitude to elastic volumetric strains and this can not be reproduced adopting a simple Mohr-Coulomb model.

The difference between experimental results and model outputs is mainly due to the simplistic nature of the elastic-perfectly plastic Mohr-Coulomb model and its inability to account for the non-linearity of unreinforced sand behaviour, especially at small strains. The use of more

complex models which capture this non-linearity would result in smoother simulated curves and a better match between experimental data and simulation.

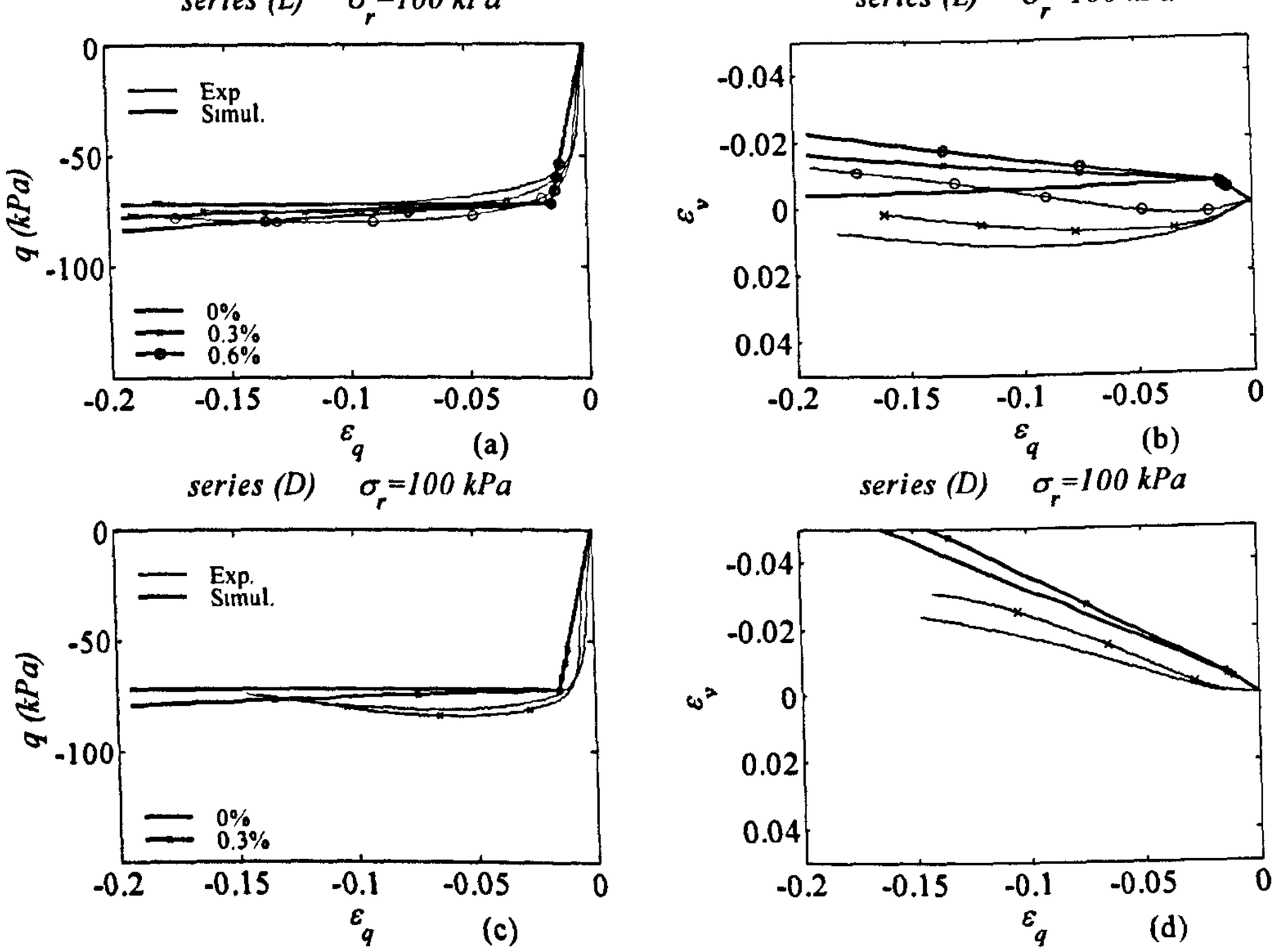

Fig. 7.10 Extension triaxial test results and model simulations for reinforced and unreinforced specimens at 100 kPa confining cell pressure (legend indicates the fibre content)

The dilatancy relationship governs the volumetric deformation of the sand matrix that in turn influences the elongation of the reinforcement within the soil. The stresses developed in the fibres are indeed greater for denser specimens which have a greater tendency to dilate. The model computes the stresses developed in the fibres from the deformation of the sand matrix, therefore the contribution of fibres is proportional to the relative density of the sand matrix as shown in the simulation in Fig. 7.11. However, fibres need strain to mobilise their strength, therefore the difference in stiffness on the initial part of the stress strains response is mainly due to the sand matrix. The adoption of a more sophisticated elastic relationship for the sand matrix

might permit the simulation of the increasing of the initial stiffness with density of the specimen.

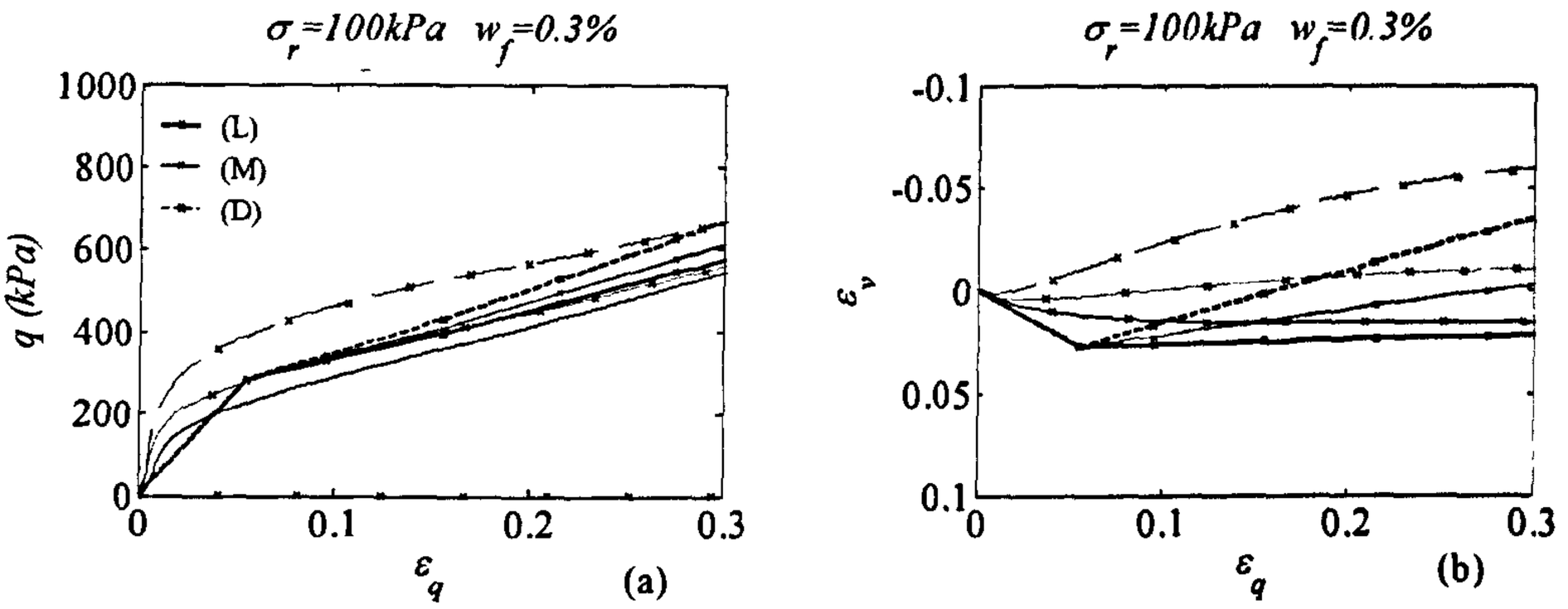

Fig. 7.11 Influence of relative density on experimental results and simulations on specimens reinforced with 0.3% of fibres and tested at 100 kPa cell confining pressure (legend indicates the fibre content)

7.5.2.3 Effect of variation of individual constitutive parameters

The simulation of fibre contribution requires the definition of three different quantities: the orientation distribution, the elastic modulus and the sliding function. The importance of assuming the correct orientation distribution is shown in Fig. 7.12 where the simulations are shown by assuming the real orientation distribution of fibres and an assumed isotropic one. The simulations have been performed for the loosest specimens confined at 100 kPa cell pressure and the experimental results are also reported as a reference. When an isotropic orientation of fibres is assumed, the performances of the specimens are underestimated in compression and overestimated in extension. In short, the adoption of a non real fibre orientation distribution may lead to a non correct estimation of the relative contribution of fibres in compression and extension.

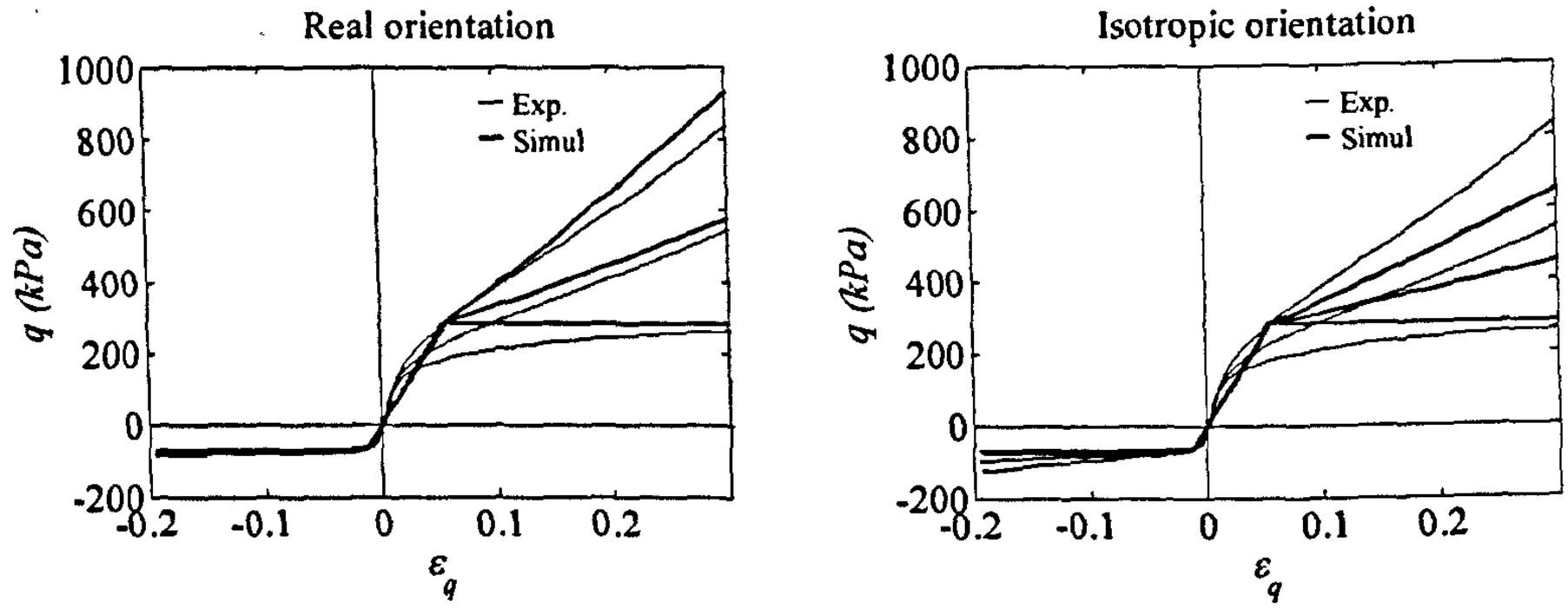

Fig. 7.12 Influence of the fibres orientation on the model simulations

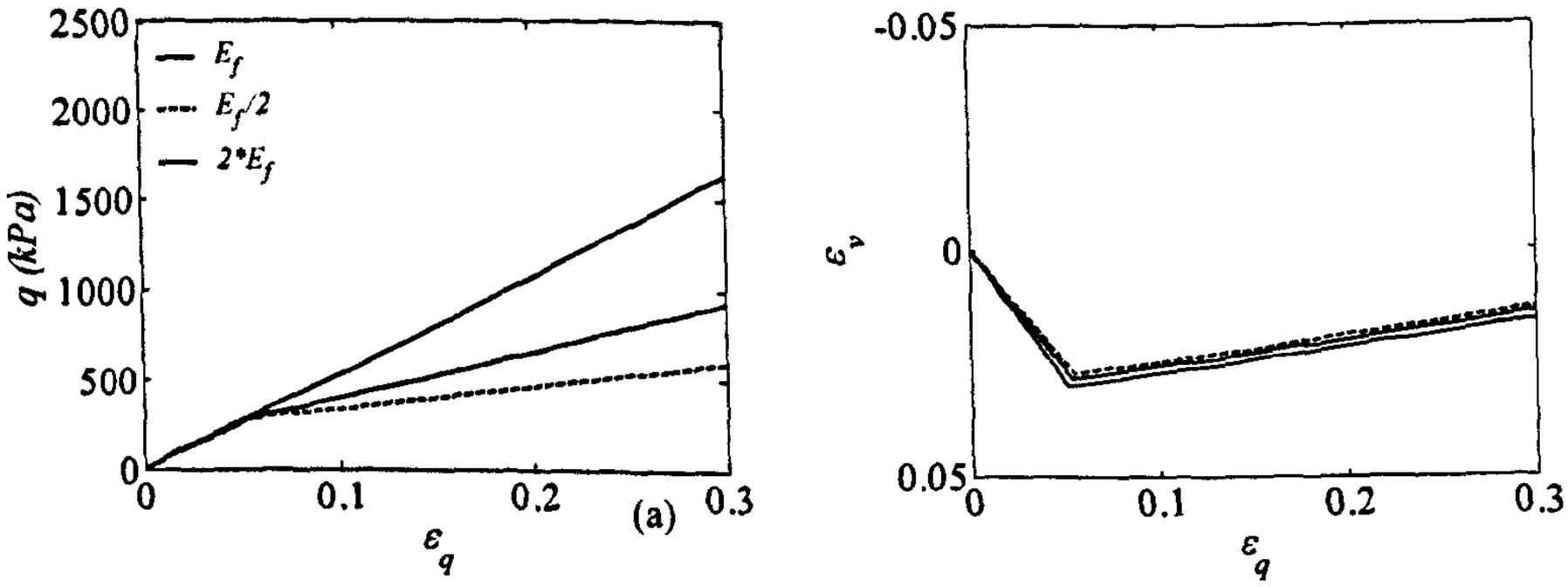

Fig. 7.13 Influence of the elastic modulus of the fibres on the model simulations

The extra confining of the sand matrix by the reinforcement is proportional to the elastic modulus and the sliding function between fibres and sand grains. The influence of the value of the elastic modulus for the fibres is shown in fig. 7.13 where the elastic modulus has been halved and doubled in respect to the selected one. The strength performances of the composite materials obviously increase with the stiffness of the fibres. On the volumetric plane, stiffer reinforcement results in a more compressive behaviour of the reinforced material. Differences in the volumetric plane are not so evident because the dilation angle of the sand matrix is adjusted in order to account for the confining pressure of the fibres and in order to have a

dilation angle of the composite equal to ψ_{max}. Differences arise in the elastic part of the volumetric trend.

The strains and the stresses developed in the fibres are dependent on the relative sliding between sand grains and fibres. The introduced sliding function can vary between 0 and 1 with f_b =1 for perfect bonding and f_b =0 for full sliding. Simulation with a perfect bonding and full sliding are reported in Fig. 7.14 together with the assumed sliding function as defined in Eq. (7.49). In full sliding condition, the stress-strain behaviour is that for an unreinforced specimen even if there are fibres while the volumetric behaviour is characterised by a less compressive behaviour if compared with an unreinforced specimens because the fibres occupy some volume and they make the sand matrix denser. When a perfect bonding is imposed, the contribution of the fibres is a maximum and the volumetric behaviour becomes more compressive. Again differences in the volumetric behaviour arise only on the elastic part, because the dilation angle of the sand is adjusted to ensure that the angle of dilatancy of the composite is ψ_{max}.

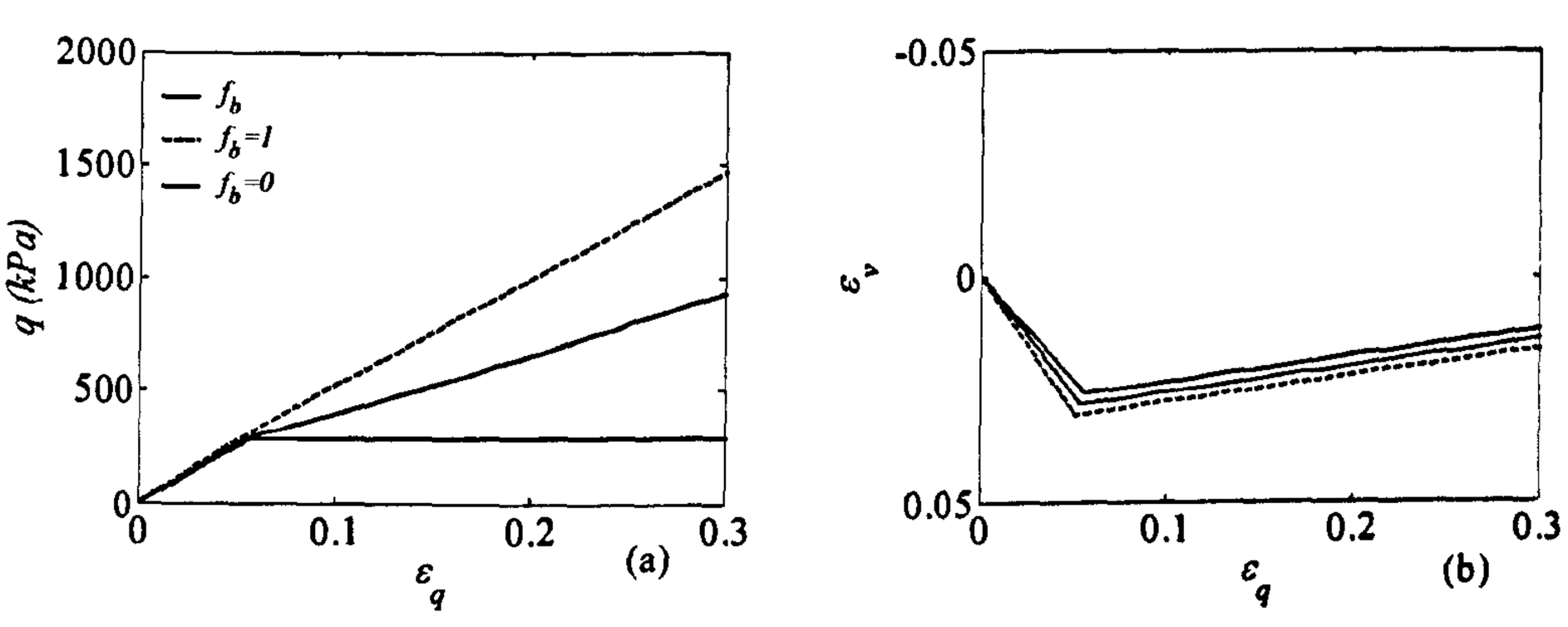

Fig. 7.14 Influence of the sliding function (f_b) between fibres and sand grains on the model simulations

The volumetric behaviour for the reinforced composite is reproduced by means of the correction to the dilatancy angle proposed in Appendix 1 in Diambra et al. (2010). If the correction is not applied the simulation of the volumetric behaviour for the reinforced specimens is not correct. Fibres produce an extra confining stresses to the sand matrix whose behaviour becomes very compressive with strains (Fig. 7.15b). The mobilization of the strength

in the fibres is obviously dependent on the deformation of the composite and the lower deviatoric strength corresponds to the more compressive behaviour (Fig. 7.15a).

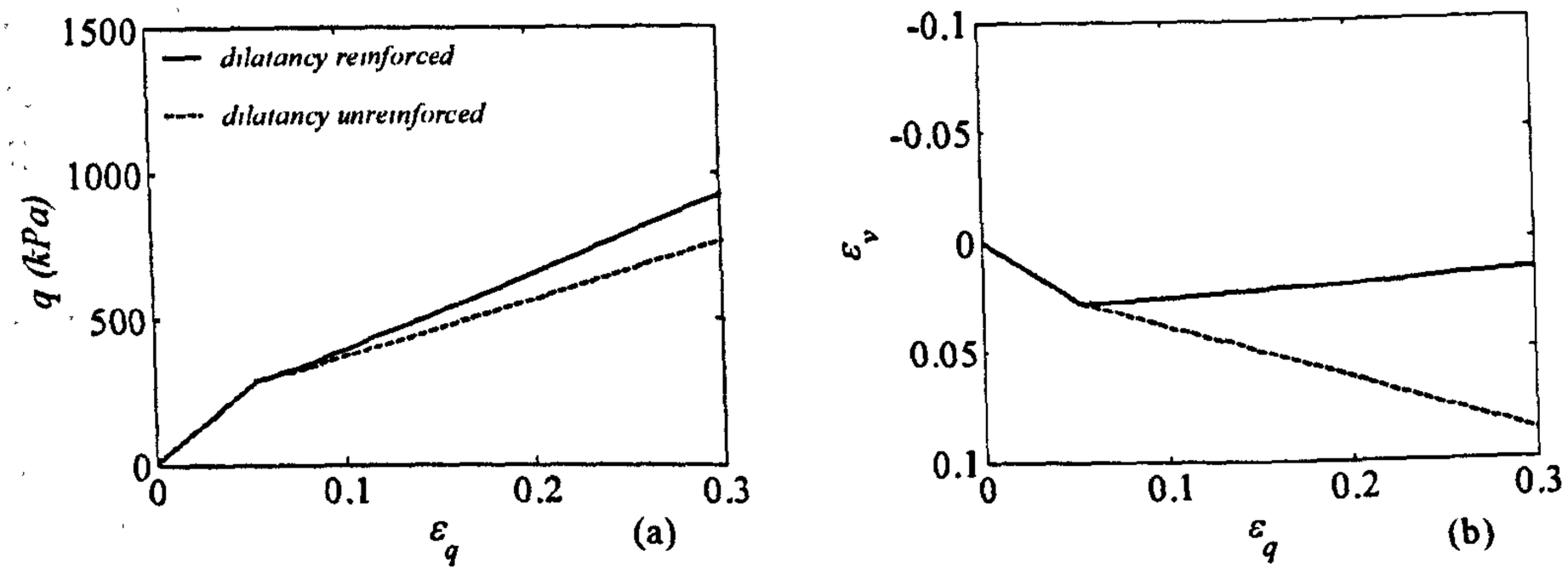

Fig. 7.15 Influence of the dilation angle on the model simulations

7.6 Application 2: Severn-Trent model for sand

It has been demonstrated that the proposed modelling framework applied with a very simple model for the sand matrix generally simulates the key characteristics of the response observed in the experimental tests. However, some discrepancies between simulation and experimental results can be attributed to the simplicity of the basic sand model adopted and this may be improved by considering more complex model developments with the capability of capturing the non-linear behaviour of materials. Also the simulation of the undrained tests requires the selection of a more complex model for the sand able to more accurately reproduce the volumetric behaviour of soils. Therefore, the modelling framework proposed in this chapter is now implemented by assuming the Severn-Trent model (Gajo and Muir Wood, 1999a) for the sand matrix. The appealing feature of the modelling framework presented here is that any constitutive model for describing the stress-strain behaviour of the sand may be used to obtain the stiffness matrix for the unreinforced sand. The Severn-Trent model has already been successfully applied for the simulation of the behaviour of Hostun sand in conventional triaxial tests (Gajo and Muir Wood, 1999a) and in the multiaxial space (Gajo and Muir Wood, 1999b ; Jafarzadeh et al. 2008)- The model will be challenged for the simulation of the behaviour of

soils reinforced with the three types of reinforcement. It will be shown that the simple introduction of minor adjustments to the interaction mechanism between fibres and sand grains results in a correct simulation of particular features on the behaviour of the composite material.

The behaviour of the soil matrix is indeed highly dependent on its relative density and this in turn depends on the voids available to the granular skeleton for deforming. The addition of fibres to the sand results in a reduction of the voids present in the specimen and therefore in a denser soil matrix which results in a more dilative behaviour of the composite material. However, the fibres may create a network within the soil matrix and they may prevent the soil skeleton from using some of the voids of the specimen (Fig. 7.1). Therefore, when a more complex model for the sand matrix like the Severn-Trent sand is adopted, more attention is required to the definition of the voids available for the sand matrix during deformation. This was not introduced when the simple elastic-perfectly plastic Mohr-Coulomb model was applied. However, the angle of dilatancy for the sand matrix was corrected in order that the dilatancy of the composite was equal to ψ_{max} and this was the account for the decreasing amount of voids available to the sand grains. The rule of mixtures as expressed in the more general case is adopted here (Eqs. 7.7 and 7.9).

7.6.1 Severn-Trent sand: the sand stiffness matrix

7.6.1.1 Basic concepts

The Severn-Trent sand model (Gajo and Muir Wood, 1999a) is developed in a critical state framework and provides a simple formulation which combines Mohr-Coulomb failure, dependence of strength and stiffness on the state parameters and a flow rule similar to that of Cam-Clay. A brief theoretical description of the model is given here but reference should be made to Gajo and Muir Wood (1999a) for further details.

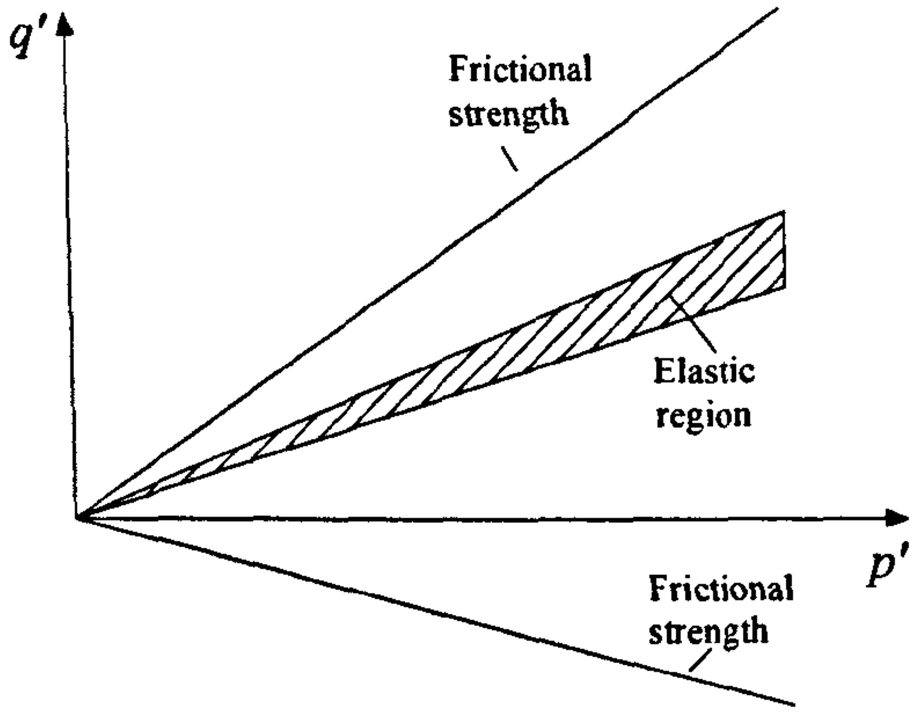

Fig. 7.16 Schematic view of the strength surface and elastic region for the Severn-Trent model (Gajo and Muir Wood, 1999a)

The model can be classified as a bounding-surface, kinematic hardening model. The strength surface is the bounding surface and it always encloses the stress state and the yield surface. In turn the stress state maybe situated within the yield surface in elastic conditions or may lie on the yield surface for elasto-plastic conditions. Both the strength and yield surfaces are wedges in the $q' \sim p'$ plane with their apexes coincident with the origin of the plane. A schematic view of the model is provided in Fig. (7.16)

The size of the current strength and yield surfaces is not constant but it is related to the size of the strength surface at the critical state through the state parameter ξ (Been and Jefferies, 1985) which is the difference between the current specific volume (v_m) and the corresponding volume at the critical state (Fig. 7.17):

$$\xi = v_m - \Gamma + \lambda \ln p' \tag{7.50}$$

The critical state line in the $v_m \sim \ln p'$ plane is a straight line, whose intercept and slope are respectively defined by Γ and λ.

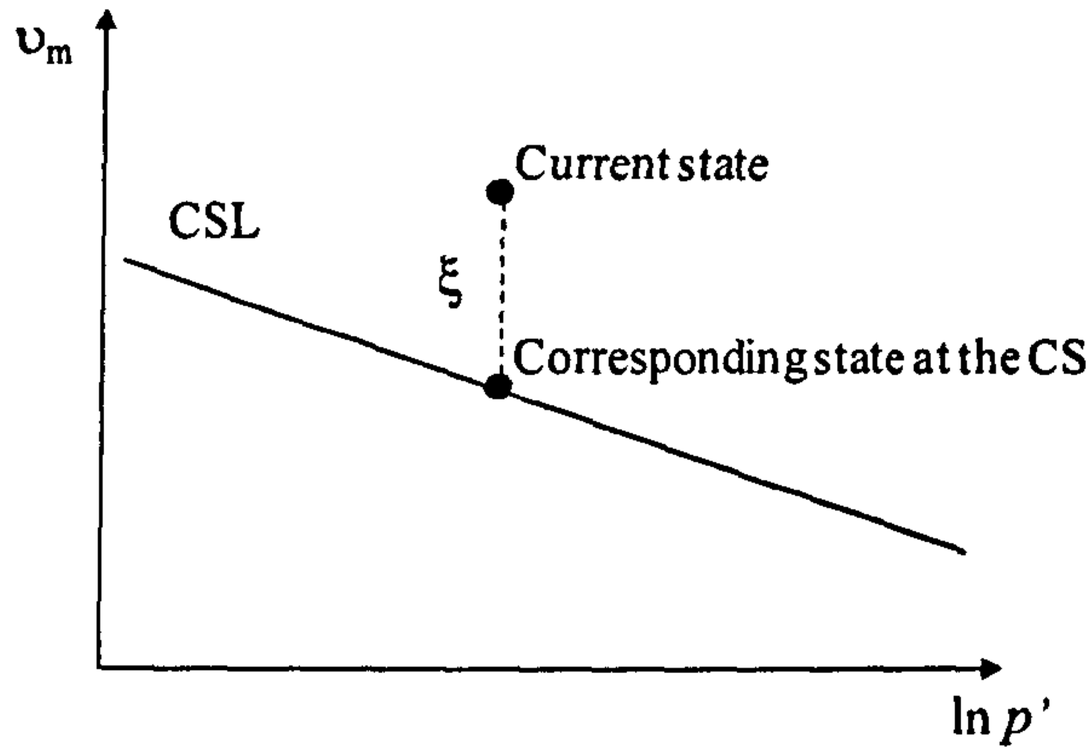

Fig. 7.17 Representation of the state parameter ξ

The angular opening of the current strength surface is related to the size of the critical state surface through the ratio r which is related to the state parameter in the following way:

$$r = 1 - k_r \xi \tag{7.51}$$

where k_r is a constitutive parameter.

The model was conveniently formulated in a "normalised" stress space in order to maintain constant the size of the strength surface. In the "normalised" stress space the deviatoric stress is divided by $r = 1 - k_r \xi$, therefore the normalised stress space is defined as $\bar{\boldsymbol{\sigma}}' = [\bar{p}', \bar{q}']^T$ where:

$$\bar{q}' = \frac{q'}{1 - k_r \xi} \quad \text{and} \quad \bar{p}' = p' \tag{7.52}$$

7.6.1.2 Strength and yield surfaces

The current strength surface or bounding surface $F(\bar{\boldsymbol{\sigma}})$ can be expressed as:

$$F(\bar{\boldsymbol{\sigma}}) = t(\bar{q}' - Mp') \tag{7.53}$$

where M represents one of two properties M_c or M_e , depending on whether triaxial compression or triaxial extension is occurring, linked to the friction angle ϕ' of the sand by the relationships(7.31) and (7.32). t distinguishes between the compression/extension approach to failure being respectively $t = +1$ and $t = -1$.

The yield or loading surface $f(\bar{\sigma})$ is subjected to a kinematic hardening which induces its rotation during loading. The direction of the surface is defined by the vector $\boldsymbol{\alpha}$ (Fig.7.18):

$$\boldsymbol{\alpha} = [\alpha_p, \alpha_q]^T \tag{7.54}$$

The expression of the yield surface is:

$$f(\bar{\sigma}) = \bar{q}'(\alpha_p - t\, n_y \alpha_q) - p'(\alpha_q - t\, n_y \alpha_p) \tag{7.55}$$

where n_y represents one of the two properties m_c or m_e, depending on whether triaxial compression or triaxial extension is occurring, linked to the friction angle ϕ_y' of yield surface of the sand by the relationships:

$$m_c = \frac{6\sin\phi_y'}{3-\sin\phi_y'} \tag{7.56}$$

$$m_e = -\frac{6\sin\phi_y'}{3+\sin\phi_y'} \tag{7.57}$$

and

$$\sin\phi_y' = R\sin\phi' \tag{7.58}$$

where R is a constitutive parameter which links the size of the yield surface to the size of the strength surface both at critical state conditions.

The unit normal vector $\mathbf{n}$, which is the normal to the yield surface and defines the direction of loading, can be computed in the "normalised" stress space::

$$\mathbf{n} = [n_p, n_q]^T \tag{7.59}$$

where

$$n_p = \frac{-\bar{\eta}}{\sqrt{1+\bar{\eta}^2}} \tag{7.60}$$

$$n_q = \frac{1}{\sqrt{1+\bar{\eta}^2}} \tag{7.61}$$

$$\bar{\eta} = \frac{\bar{q}'}{p'} \tag{7.62}$$

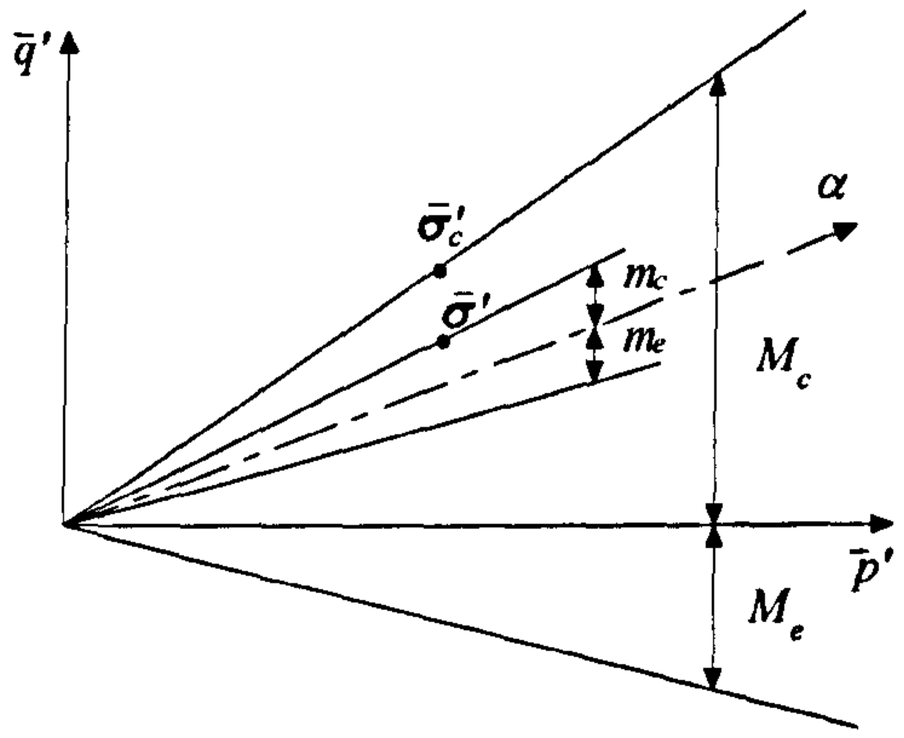

Fig. 7.18 Schematic illustration of the yield and strength surfaces of the Severn-Trent sand model in the normalised plane (Gajo and Muir Wood, 1999a)

7.6.1.3 Elasticity

Incremental elastic stresses and strains are linked through an elastic stiffness matrix $\mathbf{D}^e$:

$$\dot{\boldsymbol{\sigma}}' = [\mathbf{D}^e]\dot{\boldsymbol{\varepsilon}}_m{}^e \tag{7.63}$$

assuming isotropic elasticity:

$$\mathbf{D}^e = \begin{bmatrix} K & 0 \\ 0 & 3G \end{bmatrix} \tag{7.64}$$

where K and G are the elastic bulk and shear modulus respectively.

The elastic relationship in the normalised stress space can be computed (Gajo and Muir Wood, 1999a):

$$\dot{\bar{\boldsymbol{\sigma}}}' = [\bar{\mathbf{D}}^e]\dot{\boldsymbol{\varepsilon}}_m{}^e \tag{7.65}$$

where

$$\overline{\mathbf{D}}^e = \begin{Bmatrix} \dfrac{1}{1-k\xi} & \left[\dfrac{k\lambda q}{(1-k\xi)^2 p}\right] \\ 0 & 1 \end{Bmatrix} \mathbf{D}^e - \begin{bmatrix} 0 & \dfrac{kq\upsilon}{(1-k\xi)^2} \\ 0 & 0 \end{bmatrix} \tag{7.66}$$

7.6.1.4 Flow rule

The flow rule that is adopted is a modification of the one for the original Cam-Clay model (Roscoe and Schofield, 1963). The ratio between the plastic volumetric and deviatoric strain increments is defined as:

$$d = \frac{\dot{\varepsilon}_{mv}}{\dot{\varepsilon}_{mq}} = A\left[M_C(1+k_d\xi) - \eta\right] \tag{7.67}$$

Where A and k_d are two constitutive parameters. It can be noticed that if A=1 and k_d =0, the flow rule of the original Cam-Clay model is recovered. Even if the function of the plastic potential is not explicitly defined, the unit normal vector of the plastic flow can be derived as:

$$\mathbf{m} = [m_p, m_q]^T \tag{7.68}$$

where

$$m_p = \frac{d}{\sqrt{1+d^2}} \tag{7.69}$$

$$m_q = \frac{1}{\sqrt{1+d^2}} \tag{7.70}$$

7.6.1.5 Hardening rule

The hardening parameter H, which governs the hardening rule, is defined as:

$$H = \frac{b^2}{Bb_{\max}} \tag{7.71}$$

where B is a constitutive parameter, b depends on the distance between the actual stress state $(\bar{q}')$ and its image on the bounding $(\bar{q}_c')$ surface defined in the normalised space:

$$b = n_q(\bar{q}'_c - \bar{q}') \tag{7.72}$$

and b_{max} is the maximum possible value of b in the normalised stress space:

$$b_{\max} = n_q\left[\left(M_c - M_e\right) - \left(m_c - m_e\right)\right]p' \tag{7.73}$$

The vector of plastic strain increments is related to the normalised stress by:

$$\dot{\boldsymbol{\varepsilon}}_m{}^p = \frac{1}{H}\mathbf{m}\mathbf{n}^T\dot{\overline{\boldsymbol{\sigma}}} \tag{7.74}$$

7.6.1.6 Stress-strain relationships

The elastic-plastic constitutive relationships in the normalised stress space take the form of:

$$\dot{\overline{\boldsymbol{\sigma}}}_m = \left[\overline{\mathbf{D}}^e - \frac{\overline{\mathbf{D}}^e\mathbf{m}^*\mathbf{n}^T\overline{\mathbf{D}}^e}{H + \mathbf{n}^T\overline{\mathbf{D}}^e\mathbf{m}^*}\right]\dot{\boldsymbol{\varepsilon}}_m \tag{7.75}$$

Where $\mathbf{m}^*$ represents the unit normal vector of the plastic flow in the normalised stress space and is related to $\mathbf{m}$ by:

$$\mathbf{m}^* = \mathbf{m} + \overline{\mathbf{D}}^{e-1}\begin{bmatrix} 0 & kq\upsilon/(1-k\xi)^2 \\ 0 & 0 \end{bmatrix}\mathbf{m} \tag{7.76}$$

Once the normalised stress state $(\overline{\boldsymbol{\sigma}})$ has been calculated through Eq. (7.76), the true stress state $(\boldsymbol{\sigma})$ can be subsequently determined by adopting Eq. (7.52).

7.6.2 Model calibration for reinforcement type (1)

This more sophisticated model will be challenged for simulating the behaviour of specimens reinforced with the three types of fibres used in the experimental investigation in both drained and undrained conditions. The superposition of the effects of the sand and reinforcement for determining the performances of the composite allows the separate calibration of the parameters governing each constituent. The input parameters for the sand matrix are calibrated to obtain a good fit with the experimental results on unreinforced specimens.

7.6.2.1 Input parameters for the sand matrix

The Severn-Trent sand requires two parameters to describe the elastic behaviour and eight parameters for defining the plastic behaviour of the soil. The elastic behaviour has been determined by defining the parameters κ which is the slope of the line describing the elastic loading or unloading in the $v_m \sim \ln p'$ plane and the Poisson's ratio v and they are listed in Tab. 7.1. Although most elasto-plastic sand models calculated the elastic strain increment by using a bulk modulus K which is a power function of the mean effective stress p', for simplicity the present model assumes the bulk modulus to be proportional to the mean effective pressure p' (Bardet, 1986):

$$K = \frac{v_m p'}{\kappa} \tag{7.77}$$

$$G = \frac{3(1-2\nu)}{2(1+\nu)} K \tag{7.78}$$

The parameters needed for describing the plastic behaviour of the sand are reported in Tab. 7.1 together with a description of their meaning. They have been calibrated according to the experimental results and considering values consistent with a review of the literature.

Tab. 7.1 Values of soil parameters for Hostun sand

Parameter	Description	Value
κ	Slope of the elastic loading –unloading line on the v_m- ln p' plane	0.01
ν	Poisson' s ratio	0.1
φ'	Critical-state friction angle	36°
Γ	Intercept for critical-state line on v_m- ln p' plane at p'=1 kPa	2.08
λ	Slope of the critical-state line on v_m- ln p' plane	0.031
k_r	Link between changes in state parameter and current strength	1.5
B	Parameter controlling hyperbolic stiffness relationship	0.0025
R	Ratio of size of yield and strength surfaces	0.1
A	Multiplier in flow rule	0.75
k_d	State parameter contribution in flow rule	1.5

7.6.2.2 Input parameters for fibre type (1)

The definition of the fibres behaviour requires the calibration of four different quantities:

- the elastic modulus of the fibres;
- the orientation distribution of the fibres;
- the sliding function to define the strain in the fibres according to the strain in the composite;
- the voids "attached" to the fibres and their evolution during loading.

The same parameters as in paragraph 7.5.2.1 have been chosen to describe the stiffness of the fibres (E_f) and their orientation ($\rho(\theta)$). The sliding function (f_b) was chosen to have the same form as Eq. (7.48) but slightly different values of the parameters K_e=0.5 and c_s=0.75 have been calibrated compared with the previous application of the modelling framework. This is due to the different assumption for the volumetric fractions of the constituents which now account for the voids "belonging" to the fibre fraction.

The characteristics of the deformable behaviour of the fibre agglomerate are unknown and its accurate simulation is beyond the scope of this research. However, a general relationship describing the evolution of the deformation of the fibre agglomerate during loading is needed in order to estimate the initial void ratio of the fibres and its evolution during the tests. Information on the voids "attached" to the fibres and their evolution may be obtained by a back analysis of the experimental results on reinforced specimens. If it is considered that the sand matrix will approach a critical state during loading, this will happen both in the q'-p' and in the $v_m \sim \ln p'$ plane. The stresses of the sand matrix may be back calculated by separating the contribution of the fibres as performed to calibrate the sliding function. At first it can be considered that all the voids are "attached" to the sand particles and the difference between the critical state and the experimental point at critical state (Δv) is due to the voids "*stolen*" by the fibres (V_{vf})(Fig.7.19a). The sand matrix is considered at critical state when the volumetric behaviour of the composite start to recompress. The relationship between Δv_m and V_{vf} is the following:

$$V_{vf} = V_s \cdot \Delta\upsilon_m \tag{7.79}$$

The resulting specific volume of the fibres (υ_f) can then be linked to the external mean isotropic pressure as shown in Fig.7.19b. It should be remarked that a small error in the determination of the void ratio of the specimen may lead to a quite considerable error on the determination of the voids attached to the fibres. This is due to the very small volume of fibres compared to the volume of the sand used in the reinforced specimen. Also the procedure has the first approximation of considering the deformation of the sand equal to the one of the sand matrix, while the deformation characteristic of the composite are the sum of the deformations in the sand and the deformations in the fibres. For example, the sand may dilate while the fibres are compressing and the total volumetric strains of the composite may be zero. Therefore the procedure has been used to estimate the order of magnitude of the voids "attached" to the fibres and the shape of its evolution with the external applied stress. A trial and error procedure has been finally applied to calibrate and to choose the function of the evolution of the voids in the fibres. The chosen evolution law is of the form:

$$\upsilon_f = \upsilon_{f\min} + \frac{\upsilon_{\Delta f}}{k_\upsilon\left(p^* / p_{ref}\right)+1} \tag{7.80}$$

where $\upsilon_{f\min}$, $\upsilon_{\Delta f}$ and k_υ are three constants respectively defining the value of the minimum specific volume (for $p_c \to \infty$), the difference between the minimum and the maximum specific volume (the maximum specific volume is $\upsilon_{f\min} + \upsilon_{\Delta f}$ obtained when $p_c = 0$) and the curvature of the curve. The values selected here are reported in Tab.7.2. p_{ref} is taken here as 0.1 MPa. The use of such a formulation (Eq. 7.80) is in accord with the assumption that fibres do not offer resistance to bending or compression, therefore their contribution towards the reduction in volume has been considered negligible. For the sake of simplicity an isotropic deformation of the fibre agglomerate has been assumed in this research ($\varepsilon_{qf} = 0$). A summary of the quantities calibrated for the contribution of fibres is given in Tab.7.2.

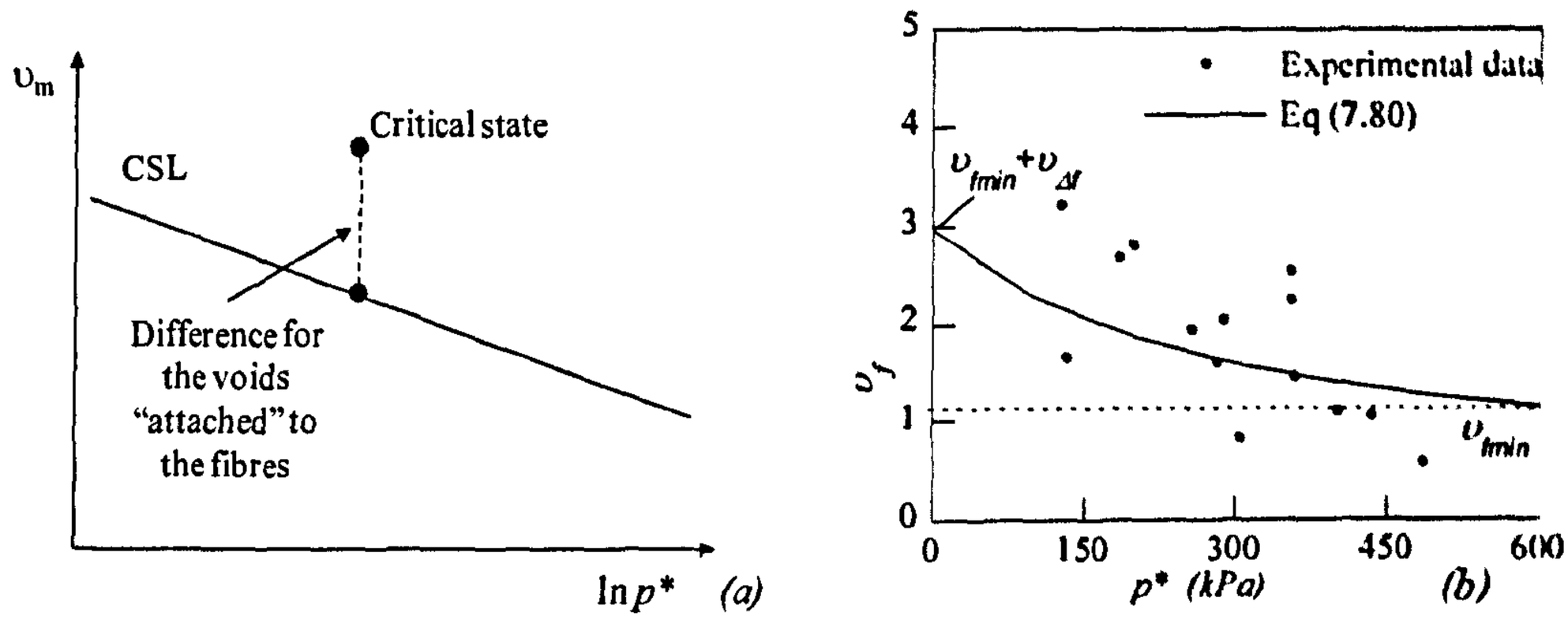

Fig. 7.19 *(a)* Approximate estimation of the voids "attached" to the fibres, *(b)* representation of Eq (7.80) on the $\upsilon_f - p^*$ plane compared with the back calculated data from experiments

Tab. 7.2 Parameters adopted for the fibres agglomerate

Parameter	Description	Value
E_f	Elastic modulus	900 Mpa
$\rho(\theta)$	Fibre orientation distribution	$\rho(\theta) = \overline{\rho}\,\frac{2ab^2\lvert\cos(\theta)\rvert}{\cos(\theta)^2(b^2-a^2)+a^2}$ $a = 1.095 \quad b = 0.449$
f_b	Sliding function	$f_b = K_s\left(1-\exp\left(-c_s\cdot\frac{p^*}{p_{ref}}\right)\right)$ $K_s = 0.5 \quad c_s = 0.75$
υ_f	Specific volume of the fibres	$\upsilon_f = \upsilon_{f\,min}+\frac{\upsilon_N}{k_\upsilon\left(p^*/p_{ref}\right)+1}$ $\upsilon_{f\,min} = 1.3 \;\; \upsilon_{\Delta f} = 2.68 \quad k_\upsilon = 0.36$

7.6.2.3 Simulation of drained tests

Typical simulations of the drained compression tests are shown in Fig. 7.20 - 7.22 in the $q \sim \varepsilon_q$ and $\varepsilon_v \sim \varepsilon_q$ planes where the tests are grouped according to the nominal density and confining cell pressure. Some discrepancies in the simulation of the behaviour of the unreinforced specimens are due to the constant friction angle selected for the sand matrix: the results from the experimental campaign showed that the angle of friction can vary between 33° and 39° depending on the stress level while a constant value of 35° was selected for the model simulation. The general comments on the simulation of the experimental results are very similar to those discussed in paragraph 7.5.2.2, therefore the attention will be addressed here only towards the improvement gained with the application of a more complex model for the sand.

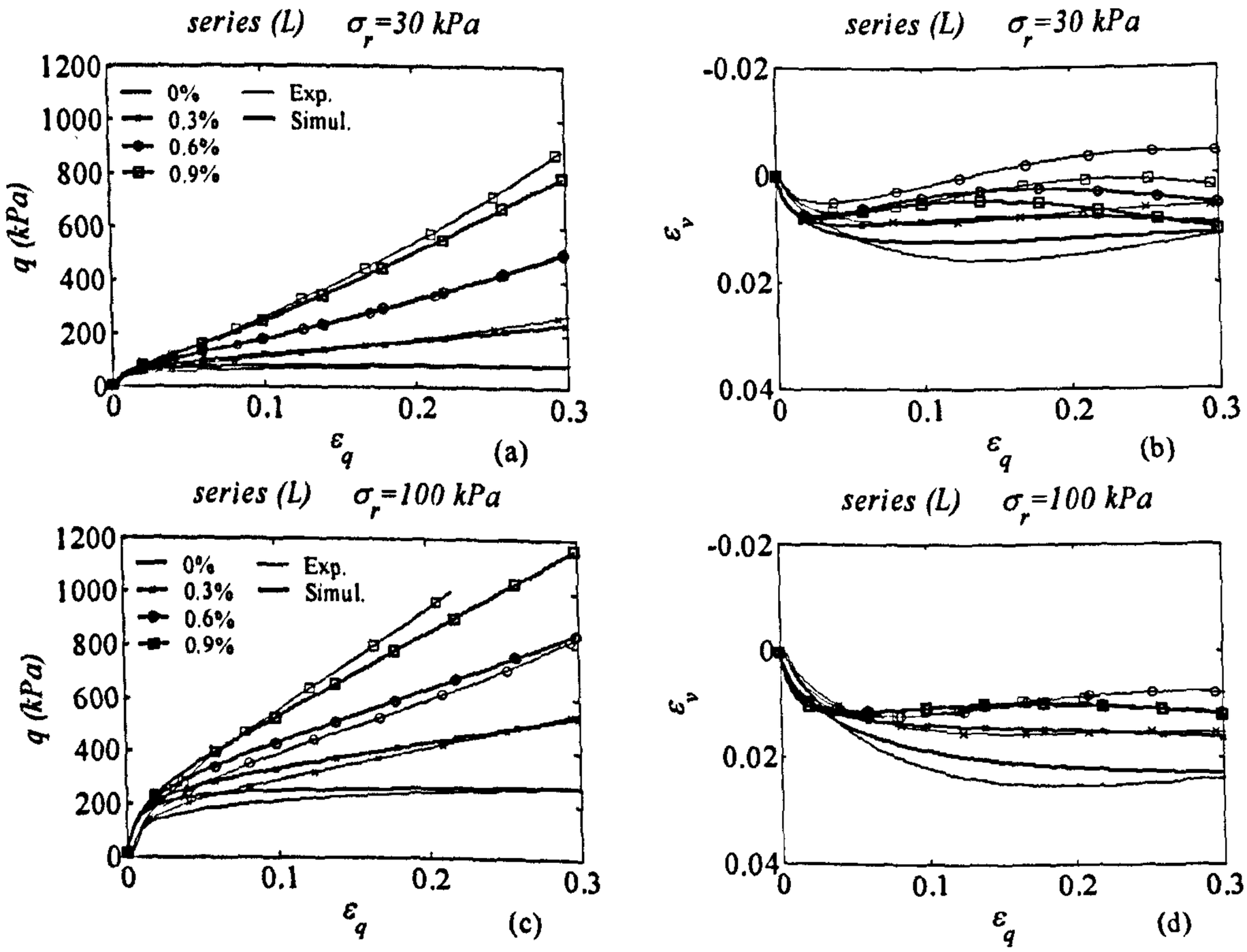

Fig. 7.20 Compression triaxial test results and model simulations for reinforced and unreinforced specimens of *(L)* test series (legend indicates the fibre content)

The use of an elastic-hardening plastic model enables the non-linearity of the deviatoric response to be reproduced and a more accurate simulation of the behaviour at low strains to be obtained. However, the more consistent improvement is achieved in the simulation of the volumetric trend. The assignment of some of the voids to the fibre agglomerate renders the sand matrix much denser resulting in a more dilative behaviour of the matrix. This more dilative behaviour initially contrasts with the effect of the extra confining pressure provided by the fibres and the compression of the voids attributed to the fibre agglomerate. At large strains, the simultaneous increase of the stresses in the fibres and the diminishing of the tendency of the sand matrix to dilate result in a predominance of the confining effect provided by the fibres. The volumetric trend for reinforced specimens reaches a constant value before the one for unreinforced specimen and this is well captured by the model. For some tests on loose reinforced specimens, a recompression at large strains is detectable and this is also predicted by the model. The sand matrix approaches its critical state line and, because of the increase of mean pressure on the matrix, undergoes a recompression following the critical state line.

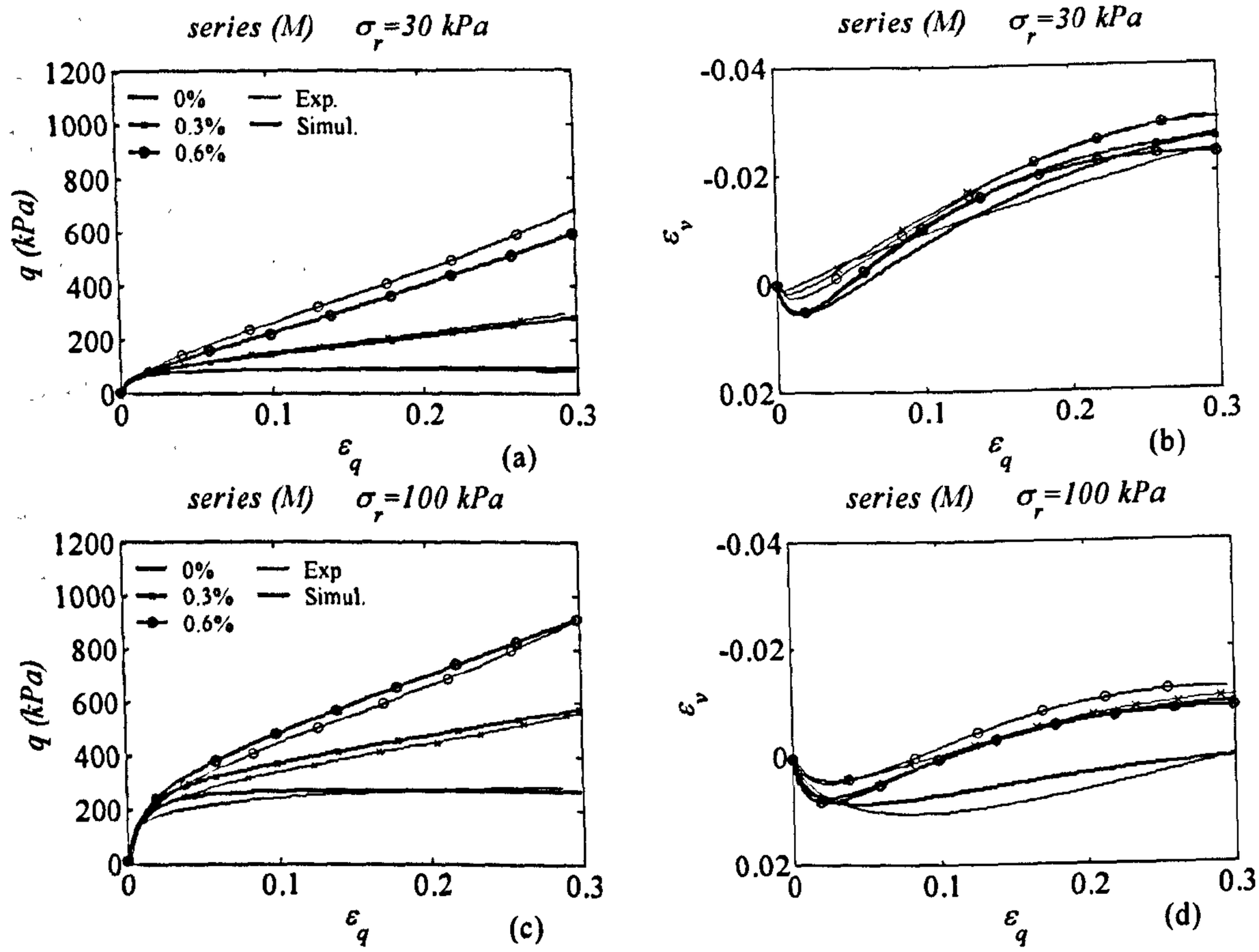

Fig. 7.21 Compression triaxial test results and model simulations for reinforced and unreinforced specimens of *(M)* test series (legend indicates the fibre content)

Figs. 7.23 – 7.24 show typical simulation of experimental results in extensive loading for unreinforced and reinforced specimens in the $q \sim \varepsilon_q$ and $\varepsilon_v \sim \varepsilon_q$ planes. A range of fibre contents is shown for a cell confining pressure of 100 kPa for respectively series *(L)* and *(D)* tests.

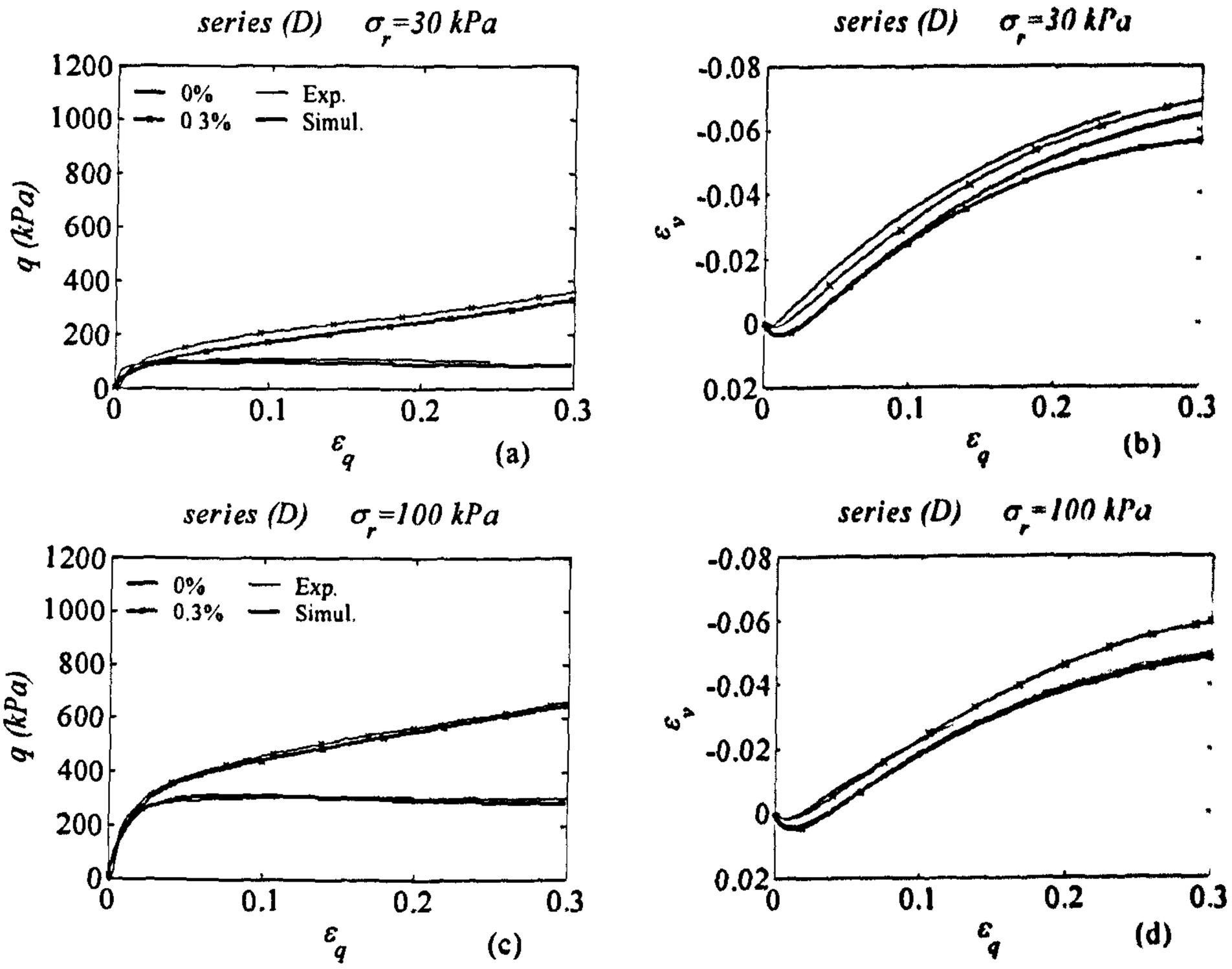

Fig. 7.22 Compression triaxial test results and model simulations for reinforced and unreinforced specimens of *(D)* test series (legend indicates the fibre content)

The poor contribution of fibres for extensive loading is well simulated. The limited strength increase for reinforced specimens is the summation of the dual contribution of the extra confining effect of the fibres and their densifying effect on the sand matrix. The selection of a more sophisticated model for the sand matrix enables the correct prediction of the volumetric trend which was not correctly reproduced in the modelling with the Mohr-Coulomb model. Even though the fibres barely affect the strength of the composite material, their influence on the volumetric behaviour is remarkable.

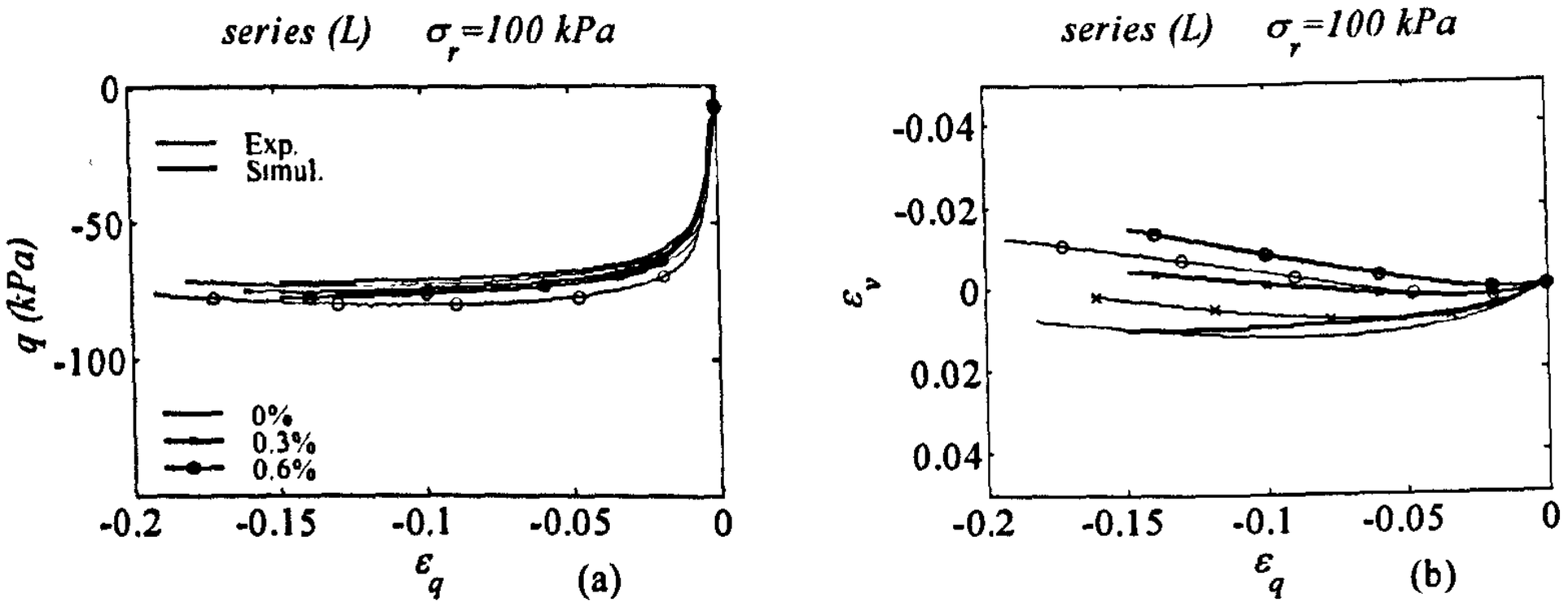

Fig. 7.23 Extension triaxial test results and model simulations for reinforced and unreinforced specimens of *(L)* test series (legend indicates the fibre content)

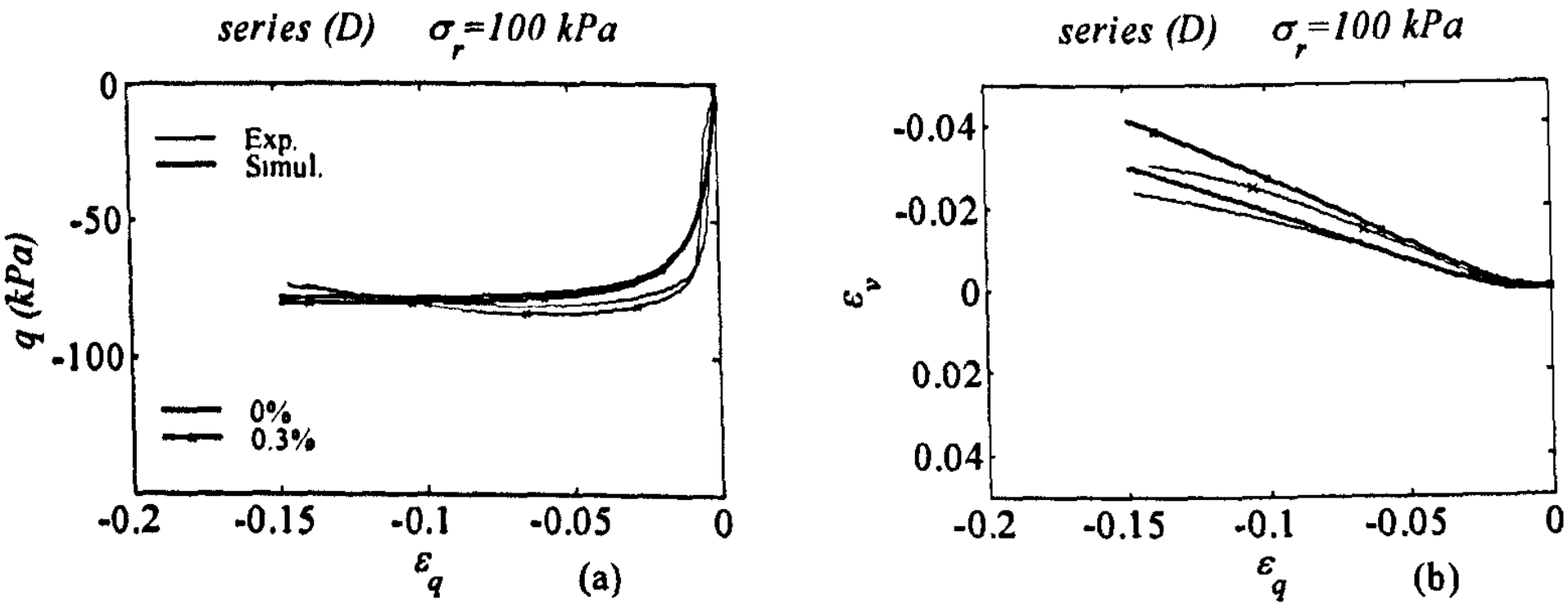

Fig. 7.24 Extension triaxial test results and model simulations for reinforced and unreinforced specimens of *(D)* test series (legend indicates the fibre content)

The employment of a hardening model for the sand matrix permits the reproduction of density dependent behaviour of the sand matrix and it results in a better simulation of the deviatoric response of the reinforced composite. The variation of the density of the specimen influences not only the stresses developed in the fibres but also the response of the sand matrix itself and this enables a more accurate simulation of the increase in strength at low to medium strains for denser specimens as shown in Fig. 7.25.

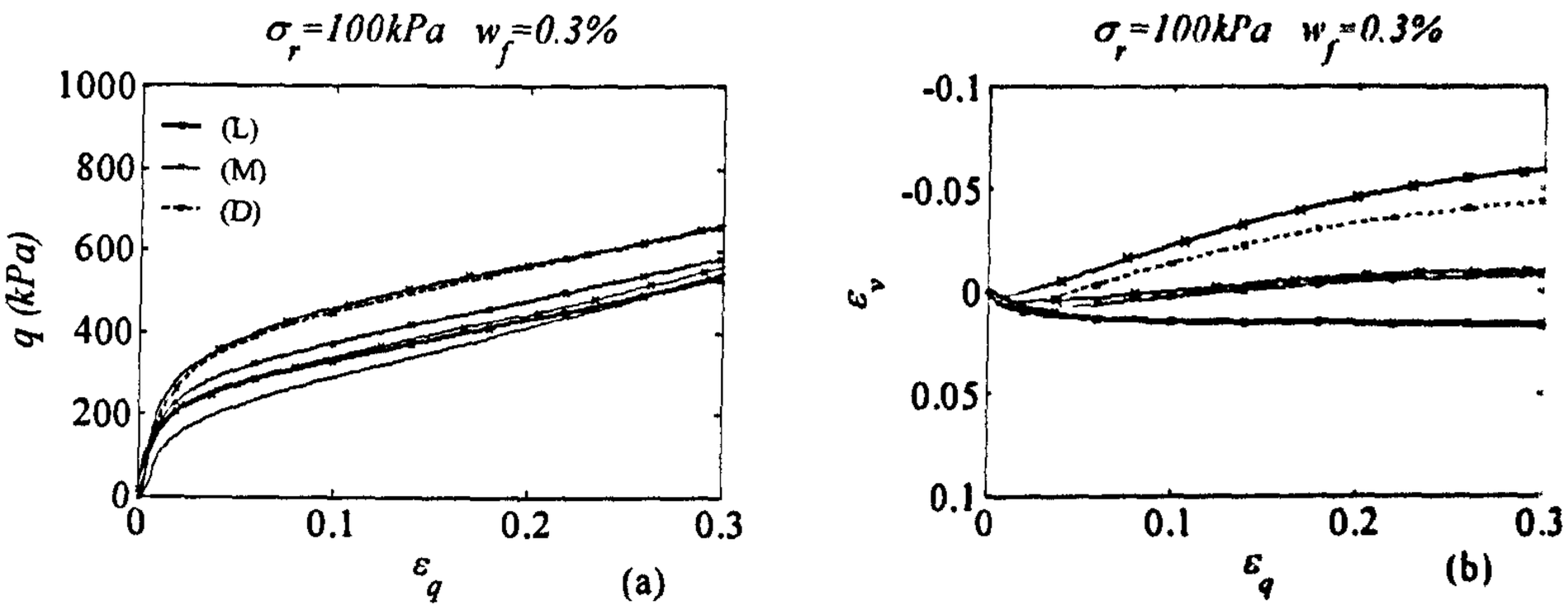

Fig. 7.25 Effect of relative density on the simulation of reinforced sand behaviour. Legend indicates the nominal density of the specimen

7.6.2.4 Influence of individual parameters on the drained behaviour

The importance of accounting for the real fibre orientation in this application of the modelling framework using Severn-Trent sand is shown in Fig.7.26. Experimental results and simulations are compared for the loosest specimen reinforced with 0.3% and 0,6% fibre content and tested at 100 kPa cell confining pressure. If an isotropic distribution is adopted, the contribution of fibres is underestimated in compression and overestimated in extension. Simulations may be improved either for compression or extension by modifying the sliding function in order to respectively enhance or damage the bonding between fibre and sand grains. However a better simulation in compression would lead to a worse simulation in extension and vice versa. The adoption of an isotropic orientation for the fibres impedes the correct prediction of the relative contribution of fibres in respect to the loading condition.

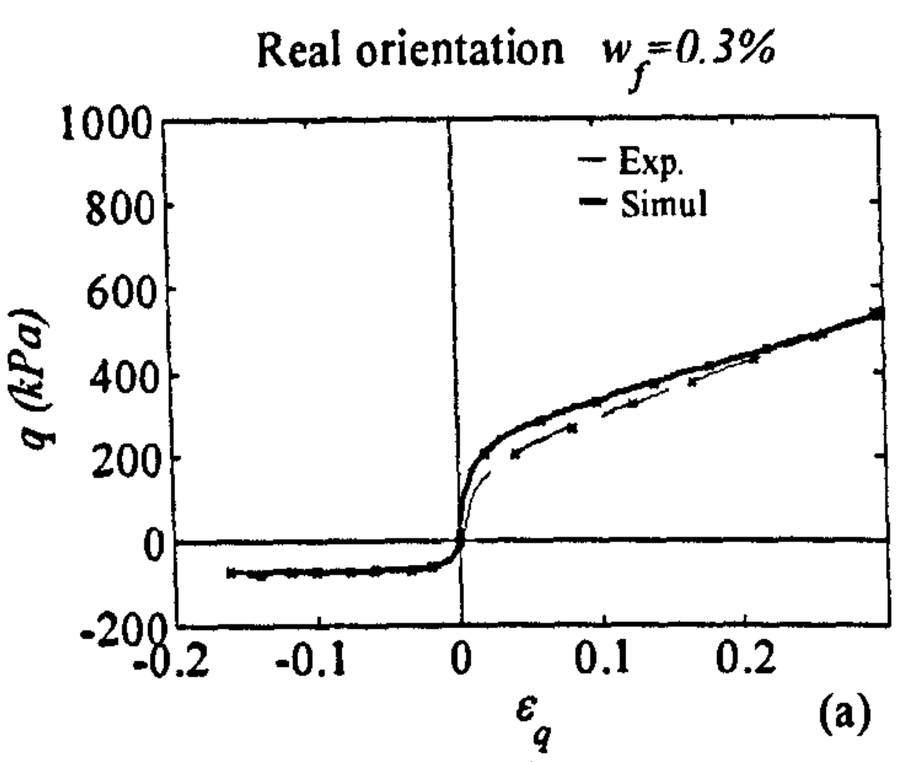

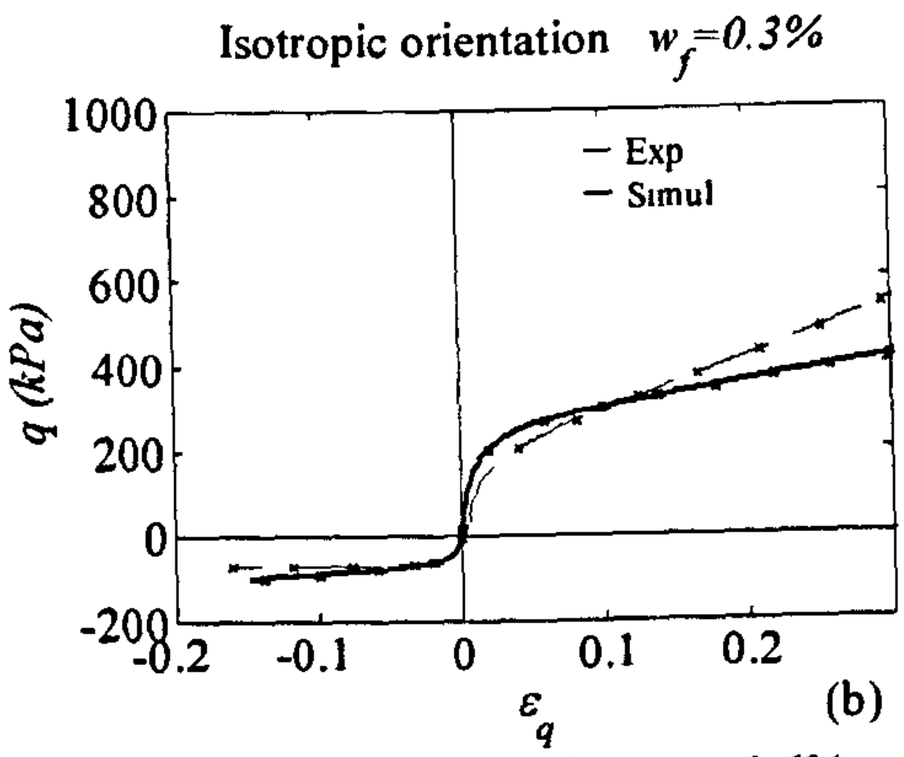

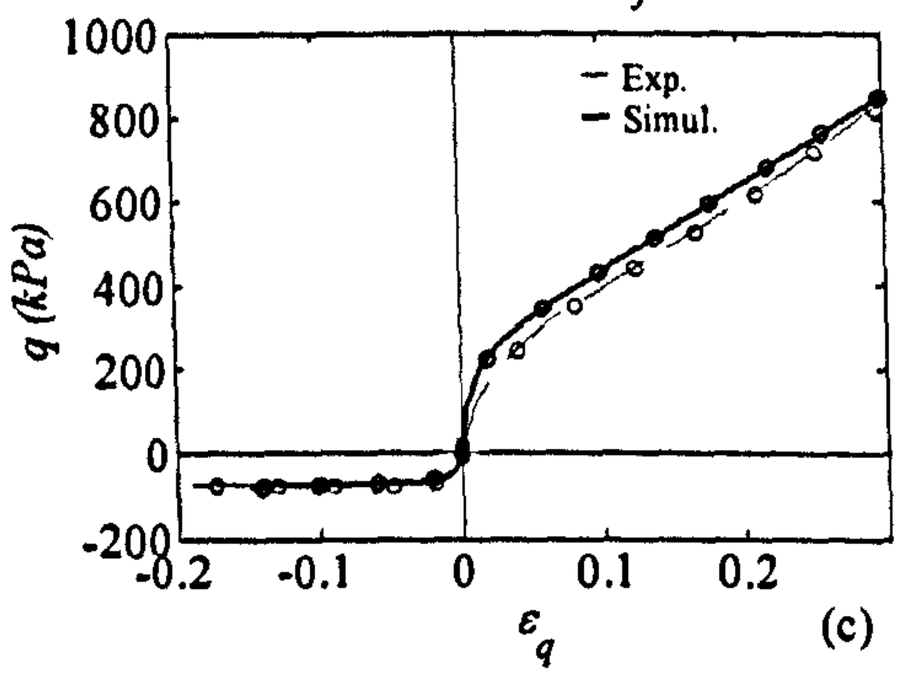

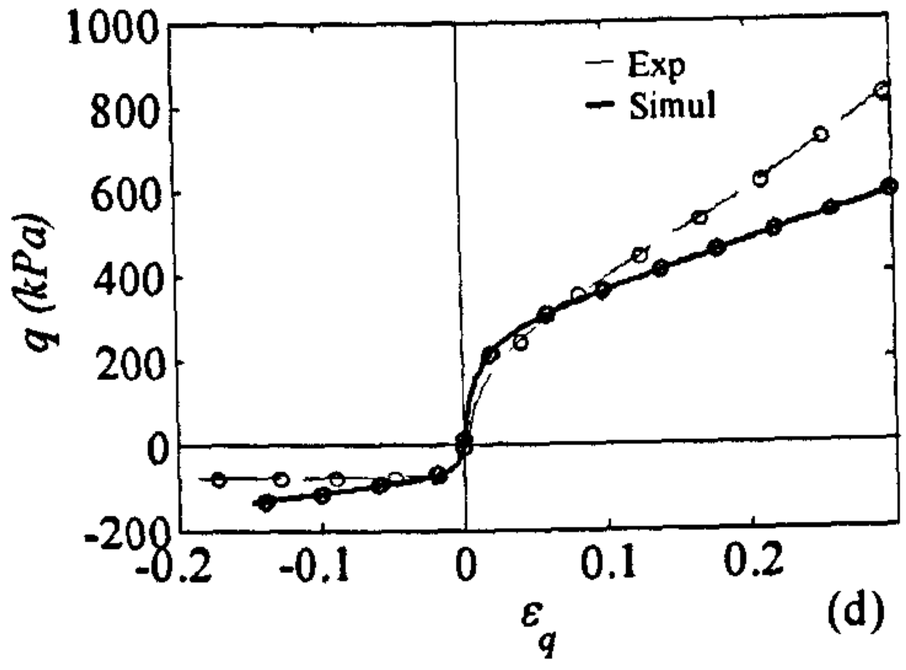

Fig. 7.26 (a) and (c) comparison between experiments and simulation considering the real fibre orientation for respectively 0.3% and 0.6% fibre content, (b) and (d) comparison between experiments and simulation considering isotropic fibre orientation for respectively 0.3% and 0.6% fibre content

For the more general case, it has been considered that fibres may prevent the sand matrix from using some of the voids during deformation. This results in a denser matrix whose tendency to dilate when sheared is increased. The increased desire to dilate is important to counterbalance the compression deriving from the extra confining pressure provided by the fibres. Fig. 7.27 compares the experimental results with simulations considering that all the voids are shared between sand and fibres or that all the voids are available to the sand for deforming. The volumetric behaviour is the most affected by this assumption (Fig 7.27 b and d) and when all the voids are "attached" to the sand the behaviour of the specimen becomes compressive without any tendency for dilation. The assumption has a lower influence on the stress-strain response (Fig 7.26 a and d) where a softer behaviour is recognised for the more compressive specimen. A more dilative behaviour of the specimen corresponds with a greater mobilisation of the stresses in the fibres.

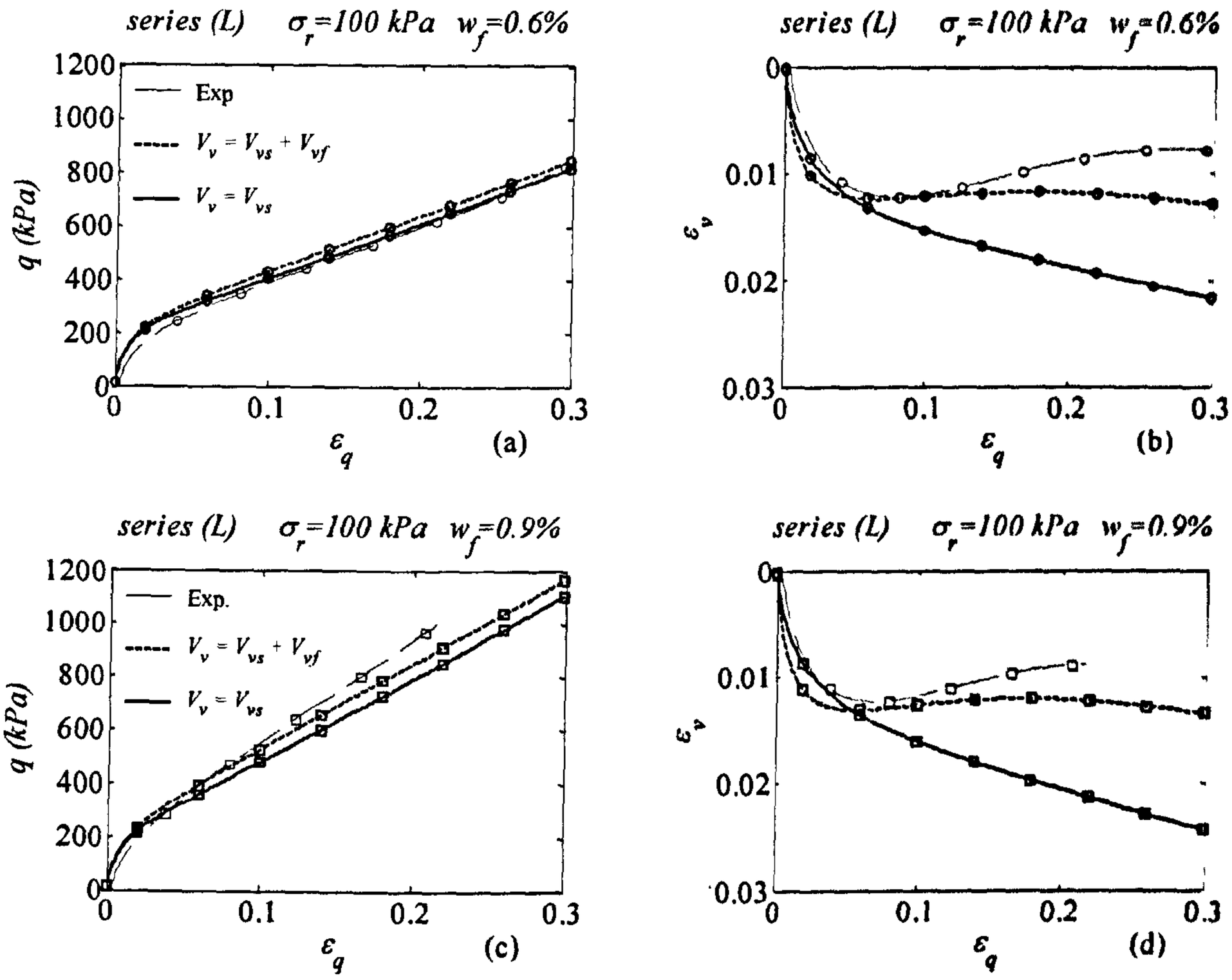

Fig. 7.27 Comparison between experiments and simulation for 0.6% and 0.9% fibre content on the ((a) and (c)) deviatoric plane and((b) and (d)) on the volumetric plane - Thin line represent the experimental value, the thick dashed lines represent simulation by allocating some voids to sand and some to fibres, while thick continuous line represents simulation by attaching all the voids to the sand

7.6.2.5 Simulation of undrained tests

Figs. 7.28 - 7.30 show the comparison between the model simulations and the experimental observation obtained in undrained compression tests on unreinforced and reinforced specimens. The tests are grouped according to the cell confining pressure and a range of fibre contents is shown in each plot. Trends are represented in the $q^* \sim \varepsilon_q$ plane, in the $q^* \sim p^*$ plane with a large scale to highlight the behaviour at small-medium strains, in the $u \sim \varepsilon_q$ plane and again in the $q^* \sim p^*$ in a smaller scale to show the general behaviour of the composite.

The undrained simulations have been obtained by applying the constraint that the volumetric deformation for each constituent to remain constant during loading; this is a simplification that

may not be correct as one of the two media may compress while the other dilates and the total volume of the specimen may remain constant. The influence of this assumptions and its relevance on the simulation of the composite behaviour will be explore in section 7.6.2.6.

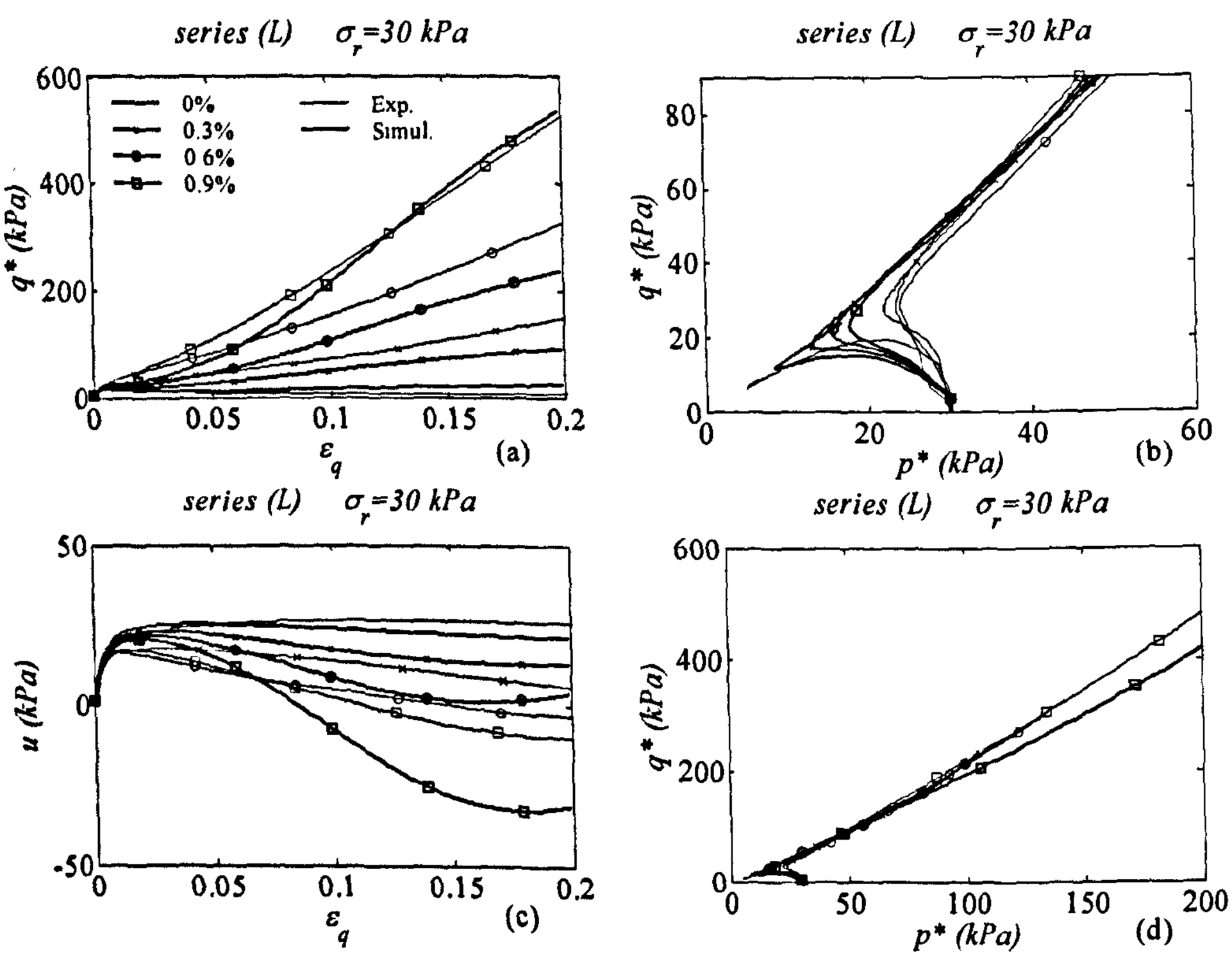

Fig. 7.28 Simulation of experimental undrained tests results on *(L)* series specimens tested at 30 kPa cell confining pressure (legend indicates fibres content)

The increase of the peak and residual deviatoric strength with the fibre content is generally well reproduced. When fibres are added to the specimens, the behaviour switches from a liquefiable to a hardening behaviour. The assignment of some voids to the fibre agglomerate renders the sand matrix denser allowing the simulation of this feature. The trend of the pore pressure with strains according to the fibre content is generally captured. However, the simulations show a stiff increase of the pore pressure with a maximum value that is reached at lower strains than in the experiment. This leads to an overestimation of the maximum pore pressure for the reinforced specimens and to softer deviatoric strength between about 2% to 10% deviatoric

strain. In the $q^* \sim p^*$ plane this becomes a delayed transition from a liquefiable soil to a hardening one. The slope of the stress path in the $q^* \sim p^*$ plane for a reinforced soil is different from that of an unreinforced sand. This is generally well predicted by the model and divergences become evident only at large strains for 0.9% of reinforcement when the simulation of the pore pressure build up becomes poorer.

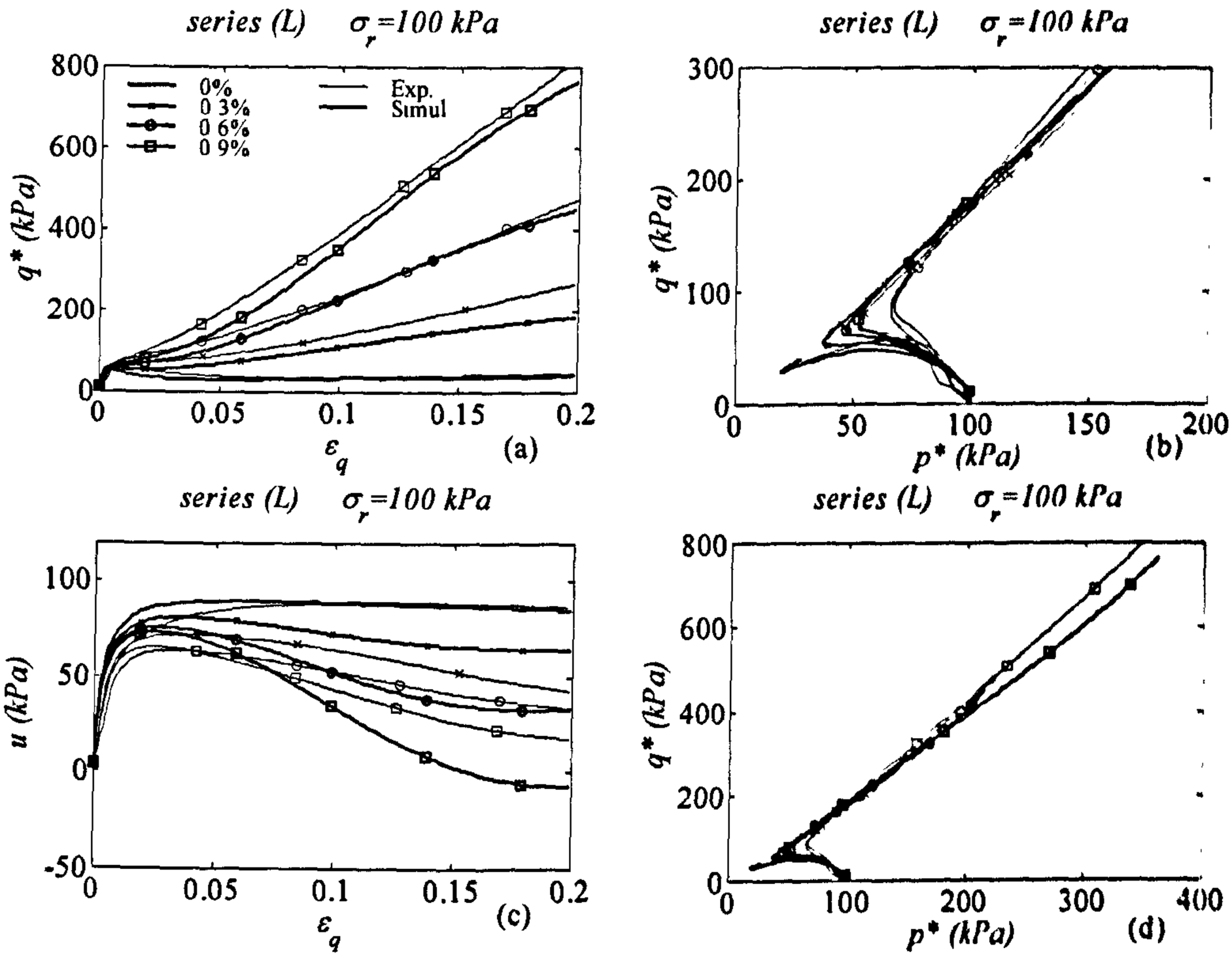

Fig. 7.29 Simulation of experimental undrained tests results on *(L)* series specimens tested at 100 kPa cell confining pressure (legend indicates fibres content).

The simulation of the pore pressure trend is a very complex issue for such loose specimens. An erroneous estimation of the initial void ratio which may derive from the slight collapse of the structure during sample installation may lead to error on the estimation of the pore pressure build up. Also it has been assumed that membrane penetration is negligible for reinforced specimens and this may lead again to some discrepancies between experiments and simulations.

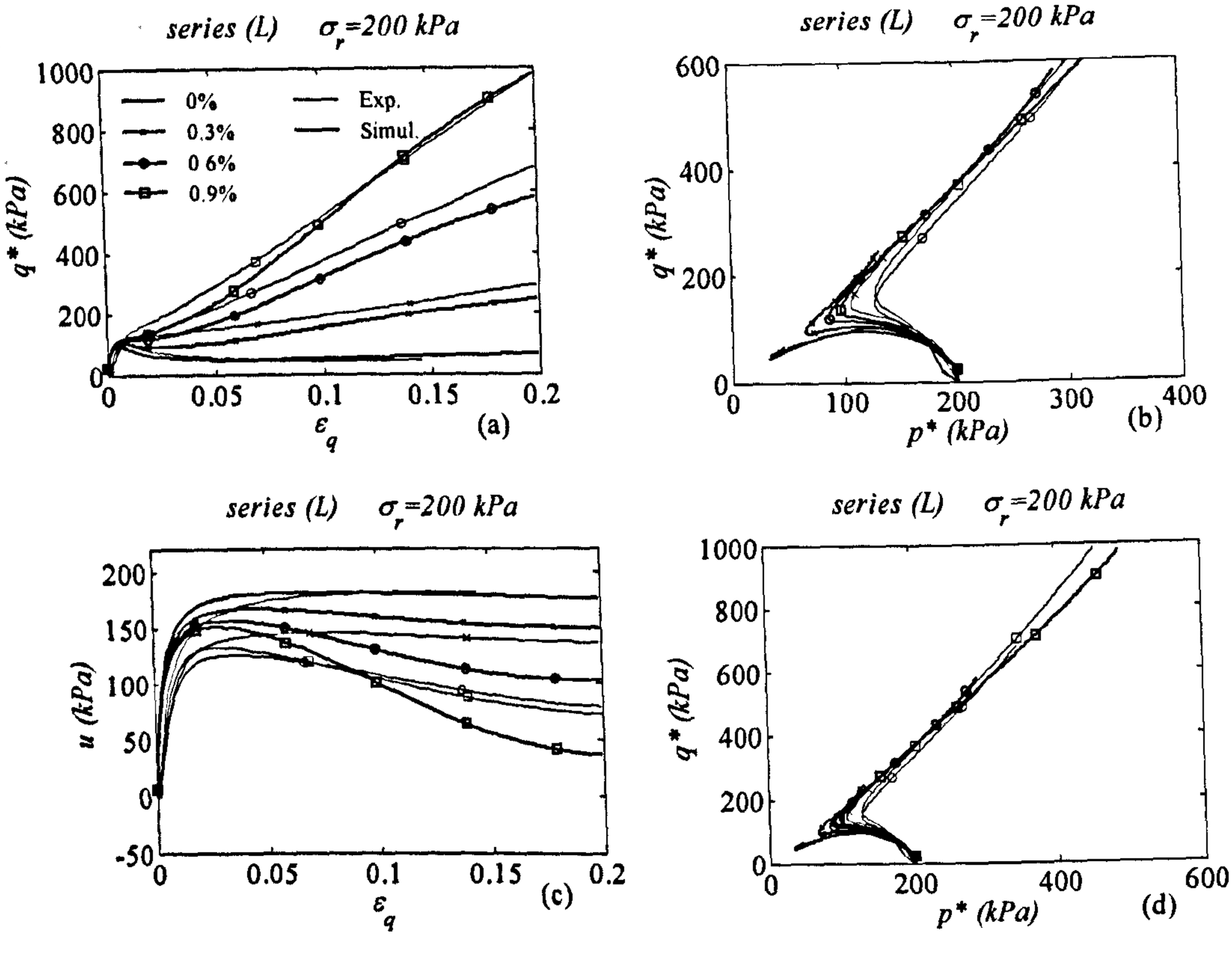

Fig. 7.30 Simulation of experimental undrained tests results on *(L)* series specimens tested at 200 kPa cell confining pressure (legend indicates fibres content)

The simulations of the undrained tests in extension are shown in Figs. 7.31-7.33 where the plots are presented in the $q^* \sim \varepsilon_q$ plane and in the $q^* \sim p^*$ plane. As observed for the drained tests, the contribution of the fibres to the strength of the material is limited for this loading condition as compared with compressive loading. However, the liquefiable behaviour is prevented by the addition of fibres because their inclusion makes the sand matrix denser. The slope of the stress-path in the $q^* \sim p^*$ plane is now the same for the unreinforced and reinforced specimens, since the extra confining stress of the fibres is almost negligible. Discrepancies between the experimental results and the simulations are due to the constant friction angle adopted for the sand matrix which has been chosen to accommodate a large range of confining pressure and

which underestimates the value at low confining pressure that is seen here. Overall the agreement between simulation and experiments is quite satisfactory.

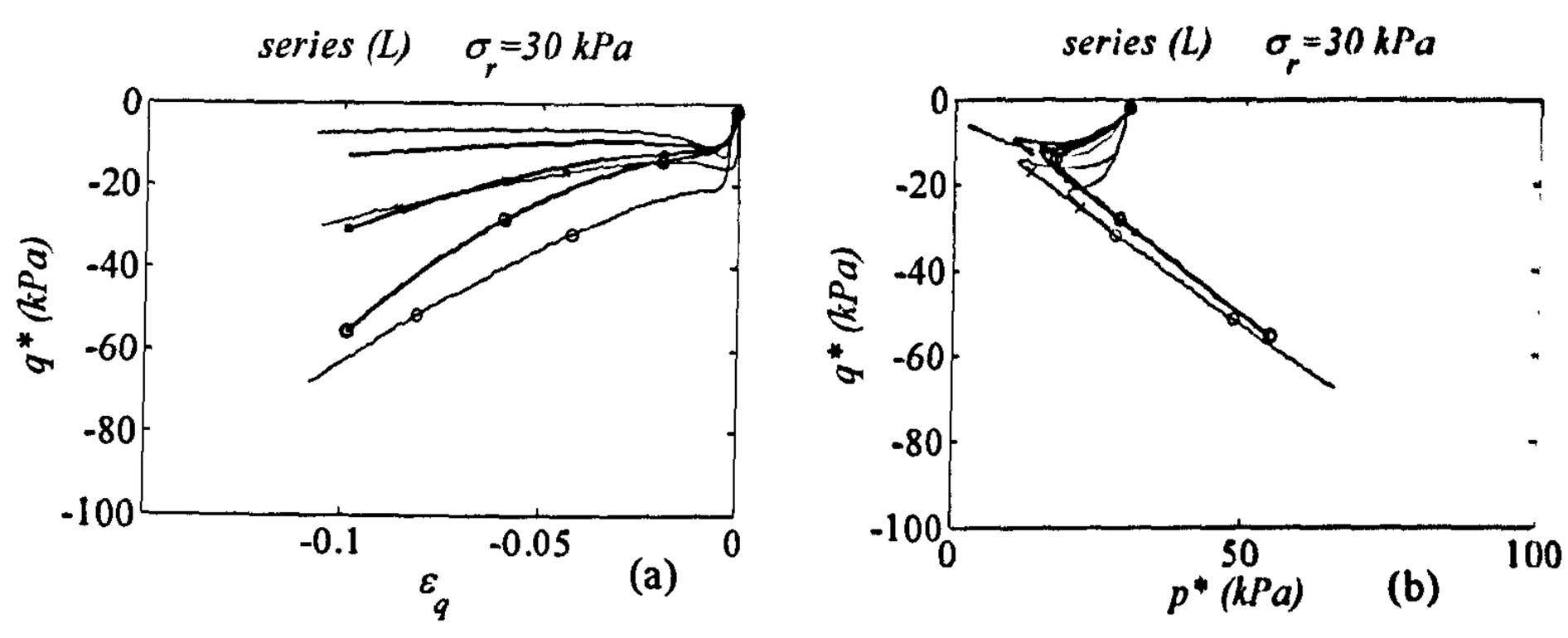

Fig. 7.31 Simulation of experimental extension undrained tests results on (L) series specimens tested at 30 kPa cell confining pressure (legend indicates fibres content)

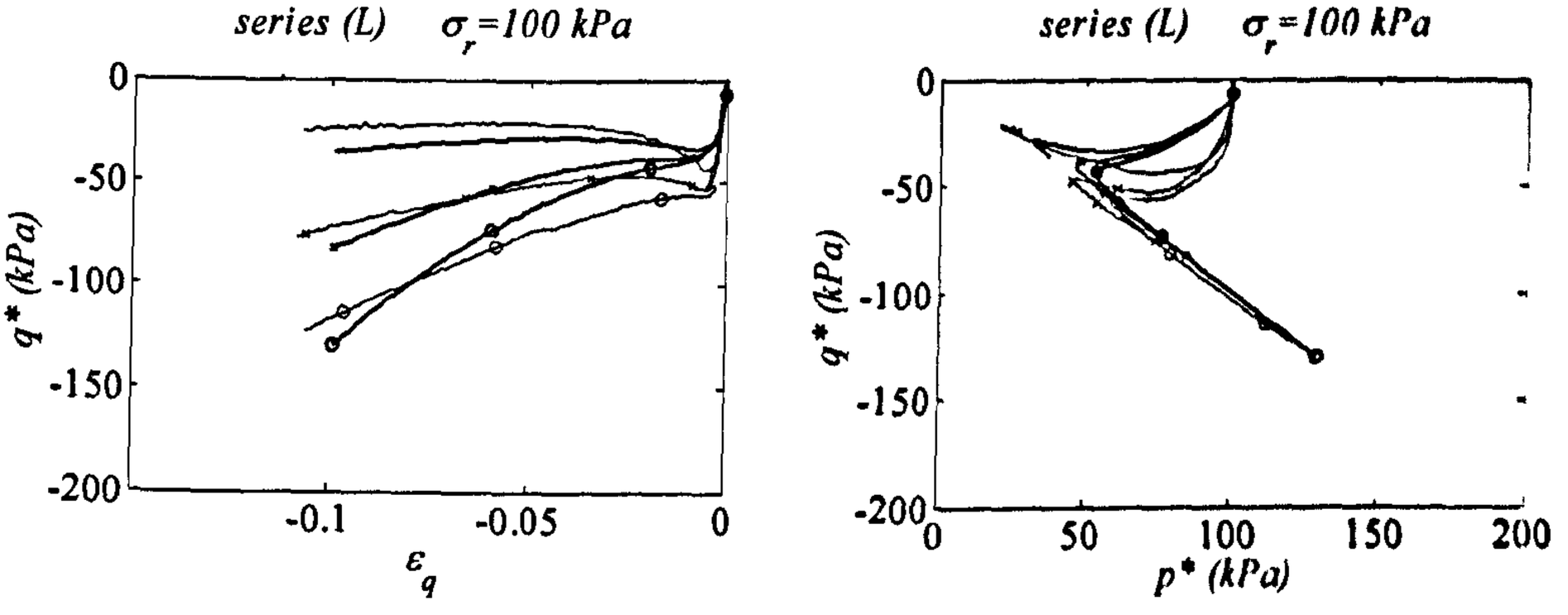

Fig. 7.32 Simulation of experimental extension undrained tests results on *(L)* series specimens tested at 100 kPa cell confining pressure (legend indicates fibres content)

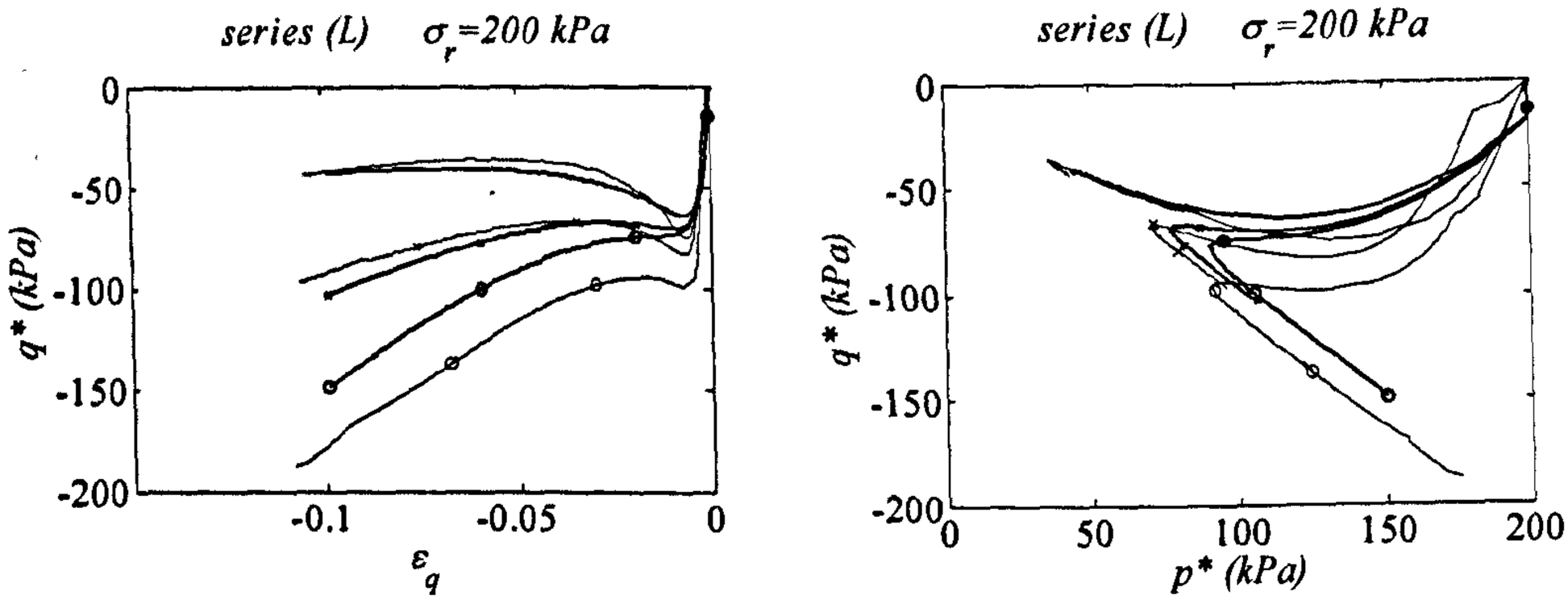

Fig. 7.33 Simulation of experimental extension undrained tests results on *(L)* series specimens tested at 200 kPa cell confining pressure (legend indicates fibres content)

From the simulation of the undrained compression tests it is noticeable that the pore pressure tends to built up again after dilation and this is analogous to the recompression at large strains observed in the drained triaxial tests. It may be interesting to study the prediction of the behaviour of the reinforced composite at large strains when the consequent build up of pore pressure may lead to some concerns for the liquefaction of the specimens. However, simulations shows that when the pore pressure increases again (Fig. 7.34c), the effective stress path abandons the straight line in the $q^* \sim p^*$ plane and follows another line in which the mean effective pressure decreases but the deviatoric stress increases (because of the increasing deviatoric stress contribution of the fibres) avoiding the subsequent liquefaction of the specimen. The stress paths are parallel for different fibre content as shown in Fig. 7.34.

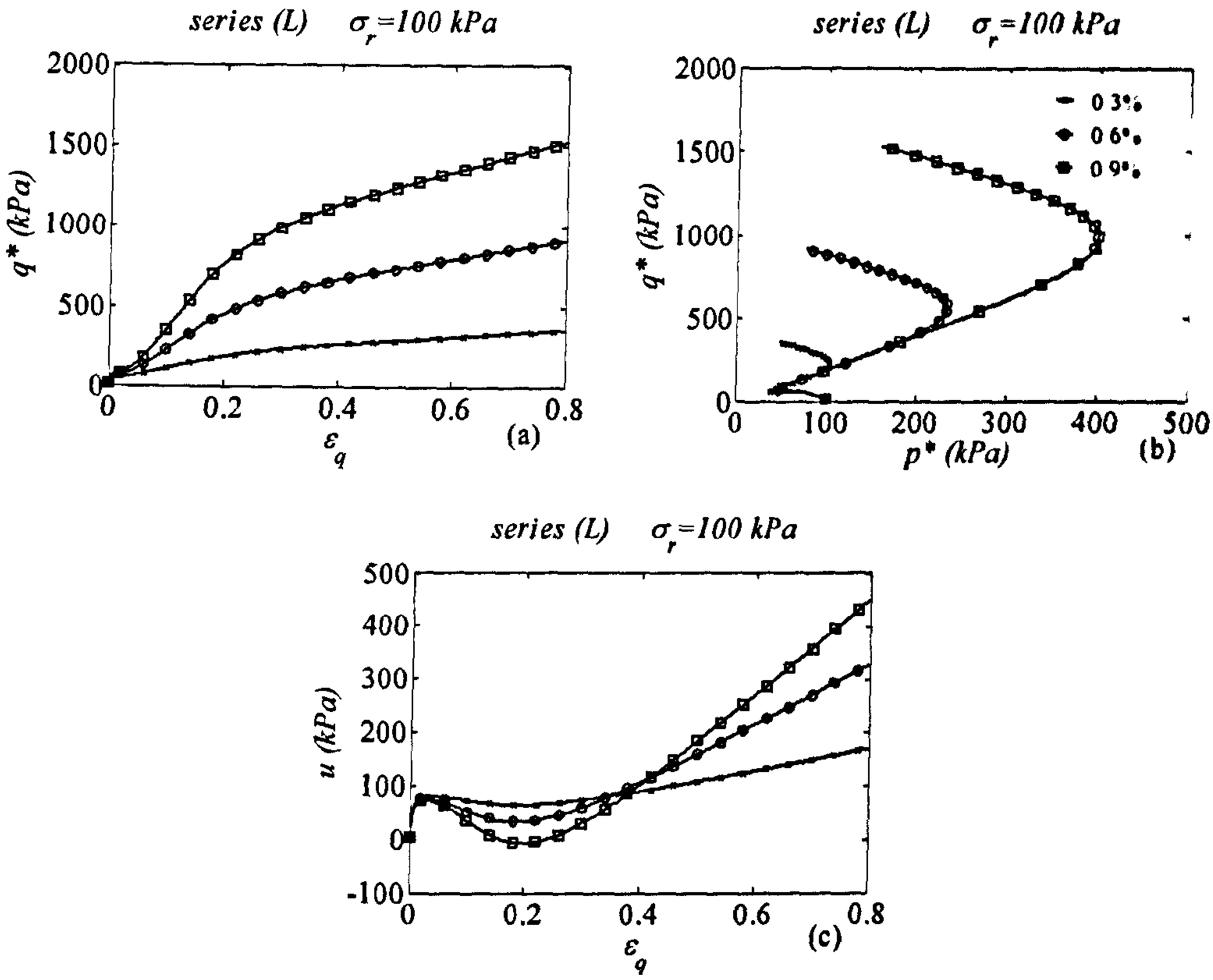

Fig. 7.34 Simulation for reinforced specimens in undrained tests at very large strains: (a) deviatoric stress-strain plot, (b) q^*-p^* plot and (c) pore pressure - deviatoric strain plot (legend gives fibre content)

7.6.2.6 Influence of the constraint on the volumetric deformation of each constituent for undrained loading

The previous simulations of the undrained experimental results have been obtained by imposing the constraint that no volumetric deformation was allowed in either constituent during loading. This is a simplification that may not be correct, as the two media may independently deform but the overall volumetric deformation of the composite may still be null. Therefore another set of simulations has been performed in which fibres and sand were allowed to deform freely with the only requirement that the total volume of the specimen should remain constant.

The new set of simulation is reported in Fig. 7.35 for compressive loading and in Fig. 7.36 for the extension case. A cell confining pressure of 100 kPa has been imposed. When compared with the previous set of simulations (Figs 7.28-7.33), this new set seems to reproduce better the

initial part of the stress strain response and also the location of the transformation point phase on the $q^* \sim p^*$ plane. However, the simulations become poorer at large strain, where the predicted recompression of the specimens results in a underestimated deviatoric strength and a divergence from the experimental effective stress path on the $q^* \sim p^*$ plane.

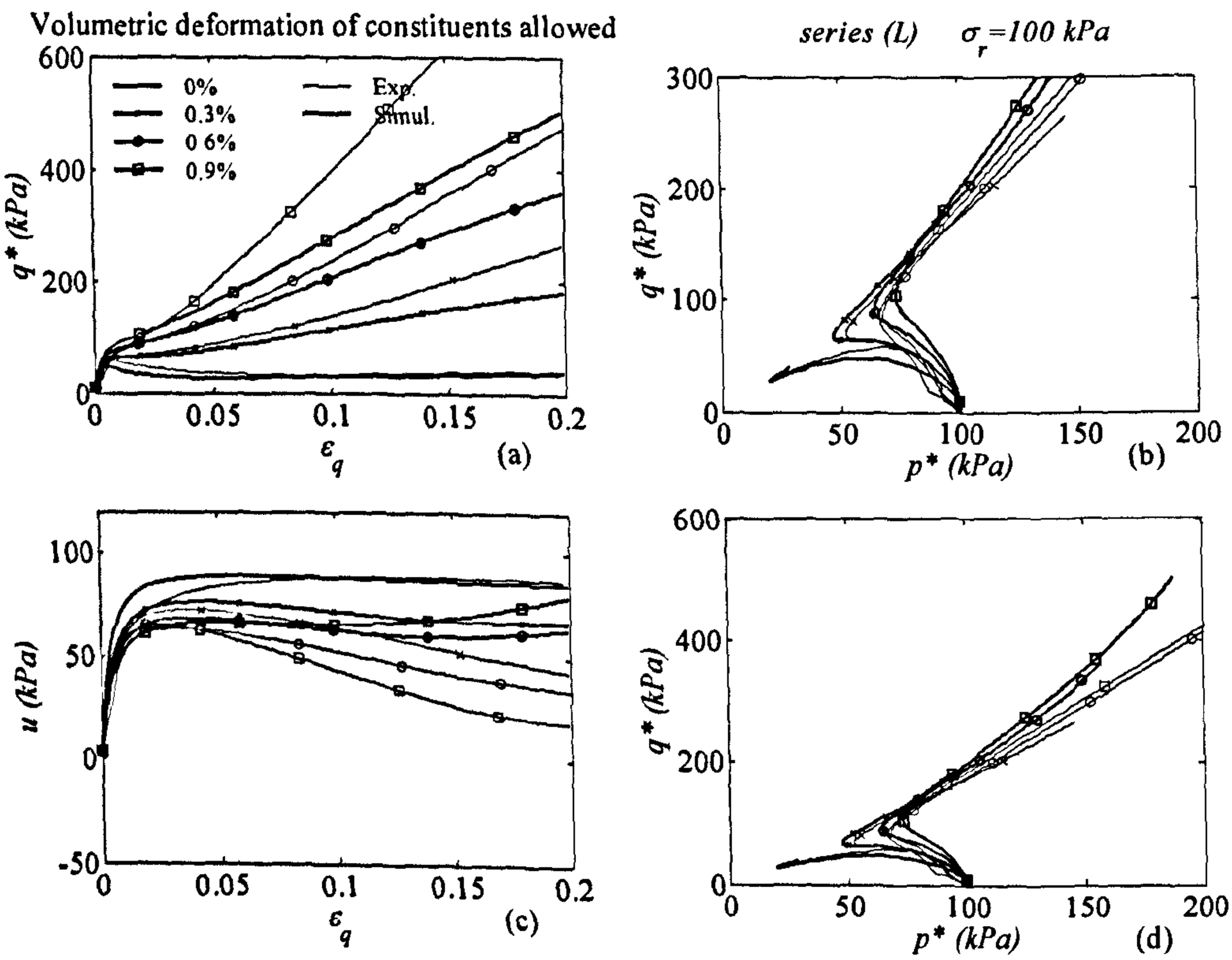

Fig. 7.35 Simulation of experimental compression undrained tests results by allowing the volumetric of each constituent. *(L)* series specimens tested at 100 kPa cell confining pressure (legend gives fibre content)

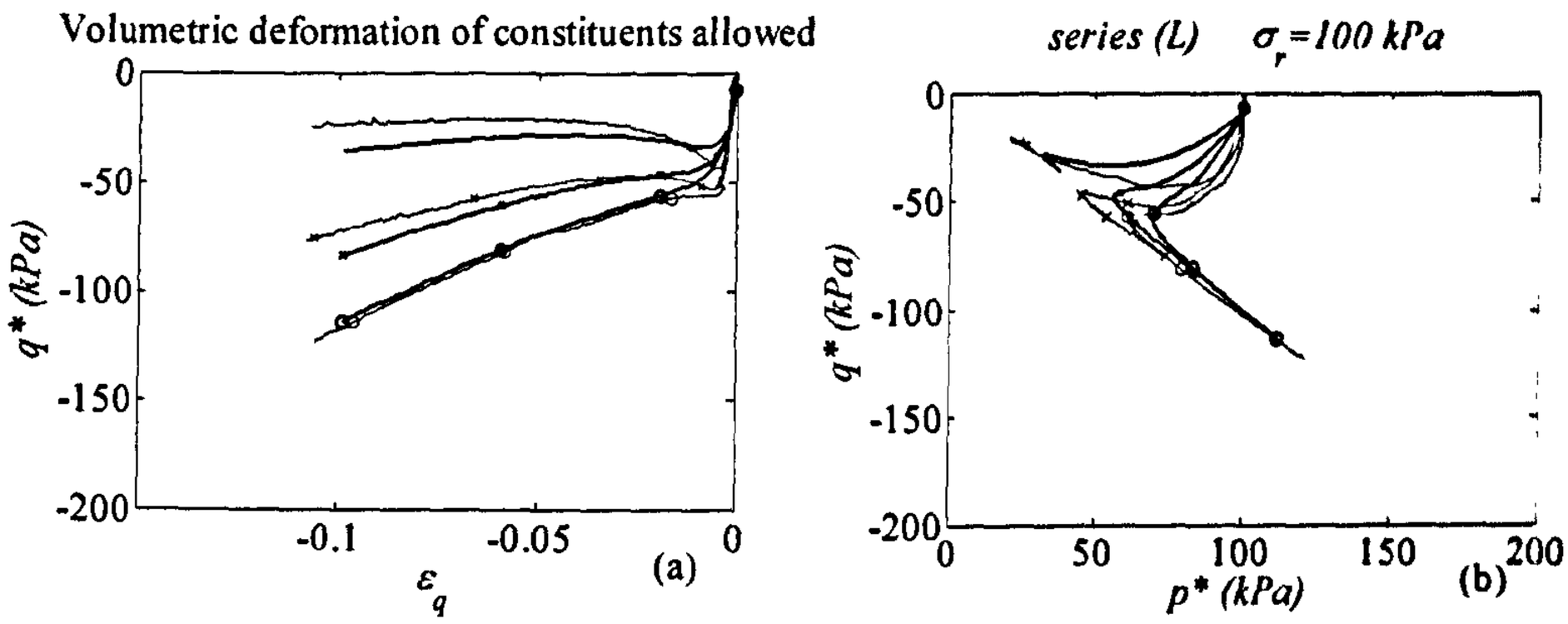

Fig. 7.36 Simulation of experimental extension undrained tests results by allowing the volumetric of each constituent. (L) series specimens tested at 100 kPa cell confining pressure. Legend indicates fibres content.

The undrained response is largely governed by the build up of pore pressure and comparison between the two sets of simulations shows that the pore pressures recorded in the experiments are somewhere between the predictions of the two sets of simulation (Figs. 7.29c and Fig.7.35c). This may suggest that the real volumetric behaviour of the constituents is somewhere in between the two assumptions made here.

7.6.2.7 Influence of individual parameters on the undrained behaviour

The two most important ingredients for correctly simulating the undrained behaviour of reinforced specimens seem to be the orientation of the fibres in respect to tensile strains and the "stolen" void ratio of the fibres. The former governs the contribution of fibres which in turn affects the slope of the stress path in the $q^* \sim p^*$ plane. The latter renders the sand matrix denser and the behaviour of the composite switches from a softening for unreinforced material to a hardening for the reinforced material.

The influence of the fibre orientation on the behaviour of reinforced sands in undrained tests has been investigated here. Simulations have been performed by adopting a preferred horizontal orientation, isotropic orientation and a preferred vertical orientation of fibres. The true orientation of fibres (Eq. 7.48) has been selected as preferred horizontal orientation.

$$\rho(\theta) = \overline{\rho}\frac{2ab^2|\cos(\theta)|}{\cos(\theta)^2(b^2-a^2)+a^2} \qquad (7.48)$$

where $a = 1.095$ and $b = 0.449$. The preferred vertical orientation was described by a vertical ellipse with a major axis having the same length as the preferred horizontal orientation (Fig. 7.37). The analytical form of the orientation distribution function for a vertical orientation of fibres is:

$$\rho(\theta) = \overline{\rho}\frac{2ab^2|\sin(\theta)|}{\sin(\theta)^2(b^2-a^2)+a^2} \tag{7.81}$$

where a=1.095 and b=1.00052.

It should be remarked that the size of the ellipses and circles in Fig. 7.36 is not related to quantity of reinforcement. The bigger dimension of the ellipse describing the vertical orientation is only related to the hypothesis of axisymmetric rotation in respect to the vertical axes and this means that there is still a consistent amount of fibres oriented in a sub-horizontal direction. It is important to mention that Eq. (7.20) is satisfied for all the three orientation distributions.

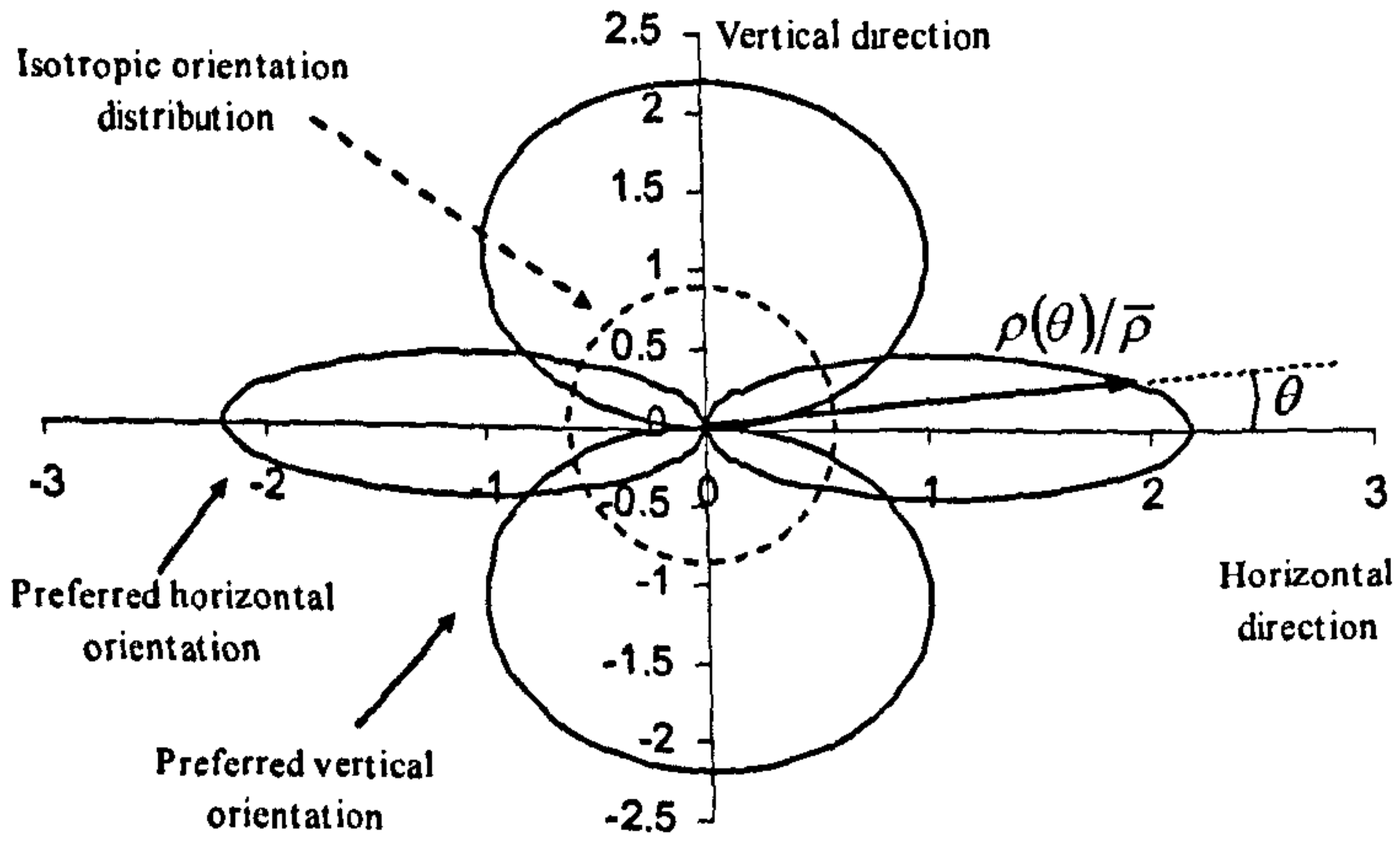

Fig. 7.37 Representation of the horizontal, vertical and isotropic orientation for fibres selected for investigating the influence of fibres orientation on the undrained behaviour

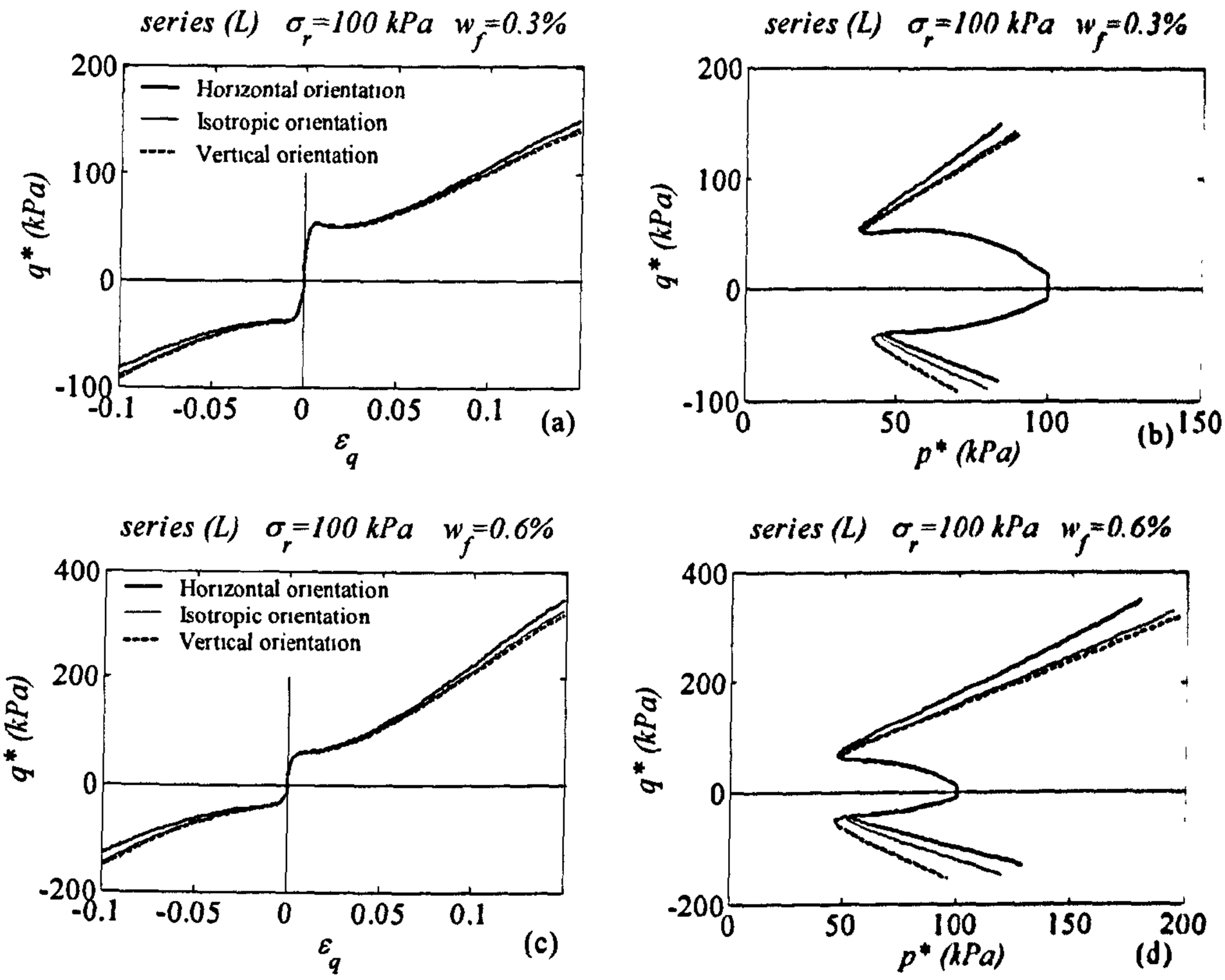

Fig. 7.38 Comparison between model predictions adopting different fibre orientation distributions in ((a) and (c)) the deviatoric stress-strain plane and ((b) and (d)) on the q^*-p^* plane for 0.3 % and 0.6% fibre content

The orientation of fibres does not strongly affect the deviatoric response of the soil which seems to be mostly governed by the quantity of reinforcement (Fig 7.38a). However, a clear dependence is noticeable in the $q^* \sim p^*$ plane where the slope of the stress path is influenced by orientation. The effectiveness of fibres is related to their orientation with respect to tensile strains (Fig 7.38b and d). The more the fibres are oriented with the tensile strains the steeper is the stress path in the $q^* \sim p^*$ plane. For undrained compression, the slope of the stress path increases as the fibres are more horizontally oriented while in extension, the slope increases when the fibres becomes more vertical. It should be mentioned that for undrained compression, there is not much difference when the isotropic and vertical orientation are assumed. The orientation of fibres is axisymmetrical with respect to the vertical direction, therefore even if a

preferred vertical orientation of fibres is chosen, many fibres still lie in a tensile strain orientation as shown in Fig. 7.37.

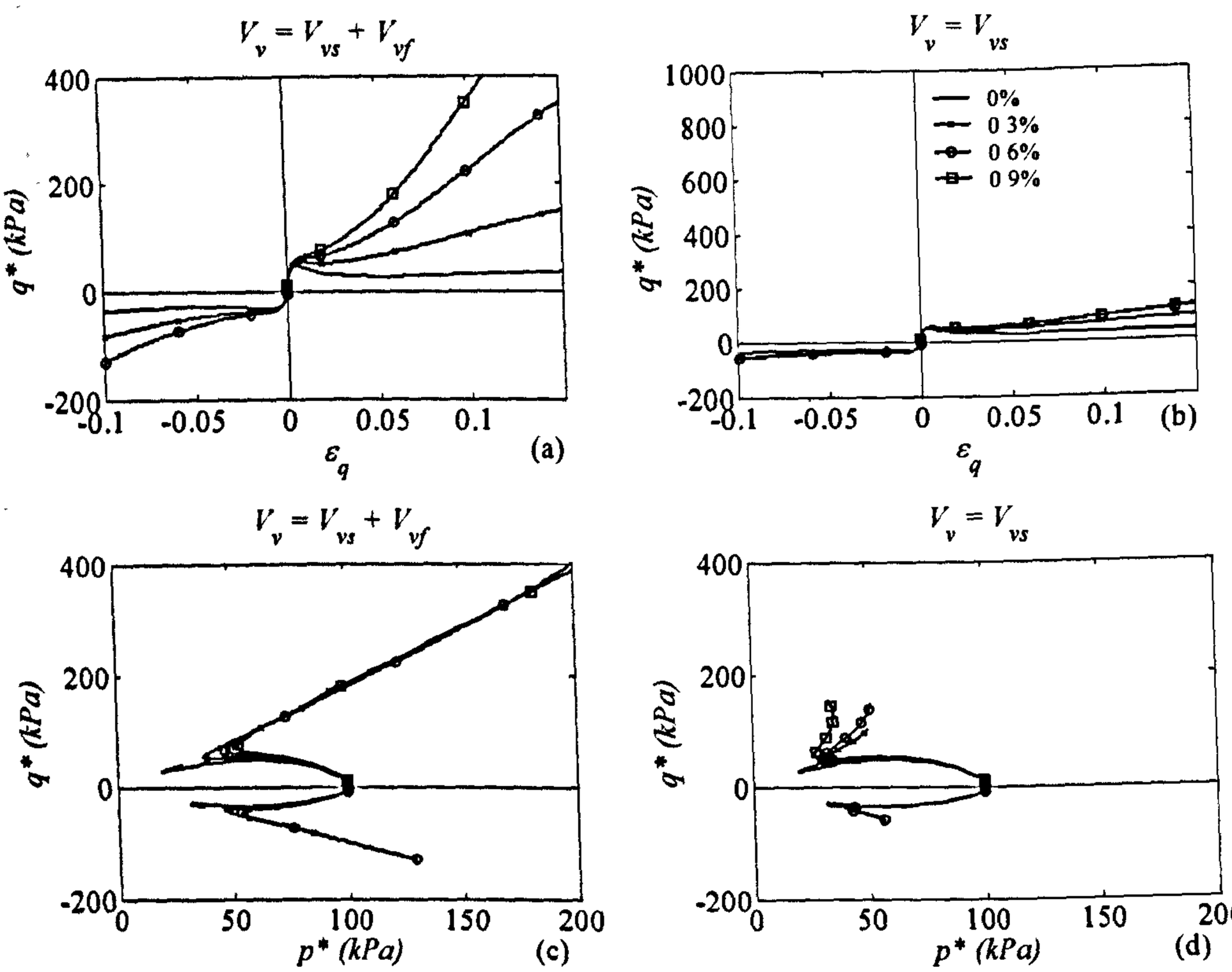

Fig. 7.39 Comparison between model predictions by considering ((a) and (c)) voids "attached" to both sand and fibres or ((b) and (d)) by allocating all the voids to the sand matrix (legend gives fibre content)

Fig. 7.39 shows the comparison between model simulations by dividing the available voids between sand and fibres ((a) and (c)) or by assigning all the voids to the sand matrix((b) and (d)). Simulations have been performed on series *(L)* specimens at 100 kPa cell confining pressure. The influence of the "stolen" void ratio is remarkable in both the deviatoric strength and on the stress plane. If all the voids are assumed to be part of the sand fraction, addition of fibres has a negligible densifying effect on the sand matrix. Therefore the effect of the extra confining stresses in the fibres becomes predominant and this induces a consistent built up on the pore pressure. This leads to an underestimation of the deviatoric strength and also to an

incorrect prediction of the stress path in the $q^* \sim p^*$ plane. However the stresses mobilised in the fibres prevent the liquefaction of the specimen.

7.6.3 Model calibration for reinforcement type (2)

The simulation of the experimental results for specimens reinforced with fibres type (2) requires a new calibration for the parameters of the reinforcement while the behaviour of the sand matrix has been modelled as already described. Experimental results on this type of fibres revealed that a limit of the resistance afforded by the reinforcement has been achieved and that it was caused by full sliding between fibres and sand grains. Therefore, a criterion to impose a limit to the performances of the reinforcement is introduced in this section.

The complete sliding between fibres and sand grains can be considered here by modifying the integration domain of tensile strain used to determine the stiffness matrix for the fibres. Fibres that are fully sliding will not develop any incremental stress and they have not to be further considered in the stiffness matrix for the fibres. The pull-out mechanism will not affect all the fibres simultaneously but it will depend on the mobilisation of fibre strength and in turn on the strain of the fibres. Obviously for triaxial compression, horizontal fibres will be the first to be affected by this limit, while in extension the vertical will slide first. If a strain limit in the fibres $\tilde{\varepsilon}_f^L$ is introduced, fibres stretched more than the strain limit $\tilde{\varepsilon}_f^L$ will fully slide while the others will still be in partial sliding conditions. Since the elongation in the fibres is related to the orientation of the fibres, a pull-out angle θ^L can be introduced to define the orientation limit for the fibres that are completely sliding. The pull-out angle can be defined with the Mohr-Circle of strains as:

$$\theta^L = \sin^{-1}\left(\sqrt{\frac{\tilde{\varepsilon}_f^L - \tilde{\varepsilon}_{f_3}}{\tilde{\varepsilon}_{f_1} - \tilde{\varepsilon}_{f_3}}}\right) \text{ if } \tilde{\varepsilon}_{f_3} > \tilde{\varepsilon}_f^L \tag{7.82}$$

and

$$\theta^L = 0 \text{ if } \tilde{\varepsilon}_{f_3} \leq \tilde{\varepsilon}_f^L \tag{7.83}$$

Therefore in triaxial compression, the fibres oriented below θ^L will slide while the other fibres will still mobilise incremental strength. The mechanism can be seen in the modified domains of the tensile stresses for the fibres (Fig.7.40). When no sliding occurs, the domain of tensile strains in the fibres is as usual (Fig.7.40a). When sliding begins to affect some fibres, the wedge of tensile strains starts to diminish (Fig.7.40b) until θ^L tends to θ^0 at large strain (Fig.7.40c) and the domain of the fibres that are not completely sliding becomes negligible.

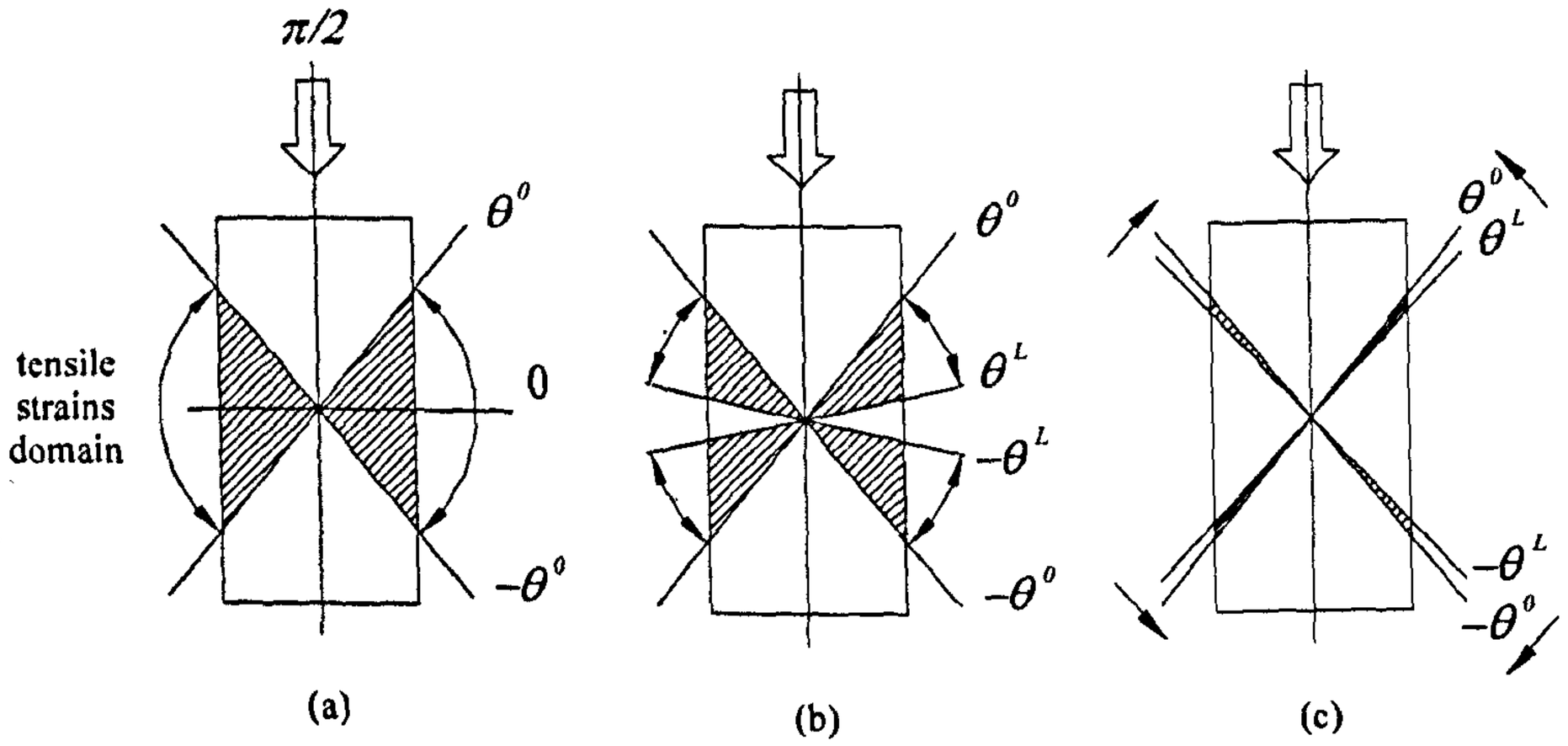

Fig. 7.40 Evolution for the tensile strains domain of fibres. (a) Absence of complete sliding, (b) initial stage of complete sliding (c) and towards the final stage of complete sliding.

A quite good agreement with the experimental data can be obtained if it is considered that the sliding mechanism takes place when the stress in the fibres reaches a certain threshold. It is as if the fibres were knotted together and these knots were undone when the stresses in the fibres reach a certain limit. Once the stress limit of the fibres σ_f^L is determined, the corresponding strain has been approximated as:

$$\tilde{\varepsilon}_f^L = \frac{\sigma_f^L}{E_f} \tag{7.84}$$

7.6.3.1 Input parameters for fibre type (2)

The calibration of the parameters governing the behaviour of fibre type (2) requires the definition of the same quantities as for fibre type (1) plus the stress limit of the fibres σ_f^L. A good agreement with experimental results was found if $\sigma_f^L = 130MPa$.

Results of tension tests of single fibres revealed that an elastic modulus E_f = 2600 MPa adequately represents the tensile behaviour of the fibres (see paragraph 3.3.2). The orientation distribution has been supposed equal to the one determined for fibre type (1) even if it was not actually supported by experimental evidence, since the procedure for determining the orientation distribution of fibres could not be applied for this type of reinforcement (see Chapter 4). The sliding function (f_b) and the evolution for the specific volume of the fibres (υ_f) have the same form as selected for fibre type (1). A summary of the parameters used for the defining the fibre stiffness matrix is given in the following Table 7.3.

Tab. 7.3 Parameters adopted for the fibres type (2)

Parameter	Description	Value
E_f	Elastic modulus	2600 MPa
$\rho(\theta)$	Fibre orientation distribution	$\rho(\theta) = \bar{\rho}\frac{2ab^2\lvert\cos(\theta)\rvert}{\cos(\theta)^2(b^2-a^2)+a^2}$ $a = 1.095 \quad b = 0.449$
f_b	Sliding function	$f_b = K_s\left(1-\exp\left(-c_s\cdot\frac{p^*}{p_{ref}}\right)\right)$ $K_s = 0.36 \quad c_s = 0.75$
υ_f	Specific volume of the fibres	$\upsilon_f = \upsilon_{f\,min} + \frac{\upsilon_N}{k_\upsilon\left(p^*/p_{ref}\right)+1}$ $\upsilon_{f\,min} = 2.1 \quad \upsilon_N = 4.8 \quad k_\upsilon = 0.22$
σ_f^L	Sliding stress limit	130 MPa

7.6.3.2 Simulation of experimental results

Figs. 7.41 and 7.42 show the comparison between the model simulation and experimental drained compression tests on sand reinforced with fibres (2) in the $q \sim \varepsilon_q$ and $\varepsilon_v \sim \varepsilon_q$ planes. Simulations are performed by keeping constant the cell pressure and the nominal density of the specimens while the fibre content is varied. The stress-strain curve is well simulated for all the fibre contents used, cell pressures and relative densities. The use of a stress threshold for defining the sliding limit between the fibres and sand grains seem supported by the satisfactory agreement between experiments and simulation. The strength of the reinforced specimen is well predicted in all the simulations.

The volumetric behaviour is also satisfactorily predicted. The addition of fibres results in a more dilative behaviour than for unreinforced composite even if the more dilative behaviour is not proportional to the fibre content. As already mentioned the volumetric behaviour is influenced by the combination of two main mechanisms (the extra confining stresses provided by the fibres and the volume they occupy) which have two opposite effects on the volumetric behaviour.

According to the simulation at large strains, when the fibres fully slide the volumetric behaviour has a quite sharp change of trend. Fibres do not further increase their confining effect, therefore the recompression of the specimen ends. This can not be confirmed by experimental results because the phenomenon takes place at large strains when the shape of the specimen may no longer be satisfactorily cylindrical.

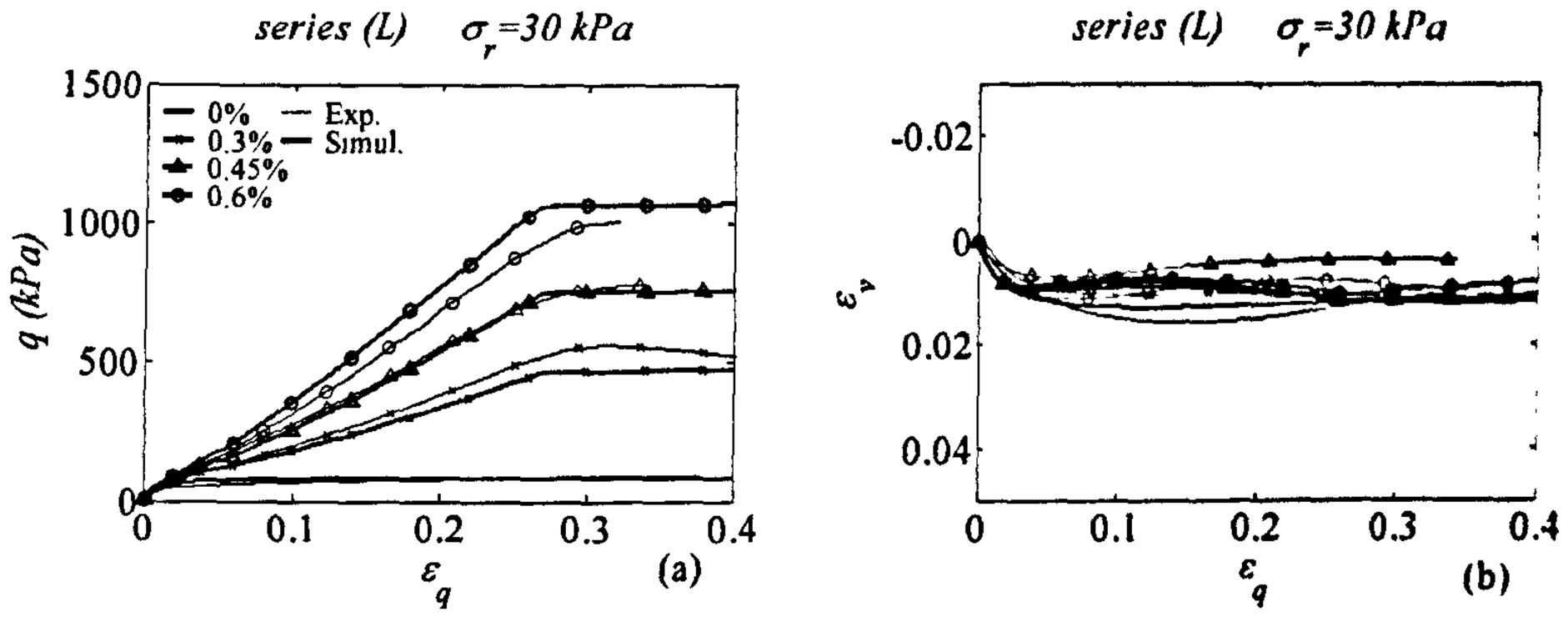

Fig. 7.41 Compression triaxial test results and model simulations for reinforced and unreinforced specimens of *(L)* test series with 30 kPa cell confining pressure (legend indicates the fibre content)

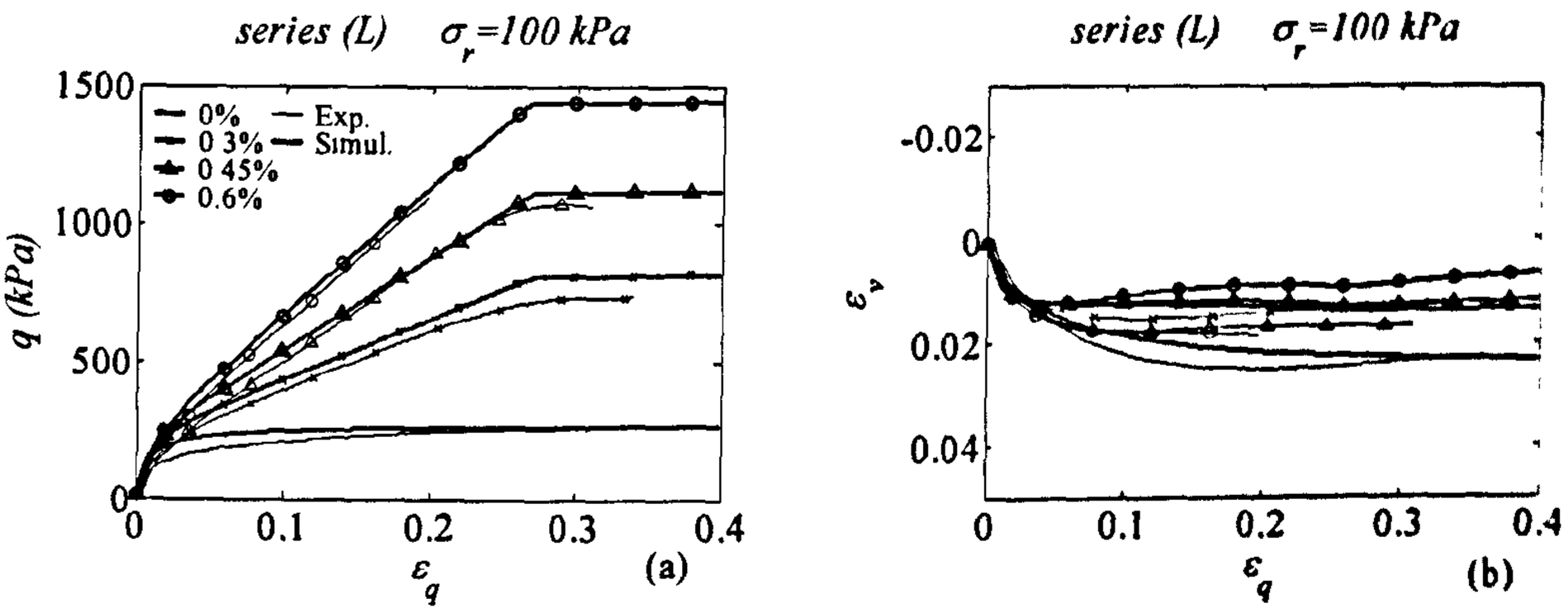

Fig. 7.42 Compression triaxial test results and model simulations for reinforced and unreinforced specimens of *(L)* test series with 100 kPa cell confining pressure (legend indicates the fibre content)

7.6.4 Model calibration for reinforcement type (3)

7.6.4.1 Input parameters for fibre type (3)

According to the experiments discussed in paragraph 5.4.4, specimens reinforced with fibre (3) do not show a proper failure, therefore a limit to the resistance provided by the fibres has not been introduced. The calibration of the parameters governing the behaviour of fibre type (3) requires the definition of three quantities as for fibre type (1).

Results for tension tests of single fibres revealed that an elastic modulus E_f = 4000 MPa can represent the tensile behaviour of the fibres (see paragraph 3.3.2). The same form of the orientation distribution as proposed in Eq.(7.48) has been used and according to the orientation distribution determined in Chapter 4, the following value for the parameters have been chosen: a=1.975, b=0.379. Comparison between the assumed orientation and the one determined from experiments is given in Fig. 7.43.

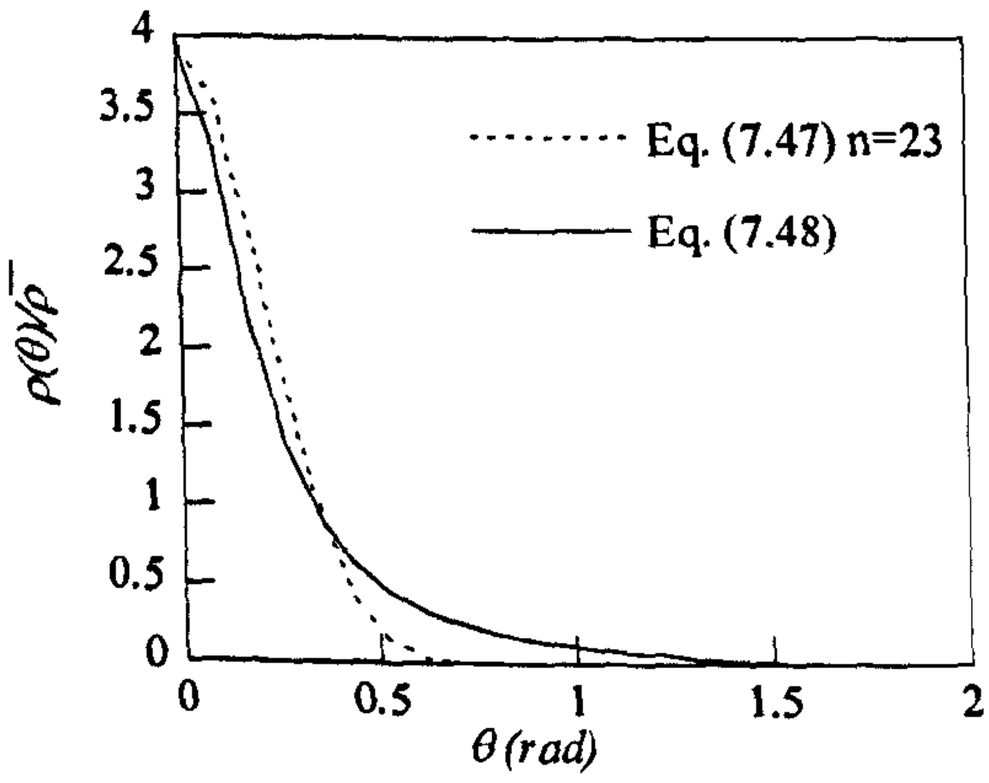

Fig. 7.43 Comparison between the assumed orientation distribution functions in Eq. (7.47) and Eq. (7.48) for fibres type (3)

The sliding function (f_b) and the evolution for the specific volume of the fibres (v_f) have the same form as selected for fibre type (1). However, the back analysis performed for the calibration of the sliding function (see paragraph 7.5.2.1 for the calibration procedure) revealed that a degradation of the bonding between the two consitutents may take place as the test proceeds. Therefore an expression for K_e that accounts for the bonding degradation is adopted:

$$K_e = K_{e0}\left(1 - k_r\left(1 - \exp\left(c_s \varepsilon_3\right)\right)\right) \tag{7.85}$$

This formulation states that bonding between the fibres and sand grains degrades from its initial value K_{e0} at the start of the test to the value $K_{e0}(1\text{-}k_r)$ at infinite strains. Graphical representation of Eq.(7.85) is given in Fig.(7.44). The rate of degradation is controlled by the

parameter c_s and the degradation is linked to the horizontal strains of the specimens which are linked to the elongation of the highly preferred horizontal fibres.

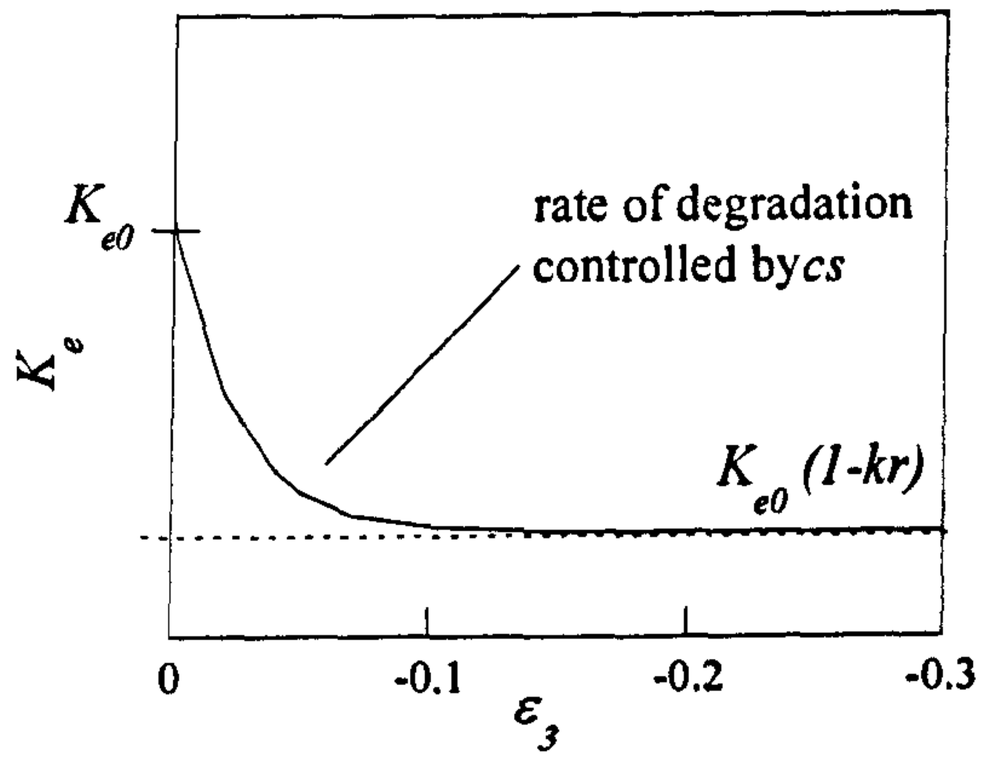

Fig. 7.44 Graphical representation of Eq(7.85) for modelling the degradation of the bonding between fibres and sand grains as test proceeds

The quantities used for the defining the fibre stiffness matrix are summarised in Table 7.4.

Tab. 7.4 Parameters adopted for the fibres type (3)

Parameter	Description	Value
E_f	Elastic modulus	2600 MPa
$\rho(\theta)$	Fibre orientation distribution	$\rho(\theta) = \overline{\rho}\dfrac{2ab^2\lvert\cos(\theta)\rvert}{\cos(\theta)^2(b^2-a^2)+a^2}$ $a = 1.975 \;,\; b = 0.379$
f_b	Sliding function	$f_b = K_e\left(1-\exp\left(-c_s\cdot\dfrac{p^*}{p_{ref}}\right)\right)$ $K_e = 0.25(1-0.86(1-\exp(50\varepsilon_3)))\;\; c_s = 0.6$
υ_f	Specific volume of the fibres	$\upsilon_f = \upsilon_{f\min} + \dfrac{\upsilon_N}{k_\upsilon(p^*/p_{ref})+1}$ $\upsilon_{f\min} = 1.1 \;\; \upsilon_N = 1.6 \;\;\; k_\upsilon = 0.2$

7.6.4.2 Simulation of experimental results

Figs. 7.45 and 7.46 show the typical comparison between the model simulation and experimental drained compression tests on sand reinforced with fibres (3). The general trend of the stress-strain behaviour for reinforced specimens shows a rather parabolic trend which is well captured by the proposed model. Some discrepancies between experimental results and simulation are only noticeable for the specimens reinforced with 0.9% fibre content. In this case the strength at large strain is overestimated at 30 kPa cell pressure and underestimated at 100 kPa cell pressure. It may be that the interaction between fibres and sand grains is more complex than has been assumed here and that other factors (e.g. fibre content) should be taken into account in the formulation of the sliding function.

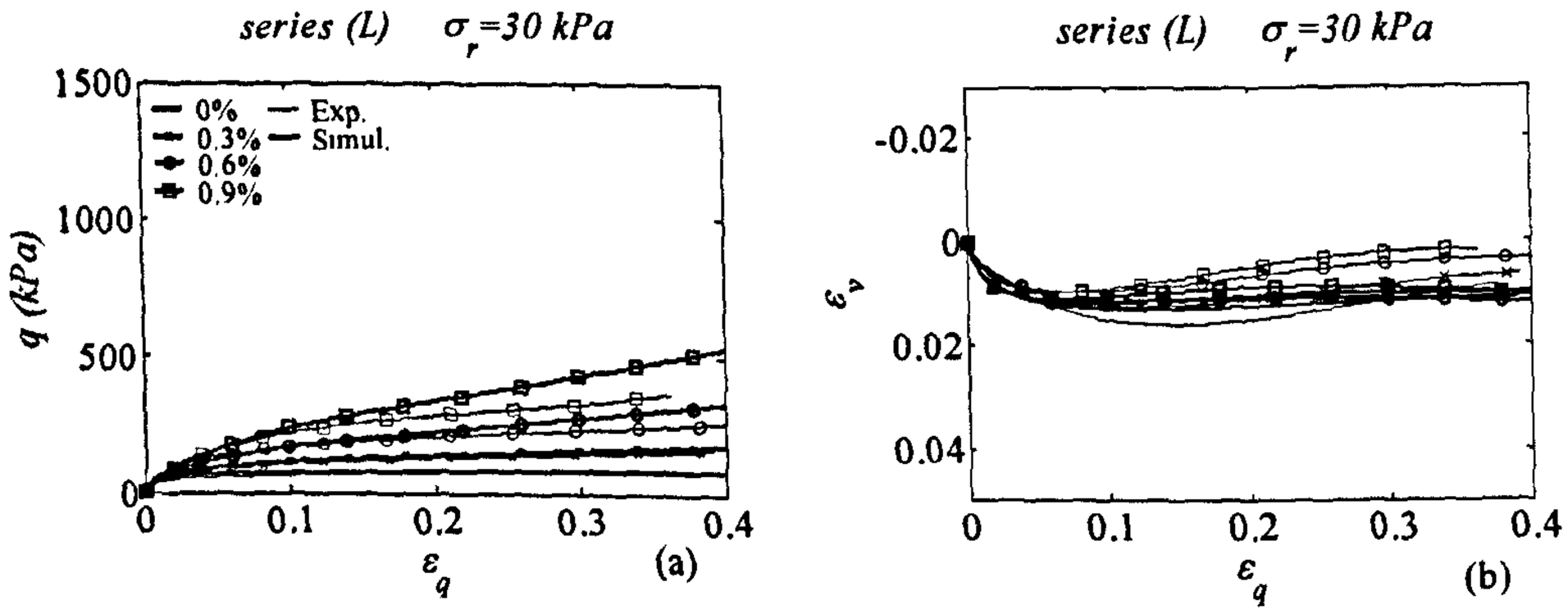

Fig. 7.45 Compression triaxial test results and model simulations for reinforced and unreinforced specimens of *(L)* test series with 30 kPa cell confining pressure (legend indicates the fibre content)

As commented in the previous simulation, the trend of the volumetric behaviour with the fibre content is not well defined. All the reinforced specimens seem to have a bit more dilative behaviour than the unreinforced specimen even if all the volumetric trends are very close. The model simulations generally respect this trend and the behaviour of reinforced composite becomes more compressive than the unreinforced sample only at large strains when the extra confining effect of the fibres becomes predominant over their densifying effect.

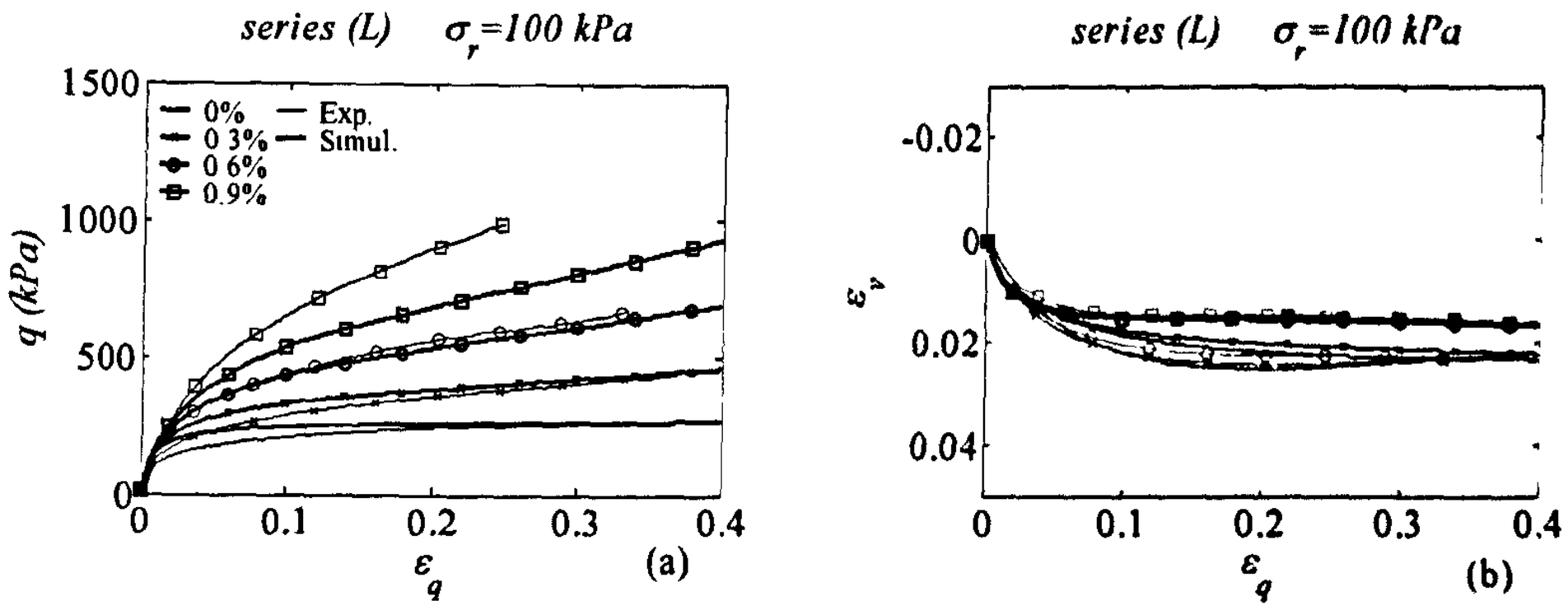

Fig. 7.46 Compression triaxial test results and model simulations for reinforced and unreinforced specimens of *(L)* test series with 100 kPa cell confining pressure (legend indicates the fibre content)

7.7 Conclusions

A simple and versatile modelling approach for predicting the constitutive behaviour of fibre reinforced sand in conventional triaxial conditions has been presented. The model is based on the rule of mixtures according to which each constituent obeys its own constitutive law. The versatility of this approach lies in the possibility of choosing the complexity of the model for characterising the behaviour of each constituent. Application of the modelling framework has been demonstrated by adopting firstly a very simple elastic-perfectly plastic model for the sand matrix and then a more complex hardening plastic model.

A stress-strain relationship for the fibre fraction has been developed by adopting a linear elastic model for the describing the tensile behaviour of a single fibre. The stiffness matrix for the fibres requires the calibration of three different ingredients: the fibre elastic modulus, the orientation distribution, the amount of sliding between fibres and sand grains. Any distribution of the fibre orientation can be incorporated in the stiffness matrix and the importance of considering the fibre orientation relative to the strain conditions has been demonstrated for triaxial extension and compression tests for both drained and undrained conditions.

The modelling framework proposed requires the definition of the volumetric fractions of its two constituents which in turn requires the separation of the voids in the specimens between them.

In fact, it was found particularly important to assign some of the voids to the fibre agglomerate in order that all the voids in the specimen are not available for the sand to deform. This feature enables the correct simulation of the volumetric behaviour in drained tests and of the resistance to liquefaction in undrained test.

Even when a very simple model for the sand matrix is adopted, the simulations of the composite exhibit key characteristics of the response observed in the experimental tests. Discrepancies between simulation and experimental results can be attributed to the simplicity of the sand model adopted but they are improved when a more complex model that captures the non-linear behaviour of the sand is selected. Simulations with the more complex model for the sand matrix have been found satisfactory for all the three types of reinforcement employed in the experimental campaign in both drained and undrained conditions. The pull-out mechanism for fibre type (2) was predicted by simple adjustment on the model formulation.

The calibration of the sliding function and the repartition of the voids between the fibres and the sand matrix is based on a back analysis procedure. However, the accurate definition of the voids belonging to the fibres is still based on a trial and error procedure which requires some refinements in future research. A more extensive and focussed experimental campaign would be useful to clarify this aspect. Further developments of the model should also account for the introduction of a more complex constitutive law for the fibres and for the extension of the modelling approach to a more general multiaxial space.

CHAPTER 8
CONCLUSIONS

8.1 Conclusions

The present project involved the experimental investigation of the performance of fibre reinforced sands and the development of a constitutive model able to predict their mechanical response. The experimental investigation consisted on testing specimens made up with Hostun sand and reinforced with three different types of short discrete polypropylene fibres. The conventional triaxial apparatus was used to carry out the investigation. Here is a summary of conclusions drawn from the work described in earlier chapters.

8.1.1 Determination of the fibre orientation distribution

For the first time, a procedure for determining the distribution of fibre orientations in sand reinforced with flexible fibres has been proposed. It has been applied to cylindrical samples prepared using moist tamping (MT) and moist vibration (MV) techniques so that the fibre orientations have a vertical axis of symmetry. However, it may be applied to samples of any shape as long as the axis of symmetry of the distribution of fibre orientation is known: it will typically be normal to the layering in a compacted sample. Conclusions from this section of the experimental investigation are summarised below:

- Both the techniques adopted for specimen preparation (MT and MV) lead to a preferred near horizontal orientation for the fibres. The orientation of fibres was found to be dependent on both fibre type and specimen preparation technique bur generally more than 80% of fibres have an orientation that lies within $\pm 30°$ of the horizontal plane. However, the MV technique seems to produce a slightly less anisotropic orientation distribution compared with that induced by MT.

- Both the procedures were found to produce a distribution of fibre orientations that was largely independent of the average volumetric concentration of fibres for the range of values considered.

- Compression triaxial test results seem to confirm the results from the orientation distribution with moist tamped specimens slightly stronger than vibrated ones for two out of the three reinforcements employed. For one reinforcement type, the deviatoric stress-strain response seems independent of the sample preparation technique.

- Comparison between triaxial compression and extension test results corroborates the conclusions given by the analysis of the fibre orientation. The fibres seem to be more effective in triaxial compression than in extension loading and the experimental results confirm the importance of the fibre orientation distribution as a key parameter which has to be considered for the design of fibre reinforced geotechnical structures.

8.1.2 Drained triaxial tests

A total number of 75 drained triaxial tests have been performed on both unreinforced and reinforced specimens. The highly anisotropic orientation of fibres and the preliminary triaxial test results mentioned above encouraged the performance of the testing in both compression and extension. The main conclusions deriving from the experimental campaign are as follows:

- The shear strength characteristics of the soil in triaxial compression loading are appreciably enhanced by all the three types of reinforcement. Addition of fibres increases both the apparent cohesion intercept and the friction angle of the material.

- The contribution of the fibres to the strength of the soil is proportional to the fibre content. Increase in relative density of the specimens has a positive effect on the contribution of fibres: dense specimens dilate more than loose ones and this induces the development of high tensile stresses in the fibres. The adoption of higher confining pressure may result in a better bonding between fibres and sand grains. At low pressures the bonding seems to improve during the test as the stresses in the specimens increases.

- For compressive loading, a limit of the strength for reinforced specimens is found only for one type of fibres. It is clear that the failure mechanism is caused by the complete sliding between sand grains and the fibres. For the other two reinforcement types, a strength limit is not reached even if the tests are continued to very large strains: a relative sliding appears to take place between the two constituents but the loss of bonding is not complete. However, samples that do not show a strength limit for compressive loading reach a resistance threshold when tested in extension.

- The effectiveness of the fibres is dependent on the loading condition and it is found to be significant in triaxial compression but limited in triaxial extension. It is clear that the effectiveness of fibres is dependent on their orientation relative to the imposed direction of tensile strain.

- The volumetric behaviour is in general more dilative when fibres are added for both compressive and extensive loading. Fibres affect the volumetric behaviour for two main reasons with contrasting effects: they increase the relative density of the specimen (because they occupy some volume and they also seem to "steal" some voids to the sand matrix) but they also provide extra confinement to the sand matrix.

8.1.3 Undrained triaxial tests

Part of the experimental campaign of this research has focussed on the prospect of altering the undrained response of a loose clean sand to reduce its liquefaction potential by mixing the sand with short flexible fibres. The analysis of undrained triaxial compression and extension tests on fibre reinforced and unreinforced sand specimens has revealed a number of points of interest:

- The presence of fibres clearly affects the undrained behaviour in compression as well as in extension and converts a strain softening response (typical of loose unreinforced sands) into a strain hardening response. Static liquefaction appears to be prevented for both loading conditions but a higher concentration of fibres is needed for the prevention of liquefaction in extension.

- Normalisation of the stress paths with the mean effective stress at the end of consolidation shows a common path once the characteristic state is reached irrespective of the fibre concentration. The mobilised angles of friction coming from the slopes of the stress paths at large strains are vastly different for compression and extension and this is a consequence of the anisotropic nature of the distribution of fibre orientations.

- The addition of fibres was also found to be beneficial in avoiding the full liquefaction that was triggered for unreinforced specimens by applying a strain reversal at the end of the monotonic loading. Considering that one of the consequences of liquefaction is the lateral spreading of the soil, it seems that the presence of fibres can limit or even prevent the occurrence of this phenomenon.

8.1.4 Constitutive modelling

A simple and versatile modelling approach for predicting the constitutive behaviour of fibre reinforced sand in conventional triaxial conditions has been presented. The model is based on the rule of mixtures according to which each constituent obeys its own constitutive law. The versatility of this approach lies in the possibility to choose the complexity of the model for characterising the behaviour of each constituent.

A stress-strain relationship for the fibre fraction has been developed by adopting a linear elastic model for the describing the tensile behaviour of a single fibre. The stiffness matrix for the fibres requires the calibration of three different ingredients: the fibre elastic modulus, the orientation distribution, the amount of sliding between fibres and sand grains. Any distribution of the fibre orientation can be incorporated in the stiffness matrix and the importance of considering the fibre orientation relative to the strain conditions has been demonstrated for triaxial extension and compression tests in both drained and undrained conditions.

The proposed modelling framework requires the definition of the volumetric fractions of its two constituents which in turn requires the repartition of the voids in the specimens between them. In fact, it was found particularly important to assign some of the voids to the fibre agglomerate in order that all the voids in the specimen are not available for the sand to deform. This feature

enables the correct simulation of the volumetric behaviour in drained tests and of the resistance to liquefaction in undrained test.

The modelling framework has been applied by adopting firstly a very simple elastic-perfectly plastic model for the sand matrix and then a more complex hardening plastic model. Even when a very simple model for the sand matrix is adopted, the simulations reproduce the key characteristics of the mechanical response observed in the experimental tests. Simulations with the more complex model for the sand matrix have been found more satisfactory and they allowed a remarkable simulation of experimental results in both drained and undrained conditions.

8.2 Further discussion

Few hints of particular interest emerged from the present work and were also discussed during the oral dissertation of this manuscript. These points are summarised and commented in the following of this section.

8.2.1 On the relative density of reinforced specimens

It has been discussed in section 2.2.2 that experimental results from previous investigations (Michalowski and Zhao, 1996; Michalowski and Čermák, 2003) revealed a different volumetric behaviour for the reinforced specimens from what presented in this dissertation: in those investigations a more compressive behaviour was observed for fibre reinforced specimens if compared to unreinforced ones, while in this work the addition of fibres generally resulted in an increased dilation. It is believed that this discrepancy can be attributed to the different definition adopted for the relative density of reinforced specimens and in turn to the different approach assumed when comparing reinforced and unreinforced samples.

In fact, since a definition of void ratio and relative density for reinforced specimens has not been agreed between researchers, there is freedom for the definition of the void ratio (and in turn the relative density) of the reinforced specimens. The void ratio (e) for unreinforced specimens is defined as the ratio between volume of voids (V_V) and volume of sand (V_s):

$$e = \frac{V_V}{V_s} \tag{8.1}$$

On the other hand, there are at least three different possibilities for defining the void ratio of reinforced soils:

1. The void ratio can be related to the sand matrix considering the volume of fibres (V_f) as part of voids

$$e = \frac{V_V + V_f}{V_s} \tag{8.2}$$

2. The void ratio can be related to the solid matrix considering the fibres as part of solids

$$e = \frac{V_V}{V_s + V_f} \tag{8.3}$$

3. The void ratio can be related to the ratio between the volume of the voids and the sand matrix, neglecting the volume of the fibres from the computation:

$$e = \frac{V_V}{V_s} \tag{8.4}$$

To any of the above mentioned definitions corresponds a different approach of comparing reinforced and unreinforced specimens at the same density state with important effects when drawing conclusions from the experimental results. Moreover, as already discussed in section 2.2.1, the maximum and minimum void ratio for reinforced specimens is different from those for unreinforced specimens and a procedure for their definition has not been yet defined. It is clear that further clarification is required in this matter and a consistent approach should be agreed among the researchers.

8.2.2 Existence of critical state for reinforced soils

The experimental results obtained in this research did not permitted to determine whether the critical state concept, which is generally applied for soils, can also be applied to reinforced soils. This is related to the limited capacity of the employed experimental equipment which did not allow to the testing under higher confining pressure or to greater axial stresses. However, experimental results published in the literature (Consoli et al., 2007b) suggest that a critical state can be detected for reinforced soils also.

It should be mentioned that the modelling approach adopted in this research implies somehow the existence of a critical state for reinforced soils. The fibre can be thought as a source of external confining stresses for the sand matrix which governs the overall behaviour of the composite and the constitutive relationship for the matrix are formulated in a critical state framework. This means that the existence of a critical state (certainly dependent on the fibre characteristics) may be a consequence of the modelling approach proposed here. However, further experimental investigation is required to clarify this point.

8.2.3 Modelling implication of existence of critical state for reinforced soils

If the critical state would be found to be applicable to reinforced soils also, it is clear that conventional continuum models for soils formulated in a critical state framework may be a suitable modelling alternative. It is expected that, in these models, fibre and sand characteristics would be fully integrated to predict the overall characteristics of the reinforced material. It should be mentioned that this route was attempted at the early stage of this investigation but the achieved experimental results did not allow the development of this modelling approach.

8.3 Suggestion for further research

Because of the novelty of this technique for reinforcing sand, there are still a number of tasks that need to be developed and further investigated before the reinforcement of soils with discrete polypropylene fibres (or other flexible fibres) could be applied at full scale to

geotechnical problems. However, the following suggestions for future research are given in relation to the research that has been reported in this thesis.

8.3.1 Fibre orientation distribution

The procedure that has been used provides a firm starting point for the determination of fibre orientation, however the following tasks may be improved to facilitate and extend its applicability:

- The procedure of sample freezing and cutting is quite laborious and it might be improved and accelerated for example by employing some kind of resin instead of freezing, and by enhancing or automating the cutting procedure;

- The procedure for counting the fibres on the cutting plane might be automated with the aid of a computer program and some form of digital image analysis;

- Different shapes of the orientation distribution function might be introduced to describe more general fibre orientations.

Moreover, since the effectiveness of fibres is considerably dependent on their orientation, the common practice should not be limited to checking the orientation of fibres in prepared specimens but a procedure for imposing a more desirable distribution of fibre orientations should be developed.

8.3.2 Experimental investigation

It has been demonstrated that the contribution of fibres is dependent on many factors related to the sand, fibres and test conditions and there are many factors whose influence is still not completely clear. However, there are some aspects that seem fundamental for the development of this reinforcing technique but they have not yet been taken into consideration:

- The contribution of fibres is dependent on their orientation in respect to tensile strains and the conventional triaxial apparatus employed here allow only a jump of the principal stresses direction by 90 degrees. The performance of an experimental

campaign using more sophisticated testing apparatus such as the Cubical Cell and the Hollow Cylinder seems necessary to investigate the influence of the direction of principal axes and their continuous rotation. The study of this feature is also fundamental as in real cases rotation of principal stress and strain rate axes almost always occurs within a soil mass.

- Fibres affect the volumetric behaviour because they increase the relative density of the specimen and they also provide extra confinement to the sand matrix. These two effects are in competition with each other (one tends to decrease and the other to increase the state parameter of the sand) and it appears fundamental to investigate their contrasting effects in order to fully understand the volumetric behaviour of reinforced composites. This would also be important for assessing the benefit of fibre addition to prevent the liquefaction of loose clean sands.

8.3.3 Theoretical modelling

The proposed constitutive model can obviously be subjected to many amendments and improvements. However, it appears that the two following tasks should have priority over other issues:

- To the author's knowledge there is a lack of published research on the constitutive modelling of agglomerates with discrete fibres and the proposed model for the fibre agglomerate is quite simple and based on a number of simplifications. For example the quantification of the voids "attached" to the fibres is still based on a trial and error procedure which requires some refinement in future research and should in some way be linked to characteristics of the sand particles and the fibres. Moreover ,other improvements (e.g. the consideration of non linear elastic and/or plastic behaviour of the fibres, the evolution of fibre orientation during loading) may be needed to enhance the predictions of the model.

- The ultimate aim of the development of a constitutive model is its implementation into a numerical program to be used for the prediction of the performance of true scale

geotechnical structures. However, the implementation in a numerical programme requires the formulation of the constitutive model in a multiaxial space and this is an essential step forward in the development of the proposed modelling framework.

8.3.4 Field Tests

Field tests on real scale geotechnical structures would be necessary to validate the experimental results and the presented modelling framework. They are also fundamental to check the reliability of the research findings and to raise the confidence of the practising engineers that the proposed technique is effective in terms of costs and performances for its application in real geotechnical problems. Moreover it is envisaged that the achievement of a uniform soil-fibre mixture on large scale is a quite complex task and field tests are required to develop an effective and efficient mixing procedure.

8.4 Closure

The ultimate objective of projects such as this is to make some contribution for the enterprise of novel technology for improving the mechanical characteristics of soils and for its use in engineering practice. This research has explored the possibility of improving the mechanical characteristics of sand by adding short discrete polypropylene fibres and it has proposed a methodology for predicting the behaviour of this composite material. It is hoped that the outcome of this research combined with the finding of further studies – e.g. as suggested here – will be beneficial for introduction of a new cost effective technique in the geotechnical market. Beneficiaries would be specialist ground treatment contractors and clients who may be able to exploit a novel technology.

REFERENCES

Abdulla, A.A. & Kiousis, P.D. (1997) Behaviour of cemented sands-II. Modelling. *International Journal for Numerical and Analytical Methods in Geomechanics*, 21, 549-568.

Al Refeai, T.O., (1991) Behaviour of granular soils reinforced with discrete randomly oriented inclusions. *Geotextiles and Geomembranes,* 10, 319-333.

ASTM D4767 - 04 Standard Test Method for Consolidated Undrained Triaxial Compression Test for Cohesive Soils.

Baldi, G. & Nova, R. (1984) Membrane penetration Effects in Triaxial Testing. *Journal of Geotechnical Engineering,* 110. No.3, 403-420.

Baldi,G., Hight,D.W. & Thomas, G.E., (1988) A Reevaluation of Conventional Triaxial Test Methods. *Advanced triaxial testing of soil and rock, ASTM STP 977, Philadelphia*: American Society for Testing and Materials, 219-263.

Bardet, J.P. (1986) Bounding surface plasticity model for sands. *Journal of Engineering Mechanics,* ASCE, 112, No.11, 1198-1217.

Been, K. & Jefferies, M.G. (1985) A state parameter for sands. *Géotechnique*, 35, No. 2, 99-112.

Bement, R.A.P. & Selby, A.R. (1997) Compaction of Granular Soils by Uniform Vibration Equivalent to Vibrodriving of Piles. *Geotechnical and Geological Engineering*, 15, No. 2, 121-143.

Bensoussan A., Lionis J.L. & Papanicolaou G. (1978) *Asymptotic analysis for periodic structures*. North-Holland Pub. Co., Amsterdam.

Bishop, A.W. & Green, G.E. (1965) The influence of end restraint on the compression strength of a cohesionless soil. *Géotechnique*, 15, 243-266.

Bjerrum, L., Kringstad, S. & Kummeneje, D. (1961) The shear strength of a fine sand. *Proc. 5th. Int. Conf. Soil. Mech. and Found. Eng.*, Paris, 1, 29-37.

Bolton, M.D. (1986) The strength and dilatancy of sands. *Géotechnique*, 36, No. 1, 65-78.

Brighenti,R. (2004) A mechanical model for fiber reinforced composite materials with elasto-plastic matrix and interface debonding. *Computational Materials Science*, 29, 475–493.

Car, E., Oller, S. & Oñate, E. (2000) An anisotropic elastoplastic constitutive model for large strain analysis of fiber reinforced composite materials. *Computer Methods in Applied Mechanics Engineering*, 185, 245-277.

Castro, G. (1969*) Liquefaction of sand*. Ph.D. Thesis, Harvard Soil Mechanics Series n° 81, Harvard University, Cambridge, MA, 112p.

Castro, G. & Christian, J.T. (1976) Shear Strength of Soils and Cyclic Loading. *Journal of Geotechnical Engineering*, 102, No. GT9, 887-894.

Castro, G. & Poulos, S. J. (1977) Factors Affecting Liquefaction and Cyclic Mobility. *Journal of Geotechnical Engineering*, 103, No. GT6, 501-516.

Chu, J. (1991) Liquefaction of Sand Under Sands Under Undrained and Non-Undrained Conditions. *Proc. 5th Int. Conf. on Soil Dynamics and Eearthquake Engineering*, Karlsruhe, Germany, 277-291.

Colliat-Dangus, J.L., Desrues, J. & Foray, P. (1988) Triaxial testing of granular soil under elevated cell pressure. *Advanced Triaxial Testing of Soil and Rock*, (R. T. Donage, R. C. Chaney and M. L. Silver ed.) ASTM, 290-310.

Consoli, N.C., Prietto, P.D.M. & Ulbrich, L.A. (1998) Influence of fiber and cement addition on behaviour of sandy soil. *Journal of Geotechnical and Geoenvironmental Engineering*, 124, No. 12, 1211-1214.

Consoli. N.C., Casagrande M.D.T., Prietto P.D.M. & Thome A. (2003) Plate Load test on fiber reinforced soil. *Journal of Geotechnical and Geoenvironmental Engineering*, 129, No. 10, 951-955.

Consoli, N.C., Casagrande, M.D.T. & Coop, M.R. (2005) Effect of fiber reinforcement on the isotropic compression behavior of a sand. *Journal of Geotechnical and Geoenvironmental Engineering*, 131, No. 11, 1434-1436.

Consoli, N.C., Casagrande, M.D.T., & Coop, M.R. (2007) Performance of a fibre-reinforced sand at large shear strains. *Géotechnique*, 57, No. 9, 751-756.

Consoli, N.C., Heineck, K.S. & Casagrande, M.D.T. (2007) Shear strength behavior of fiber-reinforced sand considering triaxial tests under distinct stress paths, *of Geotechnical and Geoenvironmental Engineering*, 133, No. 11, 1466-1469.

Costa Filho, L.M.. (1985) Measurement of Axial Strains in Triaxial Tests on London Clay. *Geotechnical Testing Journal*, 8. No. 1, 3-13.

DeGregorio, V. B. (1990) Loading Systems, Sample Preparation, and Lliquefaction. *Journal of Geotechnical Engineering*, ASCE, 116, No. 5, 805-821.

di Prisco, C., Nova, R., (1993) A constitutive model for soil reinforced by continuous threads. *Geotexiles and Geomembranes*, 12, No. 2, 161-178.

Diambra, A., Russell, A.R., Ibraim, E. & Muir Wood, D., (2007) Determination of fibre orientation distribution in reinforced sand. *Géotechnique*, 57, No. 7, 623-628.

Diambra, A., Ibraim, E., Muir Wood, D., Russell, A.R., & Bennani, Y. (2008). Effect of sample preparation on the behaviour of fibre reinforced sands. *Proceedings of the 4th Int. Symposium on Deformation Characteristic of Geomaterials*, IS-Atlanta 2008, 629-636.

Diambra, A., Ibraim, E., Muir Wood, D. & Russell, A.R., (2010) Fibre Reinforced Sands: Experiments and Modelling. *Geotextiles and Geomembranes,* 28, 3, 238-250.

Ding, D. & Hargrove, S.K. (2006) Nonlinear stress-strain relationship of soil reinforced with flexible geofibers. *Journal of Geotechnical & Geoenvironmental. Engineering*, ASCE, 132, No. 6,791-794.

Doanh, T. & Ibraim, E. (2000) Minimum undrained strength of very loose Hostun RF sand in triaxial compression and extension. *Géotechnique*, 50, No.4, 377-392.

Doanh, T., Ibraim, E. & Matiotti, R. (1997) Undrained instability of very loose Hostun sand in triaxial compression and extension. Part 1: Experimental observations. *Journal of Cohesive-Frictional Materials*, 2, 47-70.

Dvorak, G.K. & Bahei-El-Din, Y.A. (1982) Plasticity analysis of fibrous composites. *Journal of Applied Mechanics*, 49, 327-335.

Dvorak, G.K. & Bahei-El-Din, Y.A. (1987) A bimodal plasticity theory of fibrous composite materials. *Acta Mechanica*, 69, 219-241.

Eshelby, J.D, (1957) The determination of the field of an ellipsoidal inclusion and related problems. *Proceedings Royal society London A241*, 376-396.

Frydman, S., Zeitlein, J.G. & Alpan, I. (1973) The Membrane Effect in Triaxial Testing of Granular soils. *Journal of Testing and Evaluation*, 1, No.1, 37-41.

Fukushima, S. & Tatsuoka, F. (1984) Strength and deformation characteristics of saturated sand at Extremely low Pressures. *Soils and Foundations*, 24, No. 4, 30-48.

Gajo, A. & Muir Wood, D. (1999a) Severn-Trent sand: a Kinematic-hardening consitutive model: the q-p formulation. *Géotechnique*, 49, No. 5, 595-614.

Gajo, A. & Muir Wood, D. (1999b) A kinematic hardening constitutive model for sands: The multiaxial formulation. *International Journal for Numerical and Analytical Methods in Geomechanics*, 23, 925-965.

Gray, D.H. & Al-Refeai, T. O. (1986) Behaviour of fabric - versus fiber-reinforced sand, *Journal of Geotechnical Engineering*, ASCE, 112, No. 8, 804.820.

Gray, D.H. & Ohashi, H. (1983). Mechanics of fiber reinforcement in sands. *Journal of Geotechnical Engineering*, ASCE, 109, No. 3, 335-353.

Gregory, G.H. & Chill, D.S. (1998) Stabilization of earth slope with fiber reinforcement. *Proceedings 6th International Conference on Geosyntetics*, Atlanta, 1073-1078.

Heineck, C.S., Consoli, N.C. & Coop, M.R. (2005) Effect of microreinforcement of soils from very small to large shear strains. *Journal of Geotechnical and Geoenvironmental. Engineering*, ASCE, 131, No. 8, 1024-1033.

Henkel D.J. & Gilbert G.D. (1952) The effect of the rubber membrane on the measured triaxial compression strength of clay samples. *Géotechnique*, 3, No. 1, 20–29.

Hyodo, M., Tanimizu H., Yasufuku, N. & Murata, H. (1994) Undrained cyclic and monotonic triaxial behaviour of saturated loose sand. *Soils and Foundations*, 34, No.1, 19-32.

Ibraim, E. (1998) *Différents aspects du comportement des sables à partir d'essais triaxiaux: des petites déformations à la liquéfaction statique*. PhD thesis, ENTPE Lyon.

Ibraim, E. & Fourmont, S. (2006) Behaviour of sand reinforced with fibres. *Soil stress-strain behaviour: Measurement, Modelling and Analysis*, Geotechnical Symposium, Rome, March 16-17 (Ling, Callisto, Leshchinsky & Koseki Eds.) Springer, 807-918.

Ibraim, E. & Maeda, K. (2007) Numerical analysis of fibre-reinforced granular soils. *Proceedings of 5th International Symposium on Earth Reinforcement*, (Taylor&Francis Ed.) Balkema, 387-393.

Ibraim, E., Muir Wood, D., Maeda, K. & Hirabayashi, H. (2006) Fibre-reinforced granular soils: numerical approach. *Geomechanics and geotechnics of particulate media* (Hyodo, Murata & Nakata Eds.) Taylor & Francis, London, 443-448.

Ishihara, K., Tatsuoka, F. & Yasuda, Y. (1975) Undrained deformation and liquefaction of sand under cyclic stresses. *Soils and Foundations*, 15, No. 1, 29-44.

Jafarzadeh, F., Javaheri, H., Sadek, T. & Muir Wood, D. (2008) Simulation of anisotropic deviatoric response of Hostun sand in true triaxial tests. *Computers and Geotechnics*, 35, No. 5, 703-718.

Jardine, R.J., Symes, M.J. & Burland, J.B. (1984) The measurement of soil stiffness in the triaxial apparatus. *Géotechnique*, 34, No. 3, 323-340.

Jewell, R.A. & Wroth, C.P. (1987) Direct shear tests on reinforced sand. *Géotechnique*, 37, No. 1, 53-68.

Kiekbush, M. & Schuppener, B. (1977) Membrane penetrationa nd its effect on pore pressures. *Journal of Geotechnical Engineering*, ASCE, 103, No. GT11, 1267-1279.

Kirkpatrick, W.M. & Belshaw, D.J. (1968). On the Interpretation of the Triaxial Test. *Géotechnique*, 18, 336-350.

Kolymbas, D. & Wu, W. (1990) Recent results of triaxial tests with granular materials. *Powder Technology*, 60, No. 2, 99-119.

Konrad, J.M. (1990) Minimum undrained strength of two sands. *Journal of Geotechnical Engineering*, ASCE, 116, No. 6, 932-947.

Kouznetsova V., Brekelmans W.A.M. & Baaaijens F.P.T. (2001) An approach to micro-macro modeling of heterogeneous materials. *Computational Mechanics*, 27, 37-48

Kramer, L. & Seed, H.B. (1988) Initiation of soil liquefaction under static loading conditions. *Journal of Geotechnical Engineering*, ASCE, 114, No. 4, 412-430.

Kuerbis, R.H. & Vaid, Y.P. (1990) Corrections for membrane strength in the triaxial tests. Geotechnical Testing Journal, vol.13, No.4 Dec.1990, 361-369.

Kumar, S. & Tabor, E. (2003) Strength characteristics of silty clay reinforced with randomly oriented nylon fibres. EJGE paper 10.

Ladd, R. S. (1978) Preparing specimens using undercompaction. *Geotechnical Testing Journal*, 1, No. 1, 16–23.

Lade, P.V. & Hernandez, S.B. (1977) Membrane Penetration Effects in Undrained Tests. *Journal of Geotechnical Engineering*, ASCE, 103, No. GT2, 109-125.

Lade, P.V. (1992) Static Instability and Liquefaction of Loose Fine Sandy Slopes. *Journal of Geotechnical Engineering*, ASCE, 118, No. 1, 51-71.

Lade, P.V. (1993) Initiation of static instability in the submarine Nerlerk berm. *Canadian Geotechnical Journal*, 30, No. 6, 895-904.

Lancelot, L., Shahrour, I. & Al Mahmoud, M. (2006) Failure and dilatancy properties of sand at relatively low stresses. *Journal of Engineering Mechanics*, 132, No. 12, 1396-1399.

Li, J. & Ding, D.W. (2002) Nonlinear elastic behaviour of fiber-reinforced soil under cyclic loading. *Soil Dynamics and Earthquake Engineering*, 22, 997-983.

Lindenberg, J. & Koning, H.L. (1981) Critical density of sand. *Géotechnique*, 31, No. 2, 231-245.

Luccioni, B.M. (2006) Constitutive model for fiber-reinforced composite laminates. *Journal of Applied Mechanics*, 73, 901-910.

Luong, M.P. (1980) Stress-strain aspects of cohesionless soils under cyclic and transient loading. *Microstructural Science*, 1, 315-324.

Machado, S.L., Carvalho, M.F. & Vilar, O.M. (2002) Constitutive Model for Municipal Solid Waste. *Journal of Geotechnical and Geoenvironmental. Engineering*, ASCE 128, No. 11, 940-951.

Maher, M.H. & Gray, D.H. (1990) Static response of sand reinforced with fibres. *Journal of Geotechnical Engineering*, ASCE, 116, No. 11, 1661-1677.

Maher, M. H. & Ho, Y. C. (1993) Behavior of fiber-reinforced cemented sand under static and cyclic loads. *Geotechnical Testing Journal*, 16, 330–338.

Maher, M.H. & Ho, Y.C. (1994) Mechanical properties of kaolinite/fiber soil composite. *Journal of Geotechnical Engineering*, ASCE 120, No. 8, 1381–1393.

Martin, G.R., Finn, W.D.L. & Seed, H.B. (1978) Effects of system compliance on liquefaction tests. *Journal of the Geotechnical Engineering*, ASCE, 104, No. 4, 463-479.

McGown, A., Andrawes, K.Z. & Al-Hasani (1978) Effect of inclusion properties on the behavior of sand. *Géotechnique*, 28, No. 3, 327-346.

Merodio, J. & Ogden, R.W. (2005) Mechanical Response of Fibre-Reinforced incompressible non-linearly elastic solids. *International Journal of Non-Linear Mechanics*, 40, 213-227.

Michalowski, R.L. (1997) Limit stress for granular composites reinforced with continuous filaments. *Journal Engineering Mechanics*, 123, No. 8, 852–859.

Michalowski, R.L. & Čermák, J. (2002) Strength anisotropy of fiber-reinforced sand. *Computers and Geotechnics*, 29, 279-299.

Michalowski, R.L. & Čermák, J. (2003) Triaxial compression of sand reinforced with fibers. *Journal of Geotechnical and Geoenvironmental. Engineering*, ASCE, 129, No. 2, 125–136.

Michalowski, R.L. & Zhao, A. (1996) Failure of fiber-reinforced granular soils. *Journal of Geotechnical Engineering*, ASCE, 122, No. 3, 226-234.

Michałowski, R.L. (2008) Limit analysis with anisotropic fibre-reinforced soil. *Géotechnique*, 58, No. 6, 489-501.

Nash, D.F.T. (2002) *A computer control system for stress path triaxial testing*, TRIAX version 5.2, using BBC Basic for Windows (Unpublished)

Newland, P.L. & Alley, B.H. (1957) Volume changes in drained triaxial tests on granular materials. *Géotechnique*, 7, No. 1, 17-34.

Newland, P.L. & Alley, B.H. (1959) Volume changes during undrianed triaxial tests on saturated dilatant granular materials. *Géotechnique*, 9, No. 3, 174-182.

Nicholson, P.G., Seed, R.B. & Anwar, H.A. (1993) Elimination of membrane compliance in undrained testing. I. Measurement and evaluation. *Canadian Geotechnical Journal*, 30, No.5, 727-738.

Ortiz, M. & Popov, E.P. (1982) Plain concrete as a composite material. *Mechanics of Materials*, 1, 139-150.

Özkul, Z.H. & Baykal, G. (2007) Shear behaviour of compacted rubber fiber-clay composite in drained and undrained loading. *Journal of Geotechnical and Geoenvironmental Engineering*, 133, No. 7, 767-781.

Palmeira, E.M. & Milligan, G.W.E. (1989) Large scale direct shear tests on reinforced soil. *Soils and Foundations*, 29, No. 1, 18-30.

Parry, R.H.G. (1958) Correspondence: on the yielding of soils. *Géotechnique*, 8, No. 4, 183-186.

Peng, X.Q., Guo, Z.Y. & Moran, B. (2006) An Anisotropic hyperelastic constitutive model with fiber-matrix shear interaction for the human annulus fibrosus. *Journal of Applied Mechanics*, 73, 815-824.

Ponce, V. M., & J. M. Bell. (1971) Shear strength of sand at extremely low pressures. *Journal of the Soil Mechanics and Foundations Division*, ASCE, 97, No. SM4, 625-636.

Poulos, S. J. (1981) The Steady State of Deformation. *Journal of Geotechnical Engineering*, 107, No. GT5, 553-562.

Ramana, K.V., & Raju, V.S. (1982) Membrane penetration in Triaxial Tests. *Journal Geotechnical Engineering*, ASCE, 108, No. GT2, 305-310.

Ranjan, G., Vasan, R.M. & Charan, H.D., 1996. Probabilistic analysis of randomly distributed fiber-reinforced soil. *Journal Geotechnical Engineering*, ASCE, 122 , No. 6, 419-426.

Roscoe, K.H., Schofield, A.N. & Thurairajah, A. (1963) Yielding of clays in states wetter than critical. *Géotechnique*, 13, No. 3, 211-240.

Rowe, P.W. & Barden, L. (1964) Importance of free ends in triaxial testing. *Journal of the Soil Mechanics and Foundations Division*, ASCE, 90, No. SM1, 1-27.

Rowe, P.W. (1962) The stress-dilatancy relation for static equilibrium of an assembly of particles in contact. *Proceedings of the Royal Society of London*, Series A, 269, 500-521.

Sadek , T. (2006) *The multiaxial behaviour and elastic stiffness of Hostun sand*. PhD thesis, University of Bristol.

Santoni, R.L., & Webster, S.L. (2001) Airfields and roads construction using fibre stabilization of sands. *Journal of Transportation Engineering*, 127, No. 2, 96-104.

Skempton, A.W. (1954) The pore-pressure coefficients A and B. *Géotechnique* 4, 143.

Shewbridge S.E. & Sitar N. (1989) Deformation characteristics of reinforced soils in direct shear. *Journal of Geotechnical Engineering*, ASCE, 155, No.8, 1134-1147.

Sivakumar Babu, G.L., Vasudevan, A.K. & Haldar, S. (2007) Numerical simulation of fiber-reinforced sand behaviour. *Geotextiles and Geomembranes*, 26, No. 2, 181-188.

Sivathayalan, S. & Vaid, Y.P. (1998) Truly undrained response of granular soils with no membrane-penetration effects. *Canadian Geotechnical Journal*, 35, 730-739.

Sladen, J. A., D'Hollander, R. D. & Krahn, J. (1985) The liquefaction of sands, a collapse surface approach. *Canadian Geotechnical Journal*, 22, 564-578.

Spencer, A.J.M (1984) *Continuum theory of the mechanics of fibre reinforced composites.* Springer-Verlag New York, Inc , 175 Fifth Ave , New York, New York 10010, USA, 1984, 284 pp.

Sway, A.T. & Bang, S. (2007) Analysis of geofiber reinforced soils. *Proceedings of 5th International Symposium on earth reinforcement*, (Taylor&Francis Ed.) Balkema, 357-362.

Tang , C., Shi, B., Gao, W., Chen,F. & Cai,Y. (2007) Strength and mechanical behaviour of short polypropylene fiber reinforced and cement stabilized clayey soil. *Geotexiles and Geomembranes*, 25, 194-202.

Tingle, J.S., Santoni, R.L. & Webster, S.L. (2002) Full-scale field tests of discrete fibre-reinforced sand. *Journal of Transportation Engineering*, 128, No. 1, 9-16.

Toll, D.G. (1993) A computer control system for stress path triaxial testing. *Developments in Civil Construction Engineering Computing.* (Ed: Topping, B.V.) Civil-Comp press, Edinburgh. 107-117.

Vaid, Y. P. & Chern, J. C. (1983) Effect of static shear on resistance to liquefaction. *Soils and Foundations*, 23, No.1, 46-59.

Vaid, Y.P. & Sivathayalan, S. (1996) Errors in estimates of void ratio of laboratory sand specimens. *Canadian Geotechnical Journal*, 33, 1017-1020.

Verdugo R., Ishihara K. (1996) The steady State of Sandy soils. *Soils and Foundations*, 36 No.2 81-91.

Villard, P., Jouve, P. & Riou, Y. (1990) Modélisation du compertment mécanique du Texsol. *Bulletin de liaison des laboratoires des ponts et chaussees*, 168, 15-28.

Voyadijs, G.Z. & Thiagarajan, G. (1995) An anisotropic yield surface model for directionally reinforced metal-matrix composites. *International Journal of Plasticity*, 11, No. 8, 867-894.

Waldron L.J. (1977). The shear resistance of root-permeated homogeneous and stratified soil. *Soil Science Society of America Journal*, 41, No. 3, 843-849

Yetimoglu, T. & Salbas, M. (2003) A study on the shear strength of sands reinforced with randomly distributed discrete fibres. *Geotexiles and Geomembranes*, 21, 103-110.

Yetimoglu, T., Inanir, M., & Inanir, O. E. (2005) A study on bearing capacity of randomly distributed fiber-reinforced sand fills overlying soft clay. *Geotexiles and Geomembranes*, 23, 174-183.

Zhu, Y.T., Zong, G., Manthiram, A. & Eliezer, Z. (1994) Strength analysis of random short-fibre-reinforced metal matrix composite materials. *Journal of Material Science*, 29, 6281-6286.

Zornberg, J.G. (2002) Discrete framework for equilibrium analysis of fibre-reinforced soil. *Géotechnique*, 52, No. 8, 593-604.

Zornberg, J.G., LaFountain, L., & Caldwell, J.A. (2003) Analysis and Design of Evapotranspirative Cover for Hazardous Waste Landfill. *Journal of Geotechnical and Geoenvironmental Engineering*, ASCE, 129, No. 5, 427-438.